CARBON DIOXIDE AND CARBON DIOXIDE - WATER MIXTURES: P–V–T PROPERTIES AND FUGACITIES TO HIGH PRESSURE AND TEMPERATURE CONSTRAINED BY THERMODYNAMIC ANALYSIS AND PHASE EQUILIBRIUM EXPERIMENTS

By

Urs Karl Mäder

Dipl. Natw. ETH, Swiss Federal Institute of Technology, Zürich

M.Sc. (Geology), The University of British Columbia

A THESIS SUBMITTED IN PARTIAL FULFILLMENT OF

THE REQUIREMENTS FOR THE DEGREE OF

DOCTOR OF PHILOSOPHY

in

THE FACULTY OF GRADUATE STUDIES

GEOLOGICAL SCIENCES

We accept this thesis as conforming

to the required standard

THE UNIVERSITY OF BRITISH COLUMBIA

August 1990

In presenting this thesis in partial fulfilment of the requirements for an advanced degree at the University of British Columbia, I agree that the Library shall make it freely available for reference and study. I further agree that permission for extensive copying of this thesis for scholarly purposes may be granted by the head of my department or by his or her representatives. It is understood that copying or publication of this thesis for financial gain shall not be allowed without my written permission.

Department of GEOLOGICAL SCI.

The University of British Columbia
Vancouver, Canada

Date August 18, 1995

Abstract

The thermophysical properties of supercritical CO_2 and H_2O–CO_2 mixtures are reviewed and their computation and prediction improved through theory and experiment. A resolution is attempted among inconsistencies between and within data sets, including P-V-T measurements, phase equilibrium experiments and equations of state.

Pure carbon dioxide: Equations of state for CO_2 (Kerrick & Jacobs, 1981; Bottinga & Richet, 1981; Holloway, 1977) are based solely on P-V-T data up to 8 kbar and lead to deviations from phase equilibrium data at pressures greater than 10–20 kbar.

Mathematical programming analysis has been applied to the fitting of parameters for an equation of state using simultaneously constraints from phase equilibrium and P-V-T data. Phase equilibrium data up to 42 kbar are used to define a feasible region for the adjustable parameters in free energy space. Each half-bracket places an inequality constraint on the fugacity of CO_2 provided the thermophysical properties of the solid phases are known. Except for magnesite thermophysical data from the mineral data base of Berman (1988) were used. A least squares objective function served to optimize parameters to P-V-T data.

The enthalpy of formation of magnesite was revised on the basis of recent low pressure phase equilibrium experiments by Philipp (1988) to -1112.505 kJ/mole.

Piston–cylinder experiments were performed to constrain the equilibrium magnesite $\rightleftharpoons$ periclase + CO_2 at high pressure. The equilibrium boundary is located at 12.1($\pm$1) kbar, 1173–1183 °C ($\pm$10), and at 21.5($\pm$1) kbar, 1375–1435 °C ($\pm$10).

A van der Waals type equation of state with five adjustable parameters has been developed for CO_2. The function is smooth and continous above the critical region,

behaves well in the high and low pressure limits, and the calculation of $\int V dP$ for free energy does not require numerical integration. Computed free energies are consistent with all phase equilibrium data at high pressure, and computed volumes agree reasonably with P-V-T measurements. The proposed equation is:

$$P = \frac{RT}{V - b(V,T)} - \frac{A_1}{TV^2} + \frac{A_2}{V^4} \quad , \quad b = B_1 + B_2 T - \frac{B_3}{V^3 + C} \quad , \quad C = \frac{B_3}{B_1 + B_2 T}$$

with $B_1 = 28.0647$, $B_2 = 1.7287 \cdot 10^{-4}$, $B_3 = 83653$, $A_1 = 1.0948 \cdot 10^9$, $A_2 = 3.3747 \cdot 10^9$, and $R = 83.147$, in units of Kelvin, bar and cm^3/mole. The equation is recommended up to 50 kbar and above 400 K with reasonable extrapolation capabilities. A FORTRAN source code to evaluate the volume and fugacity is provided.

Thermophysical properties for the calcium carbonate polymorphs calcite–I, IV, V, and aragonite were derived that are consistent with phase equilibrium experiments.

Data required for further improvement include high pressure phase equilibria involving CO_2, constraints on the thermal expansion of magnesite, and P-V-T data to resolve inconsistencies among existing measurements.

Water–carbon dioxide mixtures: The two widely used equations of state for H_2O–CO_2 mixtures are those proposed by Kerrick & Jacobs (1981) and by Holloway (1977)–Flowers (1979).

Evaluation of existing equations and data is difficult due to inconsistencies among experimental studies. P-V-T-X data by Franck & Tödheide (1959) are inconsistent with data by Greenwood (1973) and Gehrig (1980), and cannot be reconciled with measured phase equilibria in H_2O–CO_2 fluid mixtures. Data by Greenwood and Gehrig are in loose agreement but extend only to 600 bar and do not constrain activities at higher pressures.

A procedure is developed for using experimental phase equilibrium constraints to put limits on the fugacities of components of the fluid mixture. Inconsistencies among phase equilibrium studies are discussed.

It is concluded that the data base available is not yet adequate to derive a reliable equation of state for H_2O–CO_2 mixtures. Future work must include P-V-T-X measurements to 8 kbar and phase equilibrium studies to resolve inconsistencies. These can constrain deviations from ideal mixing in the fluid phase, and constrain specific volumes at high pressures where P-V-T-X data connot be obtained.

Table of Contents

List of Tables

List of Figures

Acknowledgement

This thesis could not have been produced without the help of many friends and colleagues. I was lucky to be able to learn and profit from many outstanding scientists, particularly from Hugh Greenwood, Rob Berman, Tom Brown, 'Capi' DeCapitani, Kelly Russell, Pat Meagher and John Ross. I am indebted to Hugh Greenwood for his influence and inspiration as a scientist, a colleague and a thoughtful person. What I have achieved in the laboratory I owe to him. Rob Berman gave more of his time and help than I could possibly ask for. I always enjoyed those rather intense work sessions with Rob on the computer, in the lab, or just paddling down a river on occasion. Tom Brown stopped me thinking every now and then with one of his subtle but fundamental questions. Equally important were all the people who kept operations running smoothly: the machinists Doug Polson and Ray Rodway, John Knight who helped with electronics and performed the microprobe analyses, Stanya Horsky who spent time translating from Russian and assisting with analytical matters, Bryon Cranston, Yvonne Douma, Ed Montgomery, Mark Baker, the office staff and the crew from the inter–library loans office. John Holloway kindly provided computer codes for his equation of state. My fellow graduate students, ice hockey mates and ski bums provided stimulus and a balance to matters scientific.

The ever so important funding was arranged with grants from the Natural Sciences and Engineering Research Council (NSERC) of Canada to Hugh Greenwood and Rob Berman (Geological Survey of Canada, Ottawa), and through a grant from the Canada–British Columbia Mineral Development Agreement administerd by the B.C. Geological Survey Branch with the help of Dan Hora. The Unversity Graduate Fellowship program at UBC provided financial assistance for more than four years for which I am grateful.

My parents who did not like to see me leave Switzerland, and Ursula who did not like to see me work late nights, but married me in spite of it, deserve my deep appreciation. Stephan, ten months of age, crawling, and definitly very human set the importance of my thesis into much needed perspective during the final leg.

Preface

This thesis is a contribution towards the computation and prediction of thermophysical properties of supercritical fluids, specifically pure carbon dioxide and water–carbon dioxide mixtures. The methodology tightly interweaves theory and experiment, relevant to both synthetic and natural chemical systems. The thesis is part of an effort by the UBC–petrology group over more than two decades to create a reliable data base of thermophysical properties of minerals and fluids applicable to natural systems. This multidisciplinary approach first culminated in the publication of a comprehensive data base by Berman in 1988, and software to compute phase equilibria by Brown *et al.* (1988). Since then no petrology meeting has passed without presentations making extensive use of these powerful tools. An impressive example was this year's 'quantitative methods in petrology' symposium in Vancouver hosted by the Mineralogical Society of Canada in honour of Hugh Greenwood.

The system CO_2–H_2O is chemically simple. The large range in pressure and temperature relevant to geological problems require moving beyond rigorous theory into the world of empiricism. This empirical element introduces arbitrarily made assumptions that cannot be tested as being 'right' or 'wrong', but only as being 'practical' or 'impractical'. As a logical consequence many of the numerical values offered in this thesis are transitional in character and will change with the continuing refinement and enlargement of the experimental and natural data base, the advancement in computer technology and the development of better theories. The experimental contributions, the methodology and the assessment of existing work are expected to form a permanent contribution. The insight gained from thermodynamic modeling forms a firm basis to recommend further

experimental work that would put the most stringent constraints on the thermophysical properties of minerals and fluids.

Most aspects and results of this thesis were presented orally at meetings in Denver and Vancouver (Mäder *et al.* 1988, 1990). The first chapter without appendices was submitted to the Journal of Petrology in August, 1990 (Mäder & Berman, in review) and parts of the second chapter will appear in a special volume of the Canadian Mineralogist combining contributions to the Greenwood Symposium on 'quantitative methods in petrology' held in Vancouver, May 1990 (Mäder, in preparation). The experimental part (appendix C) will form part of a separate publication combined with an analysis of calibration and friction relevant to piston–cylinder work (Mäder, in preparation).

The two chapters are organized as stand–alone papers each having a list of references. Both chapters include its own introduction and conclusions. The table of contents, the lists of figures and tables, and the pagination combine the two parts into a single document in order to fulfill library requirements.

to Ursula

and my parents

Chapter 1

An Equation of State for Carbon Dioxide to High Pressure and Temperature

1.1 Introduction

Volumetric properties of CO_2 at high pressures are needed for the solution of a number of problems in metamorphic and igneous petrology, one of the most important being the computation of phase equilibria (i.e. Perkins *et al.*, 1986; Brown *et al.*, 1988). Because volumes have been measured up to only 8 kbar (Shmonov & Shmulovich, 1974), extrapolation using an equation of state is required.

Existing equations of state for carbon dioxide suitable for computation of geological phase equilibria include those by Holloway (1977, 1981a, 1981b), Touret & Bottinga (1979), Bottinga & Richet (1981), Kerrick & Jacobs (1981), Powell & Holland (1985, Holland & Powell, 1990), Saxena & Fei (1987a, 1987b), Shmulovich & Shmonov (1975), Mel'nik (1972), and Ryzhenko & Volkov (1971). These equations are based on a variety of theories and incorporate adjustable parameters to fit experimentally measured volumes (see Ferry & Baumgartner, 1987, Holloway, 1987 for detailed reviews, and Prausnitz *et al.*, 1986 for theory). Although most equations fit P-V-T data adequately, it has been pointed out that all of them are inconsistent with phase equilibrium data at pressures above 10 to 20 kbar (figure 1.1) (Haselton *et al.*, 1978; Berman, 1988; Mäder *et al.* 1988; Chernosky & Berman, 1989). Equations that use empirically combined parameters, and polynomial equations in particular, may achieve excellent agreement with observed data, commonly at the expense of reasonable extrapolation. Even equations based on

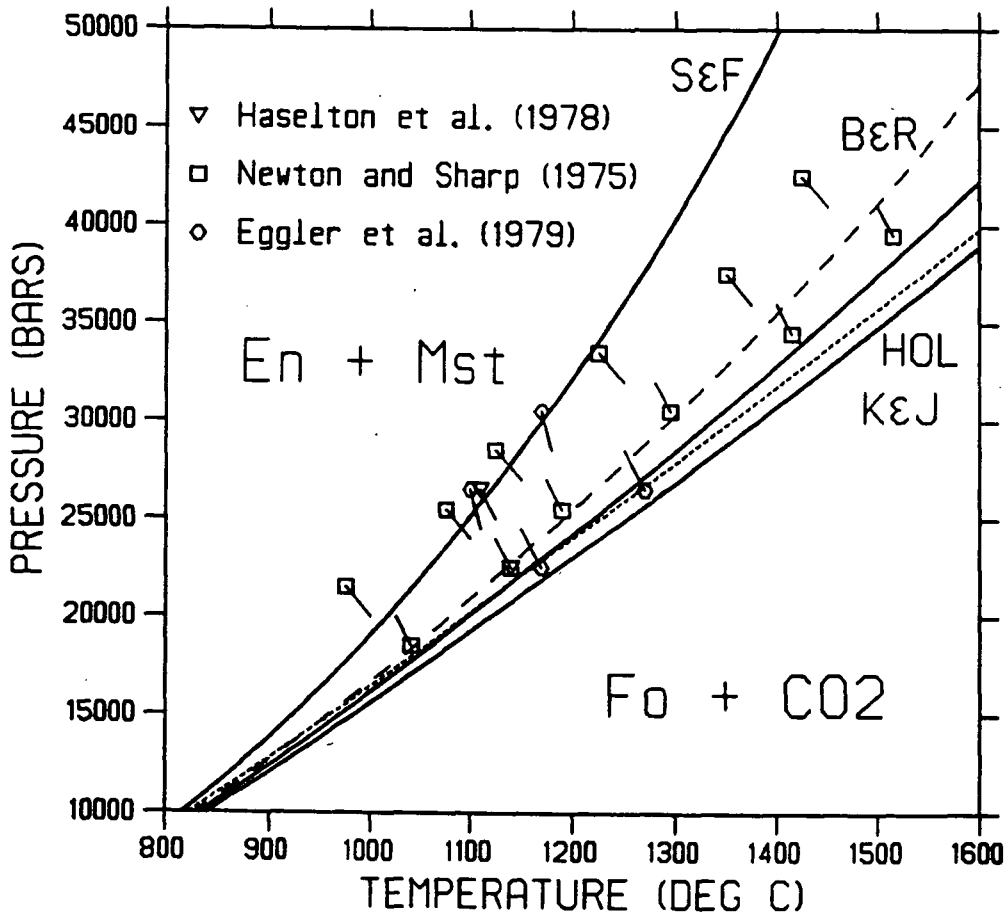

Figure 1.1: Experimental brackets on the equilibrium Mst+En $\rightleftharpoons$ Fo+CO_2 and reaction boundaries computed with the database of Berman (1988) with revised magnesite data (Chernosky & Berman, 1989, and this study) and equations of state for CO_2 by Kerrick & Jacobs, 1981 (K&J), Bottinga & Richet, 1981 (B&R), Holloway, 1977, 1981b (dotted curve, Hol), and Saxena & Fei, 1987a (S&F). The dashed curve was computed with the B&R equation with magnesite properties perturbed by its estimated uncertainties as discussed in the text. Abbreviations: En: ortho enstatite, Fo: forsterite, Mst: magnesite. The diagram was produced with GE0-Calc (Brown *et al.*, 1988).

sound theory may show unconstrained behaviour if they contain some empirical element. For example, Kerrick & Jacob's (1981) modified Redlich–Kwong equation (Redlich & Kwong, 1949) has no positive volume defined at progressively higher temperatures with rising pressure, due to the mathematical form of the $a(P,T)$ parameter. The equation proposed by Bottinga & Richet (1981) shows the best extrapolation properties to 42 kbar (Chernosky & Berman, 1989, and below), but contains discontinuities due to separate parameter fitting for different volume intervals (figure 1.4). The modified Redlich–Kwong equation adopted by Holloway (1977) from de Santis *et al.* (1974) has a b parameter (excluded volume) derived from corresponding states systematics which leads to volumes at high pressures that are too large. Powell & Holland (1985, Holland & Powell, 1990) fit a simple polynomial function directly to the logarithm of fugacities derived from the equation of state of Shmonov & Shmulovich (1974) and Bottinga & Richet (1981), which is computationally efficient but limited in its applications, i.e volumes cannot be derived reliably and extrapolation is not recommended.

To circumvent the problem of inadequate P-V-T data at high pressures, alternate approaches utilize shock wave data, although uncertainties are large. Because measurments on pure fluid CO_2 do not seem to exist, one must rely on approximations based on data for similar fluids related to one another through corresponding states systematics (e.g. Saxena & Fei, 1987a; Helffrich & Wood, 1989). The equations chosen by these authors to fit the data are based on some formulation of the intermolecular potential (e.g. Lennard–Jones), but have the disadvantage of incorporating discontinuities where they require a different function for pressures below several kilobars. Saxena & Fei (1987a) fit a virial–like equation to shock wave data valid at pressures above 5 kbar.

The purpose of the present paper is to provide metamorphic and igneous petrologists with an equation of state for carbon dioxide that is compatible with existing experimental data, both phase equilibrium and P-V-T, that extrapolates reliably to upper mantle

conditions, and that is mathematically tractable. Preliminary results were reported by Mäder *et al.*, 1988. A FORTRAN-77 coded subroutine is supplied (appendix B) that computes fugacitiy and volume at specified pressure and temperature.

1.2 Method

Provided a reliable data base of thermophysical properties of minerals is available, thermodynamic properties of CO_2 may be tested by comparing calculated and experimentally determined phase equilibria (Haselton *et al.*, 1978; Ferry & Baumgartner, 1987; Berman, 1988; Chernosky & Berman, 1989). Inspection of figure 1.1 indicates a general failure of existing equations of state for CO_2 calibrated on P-V-T measurements only, to extrapolate to high pressures. An alternate approach incorporates phase equilibrium experiments as constraints rather than merely as tests of thermodynamic parameters. This is especially important in the present context as phase equilibrium data for CO_2 extend to much higher pressures (42 kbar) than P-V-T data (8 kbar).

Before proceeding, it is important to demonstrate that the inconsistencies illustrated in figure 1.1 are due to inadequate equations of state for CO_2 and not to errors in the thermodynamic properties of the minerals. The standard state properties, $\Delta_f H^{P_r,T_r}$, S^{P_r,T_r} and V^{P_r,T_r}, of all minerals involved in the equilibria of table 1.2 are tightly constrained by calorimetry and low pressure phase equilibrium data (see Berman, 1988, for details). The enthalpy of formation for magnesite has been ajusted to a less negative value compared to Chernosky & Berman (1989) for reasons discussed in section 'Magnesite'. The most poorly constrained properties are the heat capacity and thermal expansivity of magnesite, for which the data extend only to 750 K (Kelly, 1960) and 773 K (Markgraf & Reeder, 1985), respectively. The sensitivity of the calculated phase

equilibria to possible errors in extrapolation of these magnesite properties can be examined by adjusting the functions given by Berman (1988) and Chernosky & Berman (1989) within experimental uncertainties in such a way that the inconsistencies between existing equations of state and phase equilibrium data are minimized. The heat capacity function of Berman (1988), adjusted from Berman & Brown (1985), is already aimed at minimizing inconsistencies with the Kerrick & Jacobs (1981) equation of state at high pressure, i.e. to render magnesite less stable. In order to decrease the stability of magnesite the thermal expansion was maximised while maintaining average %–deviations from measured values within 100 % of those computed with the best fit of Berman (1988). This results in an increase of 25 % of the v_4 term, and a decrease of 21 % of the v_3 term (to adjust for increased curvature) compared to Berman (1988) using his equation (5) $V^{P,T}/V^{P,T_r} = 1 + v_3(T - T_r) + v_4(T - T_r)^2$. Phase equilibria computed with this perturbed volume function for magnesite are still inconsistent with all equations of state for CO_2 (figure 1.1). It is concluded that inconsistencies cannot be attributed entirely to errors in the properties of minerals, and, instead, phase equilibrium data may be used to constrain the high pressure properties of CO_2.

Linear programming offers an appropriate mathematical formalism for such an approach, introduced to geologists by Greenwood (1967a), applied to thermodynamic analysis of phase equilibria by Gordon (1973, 1977), and extended to mathematical programming analysis by Berman *et al.* (1986) and Berman (1988). Mathematical programming is a tool to handle large optimization problems with a variety of linear or nonlinear equality or inequality constraints.The optimal solution is found by minimizing or maximizing an objective function such as a conventional least squares formulation. An optimal solution, i.e. 'best fit', is consistent with respect to all constraints and renders the smallest (or largest) possible value for the objective function. A survey of nonlinear programming codes may be found in papers by Schittkowski (1980) and Wasil *et al.* (1989).

In the present study parameters for the equation of state for CO_2 are optimized with CO_2 fugacities constrained by phase equilibrium half-brackets up to pressures of 42 kbar. The objective function achieves a best fit to P-V-T data up to 8 kbar. An acceptable mathematical solution for the parameters of the equation of state is consistent with all phase equilibrium constraints and fits volumetric data as closely as the data warrant.

For the mathematical programming analysis phase equilibrium constraints are written in such a way as to separate the unknown contributions of CO_2 to the Gibbs potential from the known contributions of all other phases involved:

$$\begin{aligned}
\Delta_R G^{P,T} &= \sum_i^{\text{solids,CO}_2} \nu_i \Delta_a G_i^{P,T} \\
&= \sum_i^{\text{solids,CO}_2} \nu_i \left[\Delta_f H_i^{P_r,T_r} - T \cdot S_i^{P_r,T_r} + \int_{T_r}^{T} C_{p_i} dT - T \cdot \int_{T_r}^{T} \left(\frac{C_{p_i}}{T} \right) dT \right] \\
&\quad + \sum_i^{\text{solids}} \nu_i \left[V_i^{P_r,T_r}(P - P_r) + \int_{P_r}^{P} (V_i^{P,T} - V_i^{P_r,T_r})\, dP \right] \\
&\quad + \nu_{CO_2} \int_{P_r}^{P} V_{CO_2}^{P,T}\, dP \qquad (1.1)
\end{aligned}$$

In equation (1.1) $\Delta_R G^{P,T}$ denotes the change in the Gibbs free energy of a reaction, $\Delta_a G^{P,T}$ the apparent free energy of a pure phase as defined in Berman (1988), $\Delta_f H^{P_r,T_r}$ the enthalpy of formation from the elements, S^{P_r,T_r}, V^{P_r,T_r}, the third law entropy and molar volume at standard pressure (P_r = 1 bar) and temperature (T_r = 298.15 K), and Cp and ν refer to the heat capacity at constant pressure and the stoichiometric coefficient. Given a reliable, internally consistent thermodynamic database for minerals, the only unknown part of equation (1.1) is the last term, $\int V_{CO_2}^{P,T}\, dP$. From the relationship $\Delta_R G^{P,T} = 0$ at equilibrium, it follows that each experimental half-bracket leads to an inequality of the form $\Delta_R G^{P,T} < 0$ or $\Delta_R G^{P,T} > 0$ depending whether products or reactants are stable, respectively. We can thus rearrange equation (1.1) accordingly and

impose an inequality constraint on $\int V_{CO_2}^{P,T}\, dP$ for each half-bracket:

$$\nu_{CO_2} \int_{P_r}^{P} V_{CO_2}^{P,T}\, dP \overset{<}{>} -\Delta_R G_{\text{known}}^{P,T} \tag{1.2}$$

where $\Delta_R G_{\text{known}}$ denotes all the terms of equation (1.1) but the last one, and the 'less than' refers to the case where products are stable. The fugacity of CO_2 is related to the volume integral by the relationship

$$RT \ln f_{CO_2}^{P,T} = \int_{P_r}^{P} V_{CO_2}^{P,T}\, dP \tag{1.3}$$

choosing $P_r = 1$ bar and assuming approximate equality of unit pressure and unit fugacity at 1 bar. R denotes the gas constant. Each inequality constraint of the form of equation (1.2) requires integration of the equation of state and is therefore nonlinear with respect to parameters of the equation of state.

For this study the internally consistent thermodynamic database of Berman (1988), including compressibility and expansivity terms, is used to compute $\Delta_R G_{\text{known}}^{P,T}$ for about 120 phase equilibrium half brackets (table 1.2). Note that in deriving the above data base high pressure equilibria involving CO_2 were not used as constraints in order to avoid introducing errors from existing equations of state. The properties of the solid phases at low pressures are biased through being forced to be consistent with the Kerrick & Jacobs (1981) equation used by Berman (1988). Incorporating the same phase equilibrium constraints will force the new equation to be consistent with Kerrick & Jacobs (1981) at low pressures within experimental uncertainties. A set of about 440 measured volumes serves to optimize the difference between computed and observed volumes (table 1.1). The nonlinear optimization problem is solved with a mainframe program using a general reduced gradient strategy (GRG2, Lasdon & Waren, 1982). An interactive interface implemented by the UBC computing center (Vaessen, 1984), together with home–grown routines for graphical and statistical progress monitoring makes this package a powerful

tool for large optimization problems. Typical runtimes for equations with 5 adjustable parameters and 100 inequality constraints that do not require numerical integration are 20 to 200 seconds on an Amdahl 5860. Numerical integration increases computing time by a factor of 10 or more. Stability problems do not occur if the mathematical form of the equation of state is chosen carefully. An initial guess of the parameters need not be feasible with respect to the constraints.

1.3 Equation of State

There are essentially four types of equations of state from which to choose: i) van der Waals type (Redlich & Kwong, 1949, Holloway, 1977, Touret & Bottinga, 1979, Kerrick & Jacobs, 1981, Bottinga & Richet, 1981), ii) virial type (Saxena & Fei, 1987a, 1987b), iii) molecular potential formulations (Helffrich & Wood, 1989) and iv) empirical functions to directly fit the logarithm of the fugacity (Powell & Holland, 1985, Holland & Powell, 1990). A van der Waals type of equation was chosen for the following reasons: simple mathematical form, favorable behaviour in the limits ($P \rightarrow \infty$, $P \rightarrow 0$), potentially small number of adjustable parameters, and the imitation of subcritical behaviour in the simplest way. Furthermore, empirical polynomials dependent on pressure or temperature were avoided to ensure reasonable extrapolation. Only continuous functions were considered in order to render derivatives meaningful. An equation discussed but not adopted by Bottinga & Richet (1981) served as a starting point for development:

$$P = \frac{RT}{V-b} - \frac{A_1}{TV^2} + \frac{A_2}{V^4} \tag{1.4}$$

where b, A_1, A_2 are adjustable parameters, and R is the gas constant. The last term of equation (1.4) becomes important at small volumes, i.e. high pressures, resulting in increased compressibility at high pressures. The b parameter, a measure of the 'incompressible volume' is commonly assumed to be a constant. This approximation is valid

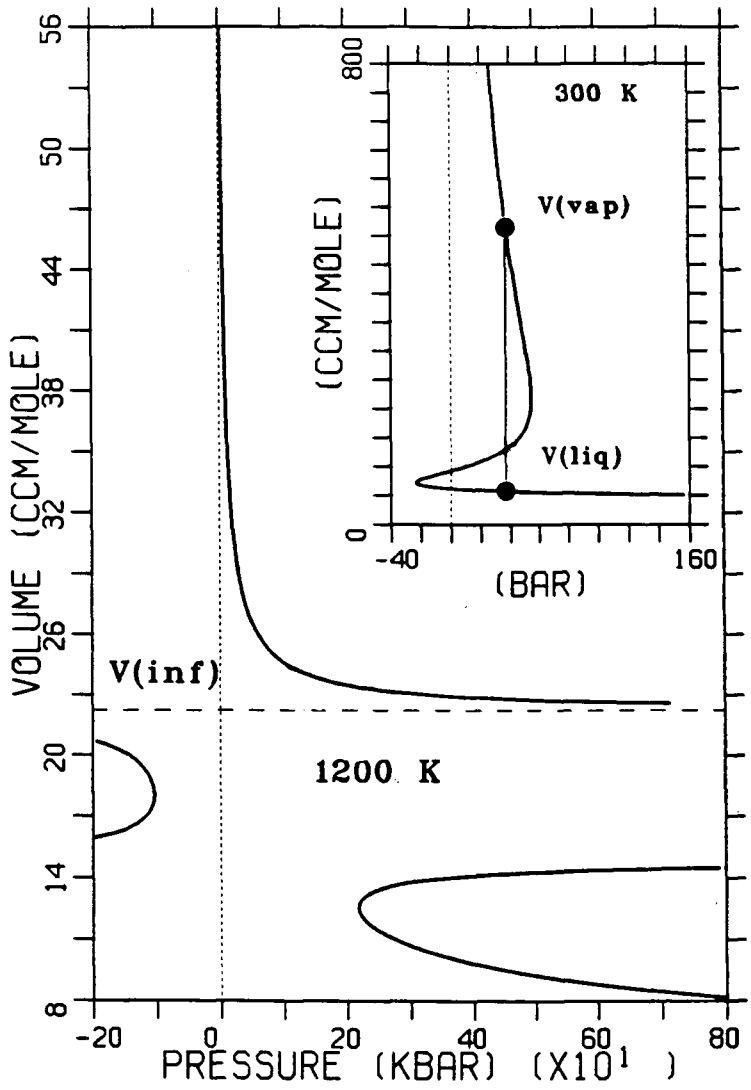

Figure 1.2: Mathematical behaviour of the Mäder & Berman equation of state. The volume at infinite pressure is labeled V(inf). Inset figure depicts the van der Waals like behaviour at subcritical pressure and temperature with volumes of the liquid, V(liq), and the vapour, V(vap), connected by a tie line.

up to 50 kbar as suggested by Holloway (1987). Corresponding states theory applied to the van der Waals equation predicts a b parameter of 43 cm^3/mole. De Santis *et al.* (1974) derived a value for b of 29.7 cm^3/mole for their modified Redlich-Kwong equation based on P-V-T data up to 1400 bar (the same value was adopted by Holloway, 1977). The smallest measured volume is 31 cm^3/mole at 7.1 kbar and 100 °C (Tsiklis *et al.*, 1971) and shock wave data (Zubarev & Telegen, 1962) on solid CO_2 indicate a volume of 18 cm^3/mole (with large uncertainties) at 180 kbar and 900 °C (as revised by Ross & Ree, 1980). It seems obvious that an equation successful at high pressures requires a compressible 'incompressible volume' which may be achieved mathematically by making b dependent on volume (see also Kerrick & Jacobs, 1981; Bottinga & Richet, 1981; Touret & Bottinga, 1979). An inverse power of the volume dependency of the b-term was determined empirically subject to the restriction of obtaining an integrable equation. A small temperature dependence of b also proved to be advantageous, resulting in the final equation:

$$P = \frac{RT}{V - (B_1 + B_2T - \frac{B_3}{V^3+C})} - \frac{A_1}{TV^2} + \frac{A_2}{V^4} \tag{1.5}$$

with $C = B_3/(B_1 + B_2T)$ and 5 independently adjustable parameters B_1, B_2, B_3, A_1, A_2. Note that the A_1/TV^2 term yields a better fit to the data than the Redlich-Kwong term $a/\sqrt{T}V(V + b)$. The function converges to the ideal gas law at very low pressures and has a smallest volume at infinite pressure dependent on temperature and parameter values (figure 1.2). The C–term ensures continuity of the equation to infinite pressure and renders the fourth-order polynomial in V of the denominator integrable (c.f. appendix A). The volume at specified pressure and temperature is determined iteratively and the integration $\int V\,dP$ may be performed analytically (cf. appendix A). At subcritical pressures and temperatures equation (1.5) behaves like the van der Waals equation (figure 1.2, inset). The equation is continuous between 0 bar and infinite pressure, and at

Author, Year	F	T [°C]	P [kbar]	#	Average % deviation			
					M&B	PVT	K&J	B&R
Shmonov & Shmulovich, 74	y	400–700	1.0–8.0	56	2.07	1.62	0.89	1.11
Tsiklis *et al.*, 1971	y	100–400	2.0–7.0	44	0.95	0.80	0.68	1.42
Juza *et al.*, 1965	y	150–475	0.7–4.0	40	1.17	0.69	0.95	0.86
Michels *et al.*, 1935	y	125–150	0.07–3.1	46	2.14	1.33	–	1.14
Kennedy, 1954	y	200–1000	0.03–1.4	72	0.79	0.55	1.17	0.47
Amagat, 1891	y	137–258	0.05–1.0	60	2.20	1.77	–	0.87
Vukalovich *et al.*, 1962	y	200–750	0.01–0.6	104	0.68	0.61	0.39	0.44
Vukalovich *et al.*, 1963a	n	125–150	0.02–0.6	43	1.54	1.24	–	0.83
Vukalovich *et al.*, 1963b	n	650–800	0.02–0.2	22	0.10	0.08	0.24	0.23
Michels & Michels, 1935	n	100–150	0.03–0.07	35	0.58	0.66	1.33	0.24

Table 1.1: Experimentally measured P-V-T properties of CO_2 used to constrain or test the equation of state. Average percent deviations of calculated volumes from measured volumes are quoted for several equations of state: M&B: Mäder & Berman equation (1.5) of this study; PVT: equation (1.5) with parameters based on P-V-T data only (see text); K&J: Kerrick & Jacobs (1981); B&R: Bottinga & Richet (1981). Column 'F' indicates data sets that were used to constrain equation (1.5) (y: yes) and data that were used for comparison only (n: no). Column '#' indicates the number of data points.

temperatures above 0 K for volumes larger than the discontinuity at V(inf) in figure 1.2.

1.4 P–V–T Data

Experimentally measured volumes were used to minimize the difference between computed and measured volumes during optimization procedures. Some data served to test the equation, particularly near the critical region. Data sets range from Amagat's (1891) classical work to Shmonov & Shmulovich's (1974) high pressure measurements (table 1.1). The more important data sets at higher pressures include Shmonov & Shmulovich (1974), Tsiklis *et al.* (1971), Juza *et al.* (1965), Michels *et al.* (1935) and Kennedy (1954).

The accuracy of the P-V-T data is almost impossible to establish. Precision at pressures below 1 kbar is generally better than 0.2 % and about 0.5 % at higher pressures

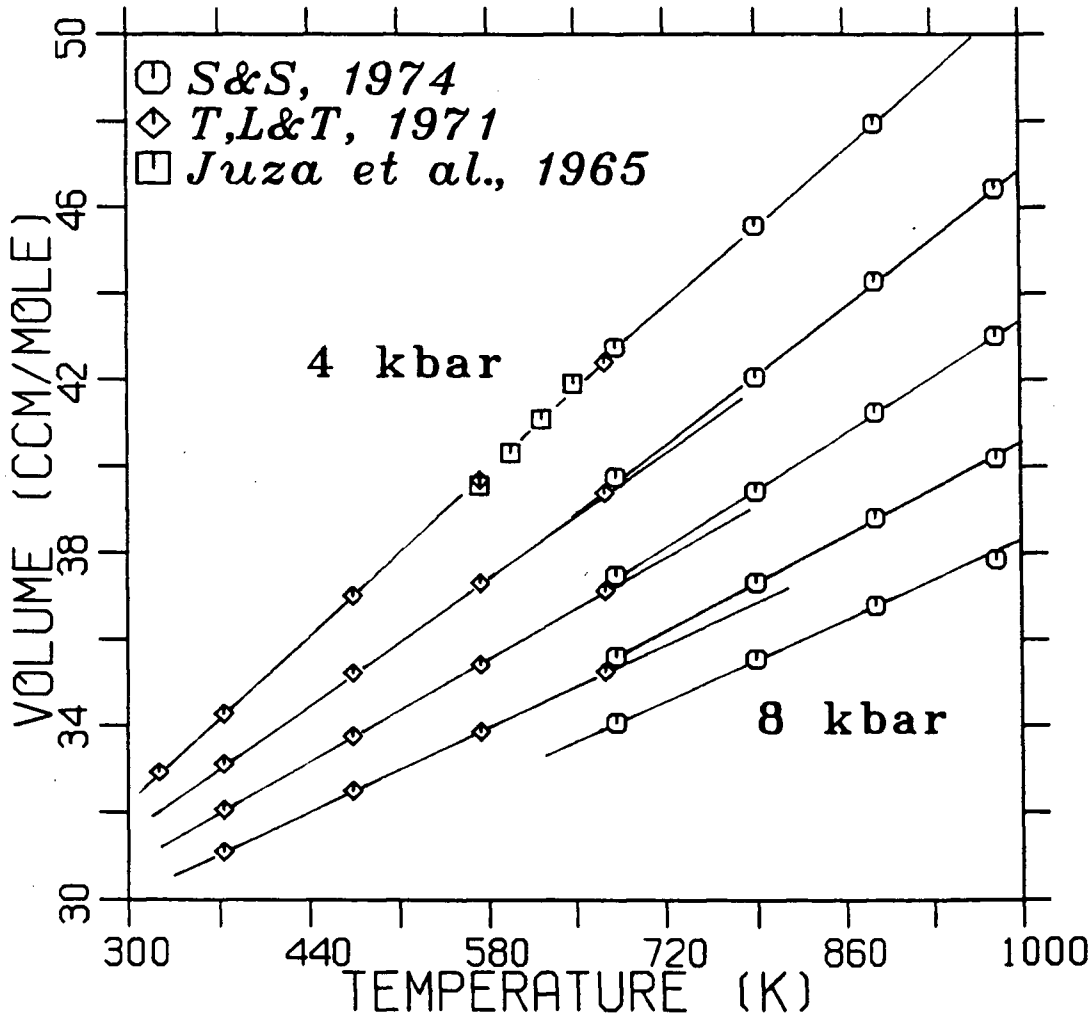

Figure 1.3: Isobaric volume–temperature diagram of high pressure P-V-T measurments (S&S: Shmonov & Shmulovich; T,L&T: Tsiklis *et al.*). Trends within individual data sets are delineated for clarity. See text for discussion.

depending on the type of equipment used. A complete review of equipment and quality of data sets up to 1972 is provided by Angus *et al.* (1973). At lower pressures and high temperatures possible problems arise from the presence of species other than CO_2, such as CO, O_2, or from the precipitation of graphite and from oxidation of the pressure vessel walls. Graphite coatings were reported by Vukalovich *et al.* (1963b) at temperatures above 800 °C. High pressure equipment is prone to uncertainties due to sealing problems, calibration, thermal gradients, pressure and temperature measurment, and deformation under pressure. The nonexistent or small areas of overlap between individual high pressure data sets make the detection of inconsistencies difficult. If, however, one extrapolates measurements from one data set into an adjacent one by some conservative method such as isobaric sections, inconsistencies of the order of 2 % or more are common (figure 1.3). One of the most disturbing discrepancies is found between the 1 kbar data of Shmonov & Shmulovich (1974) and those of Kennedy (1954) (figure 1.4). This allows for the possibility that parts of entire data sets are systematically in error by more than 2 %. Some more details are discussed in appendix D.

In summary, we estimate that the accuracy of high pressure P-V-T data is no better than 2 % and possibly much worse in some cases.

1.5 Phase Equilibrium Data

About 120 phase equilibrium experiments from 25 data sets of 16 laboratory studies (table 1.2) were used to put bounds on $\int V_{CO_2}\, dP$ according to equation (1.2). All phase equilibria used include magnesite or calcite as CO_2–bearing phases and only stoichiometric phases. High pressure data sets (> 25 kbar) involve magnesite only. Studies including dolomite were avoided because of insufficient thermodynamic data on its ordering state. Similarly, phase equilibria including geikielite, meionite, spurrite and tilleyite were not

Author	Equilibrium	P [kbar]	T [°C]	M	F	MB
S&A, 1923	Cc $\rightleftharpoons$ Lm+CO_2	0.00–0.03	890–1210	GA,DT	n	y
H&T, 1955	Mst $\rightleftharpoons$ Pe+CO_2	0.01–2.7	650–900	CS	y	y
	Cc $\rightleftharpoons$ Lm+CO_2	0.01–0.02	980–1070	CS	n	n
H&T, 1956	Cc+βQz $\rightleftharpoons$ Wo+CO_2	0.3–3.1	590–800	GA	n	y
G&H, 1961	Cc $\rightleftharpoons$ Lm+CO_2	0.01–0.08	840–1200	GA	n	n
	Mst $\rightleftharpoons$ Pe+CO_2	1.0–5.0	810–1010	GA	n	n
	Mst $\rightleftharpoons$ Pe+CO_2	1.0–10	660–1090	GA	n	n
B, 1962	Cc $\rightleftharpoons$ Lm+CO_2	0.00–0.03	900–1210	GA	n	y
W, 1963a	Cc+Fo+Di $\rightleftharpoons$ Mo+CO_2	0.07–0.54	710–890	CS	y	y
	Ak+Fo+Cc $\rightleftharpoons$ Mo+CO_2	0.5–0.7	900–930	CS	n	(y)
	Cc+Di $\rightleftharpoons$ Ak+CO_2	0.08–0.7	720–930	CS	y	y
W, 1963b	Cc+Fo $\rightleftharpoons$ Mo+Pe+CO_2	0.08–0.7	710–920	CS	n	n
J&M, 1968	Mst $\rightleftharpoons$ Pe+CO_2	0.5–1.0	700–760	CS	y	y
J, 1969	En+Mst $\rightleftharpoons$ Fo+CO_2	2.0	560	CS	y	y
S, 1974	Cc+An $\rightleftharpoons$ Wo+Ge+CO_2	0.5–0.7	840–890	PC	n	(y)
	Cc+An+Co $\rightleftharpoons$ Ge+CO_2	0.5–0.7	790–860	PC	y	y
I&W, 1975	Mst $\rightleftharpoons$ Pe+CO_2	20–36	1350–1600	PC	y	y
N&S, 1975	En+Mst $\rightleftharpoons$ Fo+CO_2	19–41	1000–1500	PC	y	y
H, 1978	Cc+βQz $\rightleftharpoons$ Wo+CO_2	10–19	1000–1330	PC	n	y
	Mst+Cs $\rightleftharpoons$ En+Fo+CO_2	37–42	1130–1200	PC	y	y
	En+Mst $\rightleftharpoons$ Fo+CO_2	24–25	1125	PC	y	y
	Mst+Ru $\rightleftharpoons$ Gk+CO_2	13–37	950–1250	PC	n	i
E, 1979	En+Mst $\rightleftharpoons$ Fo+CO_2	25–29	1110–1250	PC	y	y
P, 1988	Mst $\rightleftharpoons$ Pe+CO_2	0.4–1.2	700–760	GA,PA	y	y
M, 1990	Mst $\rightleftharpoons$ Pe+CO_2	12–21	1170–1435	PC	y	y

Table 1.2: List of phase equilibrium studies including pure CO_2 and stoichiometric phases. Column 'M': experimental method, CS: cold-seal, GA: gas apparatus (internally heated), PC: piston-cylinder, DT: differential thermal analysis, PA: pressure analysis. Column 'F' indicates data sets used for fitting (y: yes, n: no). Column 'MB' indicates consistency with Mäder & Berman equation of state of this study (y: yes, n: no, i: insufficient thermodynamic data on geikielite). See text for discussion of inconsistent data sets. Abbreviations of minerals: Cc: calcite, Lm: lime, Mst: magnesite, Pe: periclase, βQz: β-quartz, Fo: forsterite, Di: diopside, Mo: monticellite, An: anorthite, Co: corundum, Wo: wollastonite, Ge: gehlenite, Cs: coesite, En: ortho enstatite, Ru: rutile, Gk: geikielite. Abbreviations of authors: S&A: Smith & Adams, H&T: Harker & Tuttle, G&H: Goldsmith & Heard, B: Baker, W: Walter, J&M: Johannes & Metz, J: Johannes, S: Shmulovich, I&W: Irving & Wyllie, N&S: Newton & Sharp, H: Haselton *et al.*, E: Eggler *et al.*, P: Philipp, M: Mäder, this study.

considered. A thermodynamic analysis of the system CaO–SiO_2–CO_2 at high temperatures is provided by Treimann & Essene (1983) including larnite, rankinite, spurrite and tilleyite. Reactions including calcite were only used below the calcite-I – calcite-IV transition (ca. 790 °C, Mirwald 1976) because of poorly constrained properties of calcite-IV and calcite-V (see section below). The equilibrium En + Mst $\rightleftharpoons$ Fo + CO_2, constrained between 19 and 41 kbar by three studies (Newton & Sharp, 1975; Haselton *et al.*, 1978; Eggler *et al.*, 1979), forms one of the cornerstones of the present work (cf. figure 1.6). Equally important are tight constraints on the equilibrium magnesite $\rightleftharpoons$ periclase + CO_2 at low pressures (Philip, 1988) and at high pressures (new experiments, this study).

Experimental uncertainties were accounted for by displacing positions of the half-brackets away from the equilibrium based on best estimates of uncertainties in pressure and temperature. These uncertainties are indicated by tails leading to the uncorrected pressure–temperature coordinates from the symbols plotted in figures 1.1, 1.6 and 1.7. Table 1.3 shows an example of how one particular data set (Newton & Sharp, 1975) is treated to impose constraints on the fugacity of CO_2 between 19 and 41 kbar and 1373–1773 K. Many of the experimental studies used as constraints in this paper do not properly demonstrate reversibility of the phase equilibria studied. This is accounted for by increasing the range of uncertainty on that side of the equilibrium boundary approximated by stability or synthesis runs rather than reversals. This is in most cases the reactant–stable (low temperature) side. The overall consistency of the entire data set seems to indicate that reaction kinetics worked in favor of the 'abridged' approach to 'bracketing' phase equilibria in this case. Mathematical programming analysis forces one to scrutinize every experimental data point extremely carefully. Inconsistencies between data sets appear unequivocally, directing attention to problematic data. A result of this enforced scrutiny emphasizes the unfortunate fact that many experimentalists present their data inadequately, lacking tabulated run conditions, with insufficent data

to estimate uncertainties (i.e. pressure calibration in piston–cylinder work).

1.6 New Experiments on Magnesite ⇌ Periclase + CO_2

Existing experiments (Irving & Wyllie, 1975) on the equilibrium magnesite ⇌ periclase + CO_2 do not put stringent constraints on the equilibrium position at high pressure (figure 1.6). The equilibrium was therefore reversed at 12.1 kbar between 1173 and 1183 °C, and at 21.5 kbar between 1375 and 1435 °C in a piston–cylinder apparatus using 3/4-inch talc–pyrex assemblies. Friction corrections were calibrated against the melting curve of gold and silver (Mirwald *at al.*, 1975) and amounted to 2.9 kbar at 15 kbar and 3.5 kbar at 25 kbar nominal pressure. Thermal gradients were measured and the effect of pressure on the electromotive force of the Pt–Pt10%Rh thermocouples (Getting & Kennedy, 1970) was accounted for. Uncertainties are estimated at ±1.0 kbar and ±10 K. Details are reported in appendix C.

1.7 Magnesite Properties

The thermophysical properties of magnesite are crucial to this study and require close examination. At pressures below 10 kbar and temperatures below 800 °C magnesite properties are well constrained and any consistent set analysis (e.g. Berman, 1988) is not hampered by uncertainties in CO_2 properties (all existing equations of state do not deviate noticeably at pressures below 10 kbar). It is therefore possible to derive standard state thermodynamic properties of magnesite prior to the optimization of CO_2 properties at higher pressures. Chernosky & Berman (1989) revised the enthalpy of formation for magnesite (−1114.505 kJ/mole) based on experimental constraints on phase equilibria in systems with a H_2O–CO_2 fluid phase. Trommsdorff & Connolly (1990) propose an increase of the Gibbs free energy of formation for magnesite (an enthalpy

St.	P Exp. [kbar]	T Exp. [K]	P Adj. [kbar]	T Adj. [K]	$RT \ln f_{CO_2}$ Obs. [kJ]	M&B [kJ]	B&R [kJ]	K&J [kJ]	S&F [kJ]	Hol [kJ]
Re	19.0	1273	20.5	1248	> 154.6	158.9	161.7	163.2	156.6	162.5
Pr	19.0	1298	17.5	1313	< 158.2	154.7	157.8	**159.0**	153.3	157.4
Re	32.0	1523	33.5	1498	> 213.6	220.6	224.6	227.6	**213.0**	228.3
Pr	32.0	1553	30.5	1568	< 219.4	217.9	**222.4**	**225.1**	211.2	**224.3**
Re	41.0	1723	42.5	1698	> 260.0	265.2	270.1	274.4	**253.0**	275.9
Pr	41.0	1773	39.5	1788	< 268.9	264.7	**270.4**	**274.3**	253.2	**274.0**

Table 1.3: Constraints on CO_2 fugacities imposed by experimental brackets on the reaction Mst + En $\rightleftharpoons$ Fo + CO_2 (Newton & Sharp, 1975). Column 'St.' indicates whether reactants (Re) or products (Pr) are stable. Columns 'Adj.' contain pressures and temperatures adjusted for experimental uncertainties. Column 'Obs.' (observed) was computed with equation (1.2) and the data base of Berman (1988) with revised magnesite properties (Berman & Brown, 1985, Chernosky & Berman, 1989, and this study). The reminder of the columns were computed with various equations of state: M&B: Mäder & Berman equation (1.5) of this study; B&R: Bottinga & Richet (1981); K&J: Kerrick & Jacobs (1981); S&F: Saxena & Fei (1987a); Hol: Holloway (1977). Numbers printed in bold face are inconsistent with experimental brackets (column 'Obs.').

of about −1111 kJ/mole) based on field evidence on phase diagram topologies (CaO–MgO–SiO_2–CO_2–H_2O) and new phase equilibrium experiments by Philipp (1988) on the equilibrium magnesite $\rightleftharpoons$ periclase + CO_2.

A value of −1112.505 kJ/mole for the enthalpy of formation from the elements for magnesite was derived by linear programming analysis (Berman *et al.*, 1986, Berman, 1988). This value is consistent with Philipp's (1988) accurate pressure analysis experiments, as well as with the brackets on the same equilibrium determined by Harker & Tuttle (1955) and Johannes & Metz (1968) using conventional cold-seal techniques. This value used in conjunction with the data base of Berman (1988) produces the essential features of the phase diagram topologies suggested from natural mineral assemblages as outlined by Trommsdorff & Connolly (1990). The destabilization of magnesite was minimized in order not to deviate more than necessary from experimental constraints in systems including magnesite and a H_2O–CO_2 fluid mixture (e.g. magnesite + talc $\rightleftharpoons$

forsterite + H_2O + CO_2, Greenwood, 1967b). Any such discrepancy has to be counter balanced by more non–ideal mixing of H_2O–CO_2 (larger excess volume on mixing) compared to the mixing model of Kerrick & Jacobs (1981) if all other thermodynamic parameters are well constrained.

The heat capacity coefficients for magnesite of Berman & Brown (1985) were adopted, combined with the thermal expansion function of Berman (1988) and the compressibility function as revised by Chernosky & Berman (1989). The uncertainty on extrapolating heat capacity and thermal expansion (cf. section 'Method') is the largest single contribution to the uncertainty of the CO_2 properties derived in this study.

1.8 Results

As a first step the ability of equation (1.5) to fit *P-V-T* data in the absence of additional constraints from phase equilibrum experiments (figure 1.4) is demonstrated. The following equation of state parameters are derived: $B_1 = 29.5713$, $B_2 = 3.16418 \cdot 10^{-4}$, $B_3 = 10.2554 \cdot 10^4$, $A_1 = 1.10002 \cdot 10^9$, $A_2 = 2.54456 \cdot 10^9$, in units of cm^3/mole, K and bar. The results are difficult to compare to other equations of state because each was calibrated with different weights given to various sets of data. Figure 1.4 shows only the high pressure subset of all constraining *P-V-T* measurments, with the overall quality of fit of the three equations being comparable (c.f. also table 1.1). The equations share one particular feature: volumes extrapolated towards high pressures are larger than those inferred from the high pressure *P-V-T* data of Shmonov & Shmulovich (1974).

Secondly, it is important to know which phase equilibrium constraints influence the equation of state parameters. Phase equilibrium constraints at pressures below 8 kbar are fully compatible with *P-V-T* data and the equation of state (see also section on calcite polymorphs). The high pressure phase equilibrium constraints (table 1.2), however, are

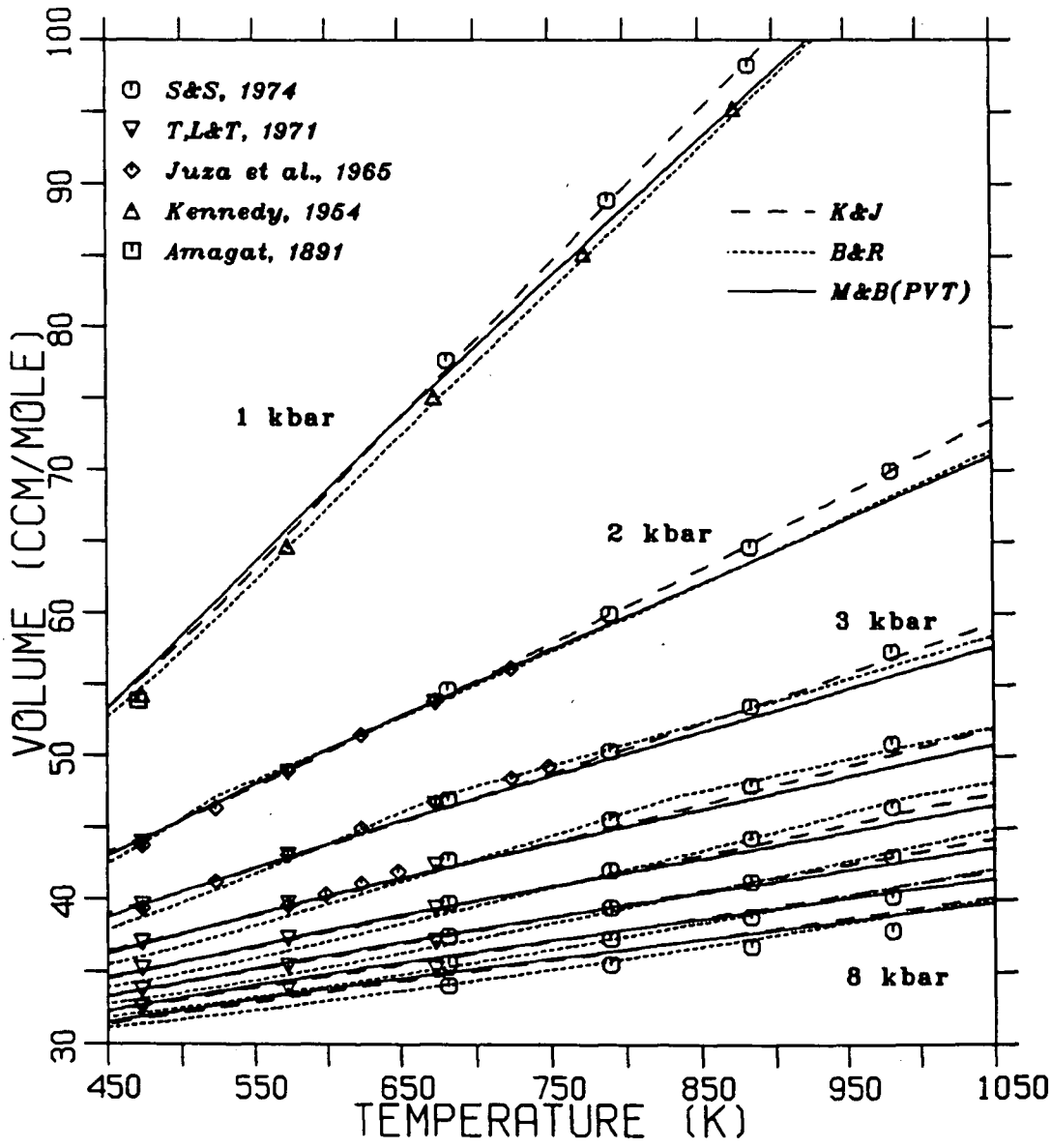

Figure 1.4: Isobaric volume–temperature diagram showing comparison of different equations of state and experimentally measured volumes. S&S: Shmonov & Shmulovich; T,L&T: Tsiklis *et al.*; K&J: Kerrick & Jacobs (1981) equation of state; B&R: Bottinga & Richet (1981) equation; M&B: Mäder & Berman equation (1.5) of this study constrained by *P-V-T* data only. The discontinuities in the slopes at 47.22 cm^3/mole of the B&R equation are a result of using separate fit parameters for different volume intervals.

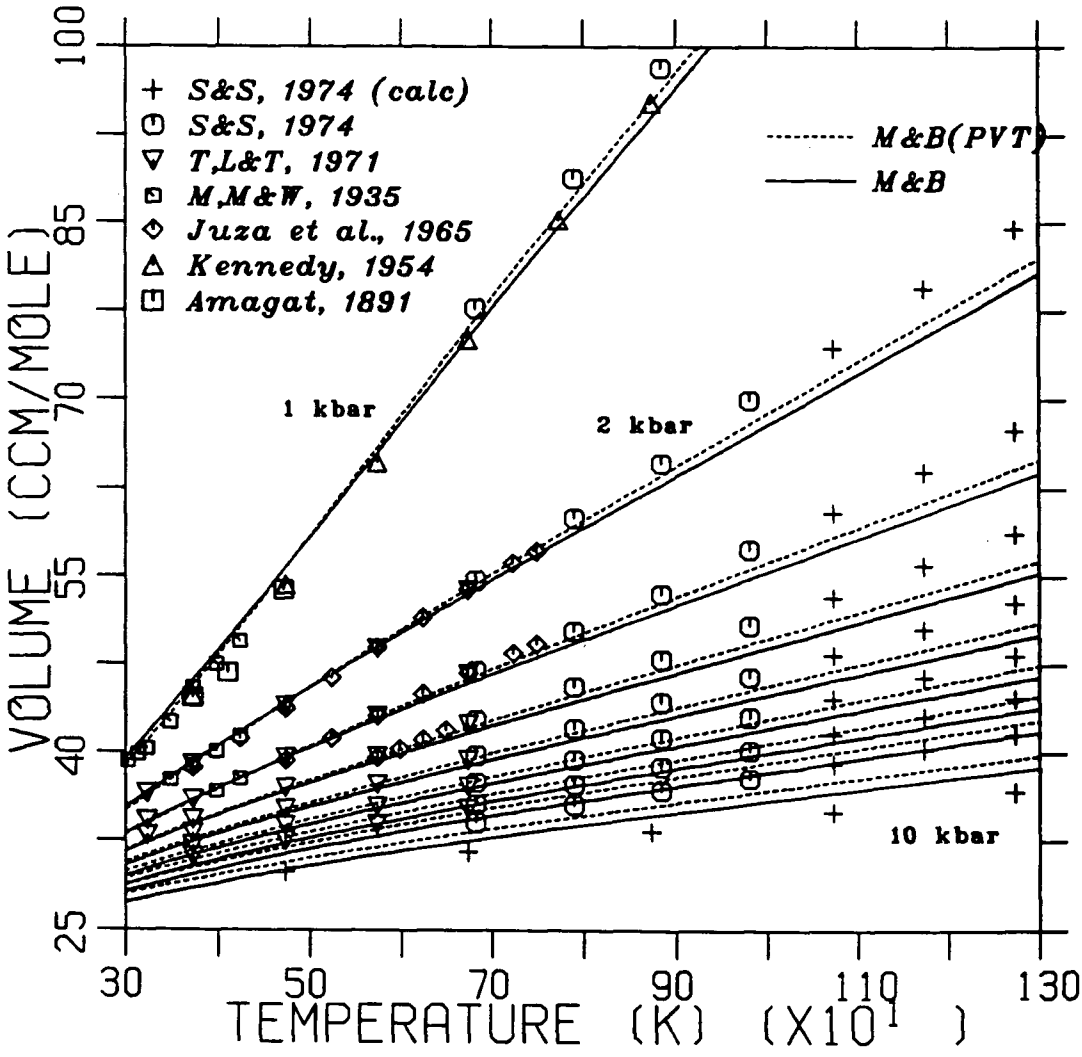

Figure 1.5: Isobaric volume–temperature diagram comparing the Mäder & Berman equation (1.5) constrained by P-V-T measurments only (M&B(P-V-T)) with equation (1.5) constrained additionally by phase equilibrium experiments (M&B). Measured volumes are overlain for comparison: S&S: Shmonov & Shmulovich; T,L&T: Tsiklis *et al.*; M,M&W: Michels *et al.*. S&S (calc) depict volumes extrapolated by Shmonov & Shmulovich (1974) based on their own experimental data. The 9 kbar data points and curves are not shown for clarity.

not compatible. The prominent feature observed is, as would be expected from figures 1.1 and 1.4, that the $RT \ln f_{CO_2}$ terms and thus the volumes are forced to become smaller (more stable CO_2) compared to predictions based on P-V-T data alone (figure 1.5). The final equation of state parameters are given below in units of cm^3/mole, K and bar:

$$B_1 = 28.0647 \qquad B_2 = 1.72871 \cdot 10^{-4} \quad B_3 = 8.36534 \cdot 10^4$$
$$A_1 = 1.09480 \cdot 10^9 \quad A_2 = 3.37475 \cdot 10^9$$

Table 1.3 lists the magnitudes of mismatch for several equations of state compared to experimental data by Newton & Sharp (1975).

Numerical convergence to a global minimum is difficult to demonstrate, but one can monitor the convergence behaviour from different initial estimates for the parameters and test solutions against those of different algorithms. The most important criterion, however, is whether the solution is acceptable in terms of fullfilling the desired task, i.e. reliable computation of geological phase equilibria and consistency with experimentally measured properties within their uncertainties. The first criterion is met by virtue of the method used: only parameters that are consistent with the constraining phase equilibria are acceptable to the algorithm. The second one, the agreement with measured volumes, can easily be tested.

Table 1.2 summarizes the consistency of the Mäder & Berman equation of state with phase equilibrium experiments involving pure CO_2 and stoichiometric phases. The two data sets inconsistent with the equation include some experiments by Goldsmith & Heard (1962) with P_{CO_2} likely less than P_{total} and one set by Walter (1936b) that is totally inconsistent (> 100 K) with any other data. Berman (1988) attributes the latter inconsistency to Walter's failure to recognize periclase in any run products. Figure 1.6 compares computed high pressure phase equilibria including magnesite with experimental data. Reactions including high temperature polymorphs of calcite, calcite-IV and calcite-V, are discussed in a separate section below. The equation of state thus performs reliably

up to at least 42 kbar.

Figure 1.5 and table 1.1 document the comparison of measured and calculated volumes. Agreement at low pressures and supercritical temperatures is excellent because the equation approximates the ideal gas law. The equation was not constrained by data below 373 K and therefore the shape of the subcritical area is only approximate and solely a result of its van der Waals like mathematical form. The critical point deduced from the equation is at 335.60 ($\pm$0.05) K, 89.22 ($\pm$0.05) bar and 115.5 ($\pm$0.5) cm^3/mole. Suggested true values (Angus *et al.*, 1973) based on experimental work, at 304.20 ($\pm$0.05) K, 73.858 ($\pm$0.05) bar and 94.07 ($\pm$0.1) cm^3/mole deviate substantially from our computed ones, but nevertheless the presence of a critical region in approximately the correct area improves the behaviour of the equation in the near–critical region (1–800 bar, 300–700 K) tremendously.

Rigorous comparisons of computed CO_2 properties with experimental phase equilibria have previously been hampered by insufficient thermophysical data of solid phases, magnesite in particular (Haselton *et al*, 1978; Bottinga & Richet, 1981). The properties of solids chosen by Saxena & Fei (1987a) lead to good agreement with CO_2 properties obtained with their equation of state, and render the Bottinga & Richet (1981) equation grossly inconsistent at 40 kbar pressure. This is in contrast with our computations (c.f. figure 1.1) which render CO_2 far too stable with the Saxena & Fei (1987a) equation. This discrepancy is at least in part due to Saxena & Fei's choice of heat capacity functions (Robie *et al.*, 1979) that are not suitable for extrapolation (i.e. beyond 750 K for magnesite).

The agreement with volumes measured at high pressures is reasonable and comparable with that of other equations of state (figures 1.4, 1.5). Equation (1.5) is able to fit measured volumes significantly better without the additional constraints from phase equilibria (figure 1.5), with the noteable exception of the volumes measured at the highest

pressures, which show excellent agreement. This may indicate too little flexibility of the equation, some systematic problems with high pressure experimental P-V-T equipment, or inaccurate mineral properties used to constrain the parameters. It seems that a more complex equation is not justified with the amount, extent and quality of P-V-T data available.

Additional volumetric constraints imposed by shock wave data could possibly improve the extrapolation properties of equation (1.5) towards pressures above 100 kbar. Shock wave measurments on solid CO_2 (or more likely a mixture of solid and liquid at initial conditions) (Zubarev & Telegin, 1962) are difficult to apply, and measurments on liquid CO_2 appear to be nonexistent. The equation of state based on shock data of similar fluids and corresponding states systematics of Saxena & Fei (1987a) is inconsistent with phase equilibrium experiments (cf. table 1.3, figure 1.1). A new approach taken by Helffrich & Wood (1989) appears to bridge shock wave data and phase equilibrium data more successfully.

In summary, the region where the Mäder & Berman equation is demonstrated to perform reliably spans 400–1773 K and 1 bar to 42 kbar. Extrapolation to higher pressures and temperatures is expected to yield useful results, possibly to 80 kbar and 2300 K.

1.9 Calcite(I-IV-V) – Aragonite

In the process of calibrating the equation of state inconsistencies became evident between constraints on CO_2 fugacities imposed by magnesite phase equilibria and those by calcite reactions. The well constrained high pressure brackets on En + Mst $\rightleftharpoons$ Fo + CO_2 and those on Mst $\rightleftharpoons$ Pe + CO_2 (figure 1.6) demand smaller CO_2 fugacities (more stable CO_2) than high pressure brackets on Cc + βQz $\rightleftharpoons$ Wo + CO_2 (figure 1.7). One likely explanation is the presence of the more stable calcite polymorphs calcite-IV and calcite-V

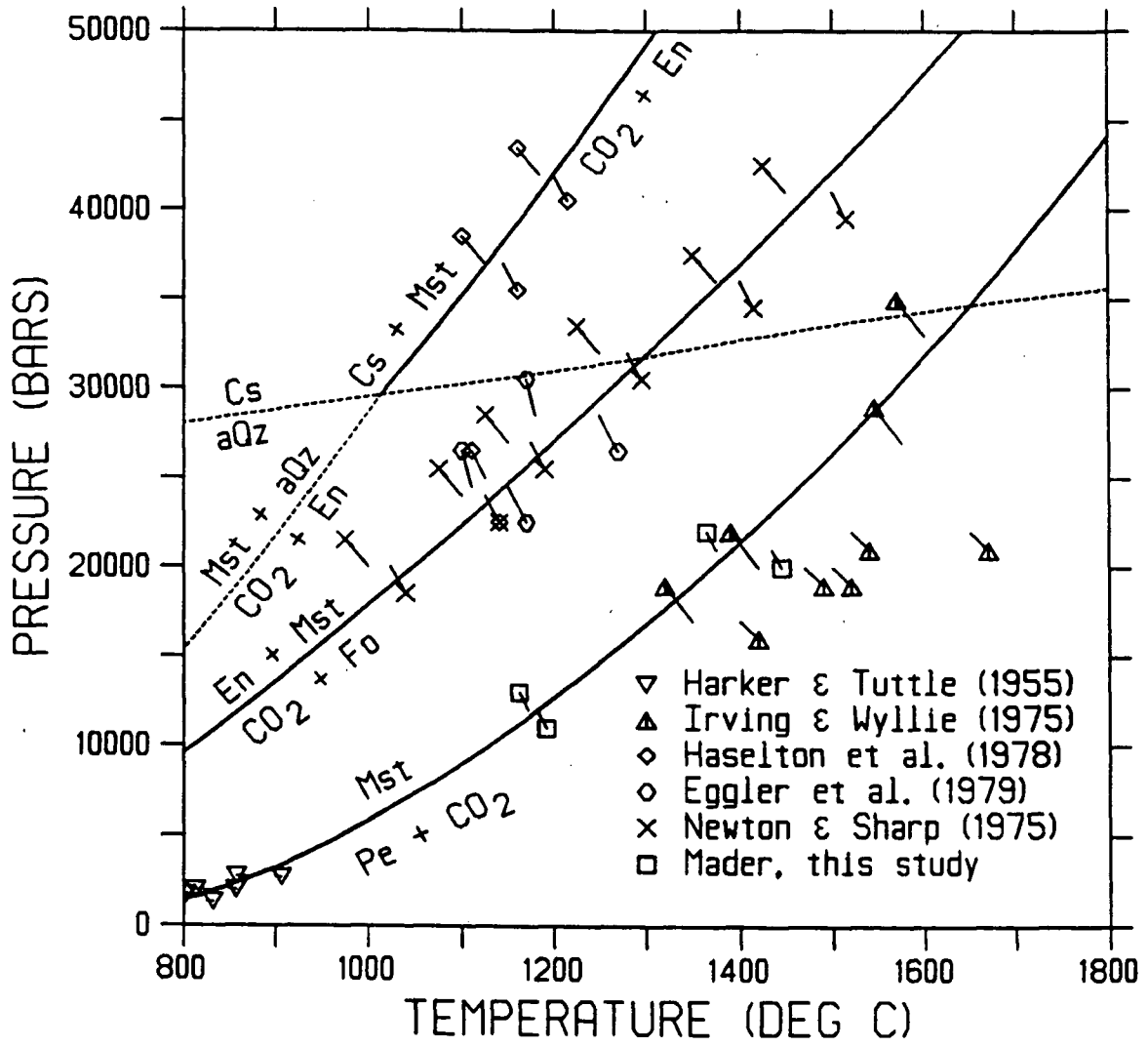

Figure 1.6: Pressure–temperature diagram with phase equilibria involving magnesite computed with the equation of state for CO_2 of this study compared to phase equilibrium experiments. A friction correction of −3 kbar was applied to the brackets by Irving & Wyllie (1975) based on calibrations by Huang & Wyllie (1975). Abbreviations of minerals: Cs: coesite, Mst: magnesite, En: ortho enstatite, Fo: forsterite, Pe: periclase, aQz: α-quartz. The diagram was produced with GEO–Calc (Brown *et al.*, 1988).

Std. state prop.	$\Delta_f H^{P_r,T_r}$ [kJ/mole]	S^{P_r,T_r} [J/mole/K]	V^{P_r,T_r} [J/bar]		Reference
Aragonite	-1207.597	87.490	3.415		(*),(*),(1)
Calcite(–I)	-1206.697	91.893	3.690		(*),(*),(B)
Calcite–IV	-1204.580	94.100	3.683		(*),(*),(*)
Calcite–V	-1199.768	97.895	3.689		(*),(*),(*)
C_P coefficients	k_0	k_1 ($\times 10^{-2}$)	k_2 ($\times 10^{-5}$)	k_3 ($\times 10^{-7}$)	
Calcite(–I)	178.19	-16.577	-4.827	16.660	(2,3,4,B)
Ar, Cc–IV, Cc–V	178.19	-16.577	-4.827	16.660	(a)
V coefficients	v_1 ($\times 10^{6}$)	v_2 ($\times 10^{12}$)	v_3 ($\times 10^{5}$)	v_4 ($\times 10^{10}$)	
Aragonite	-1.620	0.0080	3.670	227.4	(5,6,7),(5,8)
Calcite(–I)	-1.400	0.0060	0.897	227.4	(B),(a),(B),(B)
Cc–IV, Cc–V	-1.400	0.0060	0.897	227.4	(a)

Table 1.4: Thermodynamic properties of calcite polymorphs. Standard state thermodynamic properties of calcite polymorphs at 1 bar and 298.15 K, isobaric heat capacity function coefficients ($k_0 - k_3$) and volume function coefficients ($v_1 - v_4$). The heat capacity function of Berman & Brown (1985) is used: $C_P = k_0 + k_1 T^{-0.5} + k_2 T^{-2} + k_3 T^{-3}$, and the volume function of Berman (1988): $V^{P,T}/V^{P_r,T_r} = 1 + v_1(P - P_r) + v_2(P - P_r)^2 + v_3(T - T_r) + v_4(T - T_r)^2$. C_P is in units of [J/mole/K], V in [J/bar], T in [K] and P in [bar]. References: (B) Berman, 1988; (*) values derived in this study; (a) assumed, see text for discussion; (1) Robie *et al.*, 1979; (2) Stavely & Linford, 1969; (3) Jacobs *et al.*, 1981; (4) Kelly, 1960; (5) Salje & Viswanathan, 1976; (6) Madelung & Fuchs, 1921; (7) Singh & Kennedy, 1974; (8) Kozu & Kani, 1934.

(c.f. Mirwald, 1976, for nomenclature and summary) at high temperatures which would tend to shift the above equilibrium to higher temperatures.

As a first step, all experimental brackets including calcite at high temperatures were not considered as constraints on the properties of CO_2 in order to remove the possibly significant effects of calcite-IV and calcite-V. In order to test the above hypothesis, thermophysical properties of the calcite polymorphs were derived from constraints imposed by the aragonite–calcite-I–calcite-IV–calcite-V phase diagram. The equilibrium Cc(I/IV/V) + βQz $\rightleftharpoons$ Wo + CO_2 may then be recomputed with the obtained thermodynamic data to compare with experimental brackets.

Unfortunately few quantitative data are available on the unquenchable polymorphs

calcite-IV, calcite-V and the polymorphic transitions. The transition boundaries have been the subject of numerous studies (Boeke, 1912; Eitel, 1923; Clark, 1957; Crawford & Fyfe, 1964; Boettcher & Wyllie, 1968; Johannes & Puhan, 1971; Crawford & Hoersch, 1972; Cohen & Klement, 1973; Irving & Wyllie, 1975; Mirwald, 1976, 1979a, 1979b). The phase transitions between calcite–I–IV–V are most likely related to order–disorder within the anion sublattice (Lander, 1949; Salje & Viswanathan, 1976; Mirwald, 1979a, 1979b; Dove & Powell, 1989). There is, however, still some debate about the exact nature and the existence of discrete phase transitions in calcite (Markgraf & Reeder, 1985). In order to minimize the number of thermophysical parameters to be derived, all polymorphic transitions were treated as first order phase transitions with small volume discontinuities at the phase boundaries. This should lead to a reasonable approximation of the energetics of these phase transitions.

In view of the lack of data on thermal and volumetric properties the following assumptions were made. All polymorphs share the same heat capacity function. Experimental data by Kobayashi (1950b) that suggest a lower heat capacity for aragonite than calcite were disregarded due to its imprecision and inconsistency of his aragonite and calcite (Kobayashi, 1950a) data with other studies (Stavely & Linford, 1969; Jacobs *et al.*, 1981; Kelly, 1960). Calcite–IV and V are assumed to share the same expansivity and compressibility as calcite–I. X-ray data by Mirwald (1979a) suggest a larger thermal expansion for Cc–IV than for Cc–I, which is, however, not observed in Markgraf & Reeder's (1985) measurments. The extremely large thermal expansion of aragonite relative to calcite suggested by measurments up to 450 °C (Salje & Viswanathan, 1976; Kozu & Kani, 1934) was reduced by about 15 % during fitting in order to constrain the curvature of the Cc $\rightleftharpoons$ Ar equilibrium to the phase equilibrium data. The difference in compressibility between calcite and aragonite is derived from studies that include measurments on both minerals by the same technique (Salje & Viswanathan, 1976; Madelung & Fuchs, 1921).

All other thermodynamic properties were fitted to measurements as summarized in table 1.4. Calcite–I properties are nearly identical to those in Berman (1988).

The standard state properties ($\Delta_f H^{P_r,T_r}$, S^{P_r,T_r}, V^{P_r,T_r}) of Cc–IV and Cc–V were refined by a linear programming technique (Berman *et al.*, 1986, Berman, 1988) using phase equilibrium constraints (Cc-I $\rightleftharpoons$ Ar, Cc-IV $\rightleftharpoons$ Ar, Cc-V $\rightleftharpoons$ Ar, Cc-I $\rightleftharpoons$ Cc-IV, Cc-IV $\rightleftharpoons$ Cc-V; figure 1.7). The derived thermophysical properties are consistent with most phase equilibrium studies with the exception of the Ar $\rightleftharpoons$ Cc-I transition at low temperatures (< 200°C) and the Ar $\rightleftharpoons$ Cc-V transition. At 100 °C the computed Arag $\rightleftharpoons$ Cc-I boundary is located 0.5 kbar too low compared to experiments by Crawford & Fyfe (1964). Data of Mirwald (1979a) on the Ar $\rightleftharpoons$ Cc-V equilibrium are internally inconsistent and not compatible with the brackets obtained by Irving & Wyllie (1975) (figure 1.7). This boundary is therefore poorly constrained and allows some latitude in the properties of Cc-V.

Computed phase equilibria involving Cc–I, Cc–IV and Cc–V using the above refined properties (table 1.4) and the Mäder & Berman equation (1.5) for CO_2 (figure 1.7) are consistent with all phase equilibrium experiments (table 1.2) with the exception of small inconsistencies (<4 K) with one half bracket on the reaction Ak + Cc-IV + Fo $\rightleftharpoons$ Mtc + CO_2 (Walter, 1963a) and An + Cc-IV $\rightleftharpoons$ Wo + Ge + CO_2 (Shmulovich, 1974). Most importantly, however, the computed equilibria are compatible with the high pressure brackets on the reaction Cc-IV/V + βQz $\rightleftharpoons$ Wo + CO_2 (Haselton *et al.*, 1978) and the high temperature brackets on the equilibrium Cc-(IV/V) $\rightleftharpoons$ Lime + CO_2 (Smith & Adams, 1923; Baker, 1962). It appears that only the experimental data of Smith & Adams (1923) and Baker (1962) for the calcite decarbonation are reconcilable with the calorimetric data of lime and the above treatment, which are inconsistent with data by Harker & Tuttle (1955) and Goldsmith & Heard (1961). Smith's differential thermal analysis experiments are, however, not reversed in both directions and constrain only the

product–stable assemblage. The above treatment of Cc–IV and Cc–V does not put any constraints on the properties of CO_2, but allows one to estimate the effects of more stable calcite polymorphs. Additional data on the calcite polymorphs are required to permit a more accurate thermodynamic treatment that accounts explicitly for the observed order–disorder phenomena.

It is concluded that the high temperature calcite polymorphs Cc–IV and Cc–V need to be considered for computation of phase equilibria at high temperatures. The energetics of the polymorphic transitions result in an increase of the carbonate stability field that leads to good agreement with CO_2 properties calculated with the new Mäder & Berman equation of state.

1.10 Conclusions

The following points are emphasized: i) the mathematical programming technique allows significant improvements of the equation of state for CO_2, ii) phase equilibrium brackets put important constraints on the fugacity of CO_2 at pressures not accessible by conventional P-V-T measurments, and iii) some experimentally measured volumes of CO_2 at high pressures might have much larger uncertainties than previously estimated.

The data needed for further improvements include: i) more high quality phase equilibrium brackets at high pressures on reactions involving CO_2, ii) a set of carefully measured CO_2 volumes up to 12 kbar, iii) shock wave data on fluid CO_2, iv) measurments on the expansivity of magnesite to high temperatures under pressure, v) more quantitative data on the complex phase transitions undergone by calcite, and vi) progress in providing mathematically practical equations of state with a theoretical basis.

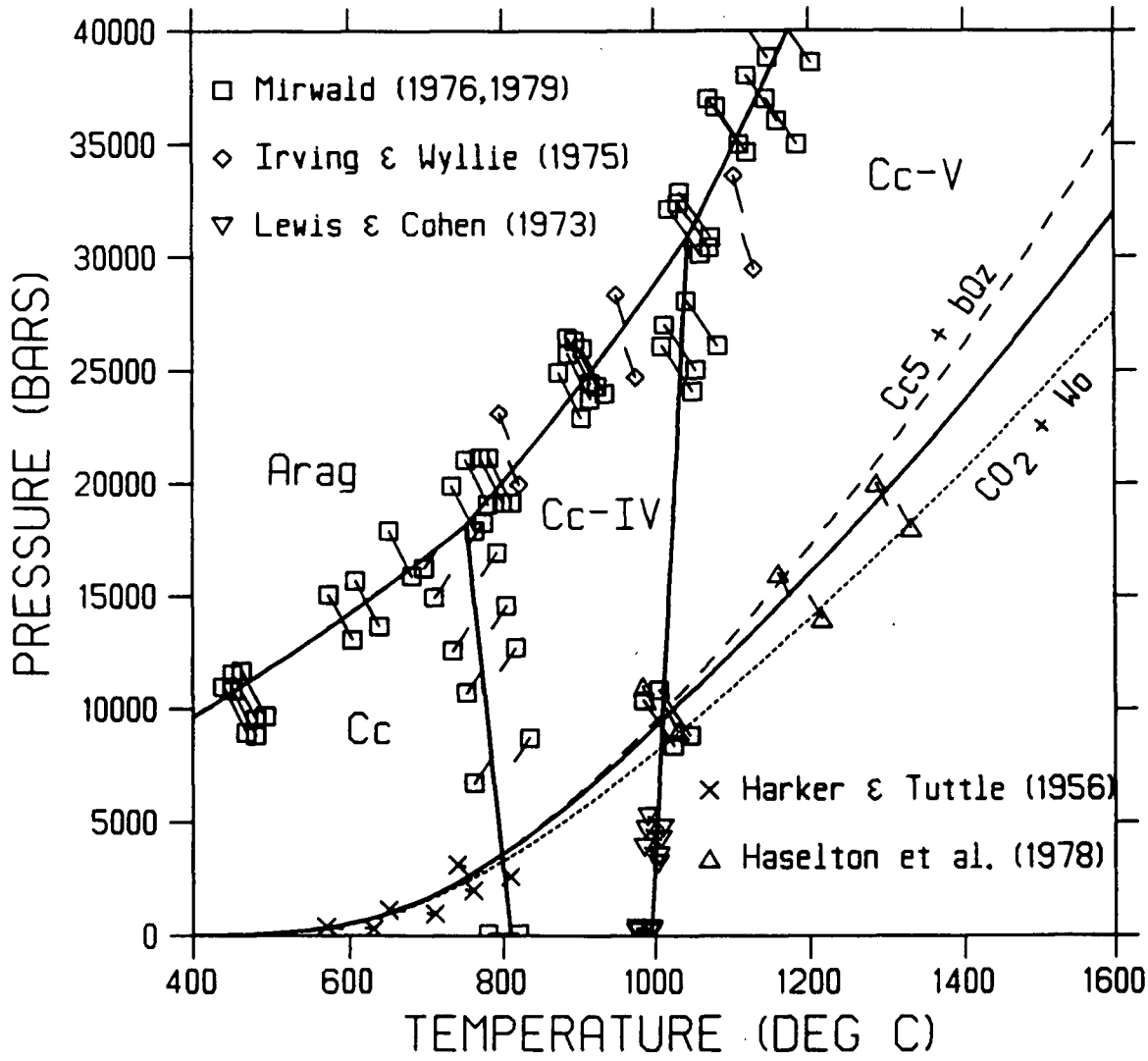

Figure 1.7: Pressure–temperature diagram with phase equilibria involving calcite polymorphs computed with thermodynamic properties of table 1.4 and Berman (1988) and the Mäder & Berman equation of state for CO_2 of this study. The dashed curve depicts the effect of omitting calcite–IV and calcite–V in order to compute the wollastonite reaction. The dotted curve was computed with the Kerrick & Jacobs (1981) equation of state not considering any of the high temperature calcite polymorphs. Abbreviations of minerals: Arag: aragonite, Cc: calcite, bQz: beta quartz, Wo: wollastonite. The diagram was produced with GE0–Calc (Brown *et al.*, 1988).

Bibliography

[1] Akella, J., 1979, Quartz $\rightleftharpoons$ coesite transition and the comparative friction measurements in piston–cylinder apparatus using talc–alsimag–glass (TAG) and NaCl high–pressure cells. *N. Jh. Miner. Monatshefte*, 217–224.

[2] Akella, J., & Kennedy, G.C., 1971, Studies on anorthite + $diopside_{50}$ $hedenbergite_{50}$ at high pressures and temperatures. *Am. J. Sci.*, **270**, 155–165.

[3] Amagat, E.M., 1880, Mémoire sur la compressibilité des gaz à des pressions élevées. *Annal. Chim. Phys.*, **19**, 345–385.

[4] Amagat, E.M., 1891, Nouveau réseau d'isothermes de l'acide carbonique. *Comptes Rendus Hebd. Séances Acad. Sci.*, **113**, 446–451.

[5] Angus, S., Armstrong, B., & de Reuck, K.M. (eds.), 1973, International Thermodynamic Tables of the Fluid State, Vol. 3: Carbon Dioxide. Pergamon Press.

[6] Baker, E.H., 1962, The calcium oxide–carbon dioxide system in the pressure range 1–300 atmospheres. *J. Chem. Soc.*, 464–470.

[7] Berman, R.G., 1988, Internally–consistent thermodynamic data for minerals in the system Na_2O–K_2O–CaO–MgO–FeO–Fe_2O_3–Al_2O_3–SiO_2–TiO_2–H_2O–CO_2. *J. Petrol.*, **29**, 445–522.

[8] Berman, R.G., & Brown, T.H., 1985, The heat capacity of minerals in the system K_2O–Na_2O–CaO–MgO–FeO–Fe_2O_3–Al_2O_3–SiO_2–TiO_2–H_2O–CO_2: representation, estimation, and high temperature extrapolation. *Contr. Miner. Petrol.*, **89**, 168–183.

[9] Berman, R.G., Engi, M., Greenwood, H.J., & Brown, T.H., 1986, Derivation of internally–consistent thermodynamic data by the technique of mathematical programming: a review with application to the system MgO–SiO_2–H_2O. *J. Petrol.*, **27**, 1331–1364.

[10] Birch, F., 1939, Thermoelectric measurement of high temperatures in pressure apparatus. *Rev. Sci. Instr.*, **10**, 137–140.

[11] Boeke, H.E., 1912, Die Schmelzerscheinungen und die umkehrbare Umwandlung des Calciumcarbonats. *N. Jh. Miner. Geol.*, **1**, 91–121.

[12] Boettcher, A.L. & Wyllie, P.J., 1968, The calcite–aragonite transition measured in the system CaO–CO_2–H_2O. *J. Geol.*, **76**, 324–330.

[13] Bohlen, S.R., 1984, Equilibria for precise pressure calibration and a frictionless furnace assembly for the piston–cylinder apparatus. *N. Jh. Miner. Monatshefte*, 404–412.

[14] Bottinga, Y., & Richet, P., 1981, High pressure and temperature equation of state and calculation of thermodynamic properties of gaseous carbon dioxide. *Am. J. Sci.*, **218**, 615–660.

[15] Boyd, F.R., & England, J.L., 1960, Apparatus for phase–equilibrium measurements at pressures up to 50 kilobars and temperatures up to 1750 °C. *J. Geophys. Res.*, **65**, 741–748.

[16] Brown, T.H., Berman, R.G., & Perkins, E.H., 1988, GE0–Calc: software package for calculation and display of pressure–temperature–composition phase diagrams using an IBM or compatible personal computer. *Comp. Geosci.*, **14**, 279–289.

[17] Chernosky, J.V., & Berman, R.G., 1989, Experimental reversal of the equilibrium: clinochlore + 2 magnesite = 3 forsterite + spinel + 2 CO_2+ 4 H_2O and revised thermodynamic properties for magnesite. *Am. J. Sci.*, **289**, 249–266.

[18] Clark, S.P.Jr., 1957, A note on calcite–aragonite equilibrium. *Am. Miner.*, **42**, 564–566.

[19] Clark, S.P.Jr., 1959, Effect of pressure on the melting points of eight alkali halides, *J. Chem. Phys.*, **31**, 1526–1531.

[20] Cohen, L.H., Klement, W., Jr., & Kennedy, G.C., 1966, Melting of copper, silver and gold at high pressures. *Phys. Rev.*, **145**, 519–525.

[21] Cohen, L.C., & Klement, W., 1973, Determination of high temperature transition in calcite to 5 kbar by differential thermal analysis in hydrostatic apparatus. *J. Geol.*, **81**, 724–726.

[22] Crawford, W.A., & Fyfe, W.S., 1964, Calcite–aragonite equilibrium at 100°C. *Science*, **144**, 1569–1570.

[23] Crawford, W.A., & Hoersch, A.L., 1972, Calcite–aragonite equilibrium from 50°Cto 150°C. *Am. Miner.*, **57**, 985–998.

[24] Dove, M.T., & Powell, B.M., 1989, Neutron diffraction study of the tricritical orientational order/disorder phase transition in calcite at 1260 K. *Phys. Chem. Miner.*, **16**, 503–507.

[25] Eggler, D.H., Kushiro, I., & Holloway, J.R., 1979, Free energy of decarbonation reactions at mantle pressures: I. Stability of the assemblage forsterite–enstatite–magnesite in the system MgO–SiO_2–CO_2–H_2O to 60 kbar. *Am. Miner.*, **64**, 288–293.

[26] Eitel, W., 1923, Über das binäre System $CaCO_3$–Ca_2SiO_4 und den Spurrit. *N. Jh. Miner. Geol. Pal. Beilageb.*, **XLVIII**, 63–74.

[27] Ferry, J.M., & Baumgartner, L., 1987, Thermodynamic models of molecular fluids at the elevated pressures and temperatures of crustal metamorphism. In: Carmichael, I.S.E. & Eugster, H.P. (eds.), Thermodynamic Modeling of Geological Materials: Minerals, Fluids and Melts. *Miner. Soc. Am., Rev. Mineral.*, **17**, 323–365.

[28] Getting, I.C., & Kennedy, G.C., 1970, Effect of pressure on the emf of chromel–alumel and platinum–platinum 10% rhodium thermocouples. *J. Appl. Phys.*, **41**, 4552–4562.

[29] Goldsmith, J.R., & Heard, H.C., 1961, Subsolidus phase relations in the system $CaCO_3$–$MgCO_3$. *J. Geol.*, **69**, 45–74.

[30] Gordon, T.M., 1973, Determination of internally consistent thermodynamic data from phase equilibrium experiments. *J. Geol.*, **81**, 199–208.

[31] Gordon, T.M., 1977, Derivation of internally consistent thermochemical data from phase equilibrium experiments using linear programming. In: Greenwood, H.J. (ed.), Short Course in Applications of Thermodynamics to Petrology and Ore–Deposits. *Miner. Assoc. Canada*, Short Course Handbook, **2**, 185–198.

[32] Greenwood, H.J., 1967a, The N–dimensional tie–line problem. *Geochim. Cosmochim. Acta*, **31**, 465–490.

[33] Greenwood, H.J., 1967b, Mineral equilibria in the system MgO–SiO_2–H_2O–CO_2. In: Abelson, P.H., (ed.), Researches in Geochemistry, v. 2. New York: John Wiley, 542–567.

[34] Hadidiakos, C.G., 1969, Solid–state temperature controller. *J. Geol.*, **77**, 365–367.

[35] Hariya, Y., & Kennedy, G.C., 1968, Equilibrium study of anorthite under high pressure and high temperature. *Am. J. Sci.*, **266**, 193–203.

[36] Harker, R.I., & Tuttle, O.F., 1955, Studies in the system CaO–MgO–CO_2. Part I: The thermal dissociation of calcite, dolomite, and magnesite. *Am. J. Sci.*, **253**, 209–224.

[37] Harker, R.I., & Tuttle, O.F., 1956, Experimental data on the P_{CO_2}–T curve for the reaction : calcite + quartz = wollastonite + carbon dioxide. *Am. J. Sci.*, **254**, 239–256.

[38] Haselton, H.T.Jr., Sharp, W.E., & Newton, R.C., 1978, CO_2 fugacitiy at high temperatures and pressures from experimental decarbonation reactions. *Geophys. Res. Lett.*, **5**, 753–756.

[39] Helffrich, G.R., & Wood, B.J., 1989, High pressure fluid P-V-T properties from fluid perturbation theory. *EOS, Trans., Am. Geophys. Union*, **70**, 487.

[40] Holland, T.J.B., & Powell, R., 1990, An enlarged and updated internally consistent thermodynamic dataset with uncertainties and correlations: the system K_2O–Na_2O–CaO–MgO–MnO–FeO–Fe_2O_3–Al_2O_3–TiO_2–SiO_2–C–H_2–O_2. *J. Metam. Geol.*, **8**, 89–124.

[41] Holloway, J.R. 1977, Fugacity and activity of molecular species in supercritical fluids. In: Fraser, D.G. (ed.), Thermodynamics in Geology. D. Reidel, Dodrecht, Holland, 161–181.

[42] Holloway, J.R. 1981a, Volatile melt interactions. In: Newton, R.C., Navrotsky, A., & Wood, B.J., (eds.), Advances in Physical Geochemistry, **1**, 266–286.

[43] Holloway, J.R. 1981b, Compositions and volumes of supercritical fluids in the earth's crust. In: Hollister, L.S., & Crawford, M.L., (eds.), Short Course in Fluid Inclusions: Applications to Petrology. *Miner. Assoc. Canada*, Short Course Handbook, **6**, 13–35.

[44] Holloway, J.R., 1987, Igneous fluids. In: Carmichael, I.S.E. & Eugster, H.P. (eds.), Thermodynamic Modeling of Geological Materials: Minerals, Fluids and Melts. *Miner. Soc. Am., Rev. Mineral.*, **17**, 211–233.

[45] Huang, W., & Wyllie, P.J., 1975, Melting reactions in the system $NaAlSi_3O_8$–$KAlSi_3O_8$–SiO_2 to 35 kilobars, dry and with excess water. *J. Geol.*, **83**, 737–748.

[46] Huang, W., & Wyllie, P.J., 1976, Melting relationships in the systems CaO–CO_2 and MgO–CO_2 to 33 kilobars. *Geochim. Cosmochim. Acta*, **40**, 129–132.

[47] Irving, A.J., & Wyllie, P.J., 1975, Subsolidus and melting relationships for calcite, magnesite, and the join $CaCO_3$–$MgCO_3$ to 36 kb. *Geochim. Cosmochim. Acta*, **39**, 35–53.

[48] Jacobs, G.K., Kerrick, D.M., & Krupka, K.M., 1981, The high temperature heat capacity of natural calcite ($CaCO_3$). *Phys. Chem. Miner.*, **7**, 55–59.

[49] Johannes, W., 1969, An experimental investigation of the system MgO–SiO_2–H_2O–CO_2. *Am. J. Sci.*, **267**, 1083–1104.

28.3C

[50] Johannes, W., 1978, Pressure comparing experiements with NaCl, AgCl, talc, and pyrophyllite assemblies in a piston cylinder apparatus. *N. Jh. Miner. Monatshefte*, 84–92.

[51] Johannes, W., & Metz, P., 1968, Experimentelle Bestimmung von Gleichgewichtsbeziehungen im System MgO–CO_2–H_2O. *N. Jh. Miner. Monatshefte*, **112**, 15–26.

[52] Johannes, W., & Puhan, D., 1971, The calcite–aragonite transition reinvestigated. *Contr. Miner. Petrol.*, **31**, 28–38.

[53] Johannes, W., Bell, P.M., Mao, H.K., Boettcher, A.L., Chipman, D.W., Hays, J.F., Newton, R.C., & Seifert, F., 1971, An interlaboratory comparison of piston–cylinder pressure calibration using the albite–breakdown reaction. *Contr. Miner. Petrol.*, **32**, 24–38.

[54] Jüza, J., Kmoníček, V., & Šifner, O., 1965, Measurement of the specific volume of carbon dioxide in the range of 700 to 4000 b and 50 to 475°C. *Physica*, **31**, 1735–1744.

[55] Kelly, K.K., 1960, Contributions to the data on theoretical metalurgy. XIII. High temperature heat–content, heat–capacity, and entropy data for the elements and inorganic compounds. *U.S. Bur. Mines Bull.*, **584**, 232 p.

[56] Kennedy, G.C., 1950, Pressure–volume–temperature relations in water at elevated temperatures and pressures. *Am. J. Sci.*, **248**, 540–564.

[57] Kennedy, G.C., 1954, Pressure–volume–temperature relations in CO_2 at elevated temperatures and pressures. *Am. J. Sci.*, **252**, 225–241.

[58] Kerrick, D.M., & Jacobs, C.K., 1981, A modified Redlich–Kwong equation for H_2O, CO_2, and H_2O–CO_2 mixtures at elevated pressures and temperatures. *Am. J. Sci.*, **281**, 735–767.

[59] Kobayashi, K., 1950a, The heat capacity of inorganic substances at high temperatures, part III. The heat capacity of synthetic calcite (calcium carbonate). *Sci. Rep. Univ. Tokyo*, **34**, 103–110.

[60] Kobayashi, K., 1950b, The heat capacity of inorganic substances at high temperatures, part IV. The heat capacity of synthetic aragonite (calcium carbonate). *Sci. Rep. Univ. Tokyo*, **34**, 111–118.

[61] Kozu, S, & Kani, K., 1934, Thermal expansion of aragonite and its atomic displacements by transformation into calcite between 450°C and 490°C in air, I. *Proc. Imp. Acad. Japan*, **10**, 222–225.

[62] Lander, J.J., 1949, Polymorphism and anion rotational disorder in the alkaline earth carbonates. *J. Chem. Phys.*, **17**, 892–901.

[63] Lasden, L.S., & Waren, A.D., 1982, GRG2 User's Guide, Dept. of Computer and Information Science, College of Business Administration, Cleveland State University, Cleveland, Ohio 44115.

[64] Madelung, E., & Fuchs, R., 1921, Kompressibiltätsmessungen an festen Körpern. *Annal. Physik*, **65**, 289–309.

[65] Mäder, U.K., & Berman, R.G., 1991, An equation of state for carbon dioxide to high pressure and temperature. Submitted to *J. Petrol.*, July, 1990.

[66] Mäder, U.K., Berman, R.G., & Greenwood, H.J., 1988, An equation of state for carbon dioxide consistent with phase equilibrium data: 400–2000 K, 1 bar – 50 kbar. *Geol. Soc. Am. Abstr. Prog.*, **20**, A190.

[67] Mäder, U.K., Berman, R.G., & Greenwood, H.J., 1990, An equation of state for H_2O–CO_2 mixtures consistent with P-V-T and phase equilibrium data. *Geol. Ass. Can. Min. Ass. Can., Prog. Abstr.*, **15**, A81.

[68] Markgraf, S.A., & Reeder, R.J., 1985, High–temperature structure refinements of calcite and magnesite. *Am. Miner.*, **70**, 590–600.

[69] Mel'nik, Y.P., 1972, Thermodynamic parameters of compressed gases and metamorphic reactions involving water and carbon dioxide. *Geochem. Int.*, **9**, 419–426. Translated from Geokhimiya, **6**, 654–662, 1972.

[70] Michels, A., & Michels, C., 1935, Isotherms of CO_2 between 0° and 150° and pressures from 16 to 250 atmospheres. *Proc. R. Soc. Lond. Ser. A*, **153**, 201–214.

[71] Michels, A., & Michels, C., & Wouters, H.H., 1935, Isotherms of CO_2 between 70 and 3000 atmospheres. *Proc. R. Soc. Lond. Ser. A*, **153**, 214–224.

[72] Mirwald, P.W., 1976, A differential thermal analysis study of the high–temperature polymorphism of calcite at high pressure. *Contr. Miner. Petrol.*, **59**, 33–40.

[73] Mirwald, P.W., 1979a, Determination of a high–temperature transition of calcite at 800°C and one bar CO_2 pressure. *N. Jh. Miner. Monatshefte*, 309–315.

[74] Mirwald, P.W., 1979b, The electrical conductivity of calcite between 300 and 1200°C at a CO_2 pressure of 40 bars. *Phys. Chem. Miner.*, **4**, 291–297.

[75] Mirwald, P.W., Getting, I.C., & Kennedy, G.C., 1975, Low–friction cell for piston–cylinder high–pressure apparatus. *J. Geophys. Res.*, **80**, 1519–1525.

[76] Mirwald, P.W., & Massonne, H.J., 1980, Quartz $\rightleftharpoons$ coesite transition and the comparative friction measurements in piston–cylinder apparatus using talc–alsimag–glass (TAG) and NaCl high pressure cells: A discussion. *N. Jh. Miner. Monatshefte*, 469–477.

[77] Newton, R.C., & Sharp, W.C., 1975, Stability of forsterite + CO_2 and its bearing on the role of CO_2 in the mantle. *Earth Planet. Sci. Lett.*, **26**, 239–244.

[78] Perkins, E.H., Brown, T.H., & Berman, R.G., 1986, *PT*–SYSTEMn *TX*–SYSTEM, *PX*–SYSTEM: three programs which calculate pressure–temperature–composition phase diagrams. *Comp. Geosci.*, **12**, 749–755.

[79] Philipp, R, 1988, Phasenbeziehungen im System MgO–H_2O–CO_2–NaCl. Ph.D. Thesis, ETH Zürich, No. 8641, unpublished.

[80] Powell, R., & Holland, T.J.B., 1985, An internally consistent thermodynamic dataset with uncertainties and correlations: 1. Methods and a worked example. *J. Metam. Geol.*, **3**, 327–342.

[81] Powell, L.R., Hall, W.J., Hyink, C.H., Jr., Sparks, L.L., Burns, G.W., Scroger, M.G., & Plumb, H.H., 1974, Thermocouple reference tables based on the IPTS–68. *NBS Monogr.*, **125**, 401 pp.

[82] Prausnitz, J.M., Lichtenthaler, R.N., & de Azevedo, E.G., 1986, Molecular Thermodynamics of Fluid–Phase Equilibria (2nd ed.). Prentice–Hall Inc., Englewood Cliffs, N.J. 07632, 600p.

[83] Redlich, O., & Kwong, J.N.S., 1949, On the thermodynamics of solutions. V. An equation of state. Fugacities of gaseous solutions. *Chem. Reviews*, **44**, 233–244.

[84] Robie, R., Hemingway, B.S., & Fisher, J.R., 1979, Thermodynamic Properties of Minerals and Related Substances at 298.15 K and 1 bar (10^5 Pascals) Pressure and Higher Temperatures. *U.S. Geol. Surv. Bull.*, **1452**, 456 p.

[85] Ross, M., & Ree, F.H., 1980, Repulsive forces of simple molecules and mixtures at high density and temperature. *J. Chem. Phys.*, **73**, 6146–6152.

[86] Ryzhenko, B.N., & Volkov, V.P., 1971, Fugacity coefficients of some gases in a broad range of temperatures and pressures. *Geochem. Int.*, **8**, 468–481. Translated from Geokhimiya, **7**, 760–773, 1971.

[87] Salje, E., & Viswanathan, K., 1976, The phase diagram calcite–aragonite as derived from the crystallographic properties. *Contr. Miner. Petrol.*, **55**, 55–67.

[88] de Santis, R., Breedveld, G.J.F., & Prausnitz, J.M., 1974, Thermodynamic properties of aqueous gas mixtures at advanced pressures. *Ind. Eng. Chem. Proc. Des. Devel.*, **13**, 374–377.

[89] Saxena, S.K., & Fei, Y., 1987a, High pressure and high temperature fluif fugacities. *Geochim. Cosmochim. Acta*, **51**, 783–791.

[90] Saxena, S.K., 1987b, & Fei, Y., 1987b, Fluids at crustal pressures and temperatures, I. Pure species. *Contr. Miner. Petrol.*, **95**, 370–375.

[91] Schittkowski, K., 1980, Nonlinear Programming Codes – Information, Tests and Performance. Lecture Notes in Economics and Mathematical Systems, No. 183, Springer–Verlag, Berlin, Heidelberg, New York. 242 pp.

[92] Shmonov, V.M., 1977, The apparatus for measuring *P-V-T* properties of gases up to 1000 K and 8000 bar (in Russian). *Och. Fiz. Khem. Petrol.*, **1**, 236–245.

[93] Shmonov, V.M., & Shmulovich, K.I., 1974, Molar volumes and equation of state of CO_2 at temperatures from 100–1000°Cand pressures from 2000–10000 bars (in Russian). *Akad. Nauk SSSR Doklady*, **217**, 935–938.

[94] Shmulovich, K.I. 1974, Phase equilibria in the system CaO–Al_2O_3–SiO_2–CO_2. *Geochem. Int.*, **11**, 883–887.

[95] Shmulovich, K.I., & Shmonov, V.M., 1975, Fugacity coefficients for CO_2 from 1.0132 to 10000 bar and 450–1300 K. *Geochem. Int.*, **12**, 202–206. Translated from Geokhimiya, **9**, 551–555, 1975.

[96] Singh, A.K., & Kennedy, G.C., 1974, Compression of calcite to 40 kbar. *J. Geophys. Res.*, **79**, 2615–2622.

[97] Smith, F.H., & Adams, L.H., 1923, The system calcium oxide–carbon dioxide. *J. Am. Chem. Soc.*, **45**, 1167–1184.

[98] Stavely, L.A.K., & Linford, R.G., 1969, The heat capacity and entropy of calcite and aragonite, and their interpretation. *J. Chem. Therm.*, **1**, 1–11.

[99] Touret, J., & Bottinga, Y., 1979, Équation d'état pour le CO_2; application aux inclusions carboniques. *Bull. Minéral.*, **102**, 577–583.

[100] Treiman, A.H., & Essene, E.J., 1983, Phase equilibria in the system CaO–SiO_2–CO_2. *Am. J. Sci.*, **283-A**, 97–120.

[101] Trommsdorff, V., & Connolly, J.A.D., 1990, Constraints on phase diagram topology for the system CaO–MgO–SiO_2–CO_2–H_2O. *Contr. Miner. Petrol.*, in print.

[102] Tsiklis, D.S., Linshits, L.R., & Tsimmerman, S.S., 1971, Measurment and calculation of molar volumes of carbon dioxide at high pressure and temperature (in Russian). *Teplofiz. Svoistva Vesch. Mater*, **3**, 130–136.

[103] Vaessen, W., 1984, UBC NLP: Nonlinear Function Optimization. Computing Center, The University of British Columbia, users manual, unpublished, 167 pp.

[104] Vukalovich, M.P., Altunin, V.V., & Timoshenko, N.I., 1962, Experimental investigation of the specific volume of carbon dioxide at temperatures from 200–750°C and pressures up to 600 kg/cm^2 (in Russian). *Teploenergetica*, **9**, 56–62.

[105] Vukalovich, M.P., Altunin, V.V., & Timoshenko, N.I., 1963a, Experimental determination of the specific volume of CO_2 at temperatures 40–150°C and pressures up to 600 kg/cm^2 (in Russian). *Teploenergetica*, **10**, 85–88.

[106] Vukalovich, M.P., Altunin, V.V., & Timoshenko, N.I., 1963b, Specific volume of carbon dioxide at high pressure and temperature (in Russian). *Teploenergetica*, **10**, 92–93.

[107] Walter, L.S., 1963a, Experimental studies on Bowen's decarbonation series: I: P–T univariant equilibria of the 'monticellite' and 'akermanite' reactions. *Am. J. Sci.*, **261**, 488–500.

[108] Walter, L.S., 1963b, Experimental studies on Bowen's decarbonation series: II: P–T univariant equilibria of the reaction: forsterite + calcite = monticellite + periclase + CO_2. *Am. J. Sci.*, **261**, 773–779.

[109] Wasil, E., Golden, B., & Liu, L., 1989, State-of-the-art in nonlinear optimization software for the microcomputer. *Computers Oper. Res.*, **16**, 497–512.

[110] Zubarev, V.N., & Telegin, G.S., 1962, The impact compressibility of liquid nitrogen and solid carbon dioxide. *Soviet Physics, Doklady*, **7**, 34–36.

Chapter 2

Properties of CO_2 – H_2O Mixtures at High Pressure and Temperature

2.1 Introduction

The importance of knowing the thermophysical properties of aqueous fluid mixtures at elevated pressure and temperature is obvious in a number of earth science applications: i) the computation and prediction of phase equilibria in metamorphic and igneous petrology (Berman, 1988, Ferry & Baumgartner, 1987, Ghiorso & Carmichael, 1987); ii) the interpretation of fluid inclusions (Roedder, 1984); iii) the modeling of mass transfer in aqueous geochemistry (Helgeson & Lichtner, 1987, Pitzer, 1987, Sverjensky, 1987); and iv) some high temperature–high pressure engineering applications, such as steam flooding to enhance oil recovery and technologies utilizing geothermal energy. In this chapter the system water–carbon dioxide is discussed which comprises the most abundant fluid species of geological interest. It will be seen that in spite of the importance of this system its properties are rather poorly known.

In addition to the variables pressure (P), specific volume (V) and temperature (T) the compositional variable (X) must be considered. This makes graphical presentation of P-V-T-X data difficult without resorting to a large number of graphs. Because a comprehensive review of such data is not available elsewhere an extensive collection of graphs is presented in appendix E.

This chapter introduces the system H_2O–CO_2 followed by a presentation of existing

equations of state in some detail. The theoretical and physical foundations of some equations of state and mixing rules are evaluated. Fundamental thermodynamic relationships for fluid mixtures are presented with special emphasis on the treatment of phase equilibrium data that are used to constrain the mixing properties of H_2O–CO_2. Subsequent sections review and evaluate the available experimental data from both *P-V-T-X* and phase equilibrium studies. A strategy and methodology is proposed for the development of an equation of state for H_2O–CO_2 mixtures that can take advantage of both *P-V-T-X* and phase equilibrium data. The chapter concludes with an assessement of where new data is most urgently required.

2.2 The System CO_2–H_2O

The system CO_2–H_2O has three components, C, H, O, and contains numerous species: CO_2, H_2O, CO, O_2, H_2, CH_4, H_2CO_3, complex hydrocarbons, and the condensed phases graphite and diamond. Charged species may be neglected on the basis of measurements of the electrical conductivity at elevated pressures and temperatures (Franck, 1956) and spectroscopic data (Franck, 1979). Hydrocarbons and other oil brine ingredients are not considered here even though some organic compounds in intermediate oxidation states may persist to metamorphic temperatures (Helgeson, 1990). Methane, carbon monoxide and in some cases hydrogen may be present in significant amounts under metamorphic conditions and in laboratory experiments at comparable conditions.

Despite the existence of numerous species it is possible to take a stoichiometric approach for the binary join H_2O–CO_2 which considers only two species, CO_2 and H_2O. The experimental data, however, on which the equation is calibrated, must be known to contain only those two species. The bulk composition of the fluid, whether experimental or natural, may be displaced from the binary join if the fugacity of one or more species

is buffered (i.e. controlled by a solid phase assemblage), or sources or sinks for C–H–O species exist. This is particularly significant in the case where graphite is stable. Care must be taken in phase equilibrium experiments involving CO_2 and H_2O to ensure that the bulk composition of the fluid remains on the binary join during the experiment and that other species than H_2O and CO_2 can be neglected if the results are to be used to constrain mixing properties of CO_2 and H_2O. Gain or loss of hydrogen is the most common problem encountered and may be solved by buffering the hydrogen fugacity at a very low partial pressure, removing likely sources or sinks for hydrogen, and keeping experimental run times as short as possible. Experimentally measured volumes of CO_2–H_2O mixtures may suffer from oxygen loss due to the oxidation of the steel pressure vessel or from hydrogen loss due to diffusion or formation of metal hydrides.

Graphite must not be stable if a binary equation of state or binary phase equilibrium and *P-V-T-X* experiments are to be used as constraining data for the binary CO_2–H_2O system. Under reducing conditions in a C–O–H system with graphite present significant mole fractions of methane may persist to high temperatures (ca. 700 °C for a quartz–fayalite–magnetite [QFM] buffered system). Carbon monoxide becomes an important species in the presence of graphite at higher temperatures (Eugster & Skippen, 1967). In the three–component system C–H–O with graphite present the state of the sytem can be fully described by specifying only 3 parameters. These are commonly taken as P, T, and the potential of one of the species such as H_2 or O_2 through the use of buffers (Eugster & Skippen, 1967, Ulmer & Luth, 1988). Under sufficiently oxidizing conditions methane, hydrogen and carbon monoxide are present only in trivial amounts and a binary C–O–H fluid consists chiefly of the species CO_2 and H_2O (see for example Holloway, 1987, Eugster & Skippen, 1967).

The two–phase region of the CO_2–H_2O binary system is encountered geologically under conditions of very low grade metamorphism, as well as under those applicable to

many hydrothermal processes. The critical curve which bounds the two–phase region extends from the critical point of pure H_2O (374.15 °C, 221.3 bar) to a temperature minimum (266 °C, 2450 bar, X_{CO_2}=0.415) and then probably to higher temperatures with increasing pressure and increasing X_{CO_2}. Experimental data on the two–phase region at high pressures extends to 3.5 kbar (Tödheide & Franck, 1963, Takenouchi & Kennedy, 1964). For CO_2–rich compositions the lower branch of the critical curve extends from the critical point of pure CO_2 (31.05 °C, 73.86 bar) to a lower critical endpoint at somewhat higher temperature and pressure which is experimentally poorly constrained. Equations of state designed for the computation of phase equilibria at temperatures below the critical point of water must therefore account for the two–phase region. Some geologically reasonable pressure–temperature–time paths like those responsible for blue schist metamorphism may intersect the two–phase region twice, once at low pressure and low temperature, and again at high pressure. Interestingly, this behaviour is predicted by the Kerrick & Jacobs (1981) equation where the two–phase region is calculated to occur at about 15 kbar and 400 °C. Another aspect of the CO_2–H_2O system that affects the physics of processes but not the thermodynamics is the density inversion at which the CO_2–rich vapour phase becomes more dense than the H_2O–rich coexisting liquid phase (Tödheide & Franck, 1963). This density inversion occurs at increasing pressure with increasing temperature and passes through the coordinates 50 °C, 800 bar and 250 °C, 2000 bar. At 2000 bar and 250 °C the 'vapour' contains 67.5 mol% CO_2 and the 'liquid' dissolves 16.6 mol% CO_2.

For computations that include fluid species other than CO_2 and H_2O it is necessary to compute the abundance of all species from the relevant equilibrium constants using a 'distribution of species' calculation. This calculation must be performed at each pressure, temperature and bulk composition of interest. The calculation involves the simultaneous solution of all mass action and mass balance equations pertaining to the fluid species

likely to be present. Some simple sample calculations are presented by Skippen & Eugster (1967), Holloway (1987) and Ferry & Baumgartner (1987). Alternately, a Gibbs potential minimization technique may be applied to achieve the same goal in a more general way (i.e. DeCapitani & Brown, 1989).

2.3 Constraints on Equations of State from Theory and Experimental Evidence

It is fair to state that the problem of the prediction of P-V-T properties of fluids and their mixtures is not so much due to the lack of theories and models but due to the lack of our ability to assess their relative merits. Models based on first principles are not yet sufficiently developed to test equations of state, and the body of experimental data is not large enough to distinguish between the extrapolation properties of the numerous semi–empirical equations. As a consequence the computation of properties of fluid mixtures heavily relies on experimentally measured quantities, semi–empirical equations of state, and in many cases arbitrarily chosen mixing rules. A physical interpretation of the constants in an equation of state is usually offered in hindsight after some combination of parameters and mixing rules is found to achieve a satisfactory fit to experimental data. Measurements on mixtures above several kilobars pressure are few and the problem of extrapolation to conditions of interest to petrologists is obvious. There are no P-V-T data obtained with static experiments on gases above 10 kbar despite the fact that current technology would permit measurements in internally heated apparati up to 15–20 kbar. It is therefore necessary to examine closely some of the theories that underly the equations predicting P-V-T-X properties and thermodynamic functions in the CO_2–H_2O system.

The exact shape of the intermolecular potential as a function of temperature and

pressure is not known, nor are the potentials resulting from their mutual interaction in mixtures. For this reason most equations of state applicable to real systems are based on macroscopic models with parameters related to the dominant intermolecular forces, namely attraction and repulsion. Examples of this class of equations are the virial–type equations, the van der Waals equation and the Redlich–Kwong (Redlich & Kwong, 1949) equation with its numerous modifications. The parameters in equations of state are either constants or some function of temperature and possibly pressure (or volume). Variations on the theme take other interactions into consideration, such as those arizing from polarizability, asymmetry, permanent dipole moments, induced dipole moments, multi–pole moments, formation of complexes and other forms of chemical association. The equation of state 'constants' may be derived from critical data (corresponding states sytematics), from low pressure data, from optimization to experimental data, or from a combination of the above. There is a spectrum from equations with a sound physical basis to those relying mainly on empiricism. Even inert gases, the simplest kind of gas systems, are difficult to treat on the basis of rigorous theory. These simple gases do not obey exactly the theory of corresponding states, making its application to more complex fluids theoretically unjustified. Corresponding–state systematics is, however, a useful tool for systems with little data and for systematic comparisons.

The behaviour of mixtures of gases may in some cases be described by equations in which the parameters are formed by some combination of the parameters for the pure gases. However, the equations must be mathematically and physically compatible. These 'mixing rules' may be independent of the nature of the endmember gases in that they simply account for geometrical effects upon mixing. If one or more of the endmember gases deviate substantially from ideal behaviour, mixing rules may be adjusted for non–geometric effects upon mixing, such as induced dipole effects, polarizability, strong electronic interactions, chemical association and others. In most cases only a two–body

interaction parameter is developed to account for these effects, and three–body and higher order interactions are neglected. The requirement that equations of the endmember gases be physically and mathematically compatible puts severe constraints on the possibility of introducing modifications to either endmember to fit experimental data. Several equations introduced to geologists have been fit piecewise to data in order to achieve an acceptable fit with a relatively simple equation (i.e. Bottinga & Richet, 1981, for CO_2; Holloway, 1977, 1981, for H_2O; Saxena & Fei, 1987b, for H_2O and CO_2; Powell & Holland, 1985, Holland & Powell, 1990, for the logarithm of the fugacity of H_2O and CO_2). The tradeoff is the introduction of discontinuities to the thermodynamic functions derived from these equations of state.

An important point that is easily underestimated is the dependency of the parameters in the equation of state on the mathematical form of the equation of state itself. Different modifications of the Redlich–Kwong equation, for example, have different values for the repulsive and the attractive parameters, although they do have the same physical significance. The same mixing rules applied to a van der Waals equation and a Redlich–Kwong equation will result in different excess properties for a mixture, even though the physical justification and the underlying assumptions may be identical. This problem is particularly pronounced for semi–empirical equations. Increased flexibility to fit measured volumes may be introduced by making the attractive term or the repulsive term more flexible, or a combination of both. Thus, an equation with a simple hard–sphere repulsive term can mimic increased compressibility at high pressure by introducing a volume (or pressure) dependency on the attractive term (see for example Kerrick & Jacobs equation). The quality of fit to observed data alone implies absolutely nothing about the physical meaning of the variation of the parameters with P, V and T, or about the correctness of the mixing rules.

Table 2.5 lists values for the b parameter, the 'excluded volume', for several equations

Equation	b [cm^3/mole]		Reference
	CO_2	H_2O	
van der Waals	$b = 42.8$	30.4	Moelwyn-Hughes, 1964
Redlich–Kwong	$b = 29.7$	21.1	Redlich & Kwong, 1949
de Santis MRK	$b = 29.7$	14.6	de Santis *et al.*, 1974
Holloway MRK	$b = 29.7$	14.6	Holloway, 1977
Kerrick & Jacobs MRK	$b = 58$	29	Kerrick & Jacobs, 1981
	$V^\infty = 14.5$	7.25	
Bottinga & Richet MRK	$b = b(V)$	–	Bottinga & Richet, 1981
Bowers & Helgeson	$b = 29.7$	14.6	Bowers & Helgeson, 1983
Mäder & Berman	$b = b(V,T)$	–	Equation 1.5, chapter 1
	$b^\circ = 28.1$		
	$b^\infty = 22 - 23$		
Critical temperature	304.2	647.3	[K]
Critical pressure	73.86	221.4	[bar]
Critical volume	94.07	55.44	[cm^3/mole]

Table 2.5: Excluded volume for H_2O and CO_2 for several equations of state. The van der Waals constants are derived from low pressure P-V-T data. The constants for the Redlich–Kwong equation are computed from the corresponding states relationship $b = 0.0867 \cdot RT_c/P_c$. MRK: modified Redlich–Kwong equation. The b paramater of Kerrick & Jacobs is not a 'true' excluded volume. V^∞ is the limiting volume at infinite pressure. b° is the value computed at 1 bar pressure and 298.15 K. b^∞ is the temperature dependent limiting value at infinite pressure. Critical data for CO_2 are from Angus *et al.* (1974) and for H_2O from Moelwyn-Hughes (1964).

based on models with a repulsive and an attractive term. The physical interpretation in these 'billiard ball' (or hard–sphere) molecule models is that b represents the volume made inaccessible to other molecules by one molecule. The excluded volume is independent of temperature and pressure according to van der Waals theory. That this assumption breaks down even at moderate pressures (10–20 kbar) has been briefly shown in chapter 1 for CO_2. In the case of water, where the molecular interaction is dominated by hydrogen bonding rather than repulsion, the definition of an 'excluded volume' is particularly questionable.

The number of parameters in an equation of state is not always correlated with the goodness of fit to data. In most equations one or more parameters, such as the

excluded volume, are fixed prior to regression to measured volumes (i.e. Kerrick & Jacobs, 1981, Holloway, 1977). For some of the mathematically more complex equations a simultaneous fit of all parameters is not possible due to problems with numerical stability during optimization (i.e. Bottinga & Richet, 1981). An equation with few parameters fit simultaneously such as the 5–parameter equation presented in chapter 1 for CO_2 may achieve a fit comparable to a 10–parameter equation such as that proposed by Kerrick & Jacobs (1981). A many–parameter equation may not extrapolate well, particularly if the parameters are combined empirically, for example in a power series expansion.

The virial equation is frequently cited as being the best equation to adopt because of its basis on sound theory, i.e. the physical meaning of the virial coefficients which can be related to the intermolecular potential functions (see Prausnitz *et al.*, 1986 for details). Application of the virial equation to mixtures requires no further assumptions and is therefore commonly preferred for mixtures of a large number of different fluid species. It is necessary to emphasize, however, that the virial equation itself is limited for practical purposes to moderate densities, not exeeding about one–half of the critical density (Prausnitz *et al.*, 1986). This is due to the lack of stringent experimental constraints on the third and higher virial coefficients which are therefore conveniently omitted by truncation or empirically estimated by some corresponding states scheme. The shape of the intermolecular potential function is not exactly known, particularly at high pressures, and therefore empirical functions are used. For most commonly used intermolecular potential models only mathematical expressions for the first and second virial coefficient are available (Prausnitz *et al.*, 1986). The difficulty experienced in fitting the virial equation to *P-V-T* data for H_2O and CO_2 is not surprising because of the polar nature of H_2O and the large quadrupole moment of CO_2. We cannot expect to predict the mixing properties with confidence using mixing rules that do not take proper account of the nature of H_2O, CO_2 and their interactions. In the geologic literature most

virial equations fit to measured data (i.e. Saxena & Fei, 1987a, 1987b) are virial-like equations in as much as the zeroth coefficient is not 1, but some value dictated by the fitting process. The sound theoretical basis is thus removed and the equations are semi-empirical in nature, offering no particular advantage over van der Waals-like equations except that mathematical manipulation may be simpler.

A detailed account of the current state of theories of fluid mixtures and their physical justifications is provided by Prausnitz *et al.* (1986). For the purpose of this study it is sufficient to address a few problems specific to water and carbon dioxide.

Carbon dioxide:

One would not expect significant changes in the nature of the CO_2 molecule in the range of pressure and temperature relevant to this study. Raman spectroscopic measurements to 490 °C and 2.5 kbar (Kruse, 1975) indicate no significant changes in the spectrum from data at low densities. Not much appears to be known about the fate of CO_2 at very high temperatures and very high densities, i.e. the extent of dissociation, ionization, or dimerization.

Water:

While the peculiar nature and properties of water compared to other liquids are well known (i.e. Franks, 1972–1984, vols.I–VII), it is not well understood how these properties change with increasing pressure and temperature. Insight is gained from experimental measurements of P-V-T properties, dielectric permittivity, Raman and infra red spectroscopy, thermodynamic properties, and more recently, from molecular dynamics simulations.

Water at low pressures and temperatures is dominated by hydrogen bonding, which leads to a highly structured liquid dominated by tetrahedrally coordinated molecules with a very open structure similar to that in the corresponding solid, ice-I. The hydrogen

bond persists to high pressures in ice (i.e. ice-VII at pressures > 21 kbar) with an increase in density due to distortion of the tetrahedral framework. The relatively low compressibility of liquid water despite the open framework indicates that the structure dominated by the hydrogen bond may persist to high pressure in the fluid state as well. There is indirect evidence that water starts to behave like a 'normal' liquid between 4 and 8 kbar pressure. A normal liquid is composed of simple molecules with attractive and repulsive interactions that are not modified by polarization, dipole moments, multipole moments, or chemical association. A comparison of compressibilities for water, methanol and hexane shows some noteworthy trends (Franck, 1981): methanol, a polar solvent, hydrogen bonded like water but without forming a three dimensional open structure, deviates significantly from water at 1–4 kbar but shows almost identical compressibilities at 8 kbar. Hexane, a 'normal' liquid, shows compressibilities similar to methanol up to 4 kbar which is the upper limit of available measurements.

The pressure limit of spectroscopic observation is limited to about 3–4 kbar which is not suffuciently high to observe the proposed collapse of the tetrahedral network at low temperatures. It is observed, however, that with increasing pressure the second–nearest and third–nearest neighbour distances decrease significantly, indicative of severe distortion of the network (Franck, 1981).

The tetrahedrally coordinated network probably does not persist to high temperatures at low pressures. Normal liquids display increasing viscosity with rising pressure. Measurements of viscosity of water at low temperatures indicate a minimum at about 2 kbar. Above 50 °C this minimum no longer exists and water appears to behave like a normal liquid (Tödheide, 1971). Spectroscopic data also indicate that at supercritical conditions H_2O has lost many of its structured characteristics which dominate at low temperatures and pressures. Supercritical water is, however, still polar in nature which is important for its ability to interact with other species. No data are available on structural changes

as a function of temperature at high pressures. At very high temperature and pressure (i.e. 100–200 kbar) water may be largely an ionic fluid due to the observed monotonic increase of the ion product with pressure and temperature (Holzapfel & Franck, 1966, Mitchell & Nellis, 1979, and discussion in Franck, 1981).

Recent progress in molecular dynamics simulations (Brodholt & Wood, 1990) at a density of 1 g/cm^3 and temperatures up to 2100 °C (38 kbar) leads to reasonable agreement with measured volumes and transport properties. This approach may allow testing of intermolecular potential formulations and equations of state in the near future. Results of numerical simulations are generally not accurate enough for the purpose of thermodynamic computations.

Designing equations of state for H_2O applicable to a wide range of pressures and temperatures is therefore not an easy task. Models based on the dominant repulsive nature of compressed gas systems will be difficult to fit to observed data. It is not surprising that in work based on corresponding states systematics or van der Waals theory H_2O is always a spoiler and requires special treatment such as more adjustable parameters or separate optimization for individual pressure or temperature intervals.

The Haar *et al.* (1984) equation used for the thermodynamic properties of supercritical water by Berman (1988) and in this study is reliable to at least 2500 K and 30 kbar. The equation is based on a formulation of the Helmholtz free energy as a function of temperature and density. The theoretical model and its empirical extensions obey the first and second laws of thermodynamics and thus allow for computation of any thermodynamic value by differentiation. The equation is consistent with virtually all experimental observations.

Mixtures of water and carbon dioxide:

As a first approximation inferences from P-V-T-X measurements about interactions

between CO_2 and H_2O may be made and tested against what limited spectroscopic and other data exist. From the strong depression of the critical composition curve to lower temperatures (see previous section) compared to mixtures with an inert gas (i.e. argon) one might expect strong chemical association up to at least 400 °C and 4 kbar. The positive deviation of the volume from ideality on mixing is presumably due to repulsive interaction, i.e. dominated by dispersion forces. This effect may be reduced or even reversed by strong chemical association. Greenwood's (1969) *P-V-T-X* measurements indicate distinct negative volumes on mixing at temperatures above 600 °C and pressures below 300–400 bar, with the most negative values being at lowest measured pressures (50 bar) and small X_{CO_2}. This would indicate that chemical association remains significant beyond 800 °C but is decreasing with increasing pressure. From theoretical considerations (Prausnitz *et al.*, 1986) one would expect chemical association to become more pronounced with increasing pressure. Franck & Tödheide (1959) interpret their *P-V-T-X* measurements in terms of deviations from a van der Waals equation of state with 'geometric' mixing rules and estimate the maximum amount of chemical association in terms of carbonic acid (see also appendix E). De Santis *et al.* (1974) use these data together with solubility measurements of carbonic acid at low pressure and temperature to formulate a temperature dependent equilibrium constant ($CO_2 + H_2O \rightleftharpoons H_2CO_3$) that is incorporated into their modified Redlich–Kwong equation of state (see below). The *P-V-T-X* data by Franck & Tödheide are considered suspect for reasons explained later, underestimating the volume effect on mixing significantly. Read's (1975) measurements on electrical conductance suggest at least some chemical association up to the limits of his experiments at 250 °C and 2 kbar.

The volume effect on mixing is most pronounced in water–rich compositions (see figures in appendix E) over most of *P–T–X* space experimentally covered by Greenwood (1969) and Gehrig (1980). The partial molar excess volume of CO_2 at high dilution is

therefore larger than that of H_2O at the same dilution. Furthermore, the activity of water in the mixture deviates significantly from ideality over almost the entire range of fluid composition, whereas the activity of CO_2 becomes nearly ideal at X_{CO_2} larger than 0.6 at temperatures above 500 °C. From this one might conclude that H_2O simply dilutes CO_2 up to some concentration above which interaction becomes significant. Conversely, the ideal behaviour at high X_{CO_2} might be fortuitous in that the interaction based on dispersion forces is offset by effects of chemical association.

Infra red and Raman spectroscopy on fluids at elevated temperature and pressure are rare due to obvious technical difficulties that put an upper pressure limit at 2–3 kbar dictated by the use of sapphire windows. The limited data available (Kruse, 1975, and summary by Franck, 1981) only show a weak band on a Raman spectrum at low temperatures which may be assigned to carbonic acid. Spectra at higher temperatures and pressures are dominated by features related to the CO_2 and H_2O molecule without clear evidence for chemical association.

While inferences on the nature of molecular interaction from P-V-T-X data are hampered by its macroscopic nature and by inconsistencies amongst data sets it is nevertheless concluded that interactions, physical or chemical, are complex and change with pressure, temperature and fluid composition. Spectroscopic data and measurements of electrical conductance do not put any quantitative constraints on chemical association at present. This makes justification for any type of equation of state and mixing rules ambiguous.

2.4 Existing Equations of State

The most commonly used equations of state that predict P-V-T-X properties of H_2O–CO_2 mixtures at conditions of interest to metamorphic and igneous petrologists include the Kerrick & Jacobs (1981) equation and the Holloway–Flowers equation (Holloway, 1977, Flowers, 1979) which are both modifications of the Redlich–Kwong equation (Redlich & Kwong, 1949). Powell and Holland (1985) and Holland & Powell (1990) fit a polynomial function for the logarithm of the fugacity to data computed with other equations of state. The mixture is modeled by a subregular, asymmetric solution model for the activities which are fit to values computed with the Kerrick & Jacobs equation. Shmulovich *et al.* (1980) present a virial equation and use a Margules formulation to model the excess volume on mixing as a function of composition from which they derive the fugacities. In many applications to geologic problems water and carbon dioxide have been assumed to mix ideally (i.e. Eugster & Skippen, 1967, Greenwood, 1967b) due to the lack of constraints on non-ideality. This may result in distorted phase diagram topologies over a wide range of temperature, pressure and fluid composition (see appendix E and below). Spycher & Reed (1988) present a pressure–explicit virial equation applicable to calculations of hydrothermal boiling, with upper limits at 1 kbar and 1000 °C. The numerous equations and modifications proposed in the chemical literature (more than 100 differently modified Redlich–Kwong equations), many of them based on corresponding states systematics, fail at pressures above 500–1000 bars and temperatures as low as 500 °C. A notable exception was a paper by de Santis *et al.* (1974) which included higher pressures and formed the basis of Holloway's (1977) adaptation of the Redlich–Kwong equation to geological problems.

Tabulations of *P-V-T-X* properties and/or fugacities or activity coefficients of CO_2–H_2O mixtures are offered in several publications, most of them based on graphical integration or some function fitting technique to experimental *P-V-T-X* data: Franck & Tödheide, 1959, Greenwood & Barnes, 1966, Greenwood, 1969, 1973, Ryzhenko & Malinin, 1971, Wood & Fraser, 1977, Shmulovich *et al.*, 1980.

Kerrick & Jacobs equation:

Kerrick & Jacobs (1981) adopt Carnahan & Starling's (1972) hard–sphere Redlich–Kwong equation with a modified attractive parameter, a, that is a function of temperature and volume (and therefore of pressure):

$$P = \frac{RT(1+y+y^2-y^3)}{V(1-y)^3} - \frac{a(V,T)}{\sqrt{T}V(V+b)} \tag{2.6}$$

with $y = b/(4V)$ and $a(V,T) = c + d/V + e/V^2$, where c, d and e are second order polynomials in temperature. This results in a total of 10 adjustable parameters, given in units of bar, K and cm^3/mole:

$$c_{H_2O} = [290.78 - (0.30276 \cdot T) + (1.4774 \cdot 10^{-4} \cdot T^2)] \cdot 10^6$$

$$d_{H_2O} = [-8374 + (19.437 \cdot T) - (8.148 \cdot 10^{-3} \cdot T^2)] \cdot 10^6$$

$$e_{H_2O} = [76600 - (133.9 \cdot T) + (0.1071 \cdot T^2)] \cdot 10^6$$

$$c_{CO_2} = [28.31 + (0.10721 \cdot T) - (8.81 \cdot 10^{-6} \cdot T^2)] \cdot 10^6$$

$$d_{CO_2} = [9380 - (8.53 \cdot T) + (1.189 \cdot 10^{-3} \cdot T^2)] \cdot 10^6$$

$$e_{CO_2} = [-368654 + (715.9 \cdot T) + (0.1534 \cdot T^2)] \cdot 10^6$$

$$b_{H_2O} = 29, \quad b_{CO_2} = 58$$

The parameters are not fit simultaneously to experimental data because of convergence problems using non–linear least squares regression techniques. A b parameter is arbitrarily chosen in such a way as to yield $a(V)$ curves for various isotherms having a

monotonic form in order to permit fitting of the simple power expansions of c, d and e to experimental data. The equation of state is thus semi–empirical and a rigorous physical interpretation of the parameters is not possible.

Simple geometric mixing rules are employed to obtain parameters for an equation for mixtures:

$$b_{\text{mix}} = \sum_i b_i X_i \tag{2.7}$$

$$a_{\text{mix}} = \sum_i \sum_j X_i X_j a_{ij} \tag{2.8}$$

where the binary interaction parameters are obtained from $a_{ij} = \sqrt{a_i a_j}$. Note that these mixing rules are of a 'geometric' nature and do not explicitly account for interactions arising from the polar nature of water, from the very different size and shape of the molecules, or from chemical association.

Thermodynamic properties of the gas mixture may be computed analytically from the equation. The expression for the fugacity coefficient of a species in the mixture is too long to be reproduced (equation 27 in Kerrick & Jacobs, 1981). The volume at specified pressure, temperature and composition has to be computed iteratively. APL and FORTRAN codes are published in a separate paper (Jacobs & Kerrick, 1981a). Jacobs & Kerrick (1981b) expand the two–species binary system to include methane. In a companion paper Jacobs & Kerrick (1981c) use their equation to compute numerous phase diagrams. The authors present results for the pure gases from about 300–1000 °C, and from 400–800 °C for mixtures. Jacobs & Kerrick (1981a) recommend the equation over the range 300–1050 °C and 1–20000 bar. Because of the functional form of the $a(V,T)$ term there is no positive volume defined for pure carbon dioxide at low temperatures. This lower temperature limit increases with rising pressure and is located at about 480 °C at 50 kbar. At 400 °C difficulties were encountered in evaluating the volumes of mixtures in a small pressure interval at about 200 bars using their published computer code (see

figures E.36 and E.37 in appendix E). This may be a convergence problem of the root finding algorithm used by the authors, or more likely the mathematical behaviour of the equation close to the two–phase region. This problem is 'invisible' for the computation of thermodynamic properties at higher pressures which require integration of the partial molar volume with respect to pressure.

In contrast to the Holloway–Flowers–de Santis equation (see below) the Kerrick & Jacobs model does not allow for chemical association and thus no negative volumetric contribution to the effect on mixing is permissible. Thus all deviations from ideality are constrained to be positive except very close to critical conditions.

Holloway–Flowers–de Santis equation:

Holloway (1976, 1977) introduced the Redlich–Kwong equation of state (Redlich & Kwong, 1949) to geologists, adapted and modified from de Santis *et al.* (1974):

$$P = \frac{RT}{V-b} - \frac{a(T)}{\sqrt{T}V(V+b)} \tag{2.9}$$

For simple, non–polar molecules the a parameter is approximately constant and may be derived from critical data (Redlich & Kwong, 1949). De Santis *et al.* (1974) introduced a temperature dependence, $a(T) = a^\circ + a'(T)$, which takes into account large dipole or quadrupole moments. The temperature dependence of $a'(T)$ was refit by Holloway to P-V-T data extending to higher pressures and temperatures (H_2O extrapolated to 1800 °C from previous extrapolations by Holloway *et al.* (1971)). The functions chosen are second or third order polynomials in temperature. The b and a° parameters are adopted from de Santis *et al.* (1974).

The mixing rules are identical to those adopted by Kerrick & Jacobs (equations 2.7 and 2.8). The binary interaction parameter a_{ij} is expanded by de Santis *et al.* (1974) to account for complications due to the formation of a complex by a reaction of the form $CO_2 + H_2O \rightleftharpoons$ complex (i.e. H_2CO_3) which is supported by experimental evidence at low

temperatures (Coan & King, 1971). The equilibrium constant K of this reaction is then entered into the binary interaction parameter a_{ij} for H_2O–CO_2 mixtures in the form:

$$a_{ij} = \sqrt{a_i^\circ a_j^\circ} + (1/2)R^2T^{5/2}K \quad (i \neq j) \tag{2.10}$$

$$b_{\text{mix}} = \sum_i b_i X_i \tag{2.11}$$

$$a_{\text{mix}} = \sum_i \sum_j X_i X_j a_{ij} \tag{2.12}$$

where R is the gas constant. The temperature dependence of the logarithm of the equilibrium constant K is expanded in a third order series of inverse powers of temperature. Numerical values of the equilibrium constant are derived from low temperature solubility data (Coan & King, 1971) and P-V-T-X data of Franck & Tödheide (1959) at 400–750 °C up to 2 kbar. Franck & Tödheide (1959) discuss the maximum possible amount of formation of carbonic acid by comparison of their measured volumes of the mixtures with those computed by a van der Waals equation with geometric mixing rules. However, the application of standard mixing rules to H_2O–CO_2 mixtures is questionable, as has been discussed above. The data of Franck & Tödheide are suspect (see discussion in section 'P-V-T-X Data on H_2O–CO_2 Mixtures' below) and the term for chemical association derived by de Santis *et al.* (1974) introduced some additional uncertainty into the equations of state of Holloway (1977), Flowers & Helgeson (1983) and Bowers & Helgeson (1983) who adapted the above treatment. Note also that equation 2.10 is derived for non–polar gases that have no significant dipole or quadrupole moments. More recent data on electrical conductance and inferences on the first ionization potential of carbonic acid by Read (1975) suggest that at least some carbonic acid is present up to 250 °C and 2 kbar which is the upper limit of the measurements. The approach by Kerrick & Jacobs is hindered because it excludes chemical association (see above). An evaluation of the de Santis *et al.* approach versus the Kerrick & Jacobs approach is not yet possible due to insufficient or contradictory experimental data.

The resulting equation for H_2O–CO_2 mixtures of Holloway (1977) has 15 parameters which are all fit to various sets of experimental data, but not simultaneously. The temperature is in °C for $a(T)$ and in Kelvin for $\ln K(T)$, pressure is in atmospheres, and the volume in cm^3/mole:

$$a^{\circ}_{CO_2} = 46 \cdot 10^6, \quad b_{CO_2} = 29.7$$

$$a^{\circ}_{H_2O} = 35 \cdot 10^6, \quad b_{H_2O} = 14.6$$

$$a'_{CO_2}(T) = 73.03 \cdot 10^6 - 71400 \cdot T + 21.57 \cdot T^2$$

$$a'_{H_2O}(T) = 166.8 \cdot 10^6 - 193080 \cdot T + 186.4 \cdot T^2 - 0.071288 \cdot T^3$$

$$\ln K = -11.07 + \frac{5953}{T} - \frac{2746 \cdot 10^3}{T^2} + \frac{464.6 \cdot 10^6}{T^3}$$

$$R = 82.05$$

Holloway (1981a, 1981b) refit the $a'(T)$ term for H_2O to an extended data base with separate polynomials for three different temperature intervals. The expression for temperatures below 400 °C was derived by J. Connolly (J.R. Holloway, written communication, June, 1990).

$$T < 600°\text{C} : a'_{H_2O}(T) = 4.221 \cdot 10^9 - 3.1227 \cdot 10^7 \cdot T + 87485 \cdot T^2 - 107.295 \cdot T^3 + 4.86111 \cdot 10^{-2} \cdot T^4$$

$$600 \leq T \leq 1200 : \quad a'_{H_2O}(T) = 166.8 \cdot 10^6 - 193080 \cdot T + 186.4 \cdot T^2 - 7.1288 \cdot 10^{-2} \cdot T^3$$

$$T > 1200°\text{C} : \quad a'_{H_2O}(T) = 140 \cdot 10^6 - 50000 \cdot T$$

$$T < 400°\text{C} : \quad a'_{H_2O}(T) = 0.987(7.4174 \cdot 10^7 + 2.132 \cdot 10^5 \cdot T - 442.1 \cdot T^2 + 0.28623 \cdot T^3)$$

Flowers (1979) pointed out that Holloway's (1977) treatement of the fluid mixture for H_2O–CO_2 violated the Gibbs–Duhem relationship (i.e. $\sum_i X_i d \ln a_i = 0$) which led to an erroneous expression for the fugacity coefficient (γ_i) that resulted in excessive deviations from ideality. The correct expression for the fugacity coefficient relative to ideal mixing

at P and T is given by Flowers (1979) and Prausnitz *et al.* (1986):

$$\ln\gamma_i = \ln\left(\frac{V}{V-b_{\rm mix}}\right) + \frac{b_i}{V-b_{\rm mix}} - \frac{2\sum_{j,i\neq j} a_{ij}X_j}{b_{\rm mix}RT^{3/2}} \cdot \ln\left(\frac{V+b_{\rm mix}}{V}\right) + \frac{a_{\rm mix}b_i}{b_{\rm mix}^2 RT^{3/2}}\left[\ln\left(\frac{V+b_{\rm mix}}{V}\right) - \frac{b_{\rm mix}}{V+b_{\rm mix}}\right] - \ln\left(\frac{PV}{RT}\right), \quad (2.13)$$

where i=CO_2 or H_2O. The same equation presented in the review article by Ferry & Baumgartner (1987, eq. 108, p. 342) contains a typographical error.

Powell & Holland equation:

Powell & Holland (1985) fit the expression $RT\ln f$ for endmember gases to a second order polynomial in temperature with coefficients that expand into power series of pressure with up to four terms. Their calibration is based on fugacity data for H_2O by Burnham *et al.* (1968) and the high pressure extrapolation of Delaney & Helgeson (1978). CO_2 fugacities are fit to data derived by Shmonov & Shmulovich (1974) up to 10 kbar and the high pressure extrapolation predicted by the Bottinga & Richet (1981) equation of state. Activities in mixtures are modeled by a subregular, asymmetric solution model with Margules parameters that have a linear dependence on temperature and pressure. The Margules parameters are fit to activities of mixtures computed with the Kerrick & Jacobs (1981) modified Redlich–Kwong equation of state. Powell & Holland's equations are stated to be applicable in the range 2–10 kbar and 400–800 °C, with separate Margules parameters to extend the pressure range below 2 kbar.

In an extended version of their thermodynamic database, Holland & Powell (1990) expand the power series of the expressions for the logarithm of the endmember fugacities to a total of 15 and 13 parameters for CO_2 and H_2O, respectively. The improved range of applicability is said to be 0.1–40 kbar and 300–1200 °C for H_2O and 300–1400 °C for CO_2. The mixtures are treated with the subregular solution model presented in 1985. The limits of appliction of the mixing model are not stated but probably coincide with

those of Kerrick & Jacobs (1981).

Bowers–Helgeson equation:

Bowers & Helgeson (1983) present a modified Redlich–Kwong equation of state for H_2O–CO_2–NaCl mixtures for the range 350–600 °C and pressures greater than 500 bars (Bowers & Helgeson, 1985). The treatement of H_2O and CO_2 is based on the work of de Santis *et al.* (1974), Holloway (1977, 1981a) and Flowers (1979). The $a(T)$ and b parameters for CO_2 are identical to those of Holloway (1977). Sodium chloride is not treated as a separate species but rather incorporated into the $a(T)$ and b terms of H_2O by making them a function of NaCl content. The authors achieve a better fit by making $a°$ for H_2O a function of temperature. The mixing rules are identical to those of de Santis *et al.* (1974), including the formulation for the effect of complex formation (see discussion above).

Spycher & Reed equation:

Spycher & Reed (1988) present quadratic, pressure–explicit virial–like equations for H_2, CO_2, CH_4, H_2O and H_2O–CO_2–CH_4 mixtures applicable to problems within the hydrothermal regime, including boiling processes. Their equations for H_2O and CO_2 and their mixtures, calibrated to P-V-T data and solubility data, are applicable up to 500 bar at temperatures below 350 °C, and up to 1000 bar for temperatures between 450 and 1000 °C.

Saxena & Fei equations:

Saxena & Fei (1987a, 1987b) present pressure–explicit or volume–explicit virial–like equations of state for many pure gas species, including H_2O and CO_2, based on shock wave data and P-V-T measurements. Efforts are under way to extend this work to fluid mixtures (Fei & Saxena, 1987). A detailed discussion and comparison of their equations must await full publication of their research. Their equation for pure carbon dioxide is

discussed in chapter 1.

2.5 Thermodynamic Relationships for Fluid Mixtures

In this section the thermodynamic relationships for fluids and fluid mixtures are developed. While most standard texts cover the subject adequately, they do not provide the necessary details relevant to our treatment of the phase equilibrium experiments. I found the following references particularly useful: Prausnitz *et al.* (1986) as a comprehensive treatise and the geologically oriented summaries of Wood & Fraser (1977), Anderson (1977) and Skippen & Carmichael (1977). The notation is tabulated for clarity in table 2.6 and also explained in the text.

Pure fluid:

The fugacity f (or 'thermodynamic pressure') is best introduced by considering the change in chemical potential μ of the pure fluid from one state to another state at constant temperature T:

$$\mu^{P_2,T} - \mu^{P_1,T} = \int_{P_1}^{P_2} \left(\frac{\partial \mu}{\partial P}\right)_T dP = \int_{P_1}^{P_2} [V(P)]_T \, dP. \tag{2.14}$$

For a perfect gas ($PV = RT$) equation 2.14 is easily integrated to obtain

$$\mu^{P_2,T} - \mu^{P_1,T} = RT \ln(P_2/P_1). \tag{2.15}$$

Lewis (1907) defined the fugacity in such a way as to preserve the mathematical form of equation 2.15

$$\mu^{\text{state 2}} - \mu^{\text{state 1}} = RT \ln\left(f^{\text{state 2}}/f^{\text{state 1}}\right) = RT \ln a \tag{2.16}$$

where states 1 and 2 are at the same temperature but may differ in fluid pressure or fluid composition. The activity a describes how 'active' a species (gas, solid, liquid, pure or in a mixture) is with respect to a standard state that needs to be specified in order to assign a numerical value to the activity.

P	pressure
P_i	partial pressure of component i
T	absolute temperature in Kelvin
V	molar volume
V_i°	molar volume of pure component i
V_i	partial molar volume of component i in a mixture
V_m	molar volume of a mixture
$\hat{V}$	volume of a mechanical (ideal) fluid mixture
V_e	molar excess volume of a mixture
V_{e_i}	partial molar excess volume of component i in a mixture
X_i	mole fraction of component i in a mixture
μ	chemical potential
μ_i	chemical potential of component i in a mixture
μ_i°	chemical potential of pure component i
f	fugacity
f_i	fugacity of component i in a mixture
f_i°	fugacity of pure component i
γ	fugacity coefficient relative to a perfect gas ($PV = RT$)
γ_i	fugacity coefficient of component i in a mixture relative to perfect gases that mix ideally
$\gamma_i^\bullet$	fugacity coefficient of component i relative to ideal mixing at pressure and temperature of interest
a	activity
a_i	activity of component i in a mixture
λ_i	activity coefficient of component i in a mixture
ν_i	stoichiometric coefficient of component i in a reaction
η_i	normalized stoichiometric coefficient of component i
R	gas constant
Superscript * refers to a variable at some standard state	
Superscript $^{\mathrm{id}}$ refers to a variable in a state of ideal mixing	
Superscript $^{\mathrm{exp}}$ refers to an experimentally measured variable	
Superscripts ^{P,T,V,X_i} refer to a variable at state P, T, V or X_i	

Table 2.6: Notation for thermodynamic equations.

If $\mu^{P_1,T}$ in equation 2.14 is chosen as a reference state at a pressure P_1 sufficiently low in order for the perfect gas law to hold true, i.e. $P_1 = 1$ bar, it follows that $f^{P_1,T} \approx P_1 = 1$ bar, and equation 2.16 will reduce to:

$$\mu^{P,T} - \mu^{1\,\text{bar},T} = RT \ln \left(f^{P,T} / 1\ \text{bar} \right) = RT \ln f^{P,T}. \tag{2.17}$$

Note that fugacity has the unit of pressure but the expression $\ln f$ is a ratio and therefore has no unit. For this particular standard state the activity a is numerically equal to the fugacity.

The fugacity coefficient γ may be introduced to describe the deviation from a perfect gas at P and T:

$$f^{P,T} = P \cdot \gamma^{P,T}. \tag{2.18}$$

Given an equation of state that relates pressure, volume and temperature for a fluid the fugacity may be readily computed by integration from equation 2.14 and 2.17

$$RT \ln f^{P,T} = \int_{1\,\text{bar}}^{P} [V(P)]_T \, dP \tag{2.19}$$

Fluid Mixtures:

The compositional variable X_i denotes the mole fraction of component i in the mixture. Equation 2.16 may be used to introduce the fugacity f_i for component i in a mixture, where now state 1 and state 2 may differ not only in fluid pressure but also in composition X_i.

$$\mu_i^{\text{state 2}} - \mu_i^{\text{state 1}} = RT \ln \left(f_i^{\text{state 2}} / f_i^{\text{state 1}} \right) = RT \ln a_i \tag{2.20}$$

For the following derivations differences of the chemical potential with respect to various standard states are examined in order to obtain fugacities, activities and volume integrals.

First, operating at constant composition:

$$\mu_i^{P_2,T,X_i} - \mu_i^{P_1,T,X_i} = \int_{P_1}^{P_2} \left(\frac{\partial \mu_i}{\partial P} \right)_{T,X_i} dP = X_i \int_{P_1}^{P_2} [V_i(P)]_{T,X_i} \, dP = RT \ln \left(\frac{f_i^{P_2,T,X_i}}{f_i^{P_1,T,X_i}} \right) \tag{2.21}$$

Defining unit fugacity at $P_1 = 1$ bar and using the perfect gas approximation and ideal mixing one can obtain $f_i^{P_1,T,X_i} = X_i P_1 = X_1 \cdot 1\,\text{bar}$ and write:

$$\mu_i^{P_2,T,X_i} - \mu_i^{1\,\text{bar},T,X_i} = X_i \int_{1\,\text{bar}}^{P_2} [V_i(P)]_{T,X_i}\, dP = RT \ln f_i^{P_2,T,X_i} - RT \ln X_i. \qquad (2.22)$$

The fugacity coefficient γ_i of component i that describes the deviation from an ideal mixture of perfect gases becomes:

$$f_i^{P,T,X_i} = X_i \cdot P \cdot \gamma_i^{P,T,X_i}. \qquad (2.23)$$

In an ideal mixture of perfect gases the fugacity coefficient becomes unity and the fugacity is equal to the partial pressure $P_i = X_i P$. In an ideal fluid mixture there is no excess volume on mixing and the fugacity is related to the fugacity of the component in its pure state by the mole fraction: $f_i^{P,T,X_i} = X_i \cdot f_i^{\circ P,T}$. Because the partial pressures must sum to the total pressure equation 2.23 leads to the relationship: $P = \sum_i P_i = \sum_i f_i/\gamma_i$.

For many practical purposes $\gamma_i^{\bullet}$ may be used relative to a state of ideal mixing of real gases at pressure and temperature of interest and equation 2.23 becomes:

$$f_i^{P,T,X_i} = X_i \cdot f_i^{\circ P,T,X_i} \cdot \gamma_i^{\bullet P,T,X_i}. \qquad (2.24)$$

This fugacity coefficient $\gamma_i^{\bullet}$ relates directly to the excess properties of a mixture.

Note that the volume V_i in equation 2.21 is the partial molar volume which may be obtained at constant P and T through differentiation of the volume of the mixture with respect to the compostional variable X_i:

$$V_i^{P,T,X_i} = \left(\frac{\partial V_m^{P,T}}{\partial X_i}\right)_{P,T}. \qquad (2.25)$$

It is possible to measure the volume V_m of a mixture experimentally as a function of P, T and X_i (see section below). In order to compute the fugacity f_i of component i the volume of the mixture at constant temperature as a function of both pressure and

composition must be known. The computation by graphical means without an equation of state requires therefore an enormous number of experimental measurements.

For a binary mixture with components A and B , and mole fractions X_A and $X_B = 1 - X_A$ one can write (see figure 2.8 for a geometrical interpretation):

$$V_A^{P,T,X_A} = V_m^{P,T} - X_B \left(\frac{\partial V_m^{P,T}}{\partial X_B}\right)_{P,T}$$

$$V_B^{P,T,X_B} = V_m^{P,T} + X_A \left(\frac{\partial V_m^{P,T}}{\partial X_B}\right)_{P,T}. \tag{2.26}$$

It is practical to introduce excess volume as the difference between the real volume of a mixture, V_m, and the volume of an hypothetical mechanical mixture $\hat{V} = \sum_i X_i V_i^\circ$. The molar excess volume of a mixture is then defined by $V_e = V_m - \hat{V}$, and the partial molar excess volume of a component on mixing becomes $V_{e_i} = V_i - V_i^\circ$. Equations 2.26 may now be rewritten in terms of excess volumes:

$$V_{e_A}^{P,T,X_A} = V_e^{P,T} - X_B \left(\frac{\partial V_e^{P,T}}{\partial X_B}\right)_{P,T}$$

$$V_{e_B}^{P,T,X_B} = V_e^{P,T} + X_A \left(\frac{\partial V_e^{P,T}}{\partial X_B}\right)_{P,T}. \tag{2.27}$$

A simple geometric interpretation of equation 2.27 is provided in figure 2.8.

Using equation 2.22 and 2.17 the integral of the excess volume with respect to pressure is related to the fugacities:

$$\begin{aligned}
\int_{1\,\mathrm{bar}}^{P} V_{e_i}^{T,X_i} dP &= \int_{1\,\mathrm{bar}}^{P} V_i^{T,X_i} dP - \int_{1\,\mathrm{bar}}^{P} V_i^{\circ T} dP \\
&= \frac{1}{X_i}\left(RT \ln f_i^{P,T,X_i} - RT \ln X_i - RT \ln f_i^{\circ P,T}\right) \\
&= \frac{1}{X_i}\left[RT \ln \left(\frac{f_i^{P,T,X_i}}{f_i^{\circ P,T}}\right) - RT \ln X_i\right] \\
&= \frac{1}{X_i}\left(RT \ln \frac{a_i^{P,T,X_i}}{X_i}\right) = \frac{1}{X_i} RT \ln \gamma_i^{\bullet P,T,X_i}.
\end{aligned} \tag{2.28}$$

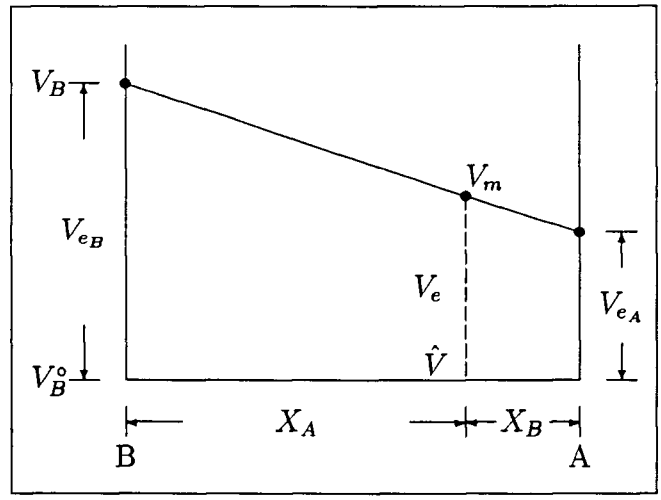

Figure 2.8: Geometric interpretation of the partial molar excess volume in a binary fluid mixture with components A and B.

Note that the standard state for the activity is the pure component at pressure and temperature of interest. Similarly the volume integral of the excess volume of the mixture may be expressed as a linear combination of the partial molar excess volumes (see figure 2.8):

$$\int_{1\,\mathrm{bar}}^{P} V_e^{P,T} dP = \sum_i X_i \int_{1\,\mathrm{bar}}^{P} V_{e_i}^{T} dP. \tag{2.29}$$

For a mixture we obtain:

$$\begin{aligned} \int_{1\,\mathrm{bar}}^{P} V_e^{P,T} dP &= \sum_i RT \ln \frac{f_i^{P,T,X_i}}{f_i^{\circ P,T}} - \sum_i RT \ln X_i \\ &= \sum_i RT \ln \frac{a_i^{P,T,X_i}}{X_i} = \sum_i RT \ln \gamma_i^{\bullet P,T,X_i}. \end{aligned} \tag{2.30}$$

Returning to equation 2.16 one can examine the change of chemical potential as a function of the compositional variable X_i at constant P and T compared to the pure state of component i:

$$\mu_i^{P,T,X_i} - \mu_i^{\circ\,P,T} = RT \ln \left(f_i^{P,T,X_i} / f_i^{\circ P,T} \right) = RT \log a_i^{P,T,X_i}. \tag{2.31}$$

This choice of standard state of the pure component at the pressure of interest is most

useful to define the activity of a component in a mixture. A pure component has thus an activity equal to unity at any pressure and temperature and the value of the activity for a component in a mixture is a number between zero and unity.

The activity coefficient λ_i may be defined to describe the deviation of a mixture from ideality ($a_i = X_i$) at constant P and T:

$$a_i^{P,T,X_i} = X_i \cdot \lambda_i^{P,T,X_i}. \tag{2.32}$$

In an ideal solution the activity coefficient is unity and the activity of a component in a mixture is equal to its mole fraction.

The fugacity coefficient is related to the activity coefficient through the relationship between the fugacity ratio and the activity, with the pure state at P and T as a standard state:

$$a_i^{P,T,X_i} = \frac{f_i^{P,T,X_i}}{f_i^{\circ\,P,T}} \quad \text{or} \quad \lambda_i^{P,T,X_i} = \frac{\gamma_i^{P,T,X_i}}{\gamma_i^{\circ\,P,T}} = \gamma_i^{\bullet P,T,X_i}. \tag{2.33}$$

Returning for a third time to equation 2.16 pressure and composition are changed simultaneously to obtain the relationship

$$\begin{aligned} \mu_i^{P_2,T,X_i} - \mu_i^{\circ\,P_1,T} &= \left(\mu_i^{P_2,T,X_i} - \mu_i^{P_1,T,X_i}\right) + \left(\mu_i^{P_1,T,X_i} - \mu_i^{\circ\,P_1,T}\right) \\ &= RT \ln\left(f_i^{P_2,T,X_i}/f_i^{P_1,T,X_i}\right) + RT \ln\left(f_i^{P_1,T,X_1}/f_i^{\circ P_1,T}\right) \end{aligned} \tag{2.34}$$

which simplifies to the following expression choosing $P_1 = 1$ bar as a reference state and assuming ideal mixing of perfect gases at 1 bar:

$$\mu_i^{P_2,T,X_i} - \mu_i^{\circ\,P_1,T} = RT \ln(f_i^{P,T,X_i}/X_i \cdot 1\text{bar}) + RT \ln(X_i \cdot 1\text{bar}/1\text{ bar}) = RT \ln f_i^{P,T,X_i}. \tag{2.35}$$

From the above relationships it is also obvious that the activity and the fugacity are not independent and only one of them needs to be specified.

Equations for the treatment of phase equilibrium data:

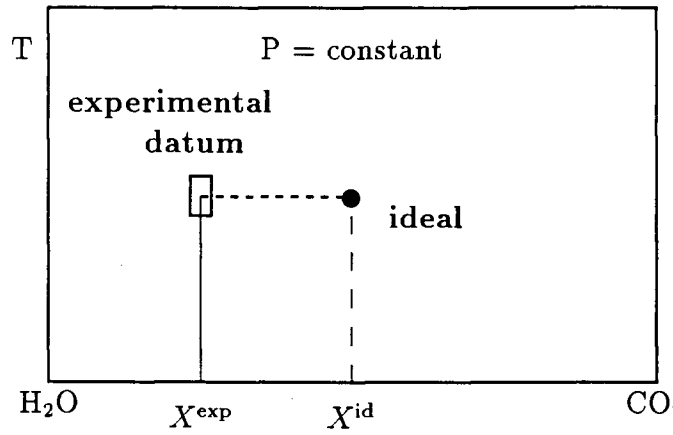

Figure 2.9: Schematic diagram of a single fluid species equilibrium. See text for explanation.

In this section expressions are derived that relate the displacement from experimentally measured phase equilibrium positions to a hypothetical position where the fluid components mix ideally. In order to use this information to constrain volumetric properties of the fluid, the observed deviation from ideality is expressed in terms of fugacities (or activities) together with the corresponding volume integrals over pressure. These relationships are used in a subsequent section to compare experimentally measured deviations from ideality of a H_2O–CO_2 fluid to non–idealities predicted by equations of state and mixing rules.

Single fluid species equilibria: First, phase equilibria are considered in which only one species in a mixture takes part in the reaction. Figure 2.9 illustrates such an equilibrium in a mole fraction *versus* temperature diagram of a binary fluid mixture at constant pressure. The solid line depicts an experimentally determined equilibrium boundary whereas the dashed boundary is that of the same equilibrium computed with the assumption of an ideally mixing fluid phase. The deviation from ideality is expressed at constant pressure and temperature as a difference in composition between X^{exp} and X^{id}. At both

locations, X^{exp} and X^{id}, the change of the Gibbs potential of a reaction is formulated:

$$\Delta_{\text{R}}G = 0 = \mathcal{G}^{P,T}[\nu_j, V_j^\star, S_j^\star, H_j^\star, (C_P)_j(T), \alpha_k(T), \beta_k(P)] + \nu_i RT \ln \frac{f_i^{P,T,X_i^{\text{exp}}}}{f_i^\star} \tag{2.36}$$

$$\Delta_{\text{R}}G = 0 = \mathcal{G}^{P,T}[\nu_j, V_k^\star, S_j^\star, H_j^\star, (C_P)_j(T), \alpha_k(T), \beta_k(P)] + \nu_i RT \ln \frac{f_i^{P,T,X_i^{\text{id}}}}{f_i^\star}, \tag{2.37}$$

where subscript j denotes all phases that take part in the reaction, k relates to solid phases only and i is the subscript for the single gas species i. The function $\mathcal{G}$ contains all contributions to the Gibbs potential from the solid phases and the contributions from the gas species with the exception of the volume integral ($RT \ln f$ term). Because the two states under consideration are at the same pressure and temperature the $\mathcal{G}$ terms cancel and one can equate the fugacity ratios directly:

$$\ln \frac{f_i^{P,T,X_i^{\text{exp}}}}{f_i^\star} = \ln \frac{f_i^{P,T,X_i^{\text{id}}}}{f_i^\star}. \tag{2.38}$$

Note that the computed $\mathcal{G}$ carries the sum of the uncertainties of the thermodynamic data of all phases involved which propagate into relationship 2.38. Remembering that for an ideal mixture $f_i = X_i f_i^\circ$ and that the fugacity ratio is equal to the activity relative to the standard state defined by the fugacity (i.e. $f_i^{\circ P,T}$) one obtains:

$$\frac{f_i^{P,T,X_i^{\text{exp}}}}{f_i^{\circ P,T}} = a_i^{P,T,X_i^{\text{exp}}} = X_i^{\text{id}}. \tag{2.39}$$

Equally well the deviation from ideality may be related to the fugacity coefficient (see equation 2.23):

$$\gamma_i^{P,T,X_i^{\text{exp}}} = \frac{X_i^{\text{id}}}{X_i^{\text{exp}}} \cdot \frac{f_i^{\circ P,T}}{P} \text{ or } \gamma_i^{\bullet P,T,X_i^{\text{exp}}} = \frac{X_i^{\text{id}}}{X_i^{\text{exp}}}. \tag{2.40}$$

Equation 2.38 is used to relate the volume integral of the partial molar excess volume V_{e_i} with respect to pressure given in equation 2.28:

$$\begin{aligned} RT \ln X_i^{\text{id}} &= RT \ln f_i^{P,T,X_i^{\text{exp}}} - RT \ln f_i^{\circ P,T} \\ &= X_i^{\text{exp}} \int_{1\,\text{bar}}^{P} V_{e_i} dP + RT \ln X_i^{\text{exp}}, \end{aligned} \tag{2.41}$$

or:

$$X_i^{\text{exp}} \int_{1\,\text{bar}}^{P} V_{e_i} dP = RT \ln \frac{X_i^{\text{id}}}{X_i^{\text{exp}}} = RT \ln \gamma_i^{\bullet P,T,X^{\text{exp}}}. \tag{2.42}$$

Equilibria in which several fluid species take part: The equations that describe deviations from an ideally mixing fluid are derived in a similar fashion as in the previous case of a single fluid species equilibrium. Only expressions for some combination of the fugacities (or activities) of the species that take part in a reaction may be obtained. Unlike the first case, the stoichiometric coefficients of the fluid species will remain in the equations.

From equations 2.36 and 2.37 that relate the change of the Gibbs potential of a reaction for the two states at X_i^{exp} and X_i^{id} it follows:

$$\sum_i \nu_i RT \ln \frac{f_i^{P,T,X_i^{\text{exp}}}}{f_i^{\star}} = \sum_i \nu_i RT \ln \frac{f_i^{P,T,X_i^{\text{id}}}}{f_i^{\star}}. \tag{2.43}$$

Using the relationship for ideal mixing $f_i = X_i f_i^{\circ}$ one can simplify and obtain:

$$\sum_i \nu_i \ln \frac{f_i^{P,T,X_i^{\text{exp}}}}{f_i^{\circ P,T}} = \sum_i \nu_i \ln a_i^{P,T,X_i^{\text{exp}}} - \sum_i \nu_i \ln X_i^{\text{id}}. \tag{2.44}$$

The activity is defined relative to a standard state of the pure species at P and T of interest.

In order to introduce the volume integrals of the fluid species into equation 2.43 equation 2.38 is used or equation 2.42 is expanded directly to obtain:

$$\sum_i \nu_i X_i^{\text{exp}} \int_{1\,\text{bar}}^{P} V_{e_i} dP = \sum_i \nu_i RT \ln \frac{X_i^{\text{id}}}{X_i^{\text{exp}}}. \tag{2.45}$$

For a mixture in which all fluid species take part in a reaction, and which all have identical stoichiometric coefficients, the left-hand-side of equation 2.45 becomes equal to the molar excess volume of the mixture (see equation 2.29):

$$\int_{1\,\text{bar}}^{P} V_e^T dP = \sum_i RT \ln \frac{X_i^{\text{id}}}{X_i^{\text{exp}}}. \tag{2.46}$$

For convenience equations 2.44 and 2.45 are made independent of the magnitude of the stoichiometric coefficients by normalizing them to unity by introducing a normalized stoichiometric coefficient η_i:

$$\eta_i = \frac{\nu_i}{\sum_i \nu_i}. \tag{2.47}$$

For computer manipulation of a large number of phase equilibrium experiemnts it is convenient to generalize the above expressions to deviations from ideality at arbitrarily chosen pressure, temperature and fluid composition. Relationships analogous to equations 2.36 and 2.37 lead to:

$$\mathcal{G}^{P^{\rm exp},T^{\rm exp}} - \mathcal{G}^{P^{\rm id},T^{\rm id}} = \sum_i \nu_i R(T^{\rm id} - T^{\rm exp}) \left(\ln X_i^{\rm id} - \ln \frac{f_i^{P^{\rm exp},T^{\rm exp},X_i^{\rm exp}}}{f_i^{\circ P^{\rm exp},T^{\rm exp}}} \right). \tag{2.48}$$

The reference state is that of a pure fluid at P and T of interest. Note that this relationship is not independent of the thermophysical properties of the minerals involved in the equilibrium. The computation of $\mathcal{G}$ is described by Berman (1988) and in chapter 1 (equation 1.1) for stoichiometric phases. For numerical optimizations where fluid properties are to be constrained and where thermophysical parameters of selected minerals are to be adjusted simultaneously, the computing time required for the algorithm may become substantial.

2.6 P–V–T–X Properties Constrained by Phase Equilibrium Data

Similar to the method developed in chapter 1 for pure CO_2 phase equilibrium experiments involving a H_2O–CO_2 mixture may be used to put bounds on the integrated partial molar excess volumes (fugacity) of CO_2 and/or H_2O. The combined bounds from many experimental half–brackets, which each put one inequality constraint of the form of equation 2.48, will confine any equation of state within feasible limits with respect to measured phase equilibria. This may be used to test existing equations of state or to constrain parameters of a new equation using numerical optimization procedures analogous to those

outlined in chapter 1.

This approach is valid if the following requirements are fulfilled: i) the thermophysical properties of the minerals involved are accurately known, ii) the constraining phase equilibrium experiments are trustworthy, iii) the standard state thermodynamic properties of the fluid (i.e. the pure species at P and T of interst) to which the excess volumes on mixing are related to is accurately known, and iv) the presence of significant species other than CO_2 and H_2O in the experimental charges can be ruled out. Some mathematical form of an equation of state must be adopted. More details and a possible approach are discussed in a later section after evaluation of the available experimental data.

This thesis proceeds only as far as a thorough review of existing data and equations of state, for reasons discussed below, and does not offer a new equation of state for H_2O–CO_2 mixtures. The approach outlined above leads to a focussed review of existing work with respect to suspect data and directing one to future experimental work that constrains thermophysical properties of fluids most efficiently.

2.7 P–V–T–X Data on H_2O–CO_2 Mixtures

Appendix E contains a series of pressure *versus* volume and fluid composition *versus* volume diagrams comparing measured volumes of H_2O–CO_2 mixtures to several equations of state already introduced in a previous section. A brief account of the experimental methods for all relevant studies is provided in the same appendix partly because several publications are written in German and in Russian.

The most striking feature apparent from inspection of the figures in appendix E are the substantial inconsistencies between data sets of Franck & Tödheide (1959), Greenwood

(1973), Gehrig (1980) and Shmulovich *et al.* (1979, 1980). There is reasonable agreement, although not within stated experimental uncertainties, between data by Greenwood (1973) and Gehrig (1980). The Kerrick & Jacobs (1981) equation of state which reproduces experimentally measured phase equilibria quite well (Berman, 1988, Jacobs & Kerrick, 1981c, and discussion below) loosely approximates the data by Greenwood and Gehrig between 400–600 °C. It is concluded that the volumes measured by Franck & Tödheide are most likely in error, particularly at pressures below 1 kbar, and should not be used. Franck & Tödheide's data were used by de Santis *et al.* (1974) for a modification of the Redlich & Kwong equation of state which was subsequently adopted by Holloway (1977), Flowers & Helgeson (1983) and Bowers & Helgeson (1983) (see discussion of equations of state above).

Franck & Tödheide's data above 1.4 kbar are not included in the figures of this appendix due to large uncertainties compared to the small volume effect on mixing at high pressures. These uncertainties are a result of not reporting P-V-T data on the pure fluids. For the computation of the excess volume below 1.4 kbar the pure gas data of Kennedy (1954) and Holser & Kennedy (1958, 1959) were used (figures E.36 to E.45 in appendix E) which Franck & Tödheide state to agree within 1 % of their measurements. The same procedure had to be adopted for the data of Gehrig (1980) who reported data of the mixtures between X_{CO_2}= 0.1–0.9 but none for the pure fluids. Shmulovich *et al.* (1980) measured volumes at 400 and 500 °C and selected fluid compositions between 1 and 5 kbar. The data are plotted up to 2 kbar in figures E.37 and E.40. Shmulovich's measurements are probably of good quality and extrapolate reasonably from data at lower pressures. Measurements by Shmulovich *et al.* (1979) at 400 and 500 °C from 150–1000 bar and 400–5700 bar show excess volumes significantly larger than all of the other data over much of the range measured.

It is not possible to relate the apparently erroneous measurements of Franck &

Tödheide (1959) to any particular cause in their experimental method (appendix E). A combination of several causes seems possible: i) the large volume of connections relative to the volume of the bomb which may introduce larger uncertainties due to thermal gradients than are suggested by their calibration; ii) the measurement of the volume of the bomb with the mercury method tends to underestimate the volume (Greenwood, 1969); iii) the copper packing of the Bridgman seal can creep, leading to an increase of the bomb volume with time and thus to underestimated volumes; and iv) the possibility of an incremental change in fluid composition each time the valve to the pressure gauge is opened.

An interesting and important feature of the measured P-V-T-X properties is the negative volumes on mixing observed by Greenwood (1969, 1973) at temperatures above 600 °C and pressures below 300-400 bar. If these measurements are correct, significant chemical association must occur in order to reverse the positive volume effect resulting from dispersion forces alone. Fugacity coefficients (the integrated partial molar excess volume weighted by its mole fraction) may be substantially smaller in this range compared to predictions from equations of state (i.e. Kerrick & Jacobs, 1981) that do not account explicitly for some mode of chemical association. The Holloway–Flowers equation (Holloway, 1977, Flowers, 1979) which accounts for formation of carbonic acid (de Santis *et al.*, 1974) does not represent Greenwood's (1973) data better (see appendix E).

In summary it is concluded that a set of P-V-T-X data on CO_2–H_2O mixtures is much needed to resolve the inconsistencies and extend the range of pressure beyond that of Greenwood (1973) and Gehrig (1980) who measured up to 500 and 600 bar.

2.8 Phase Equilibrium Data Involving H_2O–CO_2 Mixtures

Berman (1988) presented a thermodynamic analysis of all equilibria relevant to this study with extensive graphical comparison of computed equilibria with experimental measurements. Some more recent experimental data on mixed–volatile equilibria involving magnesite and clinochlore were presented by Chernosky & Berman (1989). New data on the equilibrium calcite+andalusite+quartz $\rightleftharpoons$ anorthite+CO_2 in the presence of H_2O were reported in a preliminary form by Chernosky & Berman (1990). The system CaO–MgO–SiO_2–CO_2–H_2O was most recently addressed by Trommsdorff & Connolly (1990) with respect to some inconsistencies between phase diagram topologies computed with the data base of Berman (1988) and those derived from field observations (see discussion of magnesite in chapter 1).

The following discussion of data on selected phase equilibria builds on the analysis and figures of Berman (1988), who used the Kerrick & Jacobs (1981) equation of state for the H_2O–CO_2 mixtures. The abbreviation 'B88' refers to Berman (1988).

Calcite+quartz $\rightleftharpoons$ wollastonite+CO_2 (figure 8a, B88): Data by Ziegenbein & Johannes (1974, 2–6 kbar) are inconsistent with experiments by Greenwood (1967, 1–2 kbar) and Jacobs & Kerrick (1981c, 6 kbar). The latter two data sets are in accord with the thermodynamic data base of B88. The constraints on the equilibrium with pure CO_2 (Harker & Tuttle, 1956, 0.5–3 kbar) are only compatible with Greenwood's data, indicating that the experiments by Ziegenbein & Johannes (1974) are most likely in error. Some uncertainty in the properties of calcite exists due to the fact that B88 used constraints from mixed volatile equilibria and the equation of Kerrick & Jacobs (1981) which may deviate somewhat from reality.

Wollastonite+calcite+quartz $\rightleftharpoons$ grossular+CO_2 (figure 9a-c, B88): Only data by Gordon & Greenwood (1971, 1–2 kbar) could be reconciled by B88. Experimental

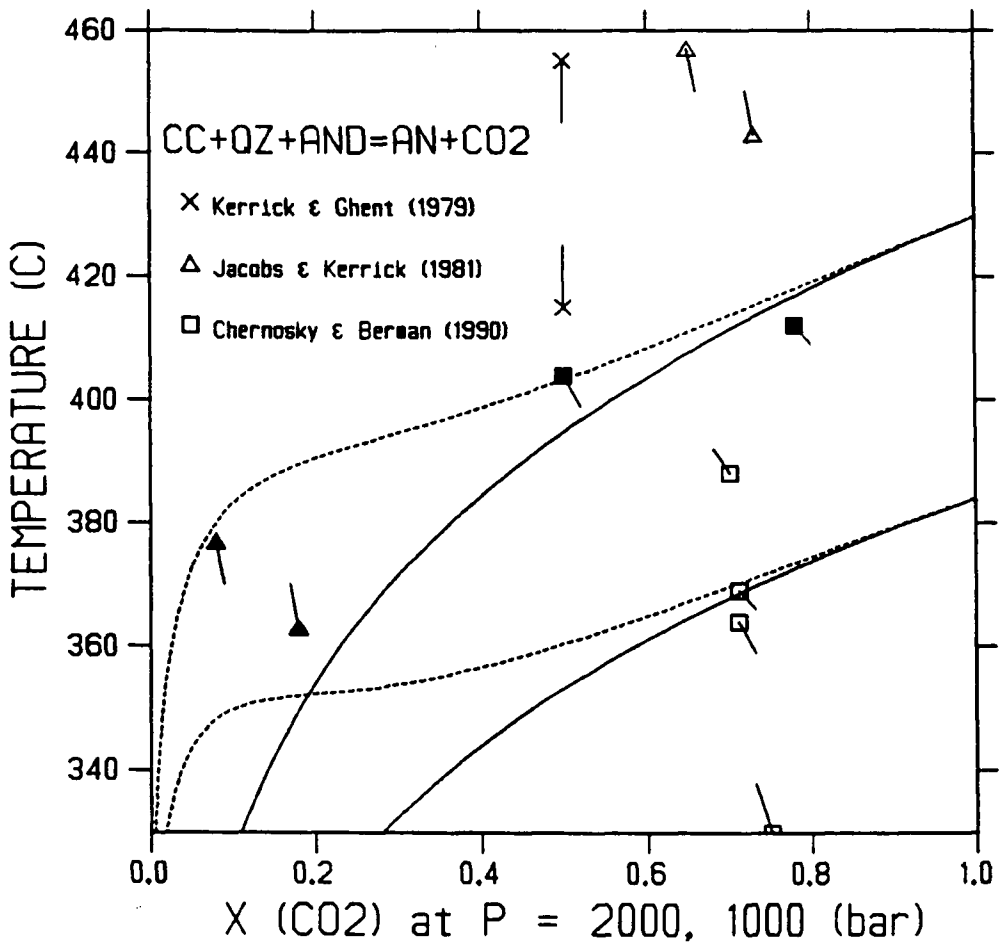

Figure 2.10: Equilibrium calcite+andalusite+quartz $\rightleftharpoons$ anorthite+CO_2 at 2 kbar. Solid curves are computed with the assumption of ideal mixing in the fluid phase. Dotted curves were computed with the Kerrick & Jacobs (1981) equation of state. See text for discussion of inconsistencies. Filled symbols refer to brackets that were used to constrain $RT \ln \gamma$ in figure 2.13. The diagram was produced with GEO-Calc (Brown *et al.*, 1988).

brackets by Shmulovich (1978, 1–6 kbar) and Hoschek (1974, 1 & 4 kbar) deviate too much from the position of the equilibrium assuming ideal mixing to be accounted for by positive deviations from ideality within the range of those computed with the Kerrick & Jacobs (1981) equation.

Calcite+andalusite+quartz $\rightleftharpoons$ anorthite+CO_2 (figure 2.10; figure 8c, B88): New data (Chernosky & Berman, 1990, 1–2 kbar) are reproduced by the B88 data base within the uncertainties of the thermodynamic properties of the minerals and render previous experiments by Jacobs & Kerrick (1981c, 2 kbar) and Kerrick & Ghent (1979, 2 kbar) distinctly inconsistent. An important implication is that the large observed deviations from ideal mixing in the fluid phase at these low tempeartures of Chernosky's experiments (350–410 °C) are reasonably reproduced by the Kerrick & Jacobs (1981) equation of state.

Calcite+kyanite+quartz $\rightleftharpoons$ anorthite+CO_2 (figure 8b, B88): Experiments by Jacobs & Kerrick (1981c, 6 kbar) and Kerrick & Ghent (1979, 6 kbar) between 450 and 580 °C are in reasonable agreement with the data base of B88, but do not put tight constraints on CO_2 fugacities.

System CaO–Al_2O_3–SiO_2–CO_2 at high T (figure 10a-f, B88): Experiments on equilibria in this system at temperatures of 670–850 °C amongst anorthite, calcite, grossular, gehlenite, corundum, wollastonite, and CO_2 diluted with H_2O have one trend in common: brackets by Hoschek (1974, 1 & 4 kbar) would demand negative deviations from ideal mixing in the fluid phase compared to the data base of B88. While negative deviations from ideality at high temperatures may be supported by P-V-T-X data of Greenwood (1973, c.f. appendix E) this discrepancy might equally well be due to errors in the data base or problems with the experimental study. One would expect that H_2O and CO_2 would mix almost ideally at these high temperatures and at an X_{CO_2} of 0.5–0.8 where this discrepancy is observed.

System CaO–MgO–SiO_2–CO_2 at high T (figure 24a-d, B88): Data by Zharikov *et al.*(1977, 1 kbar) on equilibria involving calcite, merwinite, monticellite, åkermanite, diopside, forsterite, periclase, CO_2 diluted with H_2O at temperatures of 700–950 °C demand slightly negative deviations from an ideally mixing fluid at X_{CO_2} between 0.15–0.3 which is the upper limit of the range examined. Such negative deviations from ideality at these conditions are reasonable in the light of Greenwood's (1973) P-V-T-X data which allow for negative deviations from ideality. Note that the Kerrick & Jacobs' (1981) model is virtually indistinguishable from ideality at these conditions.

System CaO–MgO–SiO_2–CO_2–H_2O (figure 27a-d & 28, B88): Experiments including tremolite–CO_2–H_2O±(diopside, forsterite, calcite, dolomite, quartz) at 430–700 °C (Chernosky & Berman, 1986, 1 kbar; Metz, 1967, 1 kbar; Metz, 1976, 5 kbar; Eggert & Kerrick, 1981, 6 kbar; Slaughter *et al.*, 1975, 2 kbar) are consistent with the data base of B88 with two exceptions: brackets on the reaction dolomite+tremolite ⇌ forsterite+ calcite+CO_2+H_2O at 0.5 kbar (Metz, 1967), and experiments on the equilibrium calcite+quartz+tremolite ⇌ diopside+H_2O+CO_2 at 1 and 5 kbar (Metz, 1970). This discrepancy is not fully explained by the effects of composition of Metz' natural tremolite (Campolungo, Switzerland) according to B88. Data by Slaughter *et al.* (1975, 1 & 5 kbar) on the latter reaction is consistent with the analysis of B88.

The equilibrium **quartz+dolomite+H_2O⇌ calcite+talc+CO_2** (figure 2.11) studied at 400–550 °C by Gordon & Greenwood (1970, 1–2 kbar), Metz & Puhan (1970, 1971, 1–5 kbar), Skippen (1970, 1–2 kbar) and Eggert & Kerrick (1981, 6 kbar) is consistent with the data base of B88 at pressures above 2 kbar. Data at 2 kbar at 425–450 °C and particularly at 1 kbar and 400 °C suggest more positive deviations from ideal mixing in the fluid phase than computed with the Kerrick & Jacobs (1981) equation of state.

Note that there is some uncertainty as to the ordering state of dolomite at higher temperatures (see discussion in B88).

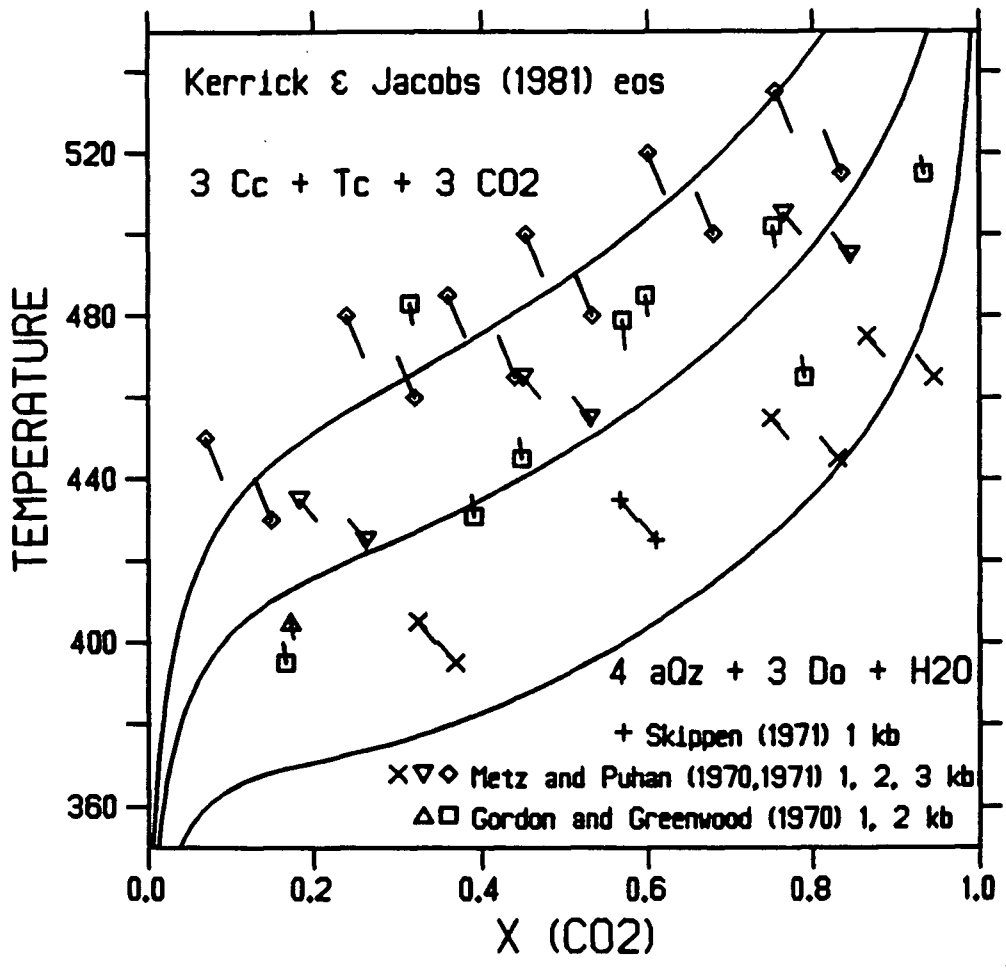

Figure 2.11: Equilibrium quartz+dolomite+H_2O $\rightleftharpoons$ calcite + talc+CO_2 at 1, 2 and 3 kbar. Curves were computed with the Kerrick & Jacobs (1981) equation of state. Experimental data at 5 and 6 kbar are not shown for clarity. See text for discussion of inconsistencies. The diagram was produced with GEO-Calc (Brown *et al.*, 1988).

System Al_2O_3–SiO_2–H_2O–CO_2 (figure 33a-b, B88): Experiments on equilibria involving clinochlore–calcite–diopside–forsterite–spinel–CO_2–H_2O± dolomite at 550–700 °C by Chernosky & Berman (1986, 1–2 kbar) and Widmark (1980, 1–4 kbar) are in reasonable agreement with the data base of B88. See discussion in B88 about the temperature dependence of the aluminum content of clinochlore which makes careful characterization of experimental charges nesessary.

Clinochlore+magnesite ⇌ forsterite+spinel+H_2O+CO_2 (figure 34a, B88): - Brackets on this equilibrium by Chernosky & Berman (1986, 1–4 kbar, 530–670 °C) are in good agreement with the data base of B88, but are displaced to slightly higher temperatures at 1–2 kbar using the new enthalpy for magnesite of chapter 1 which renders magnesite less stable. This discrepancy might be explained by more nonideal mixing in the fluid phase, although the effects of uncertainties in the order–disorder state of spinel could be significant as well.

System MgO–SiO_2–CO_2–H_2O (figure 34b-c & 35a-c, B88): Unreversed experiments that constrain only the high–temperature side of the equilibrium magnesite+ quartz+H_2O⇌ talc+CO_2 by Johannes (1969, 1–7 kbar, 330–610 °C) agree with B88.

Brackets on the reaction **magnesite+talc ⇌ forsterite+H_2O+CO_2** (figure 2.12) by Johannes (1969, 1–7 kbar, 480–660 °C) are at odds at 2 kbar with the analysis of B88 and expermemnts by Greenwood (1967, 1–2 kbar, 470–550 °C). Greenwood's data no longer agree with the computed equilibrium using the new enthalpy for magnesite derived in chapter 1. If thermodynamic properties of magnesite, talc, forsterite and the pure fluids are accurate this latter discrepancy must be due to too little positive deviation from ideality (less stable fluid phase) compared to the Kerrick & Jacobs (1981) equation, or due to problems with both Greenwood's and Johannes' experiments. There is some indication that the thermophysical properties of talc are in need of some revision (see discussion in section 'Conclusions' below).

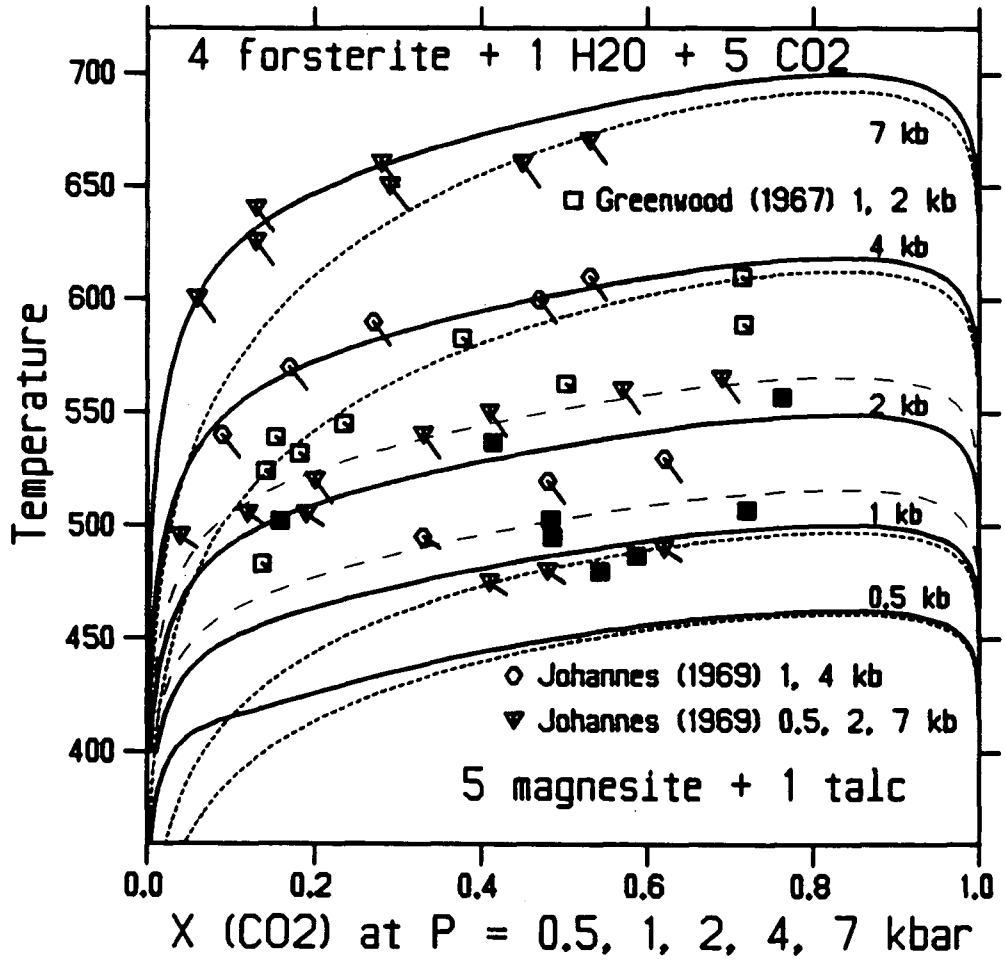

Figure 2.12: Equilibrium magnesite+talc $\rightleftharpoons$ forsterite+H_2O+CO_2 at 0.5, 1, 2, 4 and 7 kbar. Solid symbols depict experimental charges with the reactant–stable phase assemblage. Solid curves were computed with the Kerrick & Jacobs (1981) equation of state and magnesite properties as revised in chapter 1. The dotted curves at 0.5, 1, 4 and 7 kbar were computed with the assumption of ideal mixing in the fluid phase. The dashed curves at 1 and 2 kbar were computed with the magnesite properties of B88 and the Kerrick & Jacobs (1981) equation of state. See text for discussion of inconsistencies. The diagram was produced with GE0-calc (Brown *et al.*, 1988).

Brackets on three equilibria with magnesite and chrysotile (350–480 °C), talc, or anthophyllite (520–550 °C) by Johannes (1969, 1–4 kbar) at X_{CO_2} 0.03–0.08 do not put stringent constraints on the properties of the fluid mixture.

Systems with muscovite, phlogopite, paragonite, potassium feldspar, albite, H_2O, CO_2 (figure 40a-c & 41a-c, B88): Experiments on the breakdown of paragonite by Shvedenkov *et al.* (1983, 1 kbar, 460–510 °C) and that of muscovite+calcite+quartz by Hewitt (1973, 2–7 kbar, 450–620 °C) are in good agreement with the data base of B88. Brackets on the breakdown of muscovite+quartz in the presence of an H_2O–CO_2 fluid by Shvedenkov *et al.* (1973, 1 kbar, 450–520 °C) are displaced to lower temperatures relative to computed equilibria by 20–40 °C for reasons unknown (see discussion in B88). This latter equilibrium and that involving paragonite are the only reactions studied experimentally that involve H_2O diluted by CO_2.

Brackets on equilibria involving phlogopite by Bohlen (1983, 5 kbar, 775–800 °C), Puhan (1978, 4–6 kbar, 460–650 °C), Puhan & Johannes (1974, 2 kbar, 420–530 °C), Hoschek (1973, 2–6 kbar, 500–650 °C) and Hewitt (1975, 2–4 kbar, 460–520 °C) agree reasonably with the data base of B88. Several inconsistencies remain with experiments in the presence of pure H_2O. The problem of non-stoichiometry of phlogopite is discussed by Berman (1988) in this context.

Rutile+quartz+calcite $\rightleftharpoons$ sphene + CO_2 (figure 45, B88): Experiments at 6 kbar by Jacobs & Kerrick (1981c, 500–620 °C) are in good agreement with the data base of B88, but are shifted to higher temperatures at 2 kbar, 480–530 °C and X_{CO_2} at 0.4–0.8. This discrepancy of 25–45 °C is too large to be attributed solely to more nonideal mixing in the fluid phase than computed with the Kerrick & Jacobs (1981) equation of state.

While the body of experimental data including H_2O–CO_2 mixtures is substantial, incompatibilities amongst experimentalists studying the same equilibrium are disturbingly numerous. One reason for this is that such experiments are technically difficult to control with ample possibilities for errors that remain undetected. This places obvious difficulties on selecting experiments that put reasonable constraints on the deviation from ideal mixing of the fluid phase. Suggestions about which inconsistencies should be resolved experimentally are outlined in the concluding section along with proposed additional studies.

2.9 Results, Discussion and a Possible Approach

P-V-T-X data and existing equations of state:

Substantial inconsistencies exist between *P-V-T-X* data measured by different authors. The rough agreement between data of Greenwood (1969, 1973) and Gehrig (1980) and that of the Kerrick & Jacobs (1981) equation of state points towards errors in the measurements by Franck & Tödheide (1959). Data by Shmulovich *et al.* (1980) are difficult to evaluate at present but extrapolate reasonably from measurements ar lower pressures. Of particular interest is the negative volume effect on mixing observed by Greenwood at temperatures above 600 °C and pressures below 300–400 bar. Negative volumes would imply some form of chemical association which has consequences for the theoretical basis on which mixing rules are formulated. While the Holloway–Flowers–de Santis equation of state (Holloway, 1977, Flowers, 1979, de Santis *et al.*, 1974) does account for chemical association explicitly, it does not represent *P-V-T-X* data adequately. The Kerrick & Jacobs (1981) model does not allow for negative volumes on mixing but is in reasonable agreement with *P-V-T-X* data up to 600 °C and with much of the phase equilibria measured in a H_2O–CO_2 fluid.

Phase equilibrium data and constraints on fugacities:

A disturbing number of inconsistencies amongst different data sets exist which need to be resolved before all equilibria become useful as constraints on the fugacities of the fluid species in the mixture. The number of feasible experimental brackets is further decreased by those that are not very constraining due to large experimental uncertainties. Three examples of how a particular experimental datum puts a constraint on the fugacity are provided in figure 2.13 and discussed below.

Theory:

There is as yet no theory that could be adopted successfully to yield an equation of state for H_2O–CO_2 mixtures that covers the range of pressure, temperature and composition of interest to petrologists. Empirical extensions, mostly on van der Waals–like theory, are restricted by mixing rules that demand compatible mathematical forms for equations of the endmember fluids. Furthermore, analytic expressions for the fugacity of a species in the mixture are required for efficient numerical calculations, i.e. the equation of state must be integrable.

A possible approach:

Let us first consider improvements on existing equations of state. The obvious advantage of the Holloway–Flowers–de Santis equation (Holloway, 1977, Flowers, 1979, de Santis *et al.*, 1974) is that parameters for many fluid species are available, particularly those relevant to the system C–O–H. Improvements to an equation for one particular species are limited by the requirement of mathematical compatibility which dictates that the parameters a and b can only be functions of temperature. The derivation of equation 2.13, for example, includes integration at constant temperature and thus only modifications of the temperature dependence of a and b are permitted. In chapter 1 significant improvements on the equation of state for CO_2 could only be obtained by

introducing a volume (pressure) dependence of the b parameter. From P-V-T-X data and spectroscopic observations one would expect that the equilibrium constant for chemical association is a function of both temperature and pressure, and perhaps fluid composition. Again, an equilibrium constant dependent on pressure is not permissible if we must maintain mathematical compatibility. While minor improvements are possible based on an extended data base and more robust optimization techniques, major improvements would certainly demand more complex expressions for the parameters than permissible by the existing model.

A possible new approach would follow an alternate route in that the mixing properties are formulated independently of the pure fluids. This has the advantage that any equation of state for the pure fluid may be used. The disadvantage is that the extension of such a model to additional fluid species such as methane, carbon monoxide, hydrogen and oxygen is more complex. Two approaches may be taken: i) a mathematical model that describes the excess volume of the mixture as a function of pressure, temperature and fluid composition; ii) a mathematical model that directly describes the logarithm of the fugacitiy of a fluid species as a function of pressure, temperature and fluid composition.

Both approaches would require reliable P-V-T-X data over a much larger range in pressure than available at present. It may be advantagous to modify option i) such that the partial molar excess volume is expressed as a function of P, T and X_{CO_2} which would facilitate easy computation of fugacities by integration with respect to pressure. The measured excess volumes of the mixture would then constrain the combination of the partial molar excess volumes of H_2O and CO_2 which requires integration with respect to X_{CO_2}. Using option ii) care must be taken in choosing meaningful P, T and X_{CO_2} dependencies of the function describing the logarithm of the fugacity, i.e. the integrated partial molar volume. Powell & Holland (1985), for example, choose a linear dependence

on pressure and temperature which cannot be justified and must lead to significant deviations and uncertain extrapolation properties.

The dependence on fluid composition could be treated with a Margules parameter formulation which has the advantage of providing mathematically tractable expressions on integration and differentiation. One could follow traditional avenues for formulating the excess Gibbs potential on mixing, G^{ex}_{mix} (i.e. Brown, 1977, Berman & Brown, 1987):

$$G^{ex}_{mix} = W_{G12}X_1X_2^2 + W_{G21}X_1^2X_2 = RT(X_1 \ln \gamma_1 + X_2 \ln \gamma_2) \tag{2.49}$$

This two–parameter Margules expansion may easily be expanded to allow for more flexibility in the dependence of the excess properties on composition. If one were to follow the approach commonly adopted for solid solutions, the pressure and temperature dependence of the excess Gibbs potential could be incorporated by suitable expansion:

$$W_G = W_H - TW_S + (P-1)W_V \tag{2.50}$$

The last term including W_V stems from the assumption of constant volume and is not adequate for a solution of fluids where the volume term will form the largest contribution to the excess Gibbs potential. The first two terms are neglected in the subsequent treatement for simplicity but could easily be incorporated if required. Some pressure and temperature dependence of W_V is chosen arbitrarily:

$$W_G = \int_{1bar}^{P} W_V(P,T)\, dP \tag{2.51}$$

The volume of the mixture can then be obtained by differentiation of the excess Gibbs function with respect to pressure:

$$\begin{aligned} V^{ex}_{mix} &= \left(\frac{\partial G^{ex}_{mix}}{\partial P}\right)_{T,X} = \left(\frac{\partial W_{G12}}{\partial P}\right)_{T,X} X_1X_2^2 + \left(\frac{\partial W_{G21}}{\partial P}\right)_{T,X} X_1^2X_2 \\ &= W_{V12}(P,T)X_1X_2^2 + W_{V21}(P,T)X_1^2X_2 \end{aligned} \tag{2.52}$$

Although the approximate shape is known from figures E.36 to E.54, the exact mathematical form of the functions describing the W_V parameters or the partial molar excess volume has not been established. Perhaps one could borrow from some formulations used in profile fitting of diffraction patterns (Howard & Preston, 1989).

Constraints from phase equilibrium experiments may be incorporated as outlined in a previous section and discussed in detail in chapter 1. Each half–bracket puts an inequality constraint derived from equation 2.48 on the integrated partial molar excess volume. All constraints from valid experimental data combined define a feasible region for adjustable parameters in an equation of state that are consistent with all constraining equilibria. The formulation of the inequality constraints require integration and possibly differentiation of the equation of state. For all but the simplest equations of state the problem becomes non–linear.

Figure 2.13 illustrates how experimental half–brackets put constraints on the logarithm of the fugacity of CO_2. These examples are taken from an equilibrium which involve CO_2 diluted by H_2O: calcite + andalusite + quartz $\rightleftharpoons$ anorthite + CO_2 (figure 2.10). The constraints are obtained from the displacement of the experimental datum from a hypothetical position assuming ideal mixing in isobaric–isothermal sections. See section 'Thermodynamic Relationships' and figure 2.9 for details. Results are compared to several equations of state.

Mathematical programming offers an appropriate formalism for such an approach and computer codes are readily available (see chapter 1, section 'Method' for details). Parameters for the model describing the excess properties on mixing would be optimized to *P-V-T-X* data and simultaneously subject to constraints from phase equilibrium experiments. If standard state properties for selected solid phases are to be derived simultaneously the optimization may become computationally time consuming.

Walter (1963) and Ziegenbein & Johannes (1982) also tried to constrain the fugacity

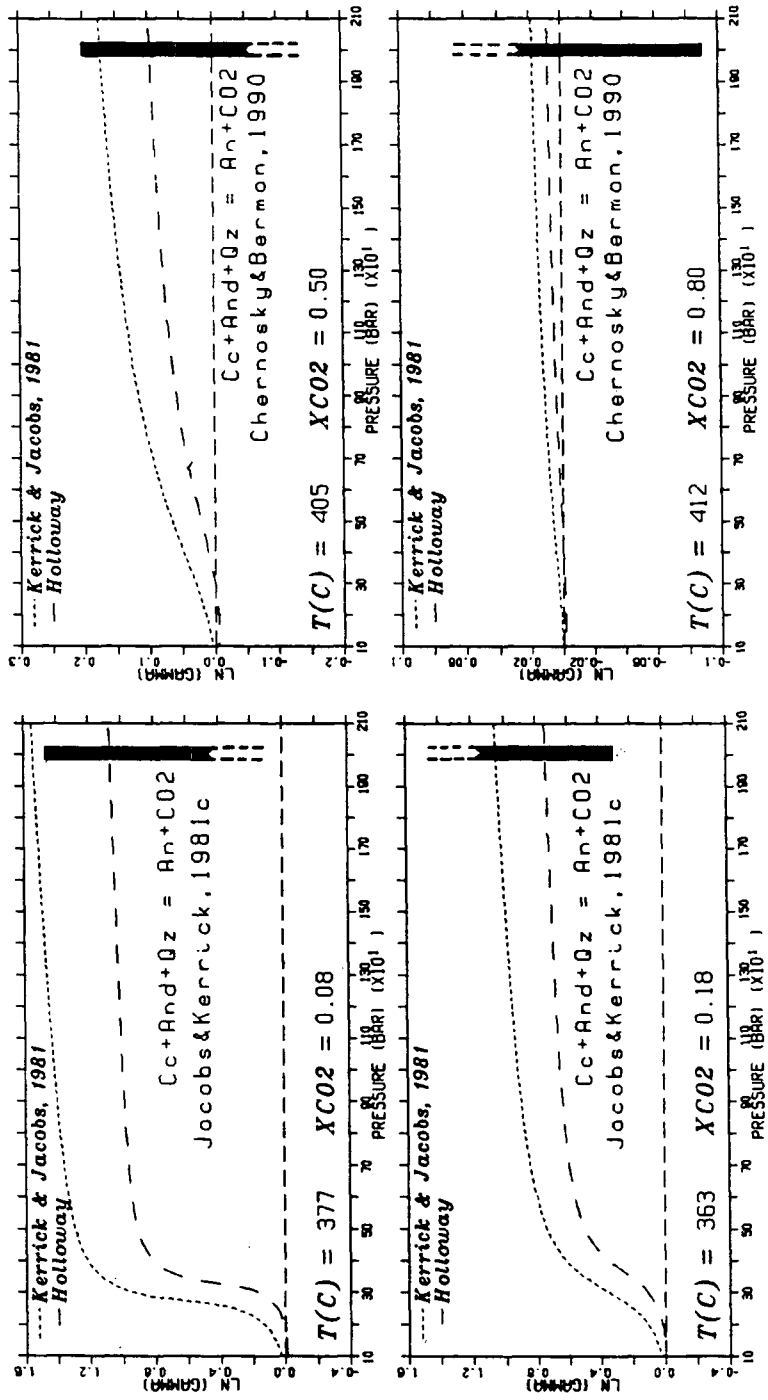

Figure 2.13: Graphs of $\ln \gamma$ *versus* pressure for CO_2 comparing phase equilibrium brackets to equations of state by Kerrick & Jacobs (1981) and Holloway, 1977 (see section 2.4 for equation of state parameters). Each vertical bar represents the range in $\ln \gamma$ permissible by one particular exparimental half–bracket on the equilibrium calcite + andalusite + quartz $\rightleftharpoons$ anorthite + CO_2. The figures on the left show two half–brackets by Jacobs & Kerrick (1981c) at 363 and 377 °C, including uncertainties. The figures on the right show half–brackets by Chernosky & Berman (1990) at 405 and 412 °C. See figure 2.10 for location of the experiemntal data.

of CO_2 in a H_2O–CO_2 mixture from experimentally measured phase equilibria. Walter (1963) used data on the equilibrium magnesite $\rightleftharpoons$ periclase + CO_2 in the presence of H_2O (Walter *et al.*, 1962), and Ziegenbein & Johannes (1982) used measurements on the reaction calcite + quartz $\rightleftharpoons$ wollastonite + CO_2 diluted with H_2O (Ziegenbein & Johannes, 1974). The results are limited by the consideration of a single equilibrium which leads to curves of activity *versus* fluid composition at constant pressure that are polythermal, i.e. the temperature is rising with increasing X_{CO_2}. Ziegenbein & Johannes (1982) derive deviations from ideal mixing that are much larger than those computed from the Holloway–Flowers (Holloway, 1977, Flowers, 1979) equation of state or those derived by Ryzhenko & Malinin (1971) from *P-V-T-X* data. This is because experimental data by Ziegenbein & Johannes (1974), on which the analysis in their 1984 paper is based, are shifted distinctly to lower temperatures compared to brackets by Greenwood (1967) and the data base of Berman (1988) and also are not compatible with experiments in pure CO_2 by Harker & Tuttle (1956).

2.10 Conclusions and Future Work

From the discussions in the previous sections and the data presented throughout chapter 2 and appendix E, it is concluded that at present insufficient experimental data and inadequate theoretical foundations are available on which to build a constrained empirical model that allows one to compute fugacities of H_2O–CO_2 mixtures over the range of pressure and temperature of interest to petrologists. However, the existing body of data is extensive enough that the effort needed to provide additional information is not insurmountable. The following problems or lack of data deserve particular attention:

1. Inconsistensies amongst existing sets of *P-V-T-X* measurements must be resolved and the range of pressure must be increased to at least 8 kbar by a complete series

of *P-V-T-X* measuruements.

2. Several inconsistencies amongst studies on phase equilibria involving H_2O–CO_2 mixtures need to be resolved in order to permit refinement of thermophysical properties of solid phases which will then provide better constraints on the fluid mixture. Numerous inconsistencies are addressed by Berman (1988) which may serve as a guide for designing the most useful experiments. Several examples are presented below.

3. Phase equilibria involving H_2O–CO_2 mixtures can be utilized to constrain deviations from ideal mixing where *P-V-T-X* data are not available. Deviations are pronounced at low temperatures where resolution would be best for experimental work. *P-V-T-X* measurements are not yet possible above 15 kbar which render phase equilibrium studies the only means with which to examine deviations from ideality at high pressures. Several equilibria that could be studied in a piston–cylinder apparatus are proposed below.

4. At present there are hardly any constraints from phase equilibrium data on the activity of H_2O in a H_2O–CO_2 mixture at any pressure and temperature. Several possible studies to supply such information are discussed below.

The last few sections below are devoted to specific experimental projects that are feasible with the technology and equipment available in many petrologic laboratories. Some of the projects may be realized in a one–month time frame while others would require two years of concentrated effort.

Proposed P-V-T-X experiments:

To resolve inconsistencies amongst existing studies (appendix E) and to form a firm basis for an equation of state, an extensive *P-V-T-X* study is required that covers at least the range 200–8000 bar and 200–800 °C and the entire compositional space. Such

experiments would best be done in an internally heated gas apparatus furnished with an expandable noble metal sample container ('accordion type') and an attached linear voltage differential transducer (LVDT) to measure linear expansion of the sample 'bag'. This linear expansion can be calibrated with well known gases (i.e. argon, water) to yield volumes of the 'bag' at measured displacements. Such a pressure vessel with a large enough volume can be purchased 'off the shelf' with modifications necessary to install the LVDT mechanism and temperature probes to control thermal gradients. Furnace assemblies can be machined from pyrophyllite to any shape desired. 'Accordion bags' are commercially available, commonly made of gold. This apparatus could be designed to hold pressures up to 12–15 kbar, but vessels with a large volume are difficult to seal at these pressures and store a dangerous amount of energy in the form of compressed hot fluids.

In order to obtain excess volumes of sufficient precision from the difference of two large numbers, the volume of the mechanical mixture and the measured volume of the mixture, the volumes of the pure fluids must be measured as precisely as possible. A precision of at least ± 0.5 % is required to yield an excess volume with a precision of ± 1 % of the volume of the mixture. At pressures below 300 bar the precision has to be much better. Because of the limited expansion of the sample bags the proposed pressure range is only accessible with repeat runs that contain different amounts of sample. The appropriate pressure intervals are approximately 200–500 bar, 500–2000 bar, and 2000–8000 bar.

While not the entire range of composition is of importance to geologists it is required to constrain the partial molar volumes which are used to compute fugacities (see section 'Thermodynamic Relationships'). In this respect it is important to undertake measurements at very small and very large mole fractions of CO_2. Ideally, one would like to obtain data at X_{CO_2}= 0.05, 0.1, 0.2, 0.3, 0.4, 0.5, 0.6, 0.7, 0.8, 0.9, and 0.95. Furthermore, any empirical equation of state gains strength from a large number of measurements.

One problem that needs attention is hydrogen diffusion through gold at elevated temperatures. Container materials different from gold could be used and run times should be kept as short as possible. Alternatively, one could impose externally a hydrogen fugacity close to the one predicted to occur in the mixture and thus remove gradients. Some monitor of speciation should be incorporated to assertain the presence of H_2O and CO_2 as the dominant species. Perhaps the hydrogen or oxygen fugacity could be measured by some means that does not affect the sample mass in an uncontrollable way.

A *P-V-T-X* project of the proposed extent is a major undertaking that probably requires 2 years of concentrated effort. The proposed phase equilibrium studies require less effort and are experimentally not as difficult as *P-V-T-X* measurements.

Proposed phase equilibrium studies:

5 magnesite + 1 talc ⇌ 4 forsterite + 1 H_2O + 5 CO_2: New brackets on this equilibrium (see figure 2.12) would resolve the inconsistencies amongst data by Johannes (1969) and Greenwood (1967). It would put further constraints on the enthalpy of magnesite as well as put some limits on the deviation from ideal mixing of the fluid phase. This is an easy experiment to do which would require only one tight bracket at 1, 2 and possibly 5 kbar, placed at the culmination of the T–X curve at a fluid composition of X_{CO_2}=5/6. An experiment with this starting fluid composition and both reactant and product assemblages present will remain at constant fluid composition during the experiment. Four to six experiments spaced 5 K apart are probably all that is required to obtain a very tight reversal at a given pressure. All minerals involved can readily be synthesized and are relatively reactive. From Greenwood's (1967b) experience it appears that run times of 15–20 days are sufficient.

Equilibria involving margarite: The proposed studies would aim at providing constraints on the activity of H_2O in a H_2O–CO_2 mixture in a temperature range where

deviations from ideality are expected to be significant. Equilibria with margarite in pure H_2O have been studied previously by Jenkins (1984), Storre & Nitsch (1974), Nitsch *et al.* (1981), Chatterjee *et al.* (1984), and Chatterjee (1974). All data are consistent with the analysis of Berman (1988, figures 13a-e) with one obvious exception of the brackets by Storre & Nitsch on the equilibrium margarite + quartz ⇌ kyanite + zoisite + H_2O that cannot be reconciled with any other data.

The two equilibria suitable for study in a mixed fluid are: 1 margarite + 1 quartz ⇌ 1 andalusite + 1 anorthite + 1 H_2O and 1 margarite ⇌ 1 anorthite + 1 corundum + 1 H_2O (figure 2.14). The range accessible to experimentation at 2 kbar fluid pressure spans 400–500 °C and X_{CO_2} = 0.0–0.7. The range in temperature may be increased by studying the equilibria at pressures below and above 2 kbar. At 1 kbar the isobarically invariant point margarite–quartz–andalusite–anorthite–calciteis predicted to be at 375 °C and X_{CO_2} = 0.78 with the data base of Berman (1988).

Margarite becomes metastable with respect to calcite + andalusite at fluid compositions larger than X_{CO_2} = 0.7. The equilibrium, 1 margarite + 1 CO_2 ⇌ 1 calcite + 2 andalusite + 1 H_2O, has a very large $\partial T/\partial X$ at constant pressure such that it could form tight constraints on the position of invariant points and thus thermodynamic properties of phases involved. The ratio of the stoichiometric coefficients of H_2O and CO_2 is 1:1 which allows one to relate deviations from ideality directly to the molar excess volume of the mixture (equation 2.46). Constraints on the temperature at the culmination of the equilibrium 1 calcite + 1 margarite + 2 quartz ⇌ 2 anorthite + 1 H_2O + 1 CO_2 at X_{CO_2} = 0.5 would pose constraints similar to those of the previous equilibrium. This reaction could be investigated with the strategy already discussed for the magnesite–talc–forsterite equilibrium.

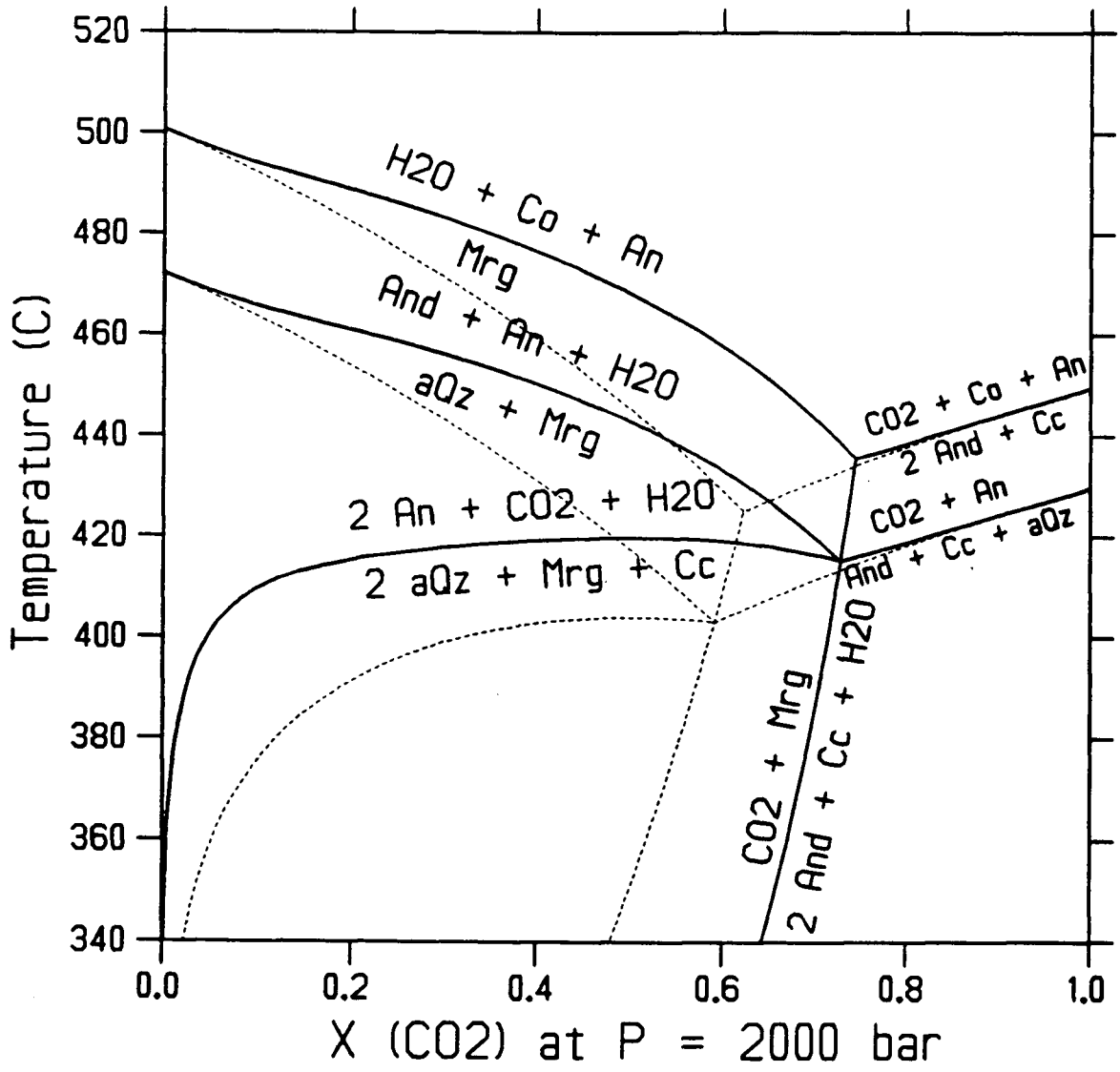

Figure 2.14: Phase diagram with equilibria involving margarite (Mrg), andalusite (And), corundum (Co), quartz (aQz), anorthite (An), H_2O and CO_2 at 2 kbar pressure. The solid curves were computed with the Kerrick & Jacobs (1981) equation of state. Dotted lines were calculated assuming ideal mixing in the fluid phase. Reactions with zoisite or grossular that modify the diagram at very H_2O–rich compositions are not shown. The diagram was computed with GEO-Calc (Brown *et al.*, 1988).

While many other hydrous phases exist, most of them are not suitable for our purposes because their stabilities are limited to water–rich fluid compositions. At temperatures above approximately 500 °C **anthophyllite** would be accessible to experimentation over a large range of fluid compositions. There is however some debate at present with respect to thermophysical properties of anthophyllite (the volume in particular) and possibly talc (B.W. Evans and R.G. Berman, pers. comm., June 1990). Experiments involving anthophyllite would therefore be appropriate in the context of resolving these uncertainties rather than deriving constraints on the fluid mixture.

Equilibria at pressures greater than 15 kbar: Such studies would aim at constraining deviations from ideal mixing in the fluid phase at pressures not accessible by *P-V-T-X* mesurements. Experiments at pressures beyond that attainable in gas apparati have to be performed in solid–media pressure vessels such as the piston–cylinder apparatus used for work presented in appendix C. The obvious disadvantages are the small sample volume and the difficulty in controlling fluid composition, speciation in the fluid phase and diffusion of hydrogen at high temperatures. Sample charges are best externally buffered at some oxidation potential high enough to ensure the absence of significant amounts of species other than H_2O and CO_2. Alternately, if the fugacities of other species are known corrections may be applied.

Suitable equilibria should include only solid phases that are thermodynamically well known and which are constrained experimentally in the presence of pure CO_2 or pure H_2O. Furthermore, only H_2O or CO_2 should take part in the reaction and the slope of these dehydration/decarbonation reactions should have a large dP/dT in order to improve resolution. Because only the relative displacement from the equilibrium in the presence of the pure fluid is sought some of the uncertainties arising from extrapolation of thermodynamic properties cancel. The possibilities are too numerous to be discussed

in detail but preference should be given to equilibria that may be studied at high pressures and relatively low temperatures in order to decrease experimental uncertainties and errors arising from extrapolated thermodynamic properties. Feasible studies include the reactions:

1. 2 diaspore $\rightleftharpoons$ corundum + 1 H_2O (580 °C at 20 kbar)
2. 1 forsterite + 1 tremolite $\rightleftharpoons$ 5 enstatite + 2 diopside + 1 H_2O (650 °C at 20 kbar)
3. 1 talc + 1 forsterite $\rightleftharpoons$ 5 enstatite + 1 water (700 °C at 20 kbar)
4. 1 talc $\rightleftharpoons$ 3 enstatite + 1 quartz + 1 H_2O (800 °C at 20 kbar)
5. 1 brucite $\rightleftharpoons$ 1 periclase + 1 H_2O (950 °C at 20 kbar)
6. 1 magnesite + 1 coesite $\rightleftharpoons$ 1 forsterite + 1 CO_2 (1100 °C at 35 kbar)
7. 1 calcite + 1 quartz $\rightleftharpoons$ 1 wollastonite + 1 CO_2 (1350 °C at 20 kbar)

In order to resolve deviations from ideal mixing in the fluid phase the best precision possible has to be achieved, which is about ± 5 K for piston–cylinder work. This author is not convinced at present whether piston–cylinder work can be successfully applied as proposed to yield results of the desired quality. Only a trial will demonstrate feasibility of such experiments.

Bibliography

[1] Anderson, G.M. 1977, Fugacity, activity, and the equilibrium constant. In: Greenwood, H.J., (ed.), Short Course in Application of Thermodynamics to Petrology and Ore Deposits. *Miner. Assoc. Canada*, Short Course Handbook, **2**, 17–37.

[2] Angus, S., Armstrong, B., & de Reuck, K.M. (eds.), 1973, International Thermodynamic Tables of the Fluid State, Vol. 3: Carbon Dioxide. Pergamon Press.

[3] Berman, R.G., 1988, Internally–consistent thermodynamic data for minerals in the system Na_2O–K_2O–CaO–MgO–FeO–Fe_2O_3–Al_2O_3–SiO_2–TiO_2–H_2O–CO_2. *J. Petrol.*, **29**, 445–522.

[4] Berman, R.G., & Brown, T.H., 1987, Development of models for multicomponent melts: analysis of synthetic systems. In: Carmichael, I.S.E. & Eugster, H.P. (eds.), Thermodynamic Modeling of Geological Materials: Minerals, Fluids and Melts. *Miner. Soc. Am., Rev. Mineral.*, **17**, 405–442.

[5] Bohlen, S.R., Wall, V.J., & Clemens, J.D., 1983, Stability of phlogopite–quartz and sanidine–quartz: a model for melting in the lower crust. *Contr. Miner. Petrol.*, **83**, 270–277.

[6] Bottinga, Y., & Richet, P., 1981, High pressure and temperature equation of state and calculation of thermodynamic properties of gaseous carbon dioxide. *Am. J. Sci.*, **218**, 615–660.

[7] Bowers, T.S., & Helgeson, H.C., 1983, Calculation of the thermodynamic and geochemical consequences of nonideal mixing in the system H_2O–CO_2–NaCl on phase relations in gelogic systems: equation of state for H_2O–CO_2–NaCl fluids at high pressures and temperatures. *Geochim. Cosmochim. Acta*, **27**, 1247–1275.

[8] Bowers, T.S., & Helgeson, H.C., 1985, Fortran programs for generating fluid inclusion isochores and fugacity coefficients for the system H_2O–CO_2–NaCl at high ressures and temperatures. *Comp. Geosci.*, **11**, 203–213.

[9] Brodholt, J., & Wood, B., 1990, Molecular dynamics simulations of water at high temperatures and pressures. *EOS, Trans., Am. Geophys. Union*, **71**, 621.

[10] Brown, T.H., 1977, Introduction to non–ideal and complex solutions. In: Greenwood, H.J., (ed.), Short Course in Application of Thermodynamics to Petrology and Ore Deposits. *Miner. Assoc. Canada*, Short Course Handbook, **2**, 126–135.

[11] Brown, T.H., Berman, R.G., & Perkins, E.H., 1988, GE0–calc: Software package for calculation and display of pressure–temperature–composition phase diagrams using an IBM or compatible personal computer, *Comp. Geosci.*, **14**, 279–289.

[12] Burnham, C.W., Holloway, J.R., & Davis, N.F., 1969, The specific volume of water in the range 1000 to 8000 bars, 20 °C to 900 °C. *Am. J. Sci.*, **267-A**, 70–95.

[13] Carnahan, N.F., & Starling, K.E., 1972, Intermolecular repulsions and the equation of state for fluids. *Am. Inst. Chem. Eng.*, **18**, 1184–1189.

[14] Chatterjee, N.D., 1974, Synthesis and upper stability limit of 2M–margarite, $CaAl_2[Al_2Si_2O_{10}(OH)_2]$. *Schweizer. Mineral. Petrograph. Mitt.*, **54**, 753–767.

[15] Chatterjee, N.D., Johannes, W., & Leistner, H., 1984, The system $CaO–Al_2O_3–SiO_2–H_2O$: new phase equilibria data, some calculated phase relations, and their petrological applications. *Contr. Miner. Petrol.*, **88**, 1–13.

[16] Chernosky, J.V., & Berman, R.G., 1986a, The stability of clinochlore in mixed volatile, $H_2O–CO_2$ fluid. *EOS, Trans., Am. Geophys. Union*, **67**, 407.

[17] Chernosky, J.V., & Berman, R.G., 1986b, Experimental reversal of the equilibrium: clinochlore + 2 magnesite = 3 forsterite + spinel + 2 CO_2 + 4 H_2O. *EOS, Trans., Am. Geophys. Union*, **67**, 1279.

[18] Chernosky, J.V., & Berman, R.G., 1989, Experimental reversal of the equilibrium: clinochlore + 2 magnesite = 3 forsterite + spinel + 2 CO_2+ 4 H_2O and revised thermodynamic properties for magnesite. *Am. J. Sci.*, **289**, 249–266.

[19] Chernosky, J.V., & Berman, R.G., 1990, The equilibrium andalusite + calcite + quartz = anorthite + CO_2 revisited. *Geol. Ass. Can. Min. Ass. Can., Prog. Abstr.*, **15**, A23.

[20] Coan, C.R., & King, A.D., 1971, Solubility of water in compressed carbon dioxide, nitrous oxide, and ethane. Evidence for hydration of carbon dioxide and nitrous oxide in the gas phase. *J. Am. Chem. Soc.*, **93**, 1857–1862.

[21] DeCapitani, C., & Brown, T.H., 1987, The computation of chemical equilibrium in complex systems containing non–ideal solutions. *Geochim. Cosmochim. Acta*, **51**, 2639–2652.

[22] Delany, J.M., & Helgeson, H.C., 1978, Calculation of the thermodynamic consequences of dehydration in subducting oceanic crust to 100 kb and 800 °C. *Am. J. Sci.*, **278**, 638–686.

[23] Eggert, R.G., & Kerrick, D.M., 1981, Metamorphic equilibria in the silicious dolomite system: 6 kbar experimental data and geologic implications. *Geochim. Cosmochim. Acta*, **45**, 1039–1049.

[24] Eugster, H.P., & Skippen, G.B., 1967, Igneous and metamorphic reactions involving gas equilibria. In: Abelson, P.H., (ed.), Researches in Geochemistry, v. 2, John Wiley & Sons, New York, 492–520.

[25] Fei, Y., & Saxena, S.K., 1987, Fluid mixtures at crustal pressures and temperatures. *EOS, Trans., Am. Geophys. Union*, **68**, 451.

[26] Ferry, J.M., & Baumgartner, L., 1987, Thermodynamic models of molecular fluids at the elevated pressures and temperatures of crustal metamorphism. In: Carmichael, I.S.E. & Eugster, H.P. (eds.), Thermodynamic Modeling of Geological Materials: Minerals, Fluids and Melts. *Miner. Soc. Am., Rev. Mineral.*, **17**, 323–365.

[27] Flowers, G.C., 1979, Correction of Holloway's (1977) adaptation of the modified Redlich–Kwong equation of state for calculation of the fugacities of molecular species in supercritical fluids of geologic interest. *Contr. Miner. Petrol.*, **69**, 315–318.

[28] Flowers, G.C., & Helgeson, H.C., 1983, Equilibrium and mass transfer during progressive metamorphism of siliceous dolomites. *Am. J. Sci.*, **283**, 230–286.

[29] Franck, E.U., 1956, Hochverdichteter Wasserdampf I, II, III. Electrolytische Leitfähigkeit und Ionendissoziation von KCl. *Z. Phys. Chem. N. Folge*, **8**, 92–106, 107–126, 192–206.

[30] Franck, E.U., 1979, High pressure chemical kinetics: phenomena in fluids at high pressures and temperatures. In: Timmerhaus, K.D., & Barber, M.S., (eds.), High Pressure Science and Technology, v. 1, Physical Properties and Material Synthesis, 6th AIRAPT Conference, Plenum Press, 609–621.

[31] Franck, E.U., 1981, Survey of selected non–thermodynamic properties and chemical phenomena of fluids and fluid mixtures. In: Rickard, D.T., & Wickman, F.E., (eds.), Chemistry and Geochemistry of Solutions at High Temperature and Pressure. *Phys. Chem. Earth.*, **13 & 14**, 65–88.

[32] Franck, E.U., & Tödheide, K., 1959, Thermische Eigenschaften überkritischer Mischumgen von Kohlendioxid und Wasser bis zu 750 °C und 2000 atm. *Z. Phys. Chem. N. Folge*, **22**, 232–245.

[33] Franck, E.U., 1979, High pressure chemical kinetics: phenomena in fluids at high pressures and temperatures. In: Timmerhaus, K.D., & Barber, M.S., (eds.), High Pressure Science and Technology, v. 1, Physical Properties and Material Synthesis, 6th AIRAPT Conference, Plenum Press, 609–621.

[34] Franck, E.U., 1981, Survey of selected non–thermodynamic properties and chemical phenomena of fluids and fluid mixtures. In: Rickard, D.T., & Wickman, F.E., (eds.), Chemistry and Geochemistry of Solutions at High Temperature and Pressure. *Phys. Chem. Earth.*, **13 & 14**, 65–88.

[35] Franck, E.U., & Tödheide, K., 1959, Thermische Eigenschaften überkritischer Mischumgen von Kohlendioxid und Wasser bis zu 750 °C und 2000 atm. *Z. Phys. Chem. N. Folge*, **22**, 232–245.

[36] Franks, F., (ed.), 1972–1984, Water, a Comprehensive Treatise, v.1–v.7, Plenum Press, New York.

[37] Gehrig, M., 1980, Phasengleichgewichte und pVT–Daten ternärer Mischungen aus Wasser, Kohlendioxid und Natriumchlorid bis 3 kbar und 550 °C. Dissertation, Hochschulverlag, Freiburg, 149 pp.

[38] Ghiorso, M.S., & Carmichael, I.S.E., 1987, Modeling magmatic systems: petrologic applications. In: Carmichael, I.S.E. & Eugster, H.P. (eds.), Thermodynamic Modeling of Geological Materials: Minerals, Fluids and Melts. *Miner. Soc. Am., Rev. Mineral.*, **17**, 467–499.

[39] Gordon, T.M., & Greenwood, H.J., 1970, The reaction: dolomite + quartz + water = talc + calcite + carbon dioxide. *Am. J. Sci.*, **268**, 225–242.

[40] Gordon, T.M., & Greenwood, H.J., 1971, The stability of grossularite in H_2O–CO_2 mixtures. *Am. Miner.*, **56**, 1674–1688.

[41] Greenwood, H.J., 1961, The system $NaAlSi_2O_6$–H_2O–argon: total pressure and water pressure in metamorphism. *J. Geophys. Res.*, *66*, 3923–3946.

[42] Greenwood, H.J., 1967a, Wollastonite stability in H_2O–CO_2 mixtures and occurrence in a contact–metamorphic aureole near Salmo, British Columbia, Canada. *Am. Miner.*, *52*, 1669–1680.

[43] Greenwood, H.J., 1967b, Mineral equilibria in the system MgO–SiO_2–H_2O–CO_2. In: Abelson, P.H., (ed.), Researches in Geochemistry, v. 2, John Wiley & Sons, 542–567.

[44] Greenwood, H.J., 1969, The compressibility of gaseous mixtures of carbon dioxide and water between 0 and 500 bars pressure and 450° and 800° centigrade. *Am. J. Sci.*, **267-A**, 191–208.

[45] Greenwood, H.J., 1973, Thermodynamic properties of gaseous mixtures of H_2O and CO_2 between 450 °C and 800 °C and 0 to 500 bars. *Am. J. Sci.*, **273**, 561–571.

[46] Greenwood, H.J., & Barnes, H.L., 1966, Binary mixtures of volatile components. In: Clark, S.P., Jr., (ed.), Handbook of Physical Constants. *Geol. Soc. Am. Memoir*, *97*, 385–400.

[47] Haar, L., Gallagher, J.S., & Kell, G.S., 1984, NBS/NRC Steam Tables. Thermodynamic and transport properties and computer programs for vapor and liquid states of water in SI units. Hemisphere Publishing Co., Washington.

[48] Harker, R.I., & Tuttle, O.F., 1956, Experimental data on the P_{CO_2}–T curve for the reaction : calcite + quartz = wollastonite + carbon dioxide. *Am. J. Sci.*, **254**, 239–256.

[49] Helgeson, H.C., 1990, Organic/inorganic reactions in metamorphic processes. *Geol. Ass. Can. Min. Ass. Can., Prog. Abstr.*, **15**, A56.

[50] Helgeson, H.C., & Lichtner, P.C., 1987, Fluid flow and mineral reactions at high temperatures and pressures. *J. Geol. Soc. London*, **144**, 313–326.

[51] Hewitt, D.A., 1973, Stability of the assemblage muscovite–calcite–quartz. *Am. Miner.*, **58**, 785–791.

[52] Hewitt, D.A., 1975, Stability of the assemblage phlogopite–calcite–quartz. *Am. Miner.*, **60**, 391–397.

[53] Holland, T.J.B., & Powell, R., 1990, An enlarged and updated internally consistent thermodynamic dataset with uncertainties and correlations: the system K_2O–Na_2O–CaO–MgO–MnO–FeO–Fe_2O_3–Al_2O_3–TiO_2–SiO_2–C–H_2–O_2. *J. Metam. Geol.*, **8**, 89–124.

[54] Holloway, J.R. 1976, Fugacity and activity coefficients of molecular species in fluids at high pressures and temperatures. *Ann. Rep. of the Director, Geophysical Laboratory*, **Year Book 75**, 771–775.

[55] Holloway, J.R. 1977, Fugacity and activity of molecular species in supercritical fluids. In: Fraser, D.G. (ed.), Thermodynamics in Geology. D. Reidel, Dodrecht, Holland, 161–181.

[56] Holloway, J.R. 1981a, Volatile melt interactions. In: Newton, R.C., Navrotsky, A., & Wood, B.J., (eds.), Advances in Physical Geochemistry, **1**, 266–286.

[57] Holloway, J.R. 1981b, Compositions and volumes of supercritical volumes in the earth's crust. In: Hollister, L.S., & Crawford, M.L., (eds.), Fluid Inclusions: Applications to Petrology, *Miner. Assoc. Canada*, Short Course Handbook, **6**, 13–38.

[58] Holloway, J.R., 1987, Igneous fluids. In: Carmichael, I.S.E. & Eugster, H.P. (eds.), Thermodynamic Modeling of Geological Materials: Minerals, Fluids and Melts. *Miner. Soc. Am., Rev. Mineral.*, **17**, 211–233.

[59] Holloway, J.R, Eggler, D.H., & Davis, N.F., 1971, An analytical expression for calculating the fugacity and free energy of H_2O to 10,000 bars and 1300 °C. *Geol. Soc. Am. Bull.*, **82**, 2639–2642.

[60] Holser, W.T., & Kennedy, G.C., 1958, Properties of water. Part IV. Pressure–volume–temperature relations of water in the range 100–400 °C and 100–1400 bars. *Am. J. Sci.*, **256**, 744–753.

[61] Holser, W.T., & Kennedy, G.C., 1959, Properties of water. Part V. Pressure–volume–temperature relations of water in the range 400–1000 °C and 100–1400 bars. *Am. J. Sci.*, **257**, 71–77.

[62] Holzapfel, W., & Franck, E.U., 1966, Leitfähigkeit und Ionendissoziation des Wassers bei 1000 °C und 100 kbar. *Berliner Bunsenges. Phys. Chemie*, **70**, 1105–1112.

[63] Hoschek, G., 1973, Die Reaktion Phlogipit + Calcit + Quarz = Tremolit + Kalifeldspat + H_2O + CO_2. *Contr. Miner. Petrol.*, **39**, 231–237.

[64] Hoschek, G., 1974, Gehlenite stability in the system CaO–Al_2O_3–SiO_2–H_2O–carbgas. *Contr. Miner. Petrol.*, **47**, 245–254.

[65] Howard, S.A., & Preston, K.D., 1989, Profile fitting of powder diffraction patterns. In: Bish, D.L., & Post, J.E., (eds.), Modern Powder Diffraction. *Miner. Soc. Am., Rev. Mineral.*, **20**, 217–275.

[66] Jacobs, G.K., & Kerrick, D.M., 1981a, APL and FORTRAN programs for a new equation of state for H_2O, CO_2 and their mixtures at supercritical conditions, *Comp. Geosci.*, **7**, 131–143.

[67] Jacobs, G.K., & Kerrick, D.M., 1981b, Methane: an equation of state with application to the ternary system H_2O–CO_2–CH_4. *Geochim. Cosmochim. Acta*, **45**, 607–614.

[68] Jacobs, G.K., & Kerrick, D.M., 1981c, Devolatilization equilibria in H_2O–CO_2 and H_2O–CO_2–NaCl fluids: an experimental and thermodynamic evaluation at elevated pressures and temperatures. *Am. Miner.*, **66**, 1135–1153.

[69] Jenkins, D.M., 1984, Upper pressure stability of synthetic margarite plus quartz. *Contr. Miner. Petrol.*, **88**, 332–339.

[70] Johannes, W., 1969, An experimental investigation of the system MgO–SiO_2–H_2O–CO_2. *Am. J. Sci.*, **267**, 1083–1104.

[71] Kennedy, G.C., 1954, Pressure–volume–temperature relations in CO_2 at elevated temperatures and pressures. *Am. J. Sci.*, **252**, 225–241.

[72] Kerrick, D.M., & Ghent, E.D., 1979, P–T–X_{CO_2} relastions of equilibria in the system: CaO–Al_2O_3–SiO_2–CO_2–H_2O. In: Zharikov, V.A., Fonarev, V.I., & Korikovskii, V.A., (eds.), Problems in Physico-Chemical Petrology. Academy of Sciences of the USSR, **2**, 32–52.

[73] Kerrick, D.M., & Jacobs, C.K., 1981, A modified Redlich–Kwong equation for H_2O, CO_2, and H_2O–CO_2 mixtures at elevated pressures and temperatures. *Am. J. Sci.*, **281**, 735–767.

[74] Khitarov, N.I., & Malinin, C.D. 1956, Experimental characteristics of a part of the system H_2O–CO_2. *Geochem. Int.*, **3**, 246–256.

[75] Khitarov, N.I., & Malinin, C.D., 1958, *Geochem. Int.*, **7**, 678.

[76] Kruse, R., 1975, Raman–Spektroskopische Untersuchungen and CO_2–H_2O Mischungen bis 490 °C und 2500 bar. Ph.D. Thesis, Universität Karlsruhe, Unpublished.

[77] Lewis, G.N., 1907, Outlines of a new system of thermodynamic chemistry. *Proc. Am. Akad.*, **43**, 260.

[78] Mäder, U.K., Berman, R.G., & Greenwood, H.J., 1990, An equation of state for H_2O–CO_2 mixtures consistent with P-V-T and phase equilibrium data, *Geol. Ass. Can. Min. Ass. Can., Prog. Abstr.*, **15**, A81.

[79] Malinin, S.D., 1958, *Geochem. Int.*, **8**, 292.

[80] Metz, P., 1967, Experimentelle Bildung von Forsterit und Calcit aus Tremolit und Dolomit. *Geochim. Cosmochim. Acta*, **31**, 1517–1532.

[81] Metz, P., 1970, Experimentelle Untersuchung der Metamorphose von kieselig dolomitischen Sedimenten: II. Die Bildungsbedingungen des Diopsids. *Contr. Miner. Petrol.*, **28**, 221–250.

[82] Metz, P., 1976, Experimental investigation of the metamorphism of siliceous dolomites III. Equilibrium data for the reaction: 1 tremolite + 11 dolomite = 8 forsterite + 13 calcite + 9 CO_2 + 11 H_2O for the total pressure of 3000 and 5000 bars. *Contr. Miner. Petrol.*, **58**, 137–148.

[83] Metz, P., & Puhan, D., 1970, Experimental Untersuchung der Metamorphose von kieselig dolomitischen Sedimenten. I. Die Gleichgewichtsdaten der Reaktion 3 Dolomit + 4 Quarz + 1 H_2O = 1 Talk + 3 Calcit + 3 CO_2 für die Gesamtgasdrucke von 1000, 3000 und 5000 Bar. *Contr. Miner. Petrol.*, **26**, 302–314.

[84] Metz, P., & Puhan, D., 1971, Korrektur zur Arbeit 'Experimental Untersuchung der Metamorphose von kieselig dolomitischen Sedimenten. I. Die Gleichgewichtsdaten der Reaktion 3 Dolomit + 4 Quarz + 1 H_2O = 1 Talk + 3 Calcit + 3 CO_2 für die Gesamtgasdrucke von 1000, 3000 und 5000 Bar'. *Contr. Miner. Petrol.*, **31**, 169–170.

[85] Mitchell, A.C., & Nellis, W.J., 1979, Water Hugoniot measurements in the range 30 to 220 GPa. In: Timmerhaus, K.D., & Barber, M.S., (eds.), High Pressure Science and Technology, v. 1, Physical Properties and Material Synthesis, 6th AIRAPT Conference, Plenum Press, 428–434.

[86] Nitsch, K.H., Storre, B., & Toepfer, U., 1981, Experimentelle Bestimmung der Gleichgewichtsdaten der Reaktion 1 Margarit + 1 Quarz $\rightleftharpoons$ 1 Anorthit + 1 Andalusit/Disthen + 1 H_2O. *Fortschritte Mineral.*, **59**, 139–140.

[87] Pitzer, K.S., 1987, A thermodynamic model for aqeous solutions of liquid-like densities. In: Carmichael, I.S.E. & Eugster, H.P. (eds.), Thermodynamic Modeling of Geological Materials: Minerals, Fluids and Melts. *Miner. Soc. Am., Rev. Mineral.*, **17**, 97–142.

[88] Powell, R., & Holland, T.J.B., 1985, An internally consistent thermodynamic dataset with uncertainties and correlations: 1. Methods and a worked example. *J. Metam. Geol.*, **3**, 327–342.

[89] Prausnitz, J.M., Lichtenthaler, R.N., & de Azevedo, E.G., 1986, Molecular Thermodynamics of Fluid–Phase Equilibria (2nd ed.). Prentice–Hall Inc., Englewood Cliffs, N.J. 07632, 600p.

[90] Puhan, D., 1978, Experimental study of the reaction: dolomite + K-feldspar + H_2O = phlogopite + calcite + CO_2 at the total gas pressure of 4000 and 6000 bars. *N. Jh. Miner. Monatshefte*, 110–127.

[91] Puhan, D., & Johannes, W., 1974, Experimentelle Untersuchung der Reaktion Dolomit + Kalifeldspat + H_2O = Phlogopit + Calcit + CO_2. Ein Methodenvergleich. *Contr. Miner. Petrol.*, **48**, 23–31.

[92] Read, A.J, 1975, The first ionization constant of carbonic acid from 25 to 250 °C and to 2000 bar. *J. Solution Chem.*, **4**, 53–70.

[93] Redlich, O., & Kwong, J.N.S., 1949, On the thermodynamics of solutions. V. An equation of state. Fugacities of gaseous solutions. *Chem. Reviews*, **44**, 233–244.

[94] Roedder, E., 1984, Fluid Inclusions. *Miner. Soc. Am., Rev. Mineral.*, **12**, 644 pp.

[95] Ryzhenko, B.N., & Volkov, V.P., 1971, Fugacity coefficients of some gases in a broad range of temperatures and pressures. *Geochem. Int.*, **8**, 468–481. Translated from Geokhimiya, **7**, 760–773, 1971.

[96] de Santis, R., Breedveld, G.J.F., & Prausnitz, J.M., 1974, Thermodynamic properties of aqueous gas mixtures at advanced pressures. *Ind. Eng. Chem. Proc. Des. Devel.*, **13**, 374–377.

[97] Saxena, S.K., & Fei, Y., 1987a, High pressure and high temperature fluif fugacities. *Geochim. Cosmochim. Acta*, **51**, 783–791.

[98] Saxena, S.K., 1987b, & Fei, Y., 1987b, Fluids at crustal pressures and temperatures, I. Pure species. *Contr. Miner. Petrol.*, **95**, 370–375.

[99] Shmonov, V.M., & Shmulovich, K.I., 1974, Molar volumes and equation of state of CO_2 at temperatures from 100–1000°Cand pressures from 2000–10000 bars (in Russian). *Akad. Nauk SSSR Doklady*, **217**, 935–938.

[100] Shmulovich, K.I., Shmonov, V.M., Zakirov, I.V., 1979, P–V–T measurements in hydrous systems at high pressure and temperature. In: Godikov, A.A., (ed.), Experimental Research Methods for Hydrothermal Solutions (in Russian). Nauka, Novosibirsk, 81–89.

[101] Shmulovich, K.I., Shmonov, V.M., Mazur, V.A., & Kalinichev, A.G., 1980, P–V–T and activity concentration relations in the H_2O–CO_2 system (homogeneous solutions). *Geochem. Int.*, **17**, 123–139.

[102] Shmulovich, K.I., 1978, Stability limits of grossular and wollastonite in the H_2O–CO_2 system up to 6 kbar. *Geochem. Int.*, **14**, 126–134.

[103] Shvedenkov, G.Y., Shvedenkova, S.V., Dashevskii, Y.A., & Kalinin, D.V., 1983, Phase equilibria in the sytem containing muscovite, paragonite, alkaline feldspars, H_2O. and CO_2. *Sov. Geol. Geophys.*, **24**, 428–436.

[104] Skippen, G.B., 1971, Experimental data for reactions in siliceous marbles. *J. Geol.*, **79**, 457–481.

[105] Skippen, G.B., Carmichael, D.M., 1977, Mixed–volatile equilibria. In: Greenwood, H.J. (ed.), Short Course in Application of Thermodynamics to Petrology and Ore Deposits. *Miner. Assoc. Canada*, Short Course Handbook, **2**, 109–125.

[106] Slaughter, J., Kerrick, D.M., & Wall, V.J., 1975, Experimental and thermodynamic study of equilibria in the system $CaO–MgO–SiO_2–H_2O–CO_2$. *Am. J. Sci.*, **275**, 143–162.

[107] Spycher, N.F., & Reed, M.H., 1988, Fugacity coefficients of H_2, CO_2, CH_4, H_2O and of $H_2O–CO_2–CH_4$ mixtures: a virial equation treatment for moderate pressures and temperatures applicable to calculations of hydrothermal boiling. *Geochim. Cosmochim. Acta*, **52**, 739–749.

[108] Storre, B., & Nitsch, K.H., 1974, Zur stabilität von Margarit im System $CaO–Al_2O_3–SiO_2–H_2O$. *Contr. Miner. Petrol.*, **43**, 1–24.

[109] Sverjensky, D.A., 1987, Calculation of the thermodynamic properties of aqueous species and the solubilities of minerals in supercritical electrolyte solutions. In: Carmichael, I.S.E. & Eugster, H.P. (eds.), Thermodynamic Modeling of Geological Materials: Minerals, Fluids and Melts. *Miner. Soc. Am., Rev. Mineral.*, **17**, 177–209.

[110] Takenouchi, S., & Kennedy, G.C., 1964, The binary system $H_2O–CO_2$ at high temperatures and pressures. *Am. J. Sci.*, **262**, 1055–1074.

[111] Tödheide, K., 1972, Water at high temperatures and pressures. In: Franks, F., (ed.), Water, a Comprehensive Treatise: v.1. The Physics and Physical Chemistry of Water. Plenum Press, New York, 463–514.

[112] Tödheide, K., & Franck, E.U., 1963, Das Zweiphasengebiet und die kritische Kurve im System Kohlendioxid–Wasser bis zu Drucken von 3500 bar. *Z. Phys. Chem. N. Folge*, **37**, 387–401.

[113] Trommsdorff, V., & Connolly, J.A.D., 1990, Constraints on phase diagram topology for the system $CaO–MgO–SiO_2–CO_2–H_2O$. *Contr. Miner. Petrol.*, in press.

[114] Ulmer, P., & Luth, R.W., 1988, The graphite–COH fluid equilibrium in P, T, f_{O_2} space: an experimental determination at high pressures. *EOS, Trans., Am. Geophys. Union*, **69**, 512.

[115] Walter, L.S., 1963, Data on the fugacity of CO_2 in mixtures of CO_2 and H_2O. *Am. J. Sci.*, **261**, 151–156.

[116] Walter, L.S., Wyllie, P.J., & Tuttle, O.F., 1962, Phase relations in the system MgO–H_2O–CO_2. *J. Petrol.*, **3**, 49–64.

[117] Welsch, H., 1973, Die Systeme Xenon–Wasser und Methan–Wasser bei hohen Drücken und Temperaturen. Dissertation, Universität Karlsruhe, unpublished, 55 pp.

[118] Wiebe, R., 1941, The binary system carbon dioxide–water under pressure. *Chem. Reviews*, **29**, 475–481.

[119] Wiebe, R., & Gaddy, V.L., 1939, The solubility in water of carbon dioxide at 50, 75, and 100 °C, at pressures to 700 atmospheres. *J. Am. Chem. Soc.*, **61**, 315–318.

[120] Wiebe, R., & Gaddy, V.L., 1940, The solubility of carbon dioxide in water at various temperatures from 12 to 40 °C and at pressures to 500 atmospheres. Critical phenomena. *J. Am. Chem. Soc.*, **62**, 815–817.

[121] Wiebe, R., & Gaddy, V.L., 1941, Vapor phase composition of carbon dioxide–water mixtures at various temperatures and pressures to 700 atmospheres. *J. Am. Chem. Soc.*, **63**, 475–477.

[122] Widmark, E.T., 1980, The reaction chlorite + dolomite = spinel + forsterite + calcite + carbon dioxide + water. *Contr. Miner. Petrol.*, **72**, 175–179.

[123] Wood, B.J., & Fraser, D.G., 1977, Elementary Thermodynamics for Geologists. Oxford University Press, 303 pp.

[124] Zharikov, V.A., Shmulovich, K.I., & Bulatov, V.K., 1977, Experimental studies in the system CaO–MgO–Al_2O_3–SiO_2–CO_2–H_2O and conditions of high temperature metamorphism. *Tectonophysics*, **43**, 745–162.

[125] Ziegenbein, D., & Johannes, W., 1974, Wollastonitbildung aus Quarz und Calcit bei Pf = 2, 4 und 6 kb. *Fortschritte Mineral.*, **44**, 77–79.

[126] Ziegenbein, D., & Johannes, W., 1982, Activities of CO_2 in supercritical CO_2–H_2O mixtures, derived from high–pressure mineral equilibrium data. In: Schreyer, W., (ed.), High–Pressure Researches in Geoscience, E. Schweizerbart'sche Verlagsbuchhandlung, Stuttgart, 493–500.

Appendix A

Integration of the Equation of State

The quantity $\int_{P_0}^{P} V_{CO_2}^{T}\, dP$ is most easily obtained from the relationship

$$\begin{aligned}\int_{P_0}^{P} V\, dP &= \int_{V_P}^{V_0} P\, dV + V_P(P - P_0) - P_0(V_0 - V_P) \\ &= \int_{V_P}^{V_0} \frac{RT}{V - (B - \frac{B_3}{V^3+C})}\, dV - \int_{V_P}^{V_0} \frac{A_1}{TV^2}\, dV + \int_{V_P}^{V_0} \frac{A_2}{V^4}\, dV \\ &\quad + V_P(P - P_0) - P_0(V_0 - V_P) \end{aligned} \tag{A.53}$$

with $B = B_1 + B_2T$ and $C = B_3/B$.

The attractive terms (A_1 and A_2 terms) become upon integration:

$$\frac{A_1}{T}\left(\frac{1}{V_0} - \frac{1}{V_P}\right) - \frac{A_2}{3}\left(\frac{1}{V_0^3} - \frac{1}{V_P^3}\right) \tag{A.54}$$

The repulsive term (RT term) requires integration of a rational function of the form

$$\int_{V_P}^{V_0} \frac{mV^3 + n}{V(aV^3 + bV^2 + cV + d)}\, dV \tag{A.55}$$

with $m = RT$, $n = RTC$, $a = 1$, $b = -B$, $c = 0$, $d = C = B_3/B$ and $B = B_1 + B_2T$.

Integral (A.55) may be solved after splitting into partial fractions provided the real roots of the polynomial $aV^3 + bV^2 + cV + d$ are known.

Case I: polynomial $aV^3 + bV^2 + cV + d$ yields 3 real roots X_1, X_2, X_3

Integral (A.55) may be split into partial fractions by solving

$$\frac{mV^3 + n}{V(aV^3 + bV^2 + cV + d)} = \frac{I}{V} + \frac{J}{V - X_1} + \frac{K}{V - X_2} + \frac{L}{V - X_3} \tag{A.56}$$

Cross multiplication and collecting terms in powers of V yields four equations in four unknowns (I, J, K, L) by comparing coefficients:

$$n = I(-X_1X_2X_3) \tag{A.57}$$

$$0 = I(X_1X_2 + X_1X_3 + X_2X_3) + J(X_2X_3) + K(X_1X_3) + L(X_1X_2) \tag{A.58}$$

$$0 = I(X_1 + X_2 + X_3) + J(X_2 + X_3) + K(X_1 + X_3) + L(X_1 + X_2) \tag{A.59}$$

$$m = I + J + K + L \tag{A.60}$$

Equations (A.57) through (A.60) are solved simultaneously to obtain:

$$I = -\frac{n}{X_1X_2X_3} \tag{A.61}$$

$$J = -\frac{mX_1^3+n}{X_1(-X_1^2+X_1X_2-X_2X_3+X_1X_3)} \tag{A.62}$$

$$K = \frac{mX_2^3+n}{X_2(X_2^2-X_1X_2-X_2X_3+X_1X_3)} \tag{A.63}$$

$$L = \frac{mX_3^3+n}{X_3(X_3^2+X_1X_2-X_2X_3-X_1X_3)} \tag{A.64}$$

Integral (A.55) may now be integrated by parts to obtain:

$$I\ln\left(\frac{V_0}{V_P}\right)+J\ln\left(\frac{V_0-X_1}{V_P-X_1}\right)+K\ln\left(\frac{V_0-X_2}{V_P-X_2}\right)+L\ln\left(\frac{V_0-X_3}{V_P-X_3}\right) \tag{A.65}$$

Case II: polynomial aV^3+bV^2+cV+d yields 1 real root X_1

Integral (A.55) may be split into partial fractions by solving:

$$\frac{mV^3+n}{V(aV^3+bV^2+cV+d)} = \frac{I}{V}+\frac{J}{V-X_1}+\frac{KV+L}{V^2+\alpha V+\beta} \tag{A.66}$$

with $\alpha = b/a+X_1$ and $\beta = c/a+X_1\alpha$ which yields four equations in four unknowns (I, J, K, L):

$$n = -I\beta X_1 \tag{A.67}$$

$$0 = I(\beta-\alpha X_1)+J\beta-LX_1 \tag{A.68}$$

$$0 = I(\alpha-X_1)+J\alpha-KX_1+L \tag{A.69}$$

$$m = I+J+K \tag{A.70}$$

Equations (A.67) through (A.70) are solved simultaneously to obtain:

$$I = -\frac{n}{\beta X_1} \tag{A.71}$$

$$J = -\frac{mX_1^3+n}{X_1(\alpha X_1+\beta+X_1^2)} \tag{A.72}$$

$$K = \frac{\alpha\beta mX_1+\alpha n+\beta^2m+nX_1}{\beta(\alpha X_1+\beta+X_1^2)} \tag{A.73}$$

$$L = \frac{\alpha^2n+\alpha nX_1+\beta^2mX_1-\beta n}{\beta(\alpha X_1+\beta+X_1^2)} \tag{A.74}$$

The last term of equation (A.66) is expanded to standard integrals by appropriate substitutions:

$$\int \frac{KV+L}{V^2+\alpha V+\beta}\,dV = \int \frac{Kz}{z^2+t^2}\,dz + \int \frac{L-Ks}{z^2+t^2}\,dz \tag{A.75}$$

with $z = V + s$, $s = \alpha/2$, $t = \sqrt{\beta - s^2}$ and $dV = dz$.

Integration of (A.55) yields:

$$\begin{aligned} &I \ln\left(\frac{V_0}{V_P}\right) + J \ln\left(\frac{V_0 - X_1}{V_P - X_1}\right) + \frac{K}{2} \ln\left(\frac{(V_0+s)^2+t^2}{(V_P+s)^2+t^2}\right) \\ &\quad + \frac{L-Ks}{t}\left[\arctan\left(\frac{V_0+s}{t}\right) - \arctan\left(\frac{V_P+s}{t}\right)\right] \end{aligned} \tag{A.76}$$

with $\alpha = b/a + X_1$, $\beta = c/a + \alpha X_1$, $s = \alpha/2$ and $t = \sqrt{\beta - s^2}$.

Appendix B

FORTRAN–77 Subroutine

This appendix contains the listing of a FORTRAN–77 subroutine that computes the volume and the fugacity, f, of carbon dioxide at a specified pressure and temperature. The compressibility factor $z = PV/RT$, density, fugacity coefficient $\gamma = f/P$ and the volume integral $\int V dP = RT \ln f$ may also be retrieved. Quantities that are not required may be removed from the program with the appropriate variables blanked out in the calling sequence of the subroutine and its corresponding argument list. The computing efficiency gained by this procedure is not significant in the case where the fugacity is required. If the volume is the only quantity sought then the parts and subroutines designed for the fugacity computations should be removed to make the code more efficient. The comment statements provided with the code are sufficient for this purpose.

```
C  ************************************************************
C  #  MADER & BERMAN EQUATION OF STATE FOR CO2                 #
C  #                                                           #
C  #       Ref:  - Mader et al., 1988,                         #
C  #               Geol. Soc. Amer., Abstr. w. Progr., p.A190  #
C  #             - Mader & Berman, 1991                        #
C  #               In prep. (J. Pet.)                          #
C  ************************************************************
C   These subroutines compute the volume and fugacity of CO2
C   at specified pressure and temperature:
C
C   P = RT / (V-B) - A1 / T*V**2 + A2 / V**4
C     B = B1 + B2*T - B3/(V**3+C);  C = B3/(B1+B2*T)
C
C   Program written by Urs Mader, June 1987
C     modified: Sept. 1988, by Urs  (better volume iteration routine)
C     modified: July  1989, by Urs  (clean up integration code)
C     modified: March 1990, by Urs  (fool proof volume iterator)
C
C   Program is written in standard FORTRAN 77
C
C   Note: Rootfinder is not designed to handle subcritical pressure and
C   temperature simultaneously (i.e. 89.2 bar, 335.6 K). To do so, the
C   rootfinder must be capable of recognizing subcritical conditions and
C   find the saturated volumes by equating f(vap) = f(liq).
C
C   List of subroutines:
C     MABE90: main subroutine, returns volume, fugacity, etc. at P,T
C     CO2VOL: computes volume at P,T using CO2BIS,CO2R00,CO2FUN
C     CO2INT: computes int(V)dP using CO2R00,CO2IN3,CO2IN1,CO2TIR
C       CO2BIS: converges to V at P,T by interval halfing
```

```
C         CO2FUN: returns the function value of the equation of state
C       CO2ROO: finds root(s) of 3rd order polynomial
C       CO2IN3: integrates attractive term (1st case, 3 real roots)
C       CO2IN1: integrates attractive term (2nd case, 1 real root)
C         CO2TIR: auxiliary routine for CO2IN1
C
C   List of variables:
C     PBAR,P    : pressure [bar]
C     TK,T      : temperature [K]
C     VO        : volume at 1 bar and T [cm**3/mole]
C     VP,V      : volume at P and T [cm**3/mole]
C     VJ        : volume at P and T [Joule/bar]
C     R         : 10*gas constant (10*8.3147 [Joule/mole/K])
C     RTLNF     : R/10*T*ln(f)CO2 [Joule]
C     FUG       : fugacity [bar]
C     FUGLN     : ln(FUG)
C     FUGCOE    : fugacity coefficient
C     Z         : compressibility  {=R*T/(P*V)}
C     RHO       : density [kg/m**3]
C     RHOCGS    : density [g/cm**3]
C     A1,A2,B1,B2,B3 : constants for equation of state
C     B         : = B1 + B2*T
C     C         : = B3/B
C     MAXIT     : iteration limit for routine CO2BIS
C     V1,V2     : volumes used during iteration
C     NROOT     : no. of roots of 3rd order polynomial
C     X1,X2,X3 : roots of 3rd order polynomial
C -------------------------
C example of a main program
C     PROGRAM MAIN
C     IMPLICIT REAL*8(A-H,O-Z)
C     PBAR=1000.0D00
C     TK=1073.0D00
C     CALL MABE90(PBAR,TK,VP,VJ,FUG,FUGCOE,FUGLN,RTLNF,Z,RHO,RHOCGS)
C     STOP
C     END
C
C ---------------------------------------------------------------------
C main subroutine
      SUBROUTINE MABE90(PBAR,TK,VP,VJ,FUG,FUGCOE,FUGLN,RTLNF,Z,RHO,RHOCGS)
      IMPLICIT REAL*8(A-H,O-Z)
      COMMON /PAR/ R,B,B3,C,A1,A2
      COMMON /LIMIT/ MAXIT
      LOGICAL FIRST
      DATA FIRST/T/
C
      IF(.NOT.FIRST) GOTO 11
      FIRST = .FALSE.
C fit parameters: March 26, 1990
C                 121 phase equil. constraints, 440 PVT
      B1 = 28.064740D00
      B2 = 1.7287123D-4
      B3 = 8.3653408D04
      A1 = 1.0948021D09
      A2 = 3.3747488D09
      R  = 83.147D00
      MAXIT = 50
 11   B  = B1+B2*TK
```

```
      C  = B3/B
C test for subcritical P and T
      IF((PBAR.LT.89.2D0).AND.(TK.LT.335.6D0)) WRITE(6,*)
     & 'subcritical P or T in CO2 routine'
C compute VP,VJ,Z,RHO at PBAR,TK
      CALL CO2VOL(VP,VO,PBAR,TK)
      VJ = VP/10.0
      Z      = PBAR*VP/R/TK
      RHOCGS = 44.010/VP
      RHO    = RHOCGS*1000.0
C compute RTLNF,FUGLN,FUGCOE,FUG at PBAR,TK
      CALL CO2INT(RTLNF,PBAR,TK,VP,VO)
      FUGLN  = RTLNF/R/TK*10.0
      FUG    = DEXP(FUGLN)
      FUGCOE = FUG/PBAR
      RETURN
      END
C ---------------------------------------
C subroutine to compute VP of CO2 at P and T
      SUBROUTINE CO2VOL(VP,VO,P,T)
      IMPLICIT REAL*8(A-H,O-Z)
      COMMON /PAR/ R,B,B3,C,A1,A2
      COMMON /LIMIT/ MAXIT
C approx. VO at 1 bar and set initial guess (V1,V2) to find VP
      VO = R*T+B
      V2 = (R*T/P+B)*1.2
C compute minimum volume VMIN at T for P = inf.
C (solve V**3 - V**2*B + C = 0; from V = B - B3/(V**3 + C))
      WP = -B
      WR = C
      CALL CO2ROO(WP,WR,X1,X2,X3,NROOT)
      V1 = X1
      IF(NROOT.EQ.3) THEN
         IF(X2.GT.V1) V1 = X2
         IF(X3.GT.V1) V1 = X3
      ENDIF
      CALL CO2BIS(V1,V2,VP,P,T)
      RETURN
      END
C -------------------------------------
C subroutine to compute int(V)dP of CO2
      SUBROUTINE CO2INT(RTLNF,P,T,VP,VO)
      IMPLICIT REAL*8(A-H,O-Z)
      COMMON /PAR/ R,B,B3,C,A1,A2
C integrate equation of state from 1 bar to P;
C note: int(V)dP = int(P)dV + V*(P-1) - (V-VO)*1
      WP=-B
      WR=C
C compute roots X1,X2,X3 of 3rd order polynominal in V
C (denominator of repulsive term of equation of state)
C and integrate repulsive term (TERM1,TERM2)
      CALL CO2ROO(WP,WR,X1,X2,X3,NROOT)
      IF(NROOT.EQ.3) CALL CO2IN3(X1,X2,X3,VO,VP,T1,T2)
      IF(NROOT.EQ.1) CALL CO2IN1(X1,WP,VO,VP,T1,T2)
      TERM1 = R*T*T1
      TERM2 = R*T*C*T2
C integrate attractive terms of equation of state
      TERM3 = A1/T*(1.0/VO-1.0/VP)
```

```
      TERM4 = -A2/3.0*(1.0/V0/V0/V0-1.0/VP/VP/VP)
      TERM5 = V0-VP
      TERM6 = (P-1.0)*VP
      RTLNF = (TERM1+TERM2+TERM3+TERM4-TERM5+TERM6)/10.0
      RETURN
      END
C -----------------------------------------------------
C subroutine for rootfinding for CO2 equation of state
      SUBROUTINE CO2BIS(X1,X2,XMID,P,T)
      IMPLICIT REAL*8(A-H,O-Z)
      COMMON /PAR/ R,B,B3,C,A1,A2
      COMMON /LIMIT/ MAXIT
      ACC = X1*1.0D-6
      X  = X2
      DX = X1-X2
      DO 11 J=1,MAXIT
         DX = DX*0.5
         XMID = X+DX
         CALL CO2FUN(XMID,FMID,P,T)
         IF(FMID.LT.0.0D00) X=XMID
         IF((DABS(DX).LT.ACC).OR.(DABS(FMID).LT.1.0D-08)) RETURN
  11  CONTINUE
      WRITE(6,*) 'MAXIT (CO2BIS) EXEEDED'
      RETURN
      END
C subroutine to evaluate equation of state
      SUBROUTINE CO2FUN(V,FV,P,T)
      IMPLICIT REAL*8(A-H,O-Z)
      COMMON /PAR/ R,B,B3,C,A1,A2
      VSQ = V*V
      FV  = R*T/(V-B+B3/(VSQ*V+C))-A1/T/VSQ+A2/VSQ/VSQ-P
      RETURN
      END
C -----------------------------------------------
C subroutines for integration of repulsive term
      SUBROUTINE CO2ROO(WP,WR,X1,X2,X3,NROOT)
      IMPLICIT REAL*8(A-H,O-Z)
C find root(s) of polynominal X**3 + WP*X**2 + WR*X
      QA = (-WP*WP)/3.0
      QB = (2.0*WP*WP*WP+27.0*WR)/27.0
      DET = QB*QB/4.0+QA*QA*QA/27.0
      IF(DET.GT.0.0) THEN
         ARGF = DSQRT(DET)-QB/2.0
         ARGE = -DSQRT(DET)-QB/2.0
         SIGF = DABS(ARGF)/ARGF
         SIGE = DABS(ARGE)/ARGE
         QF = DEXP(DLOG(DABS(ARGF))/3.0)*SIGF
         QE = DEXP(DLOG(DABS(ARGE))/3.0)*SIGE
         X1 = QF+QE-WP/3.0
         NROOT = 1
      ELSE
         PI = 3.1415926536D00
         PHI = DARCOS(-QB/2.0/DSQRT(-QA*QA*QA/27.0))
         RM = 2.0*DSQRT(-QA/3.0)
         X1 = RM*DCOS(PHI/3.0)-WP/3.0
         X2 = RM*DCOS(PHI/3.0+2.0*PI/3.0)-WP/3.0
         X3 = RM*DCOS(PHI/3.0+4.0*PI/3.0)-WP/3.0
         NROOT = 3
```

```
      ENDIF
      RETURN
      END
C integration for case with 3 real roots X1,X2,X3
      SUBROUTINE CO2IN3(X1,X2,X3,VO,V,T1,T2)
      IMPLICIT REAL*8(A-H,O-Z)
C term 1 :  V**2 / (V**3 - V**2 * B + C)
      DIV = X1*X1*(X2-X3)+X2*X2*(X3-X1)+X3*X3*(X1-X2)
      SA = X1*X1/(X1*(X1-X2-X3)+X2*X3)
      SB = X2*X2*(X3-X1)/DIV
      SC = X3*X3*(X1-X2)/DIV
      T1 = SA*(DLOG(VO-X1)-DLOG(V-X1))+SB*(DLOG(VO-X2)-DLOG(V-X2))+
     &     SC*(DLOG(VO-X3)-DLOG(V-X3))
C term 2 :  1 / V / (V**3 - V**2 * B + C)
      SA = -1.0/X1/X2/X3
      SB = 1.0/X1/(X1*(X1-X2-X3)+X2*X3)
      SC = -1.0/X2/(X2*(X1+X3-X2)-X1*X3)
      SD = 1.0/X3/(X3*(X3-X2-X1)+X1*X2)
      T2 = SA*(DLOG(VO)-DLOG(V))+SB*(DLOG(VO-X1)-DLOG(V-X1))+
     &     SC*(DLOG(VO-X2)-DLOG(V-X2))+SD*(DLOG(VO-X3)-DLOG(V-X3))
      RETURN
      END
C integration for case with 1 real root X1
      SUBROUTINE CO2IN1(X1,WP,VO,V,T1,T2)
      IMPLICIT REAL*8(A-H,O-Z)
      ALP = X1+WP
      BET = X1*(X1+WP)
C term 1
      DIV = X1*(X1+ALP)+BET
      SA = X1*X1/DIV
      SB = (ALP*X1+BET)/DIV
      SC = X1*BET/DIV
      CALL CO2TIR(SB,SC,ALP,BET,VO,V,TR)
      T1 = SA*(DLOG(VO-X1)-DLOG(V-X1))+TR
C term 2
      SA = -1.0/BET/X1
      SB = 1.0/X1/DIV
      SC = (ALP+X1)/BET/DIV
      SD = (ALP*(ALP+X1)-BET)/BET/DIV
      CALL CO2TIR(SC,SD,ALP,BET,VO,V,TR)
      T2 = SA*(DLOG(VO)-DLOG(V))+SB*(DLOG(VO-X1)-DLOG(V-X1))+TR
      RETURN
      END
C auxiliar routine for CO2IN1
      SUBROUTINE CO2TIR(S1,S2,ALP,BET,VO,V,TR)
      IMPLICIT REAL*8(A-H,O-Z)
      RDET = DSQRT(4.0*BET-ALP*ALP)
      IF(RDET.LT.1.0D-15) RDET = 1.0D-15
      TR = S1/2.0*(DLOG(VO*VO+ALP*VO+BET)-DLOG(V*V+ALP*V+BET))+
     &     (2.0*S2-ALP*S1)/RDET*(DATAN((2.0*VO+ALP)/RDET)-
     &     DATAN((2.0*V+ALP)/RDET))
      RETURN
      END
```

Appendix C

Piston-Cylinder Experiments

C.1 Piston-Cylinder Apparatus

The piston-cylinder apparatus used for this study was developed and built in the department of geological sciences at UBC with the expert help of Dr. Don Lindsley (Stony Brook). It differs from the original Boyd & England (1960) design by a concentric arrangement of the rams, modifications of the bridge, and an improved design of the upper electrode and the water cooling cycle. Two different bridges allow easy interchange between a 3/4-inch and a 1/2-inch bore pressure vessel. The ram diameter to piston diameter ratio is such that 10 kbar piston pressure require 362 bar oil pressure for the 3/4-inch assembly and 160 bar for the 1/2-inch assembly respectively. This design works reliably to 25 kbar with the 3/4-inch assembly and 40 kbar with the 1/2-inch pressure vessel. Carbides under these conditions last more than 100 runs, most likely limited by careless handling of carbide parts.

The apparatus is end-loaded with a force of 1000 kNewton (310 bar oil pressure) during operation. The 3/4-inch piston excerts a force of 431 kNewton (548 bar oil pressure) to achieve a nominal sample pressure of 15 kbar. Oil pressure is generated by a pump driven with compressed air and a manually operated piston pump to provide backup pressure for ram retraction when required. The power supply for the graphite resistance furnace is designed to provide up to 50 AC Ampères at about 25 AC Volts which is sufficient for temperatures up to 1600 °C with most furnace designs.

Thermocouple output is measured with a Leeds & Northrup 7554 Type K-4 potentiometer furnished with a constant voltage supply (Leeds & Northrup, cat. 9879) and a 1-Volt standard cell (Eppley Laboratory, Inc., cat. no. 100). Temperature is controled by a voltage balanced against the thermocouple signal with a Leeds & Northrup 9828 DC Null Detector and a KRISEL solid-state SCR controler (Hadidiacos, 1969, with modifications).

C.2 Sample Assembly

Each application demands its own optimized design of a sample assembly and choice of pressure transmitting media. The assembly developed for this study is suitable for high temperature applications ($\geq$ 900 °C) and consists of cheap, non-toxic and easily

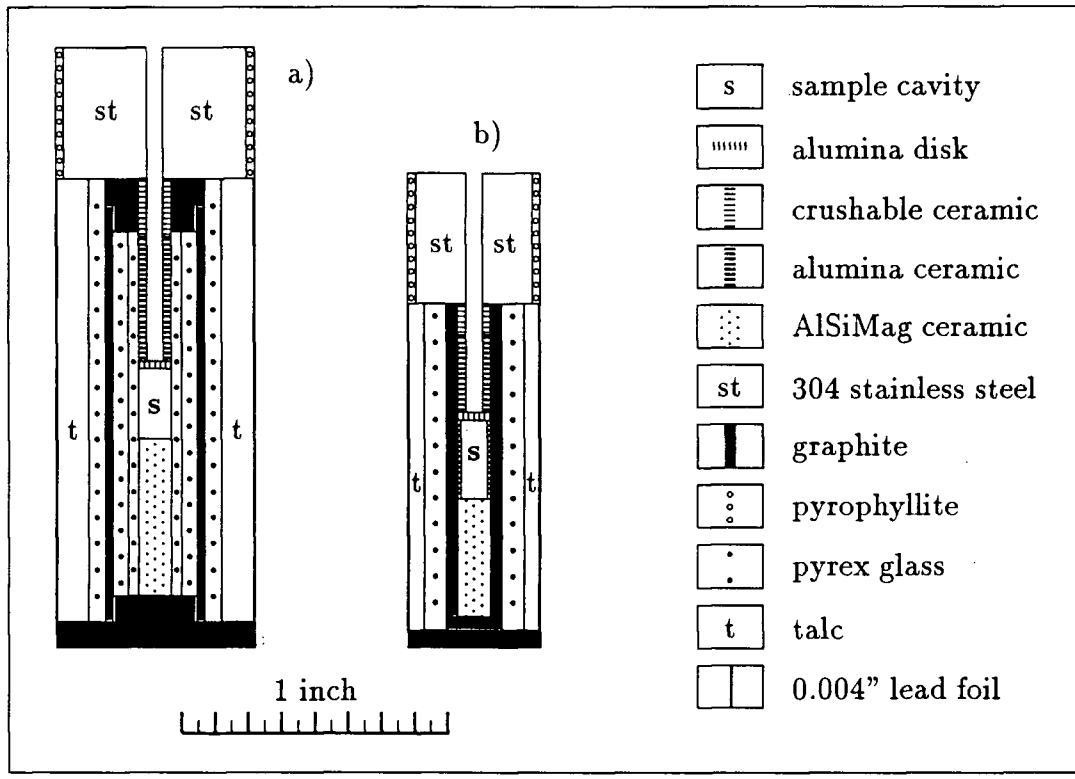

Figure C.15: Pyrex sample assembly for piston-cylinder apparatus.

machinable materials. The assembly proved to perform reliably with no failures due to thermocouple breakage and only few failures due to excessive deformation of the furnace.

The 3/4–inch assembly (figure C.15a) consists of a talc cylinder (0.743 in. OD, 0.500 in. ID) which contains the pyrex assembly made from standard 1/2 in. medium-wall and 8 mm medium-wall pyrex glass tubing embedding a 0.375 in. OD graphite cylinder furnace with a 0.06 in. wall thickness. A 0.2 in. thick graphite base disc and a 0.2 in. thick graphite plug at the top ensure good electrical contacts. The chamber within the inner pyrex tube is 35 mm long and 5 mm in diameter which allows the accommodation of relatively large sample capsules. The inner diameter can be further reduced by a 5 mm OD pyrex tube to 3 mm (1/8 in.). Machinable AlSiMag–222 ceramic rods serve as filler below the sample capsule. The two-hole thermocouple ceramic tube (McDanel MV20 mullite, 1/16 in. OD, AWG 26) is held in place by a piece of mullite ceramic tubing (McDanel MV20, 1/8 in. OD, 1/16 in. ID) sitting next to the sample capsule, and about 4 to 8 mm of crushable alumina ceramic tubing (1/8 in. OD, 1/16 in. ID) positioned below the steel plug which firmly grips the thermocouple tube during runup to prevent extrusion. The tip of the thermocouple is separated from the sample capsule by an alumina ceramic disc (0.02 in. thick). The sample capsule is packed at the top and

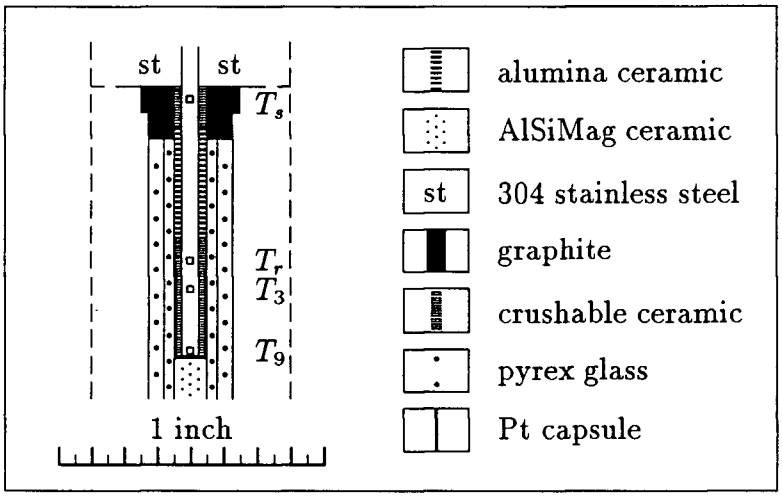

Figure C.16: Sample assembly for thermal gradient calibration. Only center part is shown (compare figure C.15).

base with pyrex powder to fill all voids due to welding seams and other irregularities in the outside of the capsule. Reduction of friction against the carbide core is achieved with a 0.004 in. thick lead foil lubricated with dry molybdenum disulfide (Molylube spray, Bel-Ray Company, Inc.). The steel plug, 0.5 in. long, is machined from 304 stainless steel with a 1/16 in. bore and an 0.03 in. thick insulator made from unfired pyrophyllite.

The 1/2-inch sample assembly (figure C.15b) consists of an outer talc cylinder (0.493 in. OD, 0.375 in. ID) and a standard 5/8 in. diameter thick-wall pyrex tube which contains the graphite furnace (0.212 in. OD, 1/8 in. ID). Sample capsules of 0.093 in. OD are contained within a thin-walled ceramic insulator (McDanel MV20, 1/8 in. OD) and packed with pyrex powder against the ceramic filler rod at the base and the ceramic tube containing the two-hole thermocouple ceramic insulator (1/16 in. OD, AWG 26) at the top. The thermocouple junction is separated from the sample by a 0.02 in. thick alumina ceramic disk. Steel plug design and friction reduction are the same as in the 3/4-inch assembly.

C.3 Temperature Calibration

Knowing the temperature of the sample at pressure within a piston-cylinder apparatus is a difficult task. Uncertainties of $\pm$ 30 °C or more are not uncommon if no special care is taken. Precision and accuracy of a temperature measurement depend on:

1. thermal gradients along the axis of the sample assembly,
2. effect of pressure on the electromotive force of the thermocouple,

3. calibration of the thermocouple,
4. calibration of the device measuring the electromotive force,
5. calibration of the ice point compensation,
6. additional voltages due to extension wires, junctions, induced emf,
7. ability to control the temperature during an experiment,
8. changes in geometry of the sample assembly during an experiment,
9. contamination of the thermocouple during an experiment.

Items 1 to 7 need to be calibrated, item 8 can be examined after the run, item 9 is negligible for short experiemnts and can be checked by recalibration after long experiments with some care.

P [kb]	T_r [°C]	T_3 [°C]	T_9 [°C]	T_s [°C]
10	900	908	893	350 ±30
	1100	1110	1096	420 ±30
	1300	1309	1300	495 ±40
	1500	1509	1507	535 ±50
15	900	908	886	
	1100	1109	1087	
	1300	1310	1292	
	1500	1508	1499	

Table C.7: Temperature measurements within the piston-cylinder apparatus made for calibration of thermal gradients. Position T_r is the location of the reference thermocouple junction (c.f. figure C.16). Positions T_3 and T_9 are located 3 mm and 9 mm below T_r. Position T_s is located at the top of the graphite furnace adjacent to the steel plug (c.f. figure C.16). Temperatures at T_s above T_r = 1200 °C are extrapolated. Uncertainties in T_s are estimated from measurements obtained from two independent experiemnts.

Thermal gradients: Gradients within the 3/4–inch assembly were measured at 10 and 15 kbar and 900–1500 °C. All calibration measurments were done with Pt–Pt10%Rh thermocouples (Johnson & Matthey Canada, Inc., 0.25 mm wire diameter) from the same spool. The gradients were determined with repeat runs each with two independent thermocouples contained within a four-hole ceramic tube (McDanel 998 Alumina, 1/16 in. OD, AWG 26) with one junction placed at the measuring position, T_r, for reference above the position of the sample capsule. The second junction was placed at depths of 3 and 9 mm, T_3 and T_9, within a dummy platinum sample capsule (3 mm OD, 10 mm long) lined with an insulator cup machined from crushable alumina ceramic tubing (figure C.16).

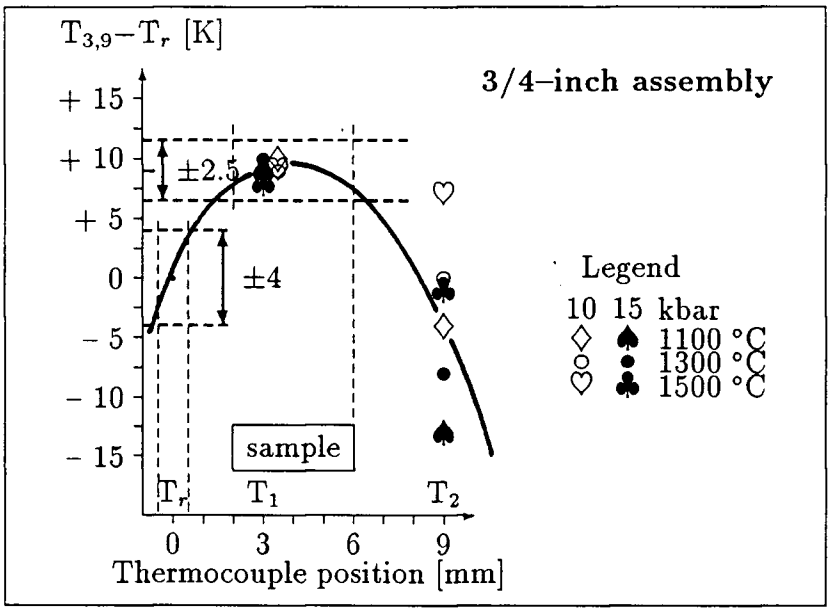

Figure C.17: Thermal gradients within the piston-cylinder apparatus. The data points at 10 kbar are offset from the T_1 position for clarity. Curve shows the inferred distribution of temperature at 1300 °C along the axis of the furnace assembly.

Temperatures were read from two $4\frac{1}{2}$–digit thermometers (Analog Devices, type AD 2051–A) which were calibrated against each other between 1000 and 1315 °C to agree within instrument precision of ± 0.5 °C. Temperatures at the top of the furnace were also determined in order to estimate the pressure seal temperature of the thermocouple wires (position T_s in figure C.16). The results are tabulated in table C.7 and plotted in figure C.17. The uncertainty has two major components: the uncertainty associated with the thermal gradient over the length of the sample capsule and the uncertainty associated with the precision with which the measuring thermocuple position can be repeated for all experiments. The position of the thermocouple was carefully monitored before and after each run and was observed to be precise to ±0.5 mm. This contribution accounts for about ±4 K and is thus the largest contribution to the overall temperature uncertainty.

The total uncertainty due to thermal gradients amounts to ± 6.5 K together with the contribution of ± 2.5 K from the thermal gradient over the length of the sample capsule. This uncertainty puts an upper limit to the precision with which runs can be duplicated. This precision also indicates that the temperature interval between runs should be at least 10 K for practical purposes. The temperature correction due to thermal gradients applied to the nominal temperatures of the experiments amounts to +9 K ± 6.5 K (cf. figure C.17).

Effect of pressure on the emf: The electromotive force (emf) of a thermocouple is affected by pressure whenever thermal gradients occur under pressure. The effect on commonly used thermocouple materials has been measured by single wire experiments within a piston–cylinder apparatus with controlled hot and cold pressure seal temperatures and approximate isobaric conditions over the length of the thermal gradient (Getting & Kennedy, 1970). Measurements on platinum and platinum–10% rhodium wire were made up to 33 kbar and 1000 °C. Extrapolation of the correction volatge to 1500 °C seems to be permissable, based on approximate linear trends of single wire voltage versus pressurized temperature interval and an approximately constant Seebeck coefficient at temperatures between 1000–1500 °C. Corrections are positive (low apparent temperature) at all pressure-temperature conditions. Uncertainties of the correction voltage are reported by Getting & Kennedy (1970) to be $\pm(10\% + 10\mu V)$ below 1000 °C and estimated to $\pm(15\% + 10\mu V)$ above 1000 °C. The corrections to be applied to experiments depend on the temperature at which the thermocouple is subject to the run pressure (pressure seal temperature). The position of the pressure seal in our experiments at 15 kbar is assumed to be at the point where the thermocouple ceramic tube is contained within a crushable alumina tube to enable a firm grip (position T_s in figure C.16 and table C.7). This approximation is based on the observation that thermocouple wires slide easily out of the part of the ceramic tube enclosed by the steel plug but do not separate from ceramic parts contained by pyrex and the furnace. The uncertainty associated with the correction is larger at 25 kbar because the steel plug appears to grip the thermocouple tube and wires at least to some extent. Table C.8 is a summary of temperature corrections and their estimated uncertainties at pressures and temperatures relevant to this study. The table entries were derived graphically from Getting & Kennedy's (1970) computed curves of correction voltage versus temperature.

P [kb]	P_{cor}	T [°C]			Correction [K]			Uncertainty [K]		
10	7.5	1000	1200	1400	+2.0	+1.8	+1.5	±1.0	±1.0	±1.5
15	12.1	1000	1200	1400	+4.2	+4.0	+3.7	±1.5	±1.5	±2.0
25	21.5	1000	1200	1400	+6.0	+5.8	+5.5	±2.0	±2.0	±2.5

Table C.8: Effect of pressure on the emf of the thermocouple calculated for pressure seal temperatures of 380 °C, 450 °C and 540 °C for run temperatures of 1000 °C, 1200 °C and 1400 °C respectively. P_{cor} denotes pressures corrected for the effect of friction.

Calibration of thermocouples: Platinum–platinum-10%Rh thermocouples (0.25 mm wire diameter) supplied by Johnson & Matthey Canada, Inc., are reliable and precise with an accuracy of better than ±0.25 % at temperatures between 538 and 1482 °C (ASTM Standard E230–72, Powell *et al.*, 1974). This will introduce an uncertainty of ±3 K at the temperatures relevant to this study. No further calibration against melting points of standard reference materials was felt necessary.

Temperature control: Temperature in all experiments was controlled automatically to better than ± 20 μV which corresponds to ± 2 °C at temperatures above 1000 °C. This uncertainty is small compared to effects of thermal gradients.

Electromotive force measurement: The emf of the thermocouple was measured with a Leeds & Northrop 7554 type K-4 potentiometer with a sensitivity of better than 1 μV. The certified 1–volt standard cell (Eppley Laboratory, Inc., cat. no. 100) was checked and calibrated against a high precision digital volt meter to an accuracy of better than $\pm 6\mu V$. Direct comparison under run conditions at 1280 °C, including the ice point compensation, against a FLUKE 8840A voltmeter showed agreement within 2 μV. The FLUKE 8840A voltmeter was calibrated against a FLUKE 8800A meter which was recently certified by the US National Bureau of Standards to an accuracy of better than $\pm 5.8\mu$V. The combined uncertainty of emf measurement, ice point compensation and all extensions and connections is therefore better than $\pm 8\mu$V which is equivalent to ± 0.8 K at temperatures above 1000 °C.

Ice point compensation: A battery powered ΩMEGA ice point compensator (type CJ) for type S and R thermocouples was used initially with an accuracy of ± 0.25 K set by factory calibration. The calibration was checked against the temperature of a well stirred ice bath and agreed to within the specifications. This unit did not perform properly at elevated temperatures creating an excessive correction voltage and thus simulating high apparent temperatures. The unit was replaced by the well-proven ice bath in a dewer flask. For the thermal analysis experiments the ice point compensation was performed at the input terminals to the KEITHLEY (Series 500) data collection system with a temperature sensor attached to the thermal mass of the terminal block. This configuration is accurate to ± 0.5 K from combined calibration uncertainties and thermal gradients amongst the input terminals.

Changes in geometry: The sample assembly was found to perform very stably under pressure and temperature. Thermocouple junction and sample capsule remained in position during all runs reported. The graphite furnace was observed to contract about 0.2 mm in diameter at mid-height, and a slightly elliptical crossection was observed in most runs at 15 kbar and 45–240 minutes duration. At 25 kbar all runs displayed a distinct elliptical cross section without any visible cracks in the furnace wall. Two 120–minute runs at 25 kbar pressure and > 1400 °C were discarded due to excessive asymmetrical deformation of the furnace. Run durations of less than 60 minutes seem to avoid the problem of excessive deformation.

Any effect from this change in geometry is accounted for by the thermal gradient calibration with an identical sample configuration and three independent runs. Each sample assembly was carefully examined after the run in order to exclude erroneous experiments due to changes in sample geometry not included in the calibrations.

Contamination of the thermocouple: Contamination is negligible for runs of short duration (1–4 hours) and at temperatures below approximately 1500 °C. Most runs of this study were shorter than two hours, with a few runs of 4 hours. All thermocouple ceramics made of mullite were boiled in hydrochloric acid as a precaution against iron contamination. McDanel MV20 two-bore and four-bore mullite ceramic tubing has an Fe_2O_3 content of less than 0.8 %, four-bore McDanel 998 alumina ceramic of less than 0.025 %. The superior mechanical properties and smaller manufacturing tolerances of the mullite tube outweigh the disadvantage of higher iron content for short runs. The high precision of the melting point determinations for pressure calibration (cf. below) preclude significant drift of the thermocouples used. Thermocouple contamination can be neglected for the run durations of the experiments of this study.

C.4 Pressure Calibration

The difference between the pressure acting on the carbide piston (i.e. oil pressure) and the pressure experienced by the sample is called 'friction' despite the fact that the actual processes leading to such a difference are not known in detail. This 'friction' can be determined by calibration against well known phase equilibria at high pressure which were determined in gas pressure apparati or with sample assemblies with negligible 'friction'. Several useful equilibria are discussed by Bohlen (1984) and Mirwald *et al.* (1975). Calibration should be performed at pressures and temperatures close to the experiment with comparable run times and procedures and identical sample assemblies. This is in most applications not possible and the uncertainty associated with the differences between calibration and experiment remains unknown.

Friction corrections for talc-pyrex assemblies similar to the design developed in this study are discussed below. The cells differ in diameter, in the type of pressure medium used within the graphite furnace (listed separately if different from pyrex) and in many details concerning the design and run procedures. Direct comparisons are therefore not possible and the actual cause of 'friction' remains speculative. Akella (1979) uses a 1/2-inch talc-pyrex-AlSiMag (a machinable, porous Mg-ceramic material) cell and reports a double value of friction of 2.5–2.9 kbar at 30 kbar and 1000–800 °C calibrated on the quartz $\rightleftharpoons$ coesite transition. The same cell, but with a boron nitride core, was used by Akella & Kennedy (1971) with a friction of about 2.2 kbar at 30 kbar derived from data on the melting curve of silver compared to Mirwald's *et al.* (1975) measurements. Chipman & Hays (in Johannes *et al.*, 1971) use a 1/2-inch talc-pyrex-pyrophyllite cell with a porcelain sample capsule sleeve and employ a −8% correction on piston-in runs calibrated on the equilibrium quartz $\rightleftharpoons$ coesite at 40 kbar and 1400 °C. The interlaboratory comparison study (Johannes *et al.*, 1971) suggests a correction of −1.5 kbar in piston-in runs and no correction for piston-out runs at 17 kbar and 600 °C based on the equilibrium albite

$\rightleftharpoons$ jadeite + quartz. Hariya & Kennedy (1968) use a 1/2-inch talc-pyrex cell with lead foil and apply a correction of −10% but offer no calibration. It is not clear whether they employed piston-in or piston-out procedures. Irving & Wyllie (1975) use a 1/2-inch talc-pyrex-boron nitride cell with lead foil and grease-base molybdenum disulfide lubricant. They use piston-out procedures, apply no correction and offer no calibration. Huang & Wyllie (1975) use a 1/2-inch talc-pyrex-boron nitride assembly, similar or identical to Irving & Wyllie (1975), and probably use lead foil and molybdenum disulfide lubrification. They use the piston-out technique and apply a correction of −3 kbar based on calibrations against the equilibria quartz $\rightleftharpoons$ coesite (30–35 kbar, 800–1100 °C) and albite $\rightleftharpoons$ jadeite + quartz (21–32 kbar, 800–1100 °C). Newton & Sharp (1975) use 3/4-inch talc–soda-lime glass and 1/2-inch talc-pyrex assemblies similar to Hariya & Kennedy (1968) but offer no calibration and assume a correction of −10% for the 1/2-inch cell and −5% for the 3/4-inch cell using piston-in procedures. Haselton, Sharp & Newton (1978) use the same assemblies and procedures as Newton & Sharp (1975) and quote a correction of −8% for the 1/2-inch cell based on a relative comparison to 3/4-inch NaCl-cell data (T.J.B. Holland, unpublished) at 1100–1200 °C on the albite $\rightleftharpoons$ jadeite + quartz equilibrium. The 3/4-inch talc–soft-glass cell is compared to NaCl-cell data at 14 kbar and 950 °C (magnesite + rutile $\rightleftharpoons$ geikielite + CO_2) indicating negligible friction.

We may conclude that the lack of consensus about what 'friction' correction to apply is a result of the variety of cells and run procedures used and, importantly, also the result of the lack of calibrations in several studies. The few calibrations available for 1/2-inch cells using piston-in procedures indicate a correction of −1.5 to −3 kbar, whereas no calibrations seem to be published for 3/4-inch talc-pyrex cells. The uncertainty of knowing the pressure may be as large as −3 kbar (± precision) if no calibration is offered.

For this work the melting curves of gold and silver were chosen as determined by Mirwald *et al.* (1975). Melting point calibration was preferred over bracketing a well studied mineral equilibrium for practical reasons: it is much faster and allows one to collect a complete calibration with one experiment. For a pressure calibration of ±0.5 kbar accuracy the melting temperature of gold or silver needs to be determined to an accuracy of ±3 K. Although the temperature dependence of the melting pressure of silver and gold is rather large there are practical reasons for chosing them: metals display a large heat effect on melting and the high densities of gold and silver permit the use of small sample beads. Furthermore, graphite containers can be used conveniently and both metals are readily available in sufficient purity.

Only few laboratories seem to routinely employ differential thermal analysis in piston–cylinder equipment, notably Mirwald (i.e. 1975) in Bochum. The writer is not aware of any direct thermal analysis experiments having been published, i.e. using a single thermocouple rather than two measuring junctions to record differences. As it will be shown below, one thermocouple combined with a near-linear heating rate is sufficient to define

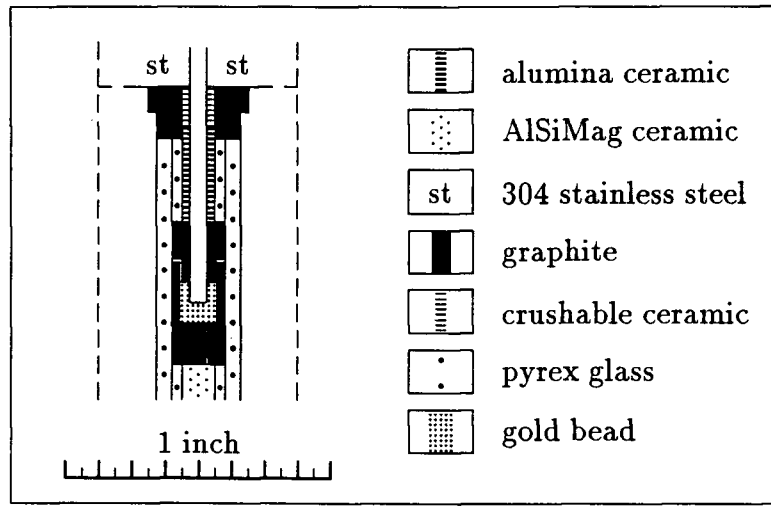

Figure C.18: Sample assembly for melting point calibration of gold and silver.

equilibria with fast reaction rates and large heats of transformation. Our piston–cylinder apparatus was adapted to thermal analysis experiments in the following manner: Temperature was recorded with a personal computer with a Kiethley Series 500 interface that performs the zero-point correction of the thermocouple signal, amplification and analog to digital conversion. Calibration of the temperature measuring system against an ice bath, including the zero–point correction, indicated a correction of +2 K. This correction was verified at run temperatures against a calibrated FLUKE 8840A voltmeter. The raw data (figure C.19 and C.20) were adjusted by +2 K (table C.9 and C.10, figure C.21). The sensitivity of the triggering system for the phase-controled (SCR) AC furnace supply was increased with an additional potentiometer placed in series with the existing set-point potentiometer of the KRISEL controller (Hadidiakos, 1969). The potentiometer was now able to control a range of 80-90 K in ten turns. A motor with variable speed attached to the potentiometer permitted smooth variation of the temperature. A heating/cooling rate of about 20 K per minute turned out to be optimal. Rates of 10 K per minute proved to be unsatisfactory due to the relatively large thermal fluctuations inherent in piston-cylinder apparati. These fluctuations produce apparent thermal arrests at slow heating rates. The biggest problem posed was the signal noise due to inductive pickup from a noisy AC environment. After proper guarding (active driven guard) and grounding, 20–30 % of the emf signals collected at the fastest sampling rate (ca. 10 per second) were unuseable due to noise. On-line software filtering effectively removed the noise with a three-stage filter that sucsessively eliminated the largest spikes and then the smaller ones down to a level of $\pm$ 20 μV ($\pm$ 2 K for a Pt-Rh thermocouple above 1000 °C). The filter had to be simple and efficient in order not to slow down the sampling program written in

BASIC. Satisfactory results were obtained with collecting 10 readings, subsequent filtering, averaging, and output to screen and floppy-disk. This procedure allowed recording a temperature measurement about every 2 seconds. Backward computed temperature differences were diplayed on the screen as a simple means of monitoring thermal arrests.

Gold: The melting of gold under pressure was determined by Mirwald *et al.* (1975), Akella & Kennedy (1971) and Cohen *et al.* (1966) in piston-cylinder apparati. Mirwald's data was obtained in a virtually frictionless salt cell (Mirwald *et al.*, 1975, Mirwald & Massonne, 1980, Johannes, 1978, Bohlen, 1984). This is as accurate a data set as one can possibly expect from piston-cylinder work and little error is introduced by calibrating against it.

Figure C.18 depicts the sample assembly used for the melting point determinations of gold and silver by thermal analysis. The graphite container is 14 mm long with a sample cavity of 4 mm length and 3.5 mm diameter to accommodate a gold bead of 0.6 grams. The gold bead was cast in graphite from acid–cleaned scrap gold tubing with a fineness of better than 99.95 and no detectable impurities measured by electron microprobe analyses (J. Knight, written communication, March, 1990). The well for the thermocouple tube (1/16 in. OD) extends through the graphite lid into the gold bead to insure measuring true sample temperature. The thermocouple junction was recessed below the tip of the mullite (MacDanel MV20 two–bore) insulater in a thin groove cut with a diamond blade and covered with Sauereisen cement for electrical insulation. The cement was sucked partway into the tube with the wires in place to ensure mechanical strength of the insulation. The sample assembly surrounding the graphite container is identical to the one depicted in figure C.15. The assembly performed very stably and survived at least 14 heating and cooling cycles. One or two tiny metal beads were detected embedded in pyrex adjacent to a hairline fissure in the wall of the graphite container in both the gold and silver experiments. One attempt for each the gold and silver calibration was successful to obtain the entire series of measurements required.

Run procedures were identical to the run procedures described for the phase equilibrium experiments including hot compaction for 20 minutes below the melting temperature of gold. The temperature was steadily increased from about 20 K below the expected melting point to about 20 K above melting and then reversed. At least four determinations were recorded at each pressure. Pressure was always increased and never decreased and time for relaxation of stresses was allowed before starting measurements at a new pressure. The measurements are remarkably precise. Only determinations at three different pressures were required to establish a relatively straight melting curve (compare figure C.21). Data are presented in figure C.19 and C.21 and in table C.9.

Silver: The melting of silver under pressure was determined by Mirwald *et al.* (1975) and Akella & Kennedy (1971) in piston-cylinder apparati. Mirwald's data was obtained in a virtually frictionless salt cell (Mirwald *et al.*, 1975, Mirwald & Massonne, 1980,

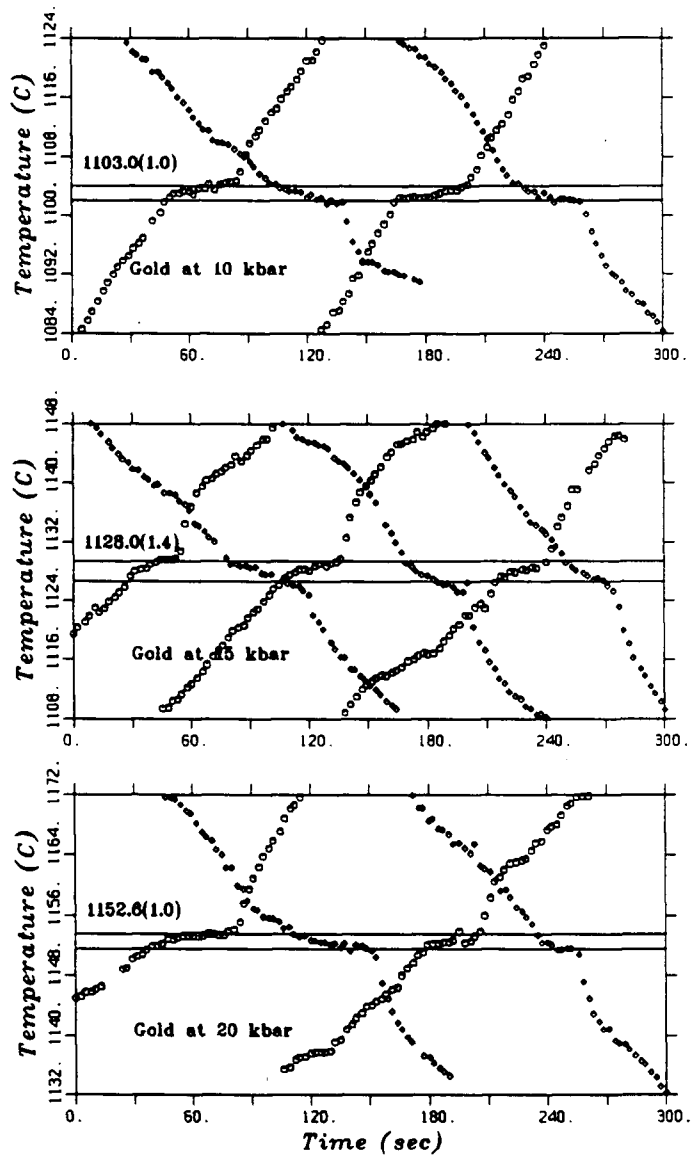

Figure C.19: Thermal analysis traces of melting of gold under pressure.

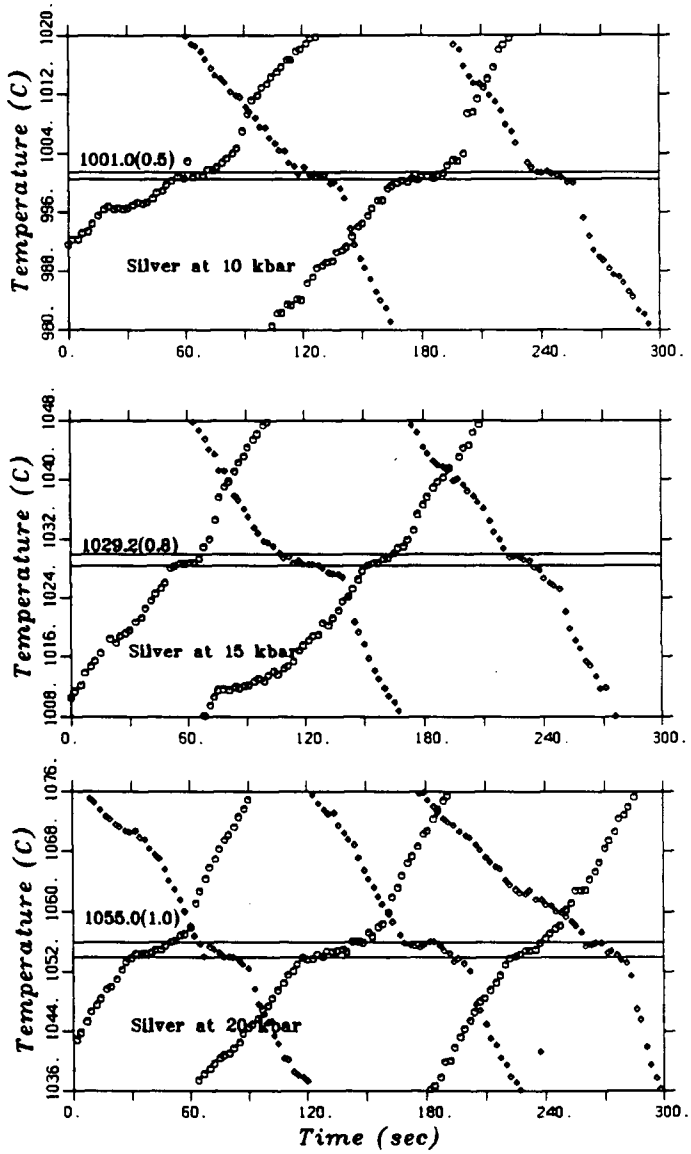

Figure C.20: Thermal analysis traces of melting of silver under pressure.

	Mirwald (1975) [°C]			Mäder [°C]					Δ(Mä–Mi)	'friction'
P [kb]	T_m	T_{corr}	unc.	N	T_m	T_{corr}	prec.	unc.	Δ T [°C]	Δ P [kb]
10.0	1118	1120	±4.0	4	1105	1107	±1.0	±4.0	-13.0±3	-2.5±0.5
15.0	1146	1150	±4.5	6	1130	1134	±1.5	±5.0	-15.0±3	-2.9±0.5
20.0	1173	1178	±5.0	4	1154.6	1159.6	±1.0	±5.0	-18.4±3	-3.5±0.5

Table C.9: Melting point determination of gold under pressure. T_m denotes the uncorrected melting temperature, T_{corr} the melting temperature corrected for the effect of pressure on the emf, 'prec.' is short for precision and 'unc.' for uncertainty. Mirwald's data is interpolated from experimental measurements at 28–56 kbar. Data for T_m (Mäder) has been corrected by +2 K from figure C.19 based on calibration (see text).

	Mirwald (1975) [°C]			Mäder [°C]					Δ(Mä–Mi)	'friction'
P [kb]	T_m	T_{corr}	unc.	N	T_m	T_{corr}	prec.	unc.	Δ T [°C]	Δ P [kb]
10.0	1018	1020	±4.0	4	1003.0	1005	±1	±4.0	-15±3	-2.9±0.5
15.0	1047	1051	±4.5	4	1031.2	1035	±1	±4.5	-16±3	-3.1±0.5
20.0	1075	1080	±5.0	6	1057.0	1062	±1	±5.0	-18±3	-3.3±0.5

Table C.10: Melting point determination of silver under pressure. T_m denotes the uncorrected melting temperature, T_{corr} the melting temperature corrected for the effect of pressure on the emf, 'prec.' is short for precision and 'unc.' for uncertainty. Mirwald's data is interpolated from experimental measurements at 28–56 kbar. Data for T_m (Mäder) has been corrected by +2 K from figure C.20 based on calibration (see text).

Johannes, 1978, Bohlen, 1984) and in a pyrophyllite cell for comparsion of friction. The salt cell data are demonstrated to be accurate and little error is introduced by calibrating against it. Akella and Kennedy (1971) used a talc-pyrex-boron nitride cell and observed melting at distinctly higher pressures compared to Mirwald *et al.* (1975) due to effects of friction or differential loading.

The sample assembly for this study is identical to the one described for the gold calibration. The silver bead (0.4 g) was machined from high purity silver. The smaller mass of the silver bead compared to the gold sample leads to a slightly less pronounced thermal arrest on melting or freezing. The measurments are presented in figure C.20 and figure C.21 and tabulated in table C.10.

Cesium Chloride: The melting curve of cesium chloride was determined in an internally heated gas pressure apparatus to 15 kbar and 1170 °C by Clark (1959) using differential thermal analysis and up to 5 kbar by Bohlen (1984) using the 'falling sphere' method. Melting was also determined by Bohlen (1984) in a piston-cylinder apparatus with a frictionless one-inch salt cell between 5 and 15 kbar employing the 'falling sphere' method. Clark's reported temperatures need to be corrected for a much exagerated pressure correction on the electromotive force of the Pt–Pt10%Rh thermocouple based on

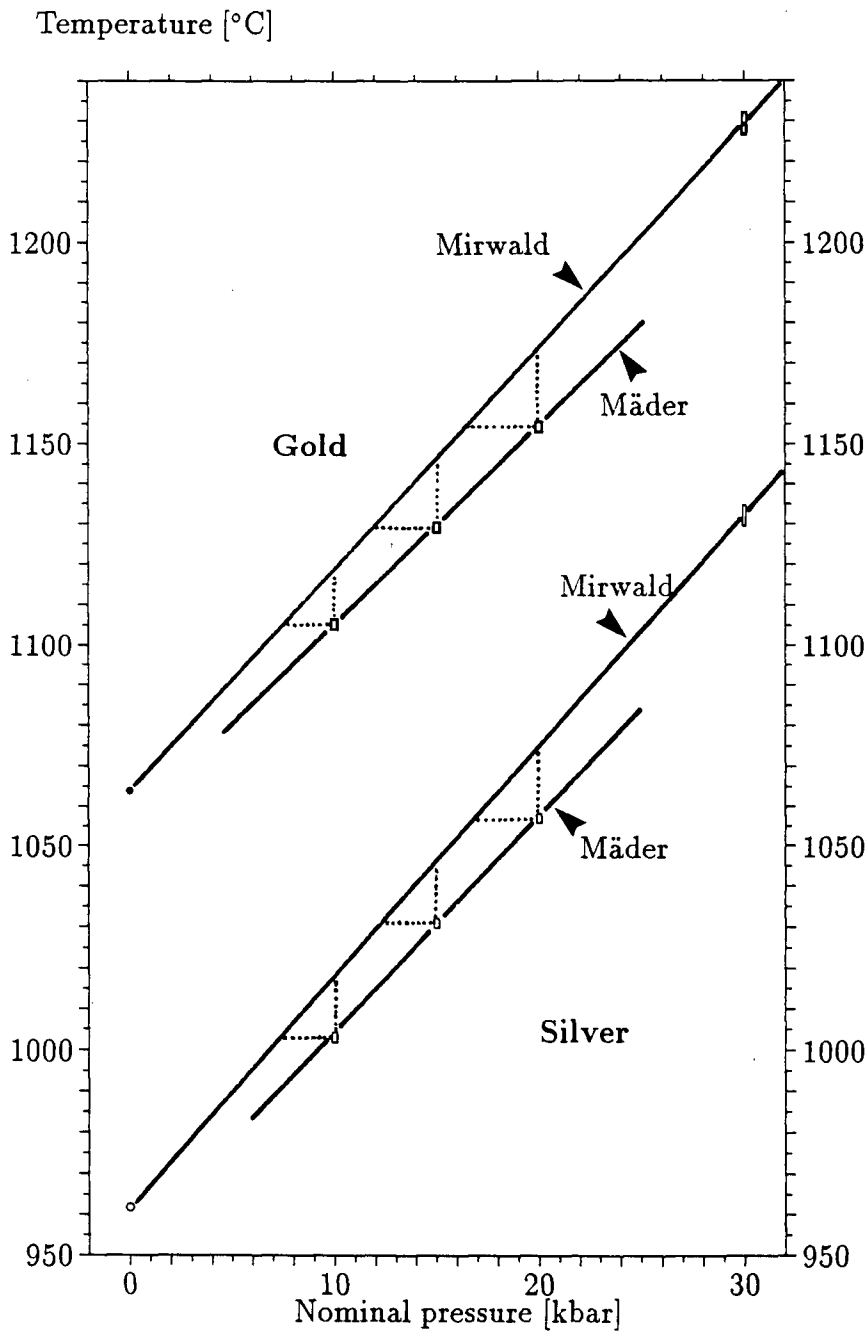

Figure C.21: Melting of gold and silver under pressure. The calibration curves labeld 'Mirwald' are interpolated from data by Mirwald *et al.* (1975) at 28–56 kbar. Dotted lines trace the measured difference in melting temperature between Mirwald and this study and the resultant pressure difference ('friction'). The size of the symbols for the data points represents the precision of the measurements.

wrongly assumed linear extrapolation (Getting & Kennedy, 1970) from Birch's (1939) measurements. Clark's temperatures need to be converted to the IPTS-68 temperature scale (Powell *et al.*, 1974) which adds about 3 K between 1000 and 1200 °C. Taking these corrections into account Clark's melting curves for CsCl, LiCl and NaCl are systematically underestimated by 10–15 °C compared to Bohlen's measurements in both solid-medium and gas-medium apparati. The reasons for this discrepancy are unclear but are partially attributed by Bohlen (1984) to reported impurities in Clark's starting materials. The temperature discrepancy translates into a difference in pressure of 0.3–0.7 kbar. Cesium chloride is nevertheless a suitable material for pressure calibration up to 20 kbar having the largest temperature gradient with respect to pressure on melting compared to other alkali chlorides and halogenides (Clark, 1959). I prefer Bohlen's data because there are more possibilities to accidentally measure too low a melting temperature than the converse.

Thermal analysis experiments with gold and silver indicate that the ideal sample mass should not be much less than 0.3 grams spread over as short a vertical dimension as possible to reduce thermal gradients. This was achieved with a 4.8 mm OD platinum capsule (0.2 mm wall) with a well (2.0 mm ID) for the thermocouple. For easy fabrication the large and small diameter tubes of 15 mm length were secured concentrically by a stainless steel cylinder, crimped together in a drill chuck and fused with a welding torch. The annular sample container was then filled with 0.28 grams of CsCl, compacted with the steel cylinder to an effective sample length of 7 mm and crimped around the inner tube with a drill chuck resulting in a bottle shaped container with a 5 mm long neck. The ring-shaped welding seam at the top with three flanges resulting from the triangular crimp required some welding experience with a plasma arc welder. An aluminum block with an appropriate bore diameter served as heat sink during welding to prevent excessive heating of the sample. Spec pure cesium chloride (SPEX Industries, Inc., lot 03781) was dried at 400 °C for 10 hours and stored at 120 °C. The capsule was placed into the 3/4-inch assembly (figure C.15) in the same fashion as the graphite container in figure C.18. All irregular spaces around the platinum capsule were filled with pyrex powder. The thermocouple junction was positioned in the platinum well with a ceramic spacer. The sample was allowed to compact at 8 kbar gauge pressure initially at a temperature below the melting of CsCl (ca. 640 °C at 1 bar) and then at slowly increasing temperature. Furnace controle and temperature recording were done with the same set-up as the gold calibration. Heating rates of about 20 °C per minute were adequate.

The recorded thermal analysis traces between 10 and 20 kbar are unfortunately useless for pressure calibration purposes. The melting signal is distinct although less clearly defined than with gold or silver with an arrest defined in most runs within ± 2 K. The pressure within the sample assembly, however, is inferred to vary with temperature and perhaps also during melting without a change in gauge pressure. It appears that the

P [kb]	Correction [kb]	Uncertainty [kb]
10.0	-2.5 (25 %)	± 1.0
15.0	-3.0 (20 %)	± 1.0
20.0	-3.3 (16 %)	± 1.0
25.0	-3.5 (14 %)	± 1.0

Table C.11: Pressure correction due to friction for the 3/4–inch talc-pyrex assembly.

large sample size and the large increase of the volume during melting of CsCl (ca. 5.6 cm^3/mole, Clark, 1959) are enough to increase sample pressure during heating within the 2–3 kbar friction interval calibrated with gold and silver where the gauge pressure is not expected to rise or fall upon heating or cooling. At 10 kbar gauge pressure 8 heating-cooling cycles were recorded yielding thermal arrests spread over a 70 K interval from 935–1005 °C which suggests a pressure interval of 2 kbar. The melting temperature at 10 kbar obtained by Clark (1959) is at 1005 °C and that obtained by Bohlen (1984) is at approximately 1117 °C. Single heating runs at 1 kbar intaervals from 11 to 17 kbar indicate a 2 kbar friction defined by the lowest measured melting signals. The scatter of the data towards higher temperatures is substantial due to the variable amount of temperature increase and therefore also pressure increase before the melting curve is intersected. Several runs also indicate 'gliding' along the melting curve for as much as 40 K or 1.3 kbar.

Friction correction: The term 'friction' applied to piston cylinder experiments lumps together contributions from friction between the sample assembly and the carbide wall, friction between the carbide piston and the carbide pressure vessel, stresses stored in the assembly materials not transmitted to the sample and various other contributions such as differential loading (negative and positive anvil effects). The magnitude of friction is a function of pressure, temperature, assembly geometry, assembly materials and run procedures. Details, such as the type of lubricant used, may play a significant role in the amount of friction observed. It is imperative that each pressure cell design be calibrated separately using identical run procedures as in the experiments to be performed. Friction correction applied by analogy with the experiences of other researchers in a different laboratory is not sufficient.

Friction corrections relevant to this study are summarized in table C.11 with uncertainties derived from calibration uncertainties of the melting point determinations. The uncertainty is the sum of the effect of temperature uncertainty (± 3 K, ± 0.5 kbar) and the uncertainty of knowing the run pressure (± 0.5 kbar). The uncertainty associated with Mirwald's *et al.* (1975) calibration is negligible compared to the above contributions.

Discussion: The relatively large friction in the talc–pyrex cell of this study is largely due to 'true friction' between the sample assembly and the carbide bore. It seems unreasonable that the talc sleeve could support a differential load of several kilobars. The

cold lower end of the sample assembly with talc, graphite and solid glass may form a plug responsible for the observed friction. In fact, such an effect is observed at the cold upper end during extrusion of the sample assembly after each run: the friction decays suddenly to about 20–30 % of the initial value after the steel plug with the pyrophyllite sleeve are pushed beyond the carbide bore. Friction may therefore be reduced substantially by introducing a pressure medium that is able to flow at low temperatures. It is hypothesized that replacing the talc sleeve with a NaCl sleeve may result in an almost negligible friction.

C.5 Run Procedures for Phase Equilibrium Experiments

The sample assembly was compacted slowly to about 8 kbar at room temperature and then softened by increasing the temperature. The softening point of pyrex under these conditions is at about 540 °C. Reactant starting materials were held at 50–100 K below the equilibrium temperature and product starting materials were quickly heated to 50–100 K above the approximate equilibrium temperature. Pressure and temperature were then increased simultaneously up to final run pressure keeping the temperature either below or above the final run temperature. The samples were held at these conditions for approximately 15 minutes in order to allow stresses within the sample assembly to relax while holding pressure constant by advancing the piston. This stress relaxation was equivalent to pumping about 10–15% of the run pressure. After pressure stabilization the final run temperature was approached and first controlled manually and after a few minutes automatically. During the subsequent 45 to 140 minutes additional relaxation occured requiring further pumping of not more than a total of 2–3% of the run pressure. All runs and calibrations were performed in the same pressure vessel with the same carbide parts which developed only insignificant damage from wear and tear.

The quench from run conditions was a temperature quench for reactant starting materials and a combined pressure quench followed by a temperature quench for product starting materials. The temperature quench proceeded at an initial rate in excess of 100 K per second.

C.6 Equilibrium magnesite $\rightleftharpoons$ periclase + CO_2

Starting materials: Synthetic periclase and magnesite were used as starting materials with silver-oxalate as the source for carbon dioxide. Reagent grade periclase was fired at 1200 °C for 6 hours and stored in a drying oven at 120 °C. Magnesite was synthesized from reagent grade basic magnesium carbonate (approx. $(MgCO_3)_4 \cdot Mg(OH)_2 \cdot 5\,H_2O$) sealed in silver or gold capsules and kept for 100–110 houres at 2 kbar gas pressure and 690–700 °C in cold-seal pressure vessels at mole fractions of water in the CO_2 fluid of

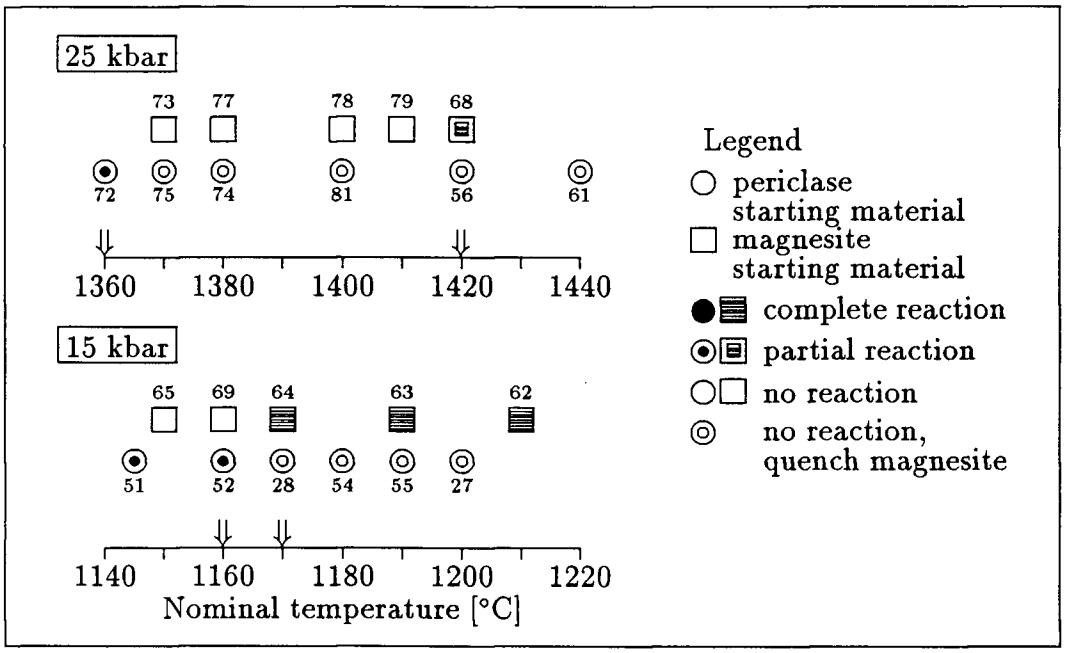

Figure C.22: Experimental brackets on the equilibrium magnesite $\rightleftharpoons$ periclase + carbon dioxide. Arrow marks define the limits of each bracket. Pressures and temperatures are nominal values and not corrected. See table C.12 and text for discussion of calibrations and corrections. Numbers refer to run numbers in table C.12.

0.3–0.4. Pure basic magnesium carbonate would produce a mole fraction of water in the fluid of approximately 0.6 on devolatilization which was diluted by adding silver oxalate as an additional source of CO_2. The synthesized material was checked by X-ray powder diffractometry and consisted of a very fine grained (5–20 μm), fluffy, euhedral magnesite with no other phases detectable (see also figure C.25b).

Carbon dioxide was added to the experimental charges in the form of silver–oxalate ($Ag_2C_2O_4$, Dixon Fine Chemichals, lot 02708), stored light–tight in a desiccator. Silver oxalate releases its carbon dioxide explosively at about 140 °C under ambient pressure. Silver is reduced in this process to the metallic state and does not participate in the reaction at run conditions. The explosive character of this reaction at ambient pressure requires cooling of the sample charges during the welding of capsule seams.

Sample preparation: Starting materials for the 3/4 inch pyrex assembly were sealed into 3 mm OD platinum capsules (2.6 mm ID), 8–9 mm long including a triangular crimp of 3–4 mm length for easy welding. The capsules contained 7–10 mg magnesite or periclase. 7–10 mg of silver-oxalate were added to magnesite and 15–20 mg were added to periclase. The triangular crimp done in a drill chuck maintains a circular cross section of the platinum capsule and provides a very strong welding seam. Welding was

done with a plasma needle–arc welder (LINDE PWM–6) or equally well with a simple graphite electrode electric welder. In either case the capsule was cooled by a few wraps of water soaked tissue contained in a bored aluminum block. Additional electrical grounding proved helpful by wrapping copper wire around the sample capsule about 2 mm below the welding seam.

The capsules were placed into the assembly with the crimped end pointing downward which results in an effective sample length of no more than 4 mm. A relatively long crimped end also provides for extra volume if required by the amount of fluid enclosed in the capsule. Any void spaces around the capsule were well packed with pyrex powder.

Results: Two brackets were reversed on the equilibrium $MgCO_3 \rightleftharpoons MgO + CO_2$, one at 15 kbar and one at 25 kbar nominal pressure, both with the 3/4–inch assembly. All runs are listed in table C.12 with uncertainties and corrections. Most capsules opened with a hiss from escaping carbon dioxide proving the presence of a CO_2 fluid at run conditions. Critical runs that did not lose gas on opening were discarded and repeated. Run products were examined under the light microscope and by X-ray powder diffraction. Some textures were further investigated under the scanning electron microscope using secondary electron imaging on gold–coated powder mounts. Reaction progress was established by three independent methods: estimated from grain mounts under the microscope, by X-ray intensities, and by the weight of CO_2 produced or consumed during the run calculated from the amount of CO_2 released on opening the capsule after the run. The accuracy of the latter method is not satisfactory with an uncertainty of approximately ± 4 mg on the amount of CO_2 produced or consumed which translates into an uncertainty of about 10 percentage points in the amount of reaction progress computed in table C.13. Details of run products are summarized in table C.13.

The equilibrium at 12.1 ± 1.0 kbar is located between 1173 ± 10 °C and 1183 ± 10 °C with a temperature interval of 10 ± 10 K where no reaction progress is observed at run times of 45–140 minutes. The bracket at 21.5 ± 1.0 kbar spans an interval of 60 ± 10 K and is located between 1375 ± 10 °C and 1435 ± 10 °C.

Textures: Textures of run products were studied under the scanning electron microscope (SEMCO Nanolab 7) in order to assist with the interpretation of the extent of reaction deduced from light microscopy and X-ray diffraction. Specifically, the study aimed towards narrowing the 60 K–interval at 21.5 kbar where no nucleation and growth of new phases were observed without ambiguity. It was anticipated that textural observations would facilitate the distinction between stably grown magnesite and magnesite formed during the temperature quench.

Loose powder or gently crushed aggregates from sample capsules were mounted on aluminum stubs. Nail polish served as binder with its stickiness controled by placing the sample spread on a dry nail polish film under acetone vapour for an appropriate amount of time. The samples were coated with gold to a thickness of about 30–40 nm. The

Run	Pressure [kbar]		Temperature [°C]		Time	Starting	Run
	nominal	corrected	nominal	corrected	[min]	materials	products
UP-24	15 (0.5)	12.1 (1)	1285 (7)	1298 (10)	55	Mc,AgOx	a(Pe),qs(Mc)
UP-25	15 (0.5)	12.1 (1)	1250 (7)	1263 (10)	65	Pe,AgOx	e(Pe),qt(Mc)
UP-26	15 (0.5)	12.1 (1)	1230 (7)	1243 (10)	50	Pe,AgOx	e(Pe),qt(Mc)
UP-27	15 (0.5)	12.1 (1)	1200 (7)	1213 (10)	65	Pe,AgOx	e(Pe),qt(Mc)
UP-28	15 (0.5)	12.1 (1)	1170 (7)	1183 (10)	85	Pe,AgOx	e(Pe),qt(Mc)
UP-50	15		1150		65	Pe,AgOx	CO_2 leak
UP-51	15 (0.5)	12.1 (1)	1145 (7)	1158 (10)	155	Pe,AgOx	e(Pe),am(Mc)
UP-52	15 (0.5)	12.1 (1)	1160 (7)	1173 (10)	100	Pe,AgOx	a(Mc),em(Pe)
UP-53	15 (0.5)	12.1 (1)	1170 (7)	1183 (10)	115	Pe,AgOx	e(Pe),qt(Mc)
UP-54	15 (0.5)	12.1 (1)	1180 (7)	1193 (10)	95	Pe,AgOx	e(Pe),qtr(Mc)
UP-55	15 (0.5)	12.1 (1)	1190 (7)	1203 (10)	105	Pe,AgOx	e(Pe),qt(Mc)
UP-56	25 (0.5)	12.1 (1)	1420 (7)	1435 (10)	115	Pe,AgOx	e(Pe),qs(Mc)
UP-57	15 (0.5)	12.1 (1)	1230 (7)	1243 (10)	110	Mc,AgOx	a(Pe),qs(Mc)
UP-58	15 (0.5)	12.1 (1)	1240 (7)	1253 (10)	105	Mc,AgOx	a(Pe),qs(Mc)
UP-59	15 (0.5)	12.1 (1)	1260 (7)	1273 (10)	115	Mc,AgOx	a(Pe),qs(Mc)
UP-60	15 (0.5)	12.1 (1)	1300 (7)	1313 (10)	130	Mc,AgOx	a(Pe),qs(Mc)
UP-61	25 (0.5)	21.1 (1)	1440 (7)	1455 (10)	115	Pe,AgOx	e(Pe),qs(Mc)
UP-62	15 (0.5)	12.1 (1)	1210 (7)	1223 (10)	120	Mc,AgOx	a(Pe),qs(Mc),t(Mc)
UP-63	15 (0.5)	12.1 (1)	1190 (7)	1203 (10)	160	Mc,AgOx	a(Pe),qs(Mc),q(Mc)
UP-64	15 (0.5)	12.1 (1)	1170 (7)	1183 (10)	140	Mc,AgOx	a(Pe),qs(Mc),q(Mc)
UP-65	15 (0.5)	12.1 (1)	1150 (7)	1163 (10)	125	Mc,AgOx	e(Mc), furnace def.
UP-66	15		1160		115	Mc,AgOx	furnace deformed
UP-67	25		1420		110	Mc,AgOx	furnace deformed
UP-68	25 (0.5)	21.5 (1)	1420 (7)	1435 (10)	55	Mc,AgOx	a(Pe),a(Mc),qs(Mc)
UP-69	15 (0.5)	12.1 (1)	1160 (7)	1173 (10)	120	Mc,AgOx	e(Mc)
UP-70	25 (0.5)	21.5 (1)	1400 (7)	1415 (10)	60	Pe,AgOx	e(Pe),qs(Mc)
UP-71	25 (0.5)	21.5 (1)	1380 (7)	1395 (10)	60	Pe,AgOx	e(Pe),qs(Mc),q(Mc)
UP-72	25 (0.5)	21.5 (1)	1360 (7)	1375 (10)	60	Pe,AgOx	a(Mc),e(Pe)
UP-73	25 (0.5)	21.5 (1)	1370 (7)	1385 (10)	45	Mc,AgOx	e(Mc)
UP-74	25 (0.5)	21.5 (1)	1380 (7)	1395 (10)	60	Pe,AgOx	e(Pe),qs(Mc),q(Mc)
UP-75	25 (0.5)	21.5 (1)	1370 (7)	1385 (10)	60	Pe,AgOx	e(Pe),qs(Mc),q(Mc)
UP-76	25		1380			Mc,AgOx	furnace failure
UP-77	25 (0.5)	21.5 (1)	1380 (7)	1395 (10)	55	Mc,AgOx	e(Ms)
UP-78	25 (0.5)	21.5 (1)	1400 (7)	1415 (10)	55	Mc,AgOx	e(Ms)
UP-79	25 (0.5)	21.5 (1)	1410 (7)	1425 (10)	55	Mc,AgOx	e(Ms)
UP-80	25					Pe,AgOx	furnace failure
UP-81	25 (0.5)	21.5 (1)	1400 (7)	1415 (10)	105	Pe,AgOx	e(Pe),qs(Mc),q(Mc)

Table C.12: List of experiments on magnesite decarbonation. Numbers in parentheses refer to precision (columns 'nominal P, T') and uncertainty (columns 'corrected P, T'). Abreviations: Pe: periclase, Mc: magnesite, AgOx: silver oxalate, m: minor, t: trace, q: quench product, s: skins, a: anhedral, e: euhedral.

electron microscope was operated with an acceleration potential of 15 kV. Secondary electron images were recorded on Polaroid 52 film.

Figures C.23, C.24, and C.25 depict the range of textures observed in a study of 15 samples. At 15 kbar the nucleation and growth of periclase appear to proceed rapidly: the decarbonation reaction went to completion in all runs above the narrowly defined equilibrium temperature (figure C.22). The growth of magnesite from periclase proceeded at a much slower rate documented by the mixtures of periclase and well crystallized magnesite quenched from run conditions. In figure C.23a thin quench skins of magnesite are visible on periclase formed from magnesite where the skin is broken at several places (i.e. left of center, near top). The peculiar shape of the magnesite crystals presumably formed from linking at random arrays of globular magnesite starting material (grain size of 5–20 μm) during reaction progress.

At 25 kbar nominal pressure difficulties in nucleating either magnesite or periclase were encountered resulting in a temperature interval of 60 K where no reaction progress was observed. The low–temperature side of the reaction was defined by growth of large magnesite crystals (figure C.23b) with relict spherical periclase inclusions clearly visible. At higher temperatures periclase starting material displayed thick skins of magnesite (figure C.24a) which were interpreted as quench products based on the lack of magnesite crystal morphologies. Rare sponge–like aggregates of probable magnesite were observed in runs 71, 74, 75 and are illustrated in figure C.24b. These aggregates are birefringent and show domains of coherent optical orientation. 'Very fine–grained spongy aggregates' of magnesite were observed by Harker & Tuttle (1955) in cold–seal experiments at 1.3 kbar and 800–850 °C employing the 'slow–quench' method using compressed air. These aggregates were not observed in runs quenched more rapidly by plunging the pressure vessel into a bucket of water. The authors therefore conclude that these magnesite aggregates were quench products. Considering the extremely fast quench rates of a piston–cylinder apparatus compared to cold–seal equipment it is unlikely that the two 'sponge–like' aggregates represent the same feature. The lack of any crystal morphology may perhaps be indicative of a quench product. The size of the aggregates is similar to the periclase grains and may therfore be a replacement of former periclase grains. Condensation from the vapour phase might also be considered a mechanism of formation, although one would expect nucleation during condensation to occur on surfaces rather than forming separate particles. While the significance of these aggregates remains enigmatic one cannot make a strong case for these features being stably formed magnesite. Runs with magnesite starting material, on the other hand, do not show any complex textures. Magnesite grains become more euhedral at 25 kbar (figure C.25a) than the hydrothermally produced starting material (figure C.25b). At a nominal temperature of 1440 °C partial decarbonation is observed marking the high–temperature side of the experimental bracket.

While this analysis of textures is interesting and may contribute towards the analysis of kinetics of reactions, it does not put tighter limits on the location of the equilibrium position at 25 kbar. It is, however, concluded that reaction rates need not be as fast as portrayed in some studies (Irving & Wyllie, 1975) where run times of only minutes were considered sufficient to let reactions proceed to completion.

Run	P	T	Starting	Products			
	[kb]	[°C]	materials	optical examination	X-ray	% R	SEM
UP-24	15	1285	Mc,AgOx	p(Pe),qs(Mc)	–	–	–
UP-25	15	1250	Pe,AgOx	e(Pe),qt(Mc)	Pe,w(Mc)	–	–
UP-26	15	1230	Pe,AgOx	e(Pe),qt(Mc)	–	–	–
UP-27	15	1200	Pe,AgOx	e(Pe),qt(Mc)	–	–	e(Pe),qs(Mc)
UP-28	15	1170	Pe,AgOx	e(Pe),qt(Mc)	–	100 Pe	e(Pe),qs(Mc)
UP-51	15	1145	Pe,AgOx	e(Pe),am(Mc)	Pe,m(Ms)	–	–
UP-52	15	1160	Pe,AgOx	a(Mc),em(Pe)	Mc,m(Pe)	67 Pe	–
UP-53	15	1170	Pe,AgOx	e(Pe),qt(Mc)	Pe,w(Mc)	100 Pe	–
UP-54	15	1180	Pe,AgOx	e(Pe),qt(Mc)	Pe,w(Mc)	100 Pe	–
UP-55	15	1190	Pe,AgOx	e(Pe),qt(Mc)	Pe,w(Mc)	100 Pe	–
UP-56	25	1420	Pe,AgOx	e(Pe),qs(Mc)	Pe,d(Mc)	96 Pe	e(Pe), Qs(Mc)
UP-57	15	1230	Mc,AgOx	p(Pe),qs(Mc)	Pe	81 Mc	–
UP-58	15	1240	Mc,AgOx	p(Pe),qs(Mc)	–	0 Mc	–
UP-59	15	1260	Mc,AgOx	p(Pe),qs(Mc)	–	0 Mc	–
UP-60	15	1300	Mc,AgOx	p(Pe),qs(Mc)	–	0 Mc	p(Pe), qs(Mc)
UP-61	25	1440	Pe,AgOx	e(Pe),qs(Mc)	Pe	0 Pe	e(Pe), Qs(Mc)
UP-62	15	1210	Mc,AgOx	p(Pe),qs(Mc),t(Mc)	Pe,w(Mc)	46 Mc	g+p(Pe), qs(Mc)
UP-63	15	1190	Mc,AgOx	p(Pe),qs(Mc),q(Mc)	Pe,d(Mc)	100 Mc	–
UP-64	15	1170	Mc,AgOx	p(Pe),qs(Mc),q(Mc)	Pe,d(Mc)	28 Mc	p(Pe), qs(Mc)
UP-68	25	1420	Mc,AgOx	a(Pe),a(Mc),qs(Mc)	–	50 Mc	–
UP-69	15	1160	Mc,AgOx	e(Mc)	–	90 Mc	f(Mc)
UP-70	25	1400	Pe,AgOx	e(Pe),qs(Mc),q(Mc)	–	q leak	–
UP-71	25	1380	Pe,AgOx	e(Pe),qs(Mc),q(Mc), S	–	q leak	–
UP-72	25	1360	Pe,AgOx	a(Mc),e(Pe)	–	58 Pe	e(Mc), r(Pe)
UP-73	25	1370	Mc,AgOx	e(Mc)	–	100 Mc	e+f(Mc)
UP-74	25	1380	Pe,AgOx	e(Pe),qs(Ms),q(Ms)	Pe	q leak	e(Pe), Qs(Mc), S
UP-75	25	1370	Pe,AgOx	e(Pe),qs(Ms),q(Ms)	Pe	72 Pe	e(Pe), Qs(Mc), S
UP-77	25	1380	Mc,AgOx	e(Mc)	–	86 Mc	–
UP-78	25	1400	Mc,AgOx	e(Mc)	–	90 Mc	e(Mc)
UP-79	25	1410	Mc,AgOx	e(Mc)	–	100 Mc	e(Mc)
UP-81	25	1400	Pe,AgOx	e(Pe),qs(Mc),q(Mc)	–	100 Pe	e(Pe), Qqs(Mc)

Table C.13: Summary of run products and textures of magnesite decarbonation experiments. Optical examination was carried out on powder mounts immersed in oil (n = 1.73). X–ray examination was performed on powder mounts on quartz slides ((**001**) surface) with Cu-K_α radiation. The '% Reaction' column indicates the amount of reaction progress expressed as a percentage of starting material not reacted. The amount of CO_2 produced or consumed was determined from the measured amount of CO_2 loss on opening of the capsule after each run and the total amount in the capsule introduced with silver oxalate and magnesite. The accuracy of this method is about 10 percentage points. Runs marked 'q leak' have experienced CO_2 leakage during the quench. See text for discussion of the textures observed under the scanning electron microscope. Abreviations: Pe: periclase, Mc: magnesite, AgOx: silver oxalate, m: minor, t: trace, q: quench product, s: skins, w: weak, d: distinct, a: anhedral, e: euhedral, Qs: thick quench skins, S: spongy aggregates (see text), g: globular, f: facetted grains with rounded corners and edges, p: periclase with 'peculiar' shape (see figure C.23a).

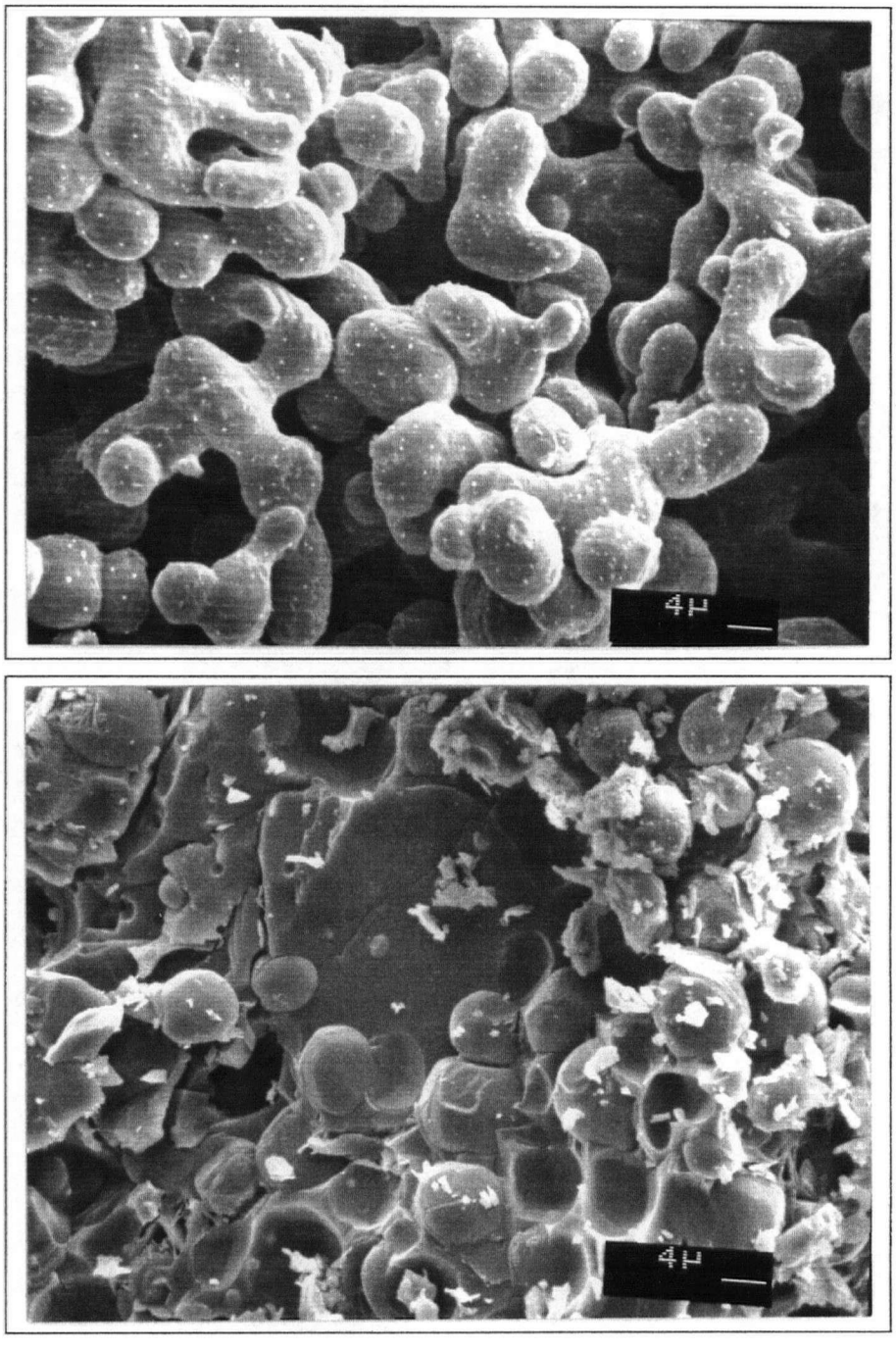

Figure C.23: Plate I of textures of experimental run products viewed under the scanning electron microscope using secondary electron imaging: a) run UP–60, 15 kbar, 1300 °C, 130 minutes, b) run UP–72, 25 kbar, 1360 °C, 60 minutes. See text for discussion of textures.

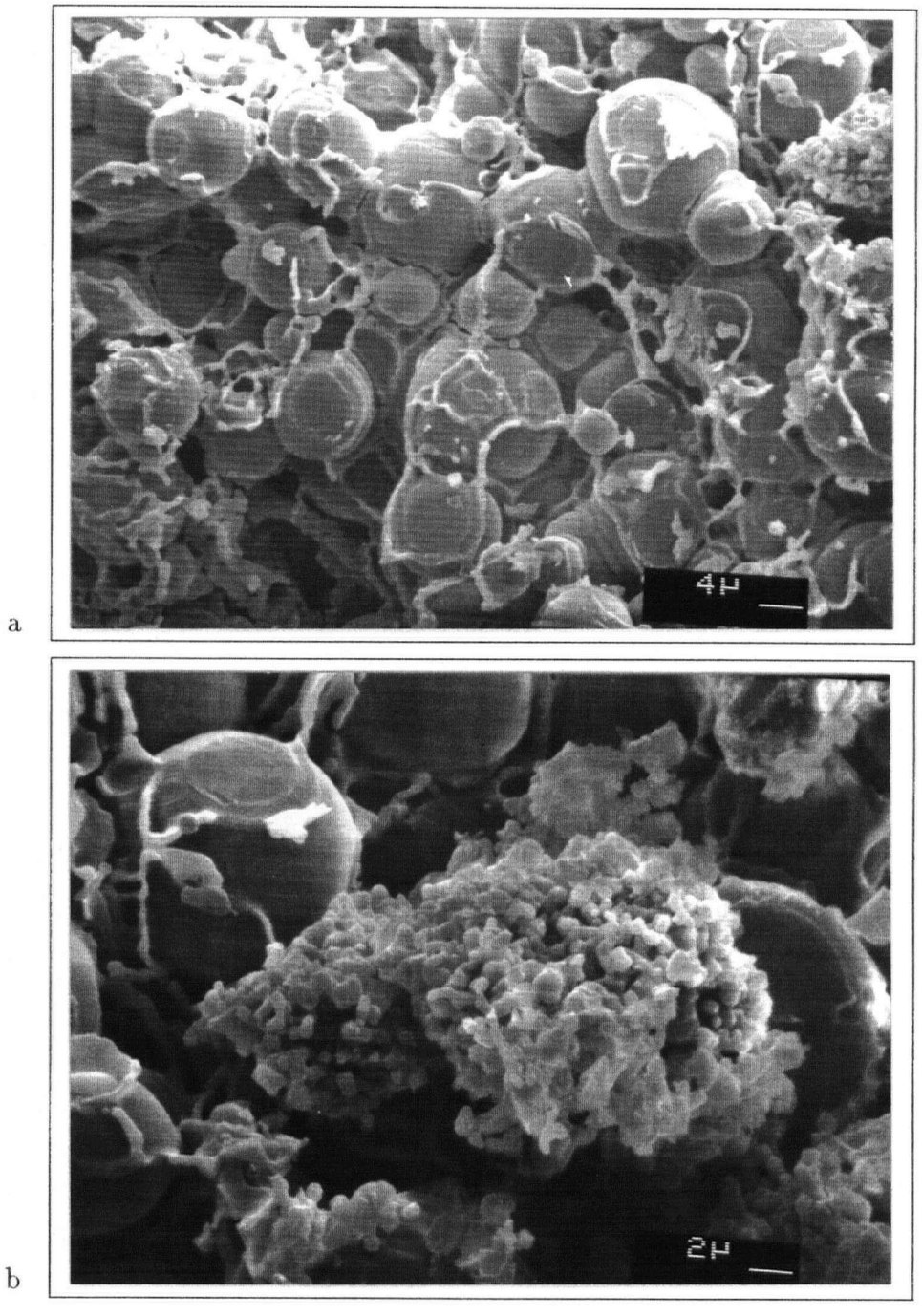

Figure C.24: Plate II of textures of experimental run products viewed under the scanning electron microscope using secondary electron imaging: a) run UP–75, 25 kbar, 1370 °C, 60 minutes, b) run UP–75, 25 kbar, 1370 °C, 60 minutes. See text for discussion of textures.

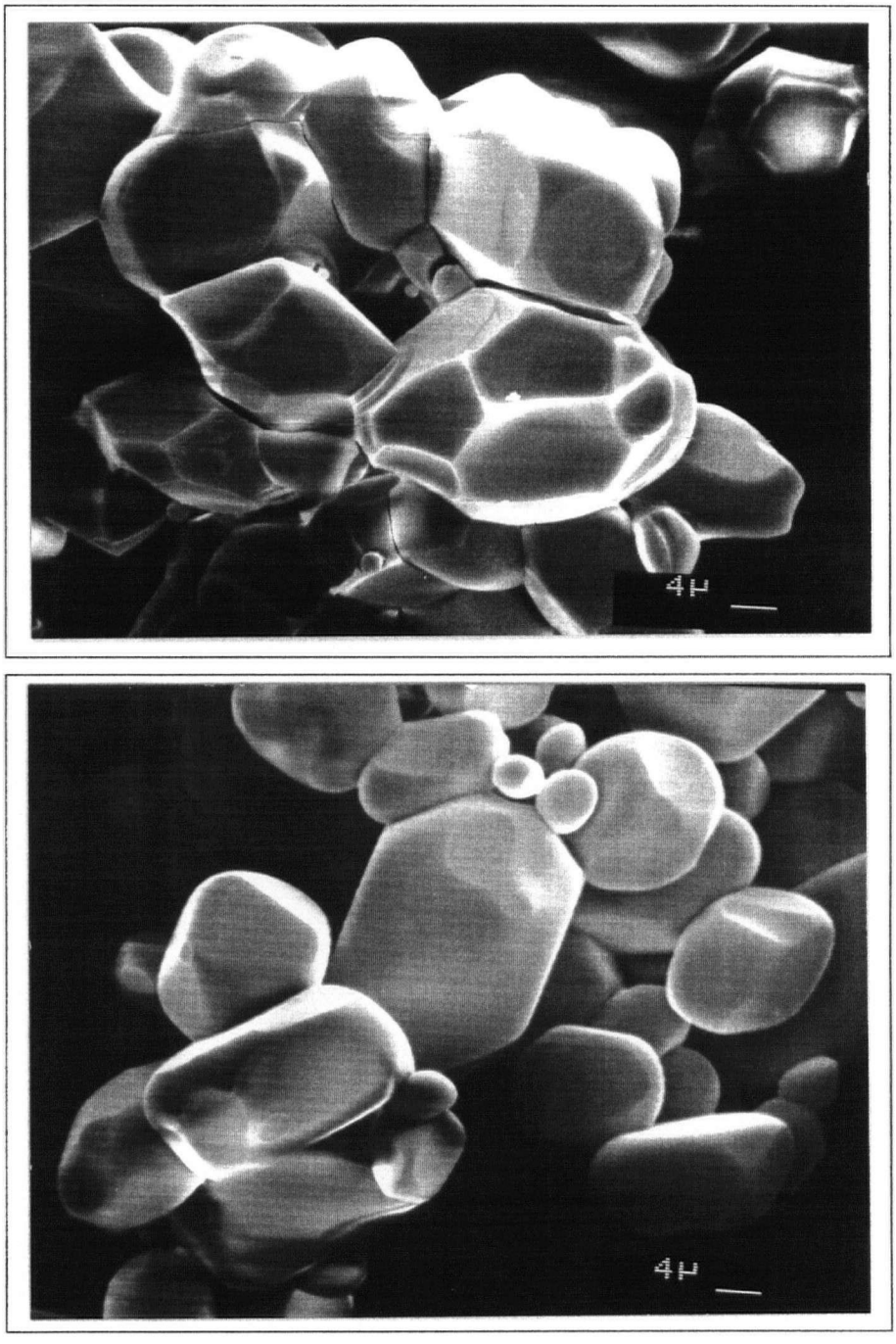

a

b

Figure C.25: Plate III of textures of experimental run products viewed under the scanning electron microscope using secondary electron imaging: a) run UP–79, 25 kbar, 1410 °C, 55 minutes, b) hydrothermal run, 2 kbar, 700 °C, 110 hours. See text for discussion of textures.

Appendix D

Comparison of Calculated Volumes with Measured Volumes

This appendix contains a collection of pressure versus percent–deviation plots (figure D.26 to figure D.35) that compare experimentally measured volumes with calculated ones using the equation of state of this study. This type of plot is a part of the output from the home–grown peripherals of the non–linear programming code used for fitting parameters of the equation of state. The figures are discussed in some detail and expand the discussion provided in chapter 1. A brief account of the experimental methods is included.

Shmonov & Shmulovich, 1974, figure D.26, 1–8 kbar, 400–700 °C: This data set covers a very important part of $P-T$ space and is the only study extending to high temperatures above 1.4 kbar. The experimental method is discribed in Shmonov (1977). The authors use a displacement method whereby the volume is extracted from the difference of two measurement series at the same temperature with sample volumes that differ by a known amount. This method has the advantage that corrections due to the deformation of the sample volume and due to thermal gradients along connections are not required. Smoothed volumes extrapolated to 10 kbar and 100–1000 °C are tabulated in Shmonov & Shmulovich (1974) and are quoted by several authors as primary measurements.

Experimental data at 1 kbar are 2.5 % too large compared to data by Kennedy (1954) (c.f. figure 1.5). Data by Tsiklis *et al.* (1971) at lower temperatures and 4–7 kbar are only 1 % smaller than measurements by Shmonov & Shmulovich (1974) at 673 K, but trends in isobaric sections (c.f. figure 1.3) would extrapolate volumes by Tsiklis *et al.* (1971) to volumes smaller by about 2–3 %. Isobaric lines on a $T-V$ diagram are almost straight but should be curved slightly downward based on van der Waals theory which would even enhance the discrepancy discussed above. Any smooth equation of state based on van der Waals–like theory constrained by data of Kennedy (1954), Tsiklis *et al.* (1971) and Shmonov & Shmulovich (1974) will therefore predict volumes which are too small relative to Shmonov & Shmulovich. Phase equilibrium data at moderate pressures (1–5 kbar) appear to demand smaller volumes (more stable CO_2) as well (c.f. figure 1.5). In figure D.26 we also observe a marked nonlinearity of the 980 K data in isobaric sections with the lower temperature data in the pressure range of 2.5–4 kbar, perhaps suggesting some experimental problem.

While this evaluation can only be relative it points towards uncertainties for P-V-T measurements at high pressure that are significantly larger than those estimated by the

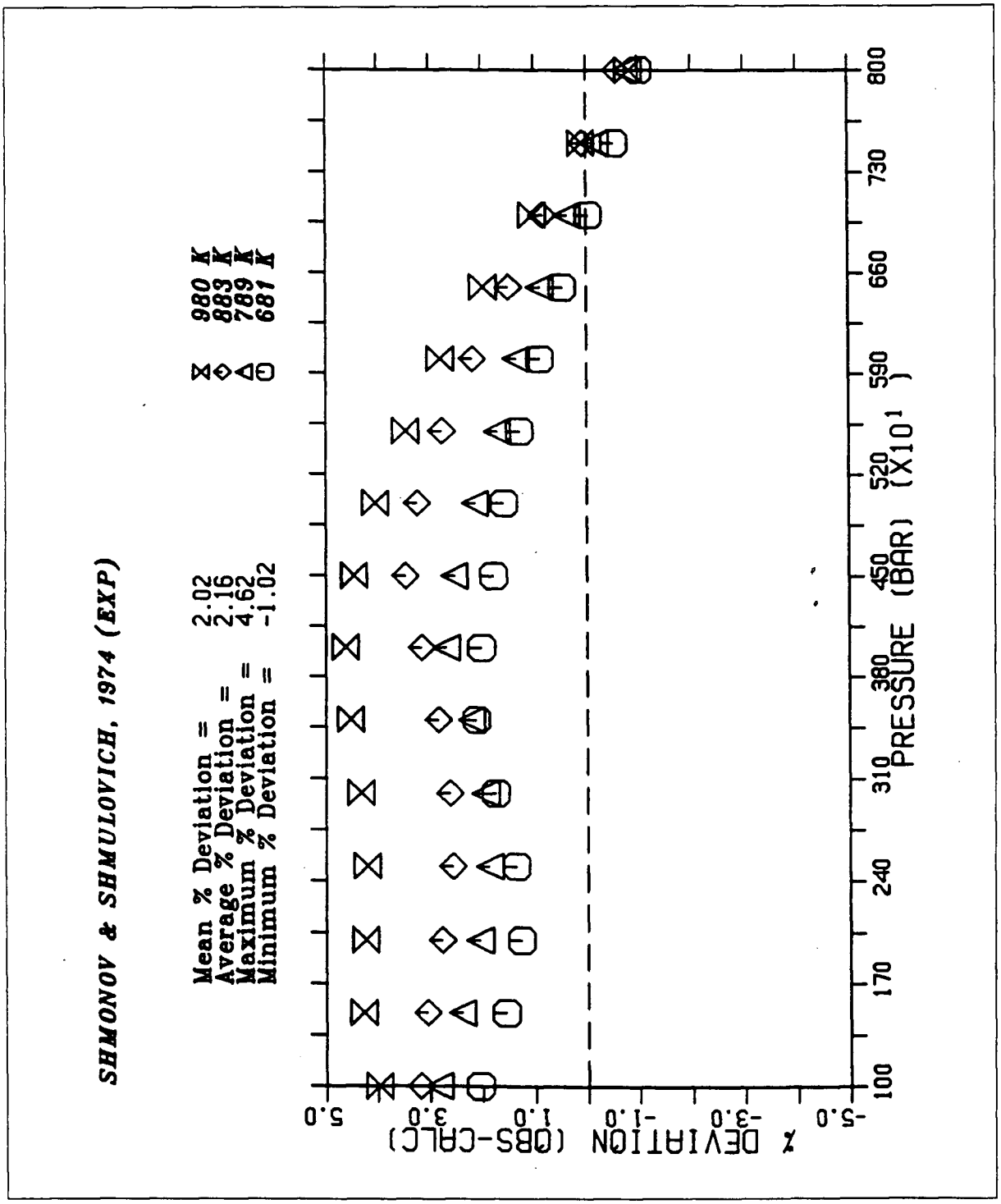

Figure D.26: Comparison of computed volumes with experimental data of Shmonov & Shmulovich (1974).

experimentalists.

Kennedy, 1954, figure D.27, 25–1400 bar, 0–1000 °C: The experiments were performed at Harvard University. The apparatus (Kennedy, 1950, 1954) consists of an externally heated pressure vessel connected to a calibrated volumeter. Two methods are used, one with known amounts of sample gas in a known volume, and one with constant but unknown amount of sample in a constant volume. The first method is tedious but yields *P-V-T* data directly whereas the latter method has to be referenced to an isotherm along which the volume is known. Most data were obtained by the latter method and a reference isotherm at 150 °C was chosen based on data by Michels *et al.* (1935) and Michels & Michels (1935) and those obtained by the first method for gas densities below the range of Michels' data. Little primary data is published. Smoothed volumes based on several thousand measurements are tabulated. Precision of the data is reported to be ±0.2 % and smoothed values do not deviate from measured ones by more than 0.4 %. The accuracy is estimated at ±0.2 % (or ±0.0001 g/cm^3) where data overlap with existing work and not stated at higher temperatures. The possibility of reaction of CO_2 with the alloy of the pressure vessel wall is mentioned but not examined.

Discrepancies with data by Shmonov & Shmulovich (1974) are discussed above. The data set is considered of inferior quality by Angus *et al.* (1973) compared to other available data below 1 kbar. Kennedy's data, however, covers an extremely wide range of temperature (373–1273 K) which is crucial to constrain the temperature dependence of paramaters in an equation of state in such a way as to permit meaningful extrapolation to higher temperatures.

The equation of state of this study does not reproduce volumes at 373–473 K adequately, particularly near the critical region (70–200 bar). Data below 473 K were not used to constrain the equation of state in order to permit a better fit to measurements at high temperatures. This trade–off demonstrates that a realistic temperature dependence of the parameters needs to be complex in order to fit the near–critical region.

Juza et al., *1965, figure D.28, 700–4000 bar, 50–475 °C:* These experiments were performed in Prague at the Czechoslovak Academy of Sciencies using an externally heated pressure vessel. The authors measure pressure and temperature of a known amount of sample in a known volume. The pressure measuring unit had to be maintained at 25 °C making necessary thermal gradient corrections for connection tubes. Uncertainties are estimated at ±0.3 %.

Only smoothed volumes are reported by Juza *et al.* (1965) but the original measurements are tabulated in Angus *et al.* (1973). The overall fit of the equation of state to the data is reasonable with the exception of some measurements at low temperatures (323–423 K) which were not used as constraints.

Tsiklis et al., *1971, figure D.29, 2–7 kbar, 50–400 °C:* The experiments were performed at the State Institute for Nitrogen Research (GIAP) in Moscow. The authors

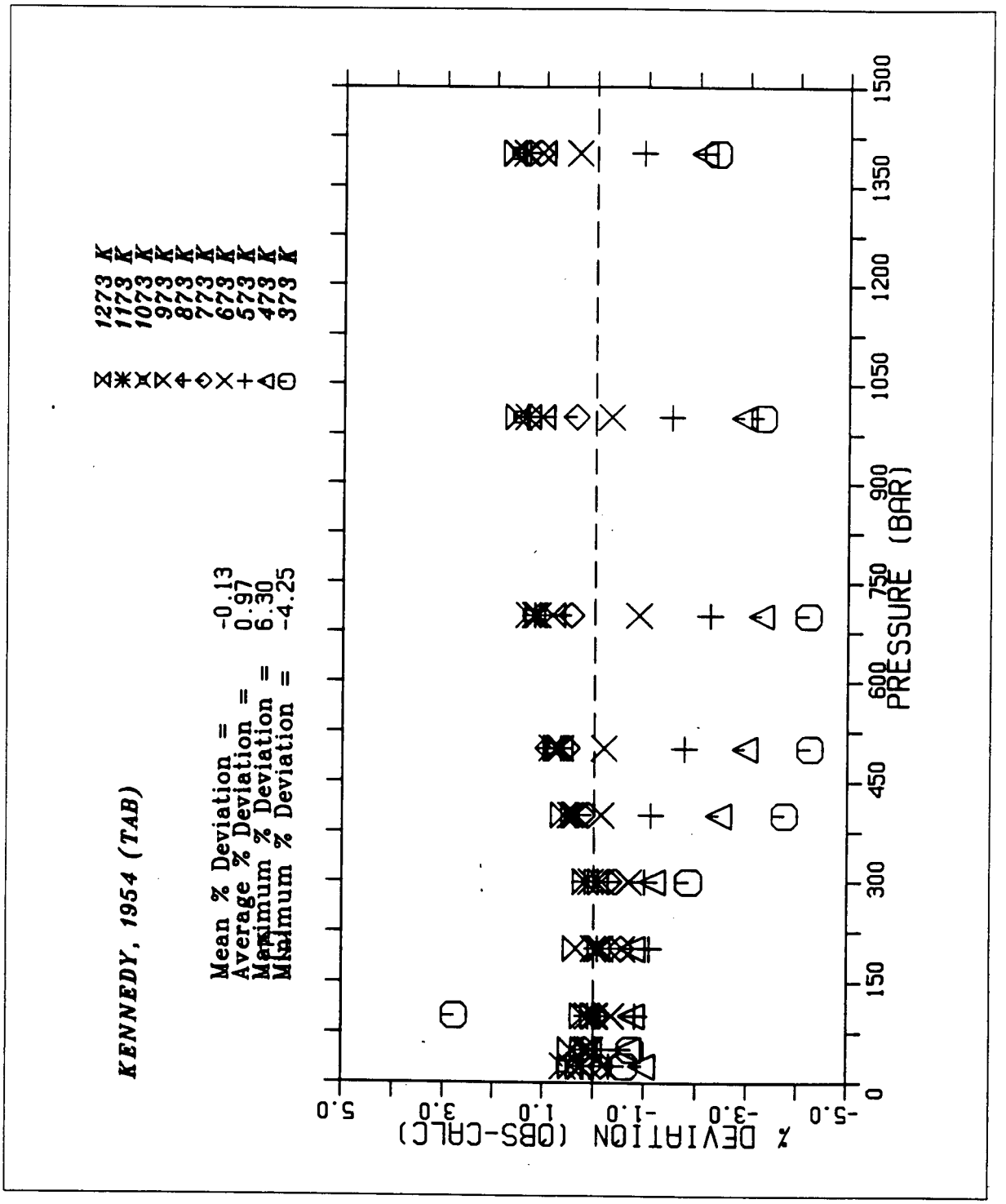

Figure D.27: Comparison of computed volumes with experimental data of Kennedy (1954).

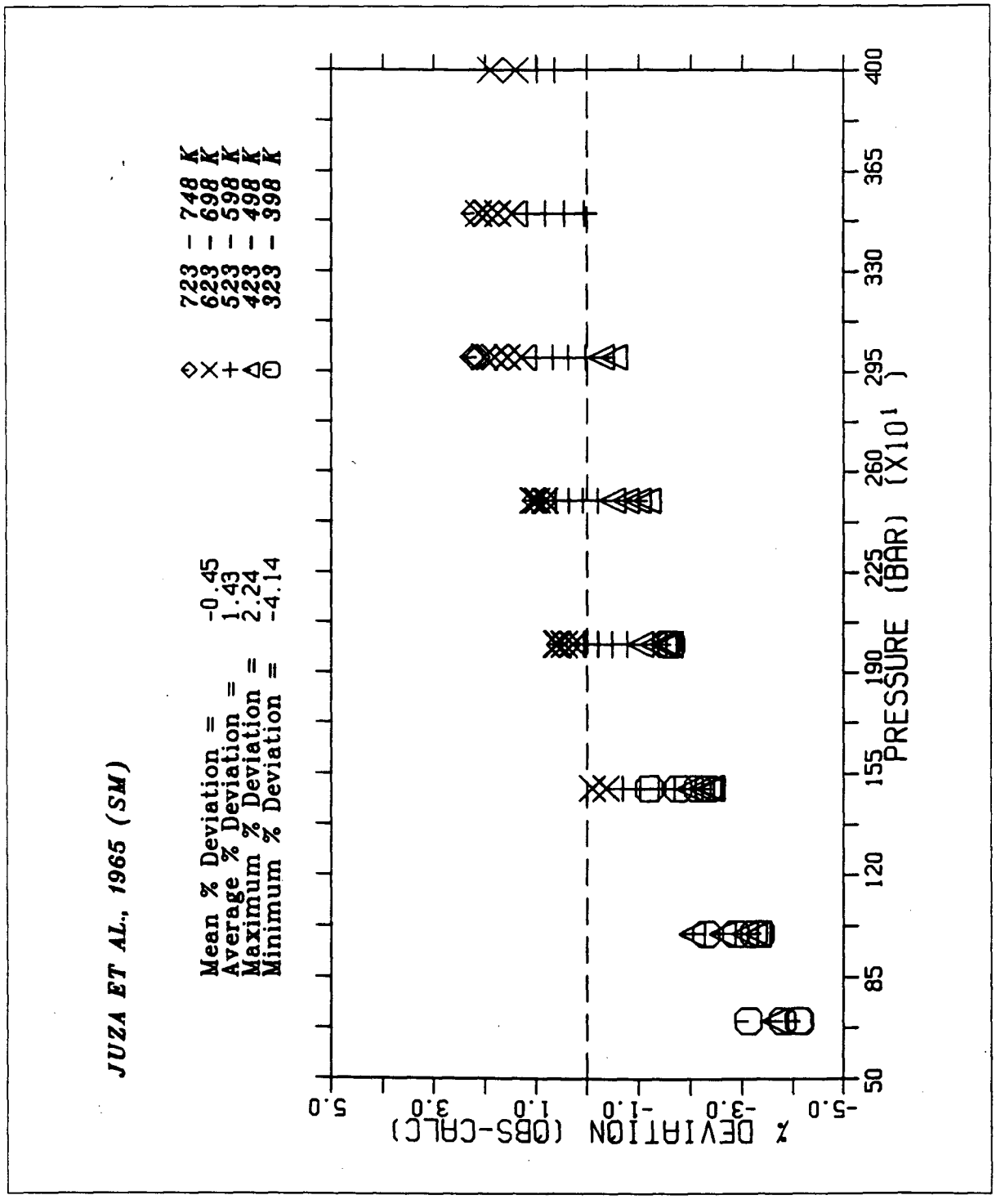

Figure D.28: Comparison of computed volumes with experimental data of Juza *et al.* (1965).

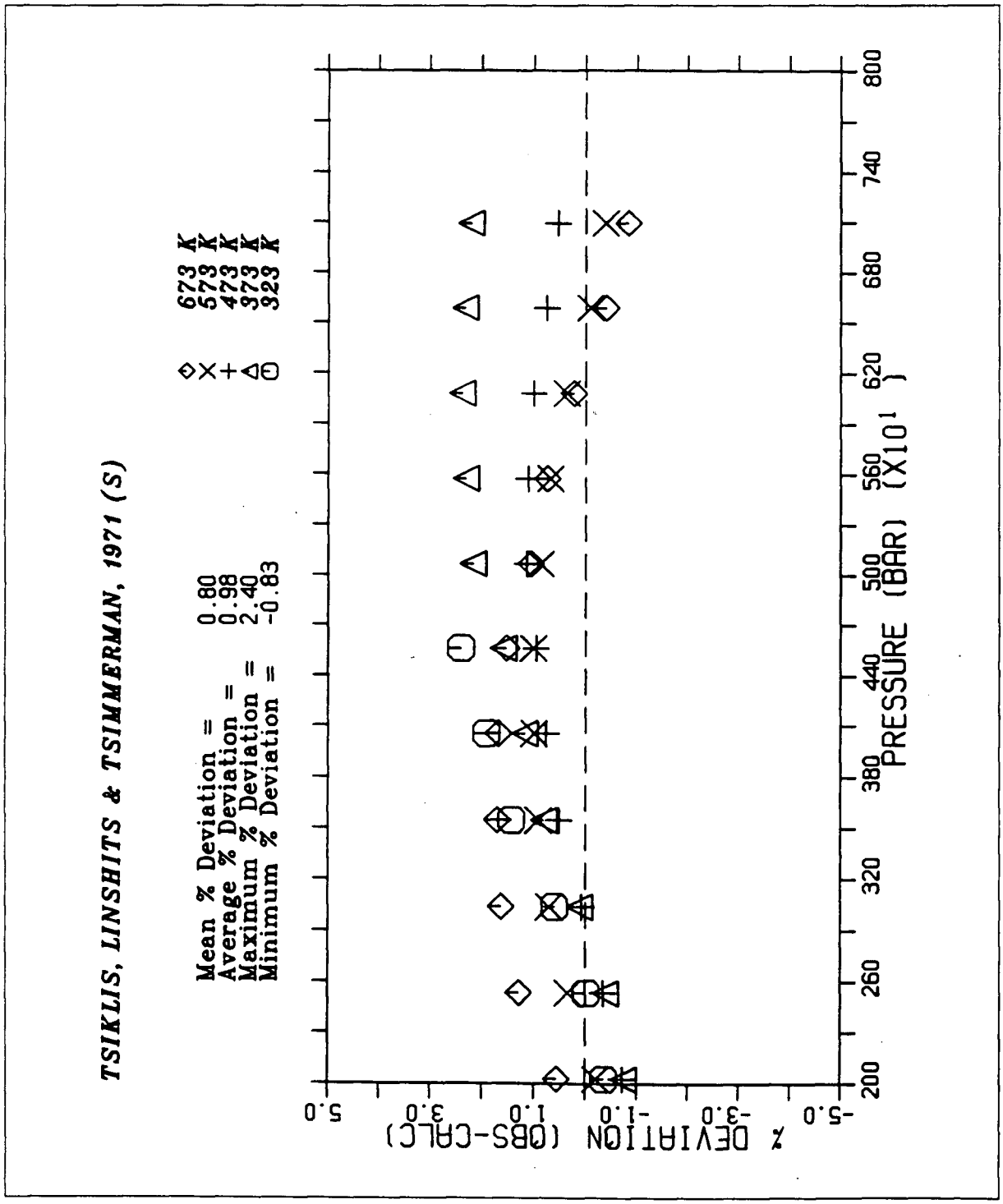

Figure D.29: Comparison of computed volumes with experimental data of Tsiklis *et al.* (1971).

use a displacement method whereby the volume is extracted from the difference of two measurement series at the same temperature with sample volumes that differ by a known amount. A measurement series consists of withrawing and weighing successive samples of fluid and monitoring pressure at constant temperature. This method has the advantage that corrections due to the deformation of the sample volume and due to thermal gradients along connections are not required.

Only smoothed P-V-T data is presented with a claimed accuracy of ± 0.5 %. Deviations from volumes measured by Juza *et al.* (1965) are as large as 1 %. The equation of state of this study represents the data well with the exception of some measurements at 323–373 K. This is an important data set which expands the range of temperature experimentally examined at high pressure from those reported by Shmonov & Shmulovich (1974). Volumes of Tsiklis *et al.* (1971) extrapolate to smaller values at higher temperatures than those measured by Shmonov & Shmulovich (c.f. figure 1.3 and discussion above).

Michels et al., *1935, figure D.30, 70–3000 atm, 25–150 °C:* These experiments were performed at the van der Waals laboratory in Amsterdam using the classical method of mercury manometry. The measurements are exceedingly precise (± 0.05 %) and likely of excellent accuracy estimated to better than ± 0.2 % by Angus *et al.* (1973). This data set therefore portrays best the inaccuracies of the equation of state in the near–critical region. Data between 373 and 398 K were not used to constrain the equation of state.

Vukalovich et al., *1962, figure D.31, 10–600 bar, 200–750 °C:* The experiments were performed at the Moscow Energetics Institute (MEI). The method is to remove and measure the amount of fluid in the pressure vessel at known temperature, pressure and volume. The authors stopped the experiemntal project at 1023 K above which they observed graphite coatings on the pressure vessel walls indicating the presence of significant carbon monoxide. The measurements agree well with those of Kennedy (1954) and other data where some overlap exists. There is some uncertainty as to the speciation of CO_2 at temperatures above 900–1000 K in the measuremnets of Kennedy (1954) which extend to 1273 K. No estimate of uncertainty is provided. Angus *et al.* (1973) assigned an uncertainty of approximately ± 0.3 % based on his analysis.

The equation of state does not represent the data within their accuracy towards higher pressures. The difficulty of fitting data well at 300–600 bar indicates too little flexibility of the equation of state to fit data to higher pressures simultaneously.

Amagat, 1891, figure D.32, 50–1000 atm, 100–260 °C: This classical experimental study was performed using mercury manometry. The apparatus is described in Amagat (1880). The measurements are of good quality and agree well with measurements of Michels *et al.* (1935) and Kennedy (1954) at 1 kbar. Data at 373 K which show the largest deviations from the equation of state were not used as constraints.

Michels & Michels, 1935, figure D.33, 16–250 atm, 0–150 °C: The experiments were

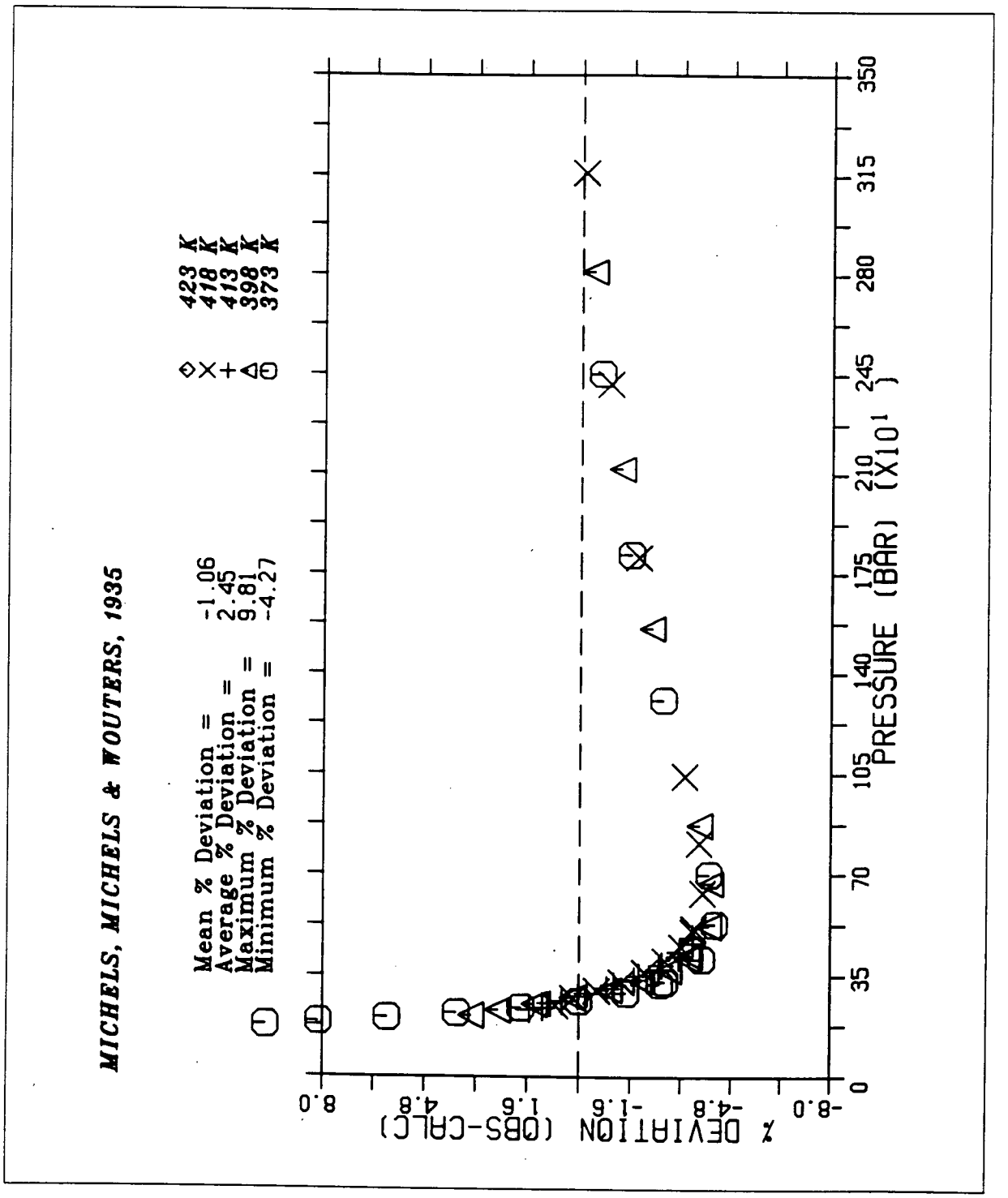

Figure D.30: Comparison of computed volumes with experimental data of Michels *et al.* (1935).

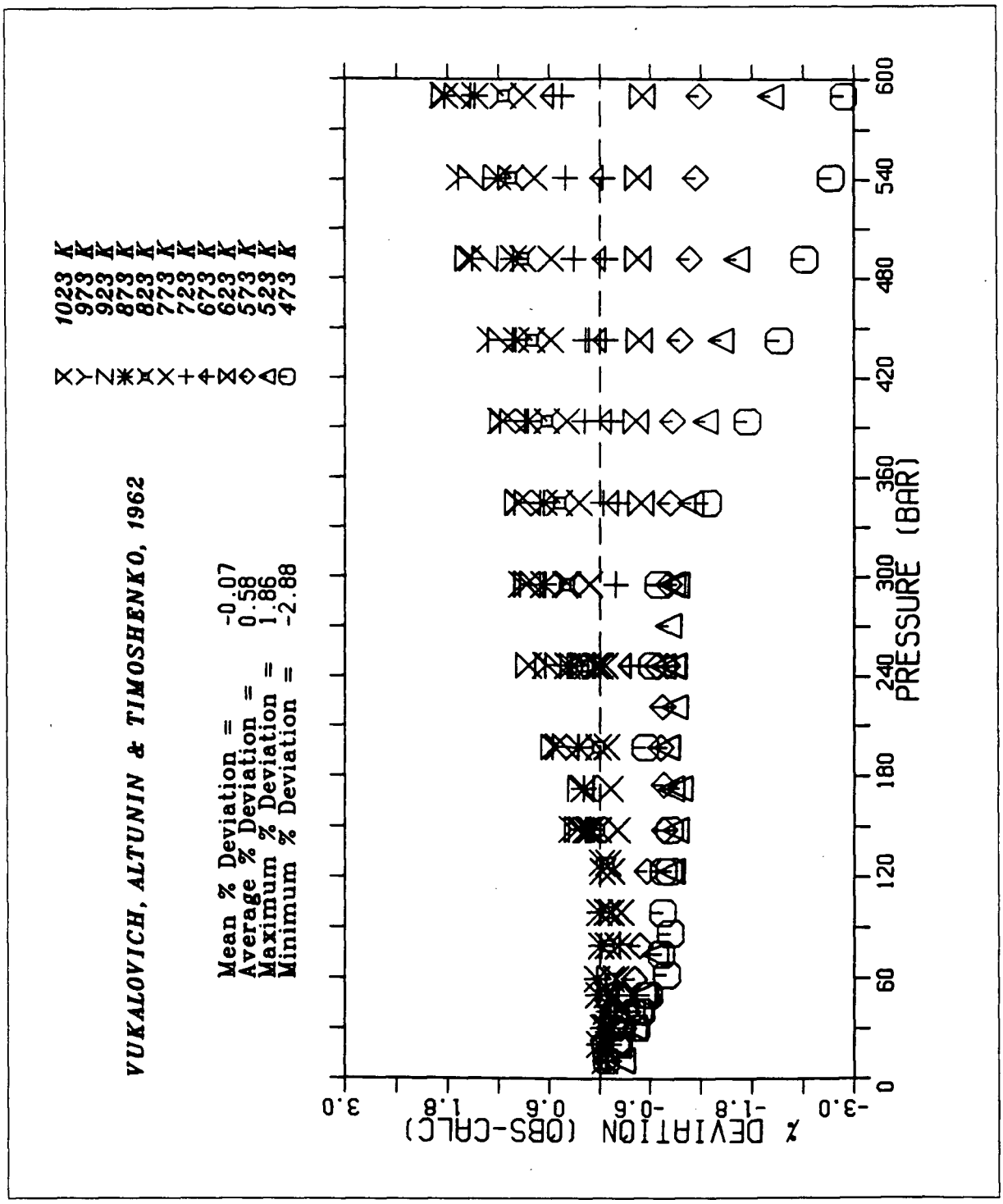

Figure D.31: Comparison of computed volumes with experimental data of Vukalovich *et al.* (1962).

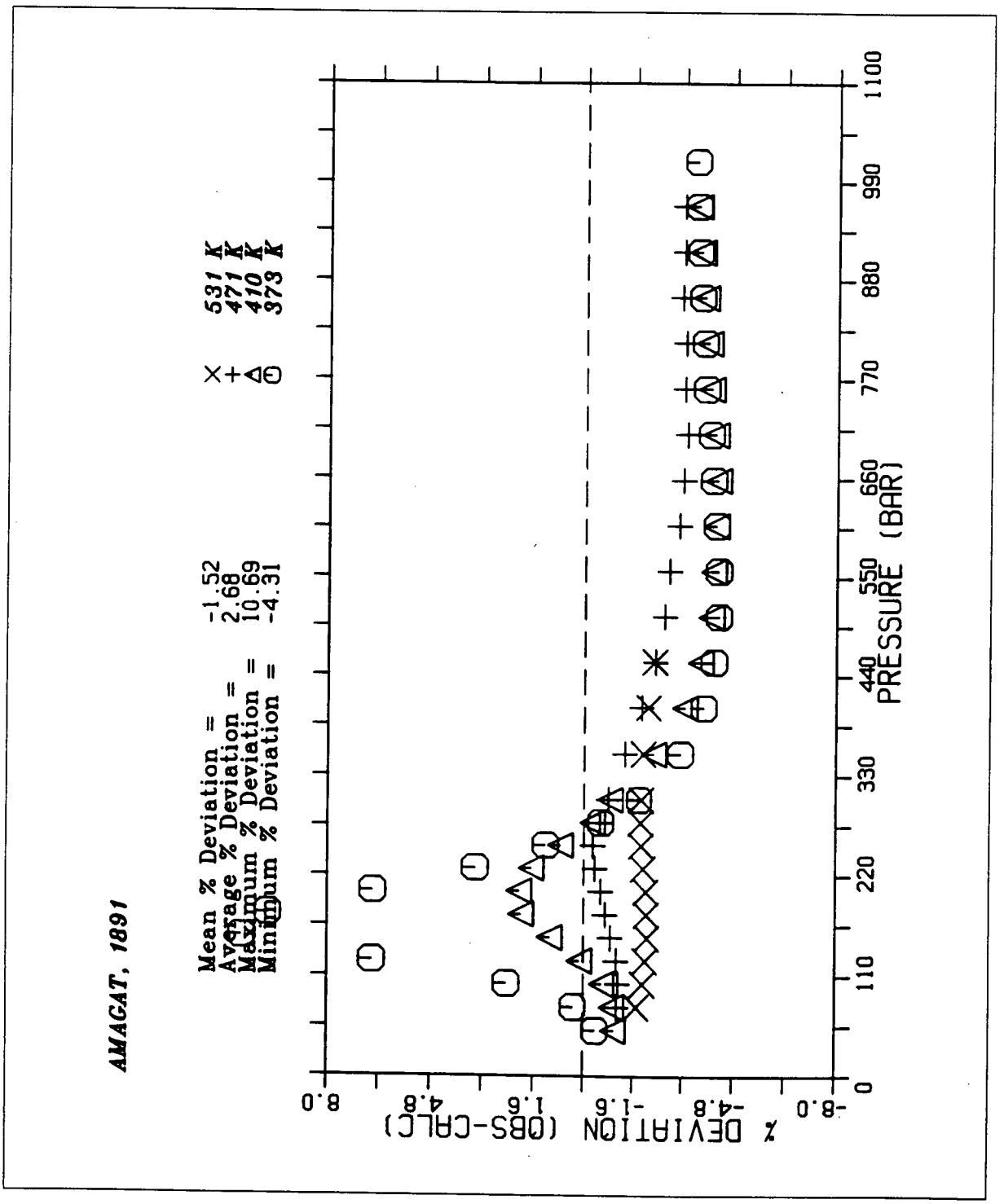

Figure D.32: Comparison of computed volumes with experimental data of Amagat (1891).

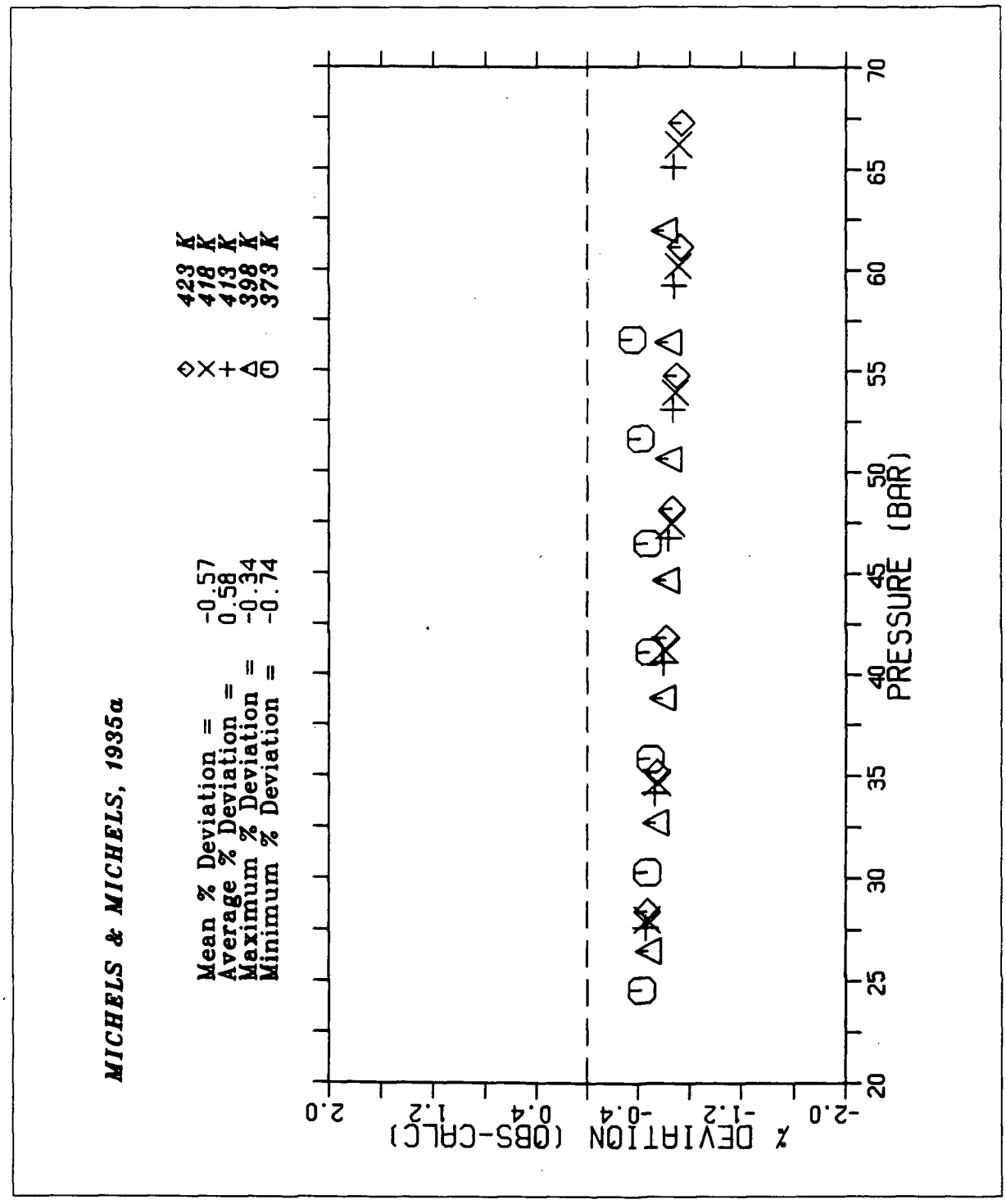

Figure D.33: Comparison of computed volumes with experimental data of Michels & Michels (1935).

performed at the van der Waals laboratory in Amsterdam (see notes on Michels *et al.*, 1935). The agreement of the measured volumes at these subcritical pressures and supercritical temperatures with the equation of state is adequate.

Vukalovich et al., *1963b, figure D.34, 20–200 bar, 650–800 °C:* These high temperature–low pressure experiments were performed at MEI (see notes on Vukalovich *et al.*, 1962). At these conditions the equation of state approximates the perfect gas law (minus the covolume b) which reproduces the measured volumes well.

Vukalovich et al., *1963a, figure D.35, 10–600 bar, 40–150 °C:* This data is an extension of the study by Vukalovich *et al.* (1962) using the same method (see above). Similar to data discussed previously (Amagat, 1891, Michels *et al.*, 1935, Kennedy, 1954) the equation of state does not represent measurements well at pressures just above the critical pressure at temperatures below 400 K. This data set was not used to constrain the equation.

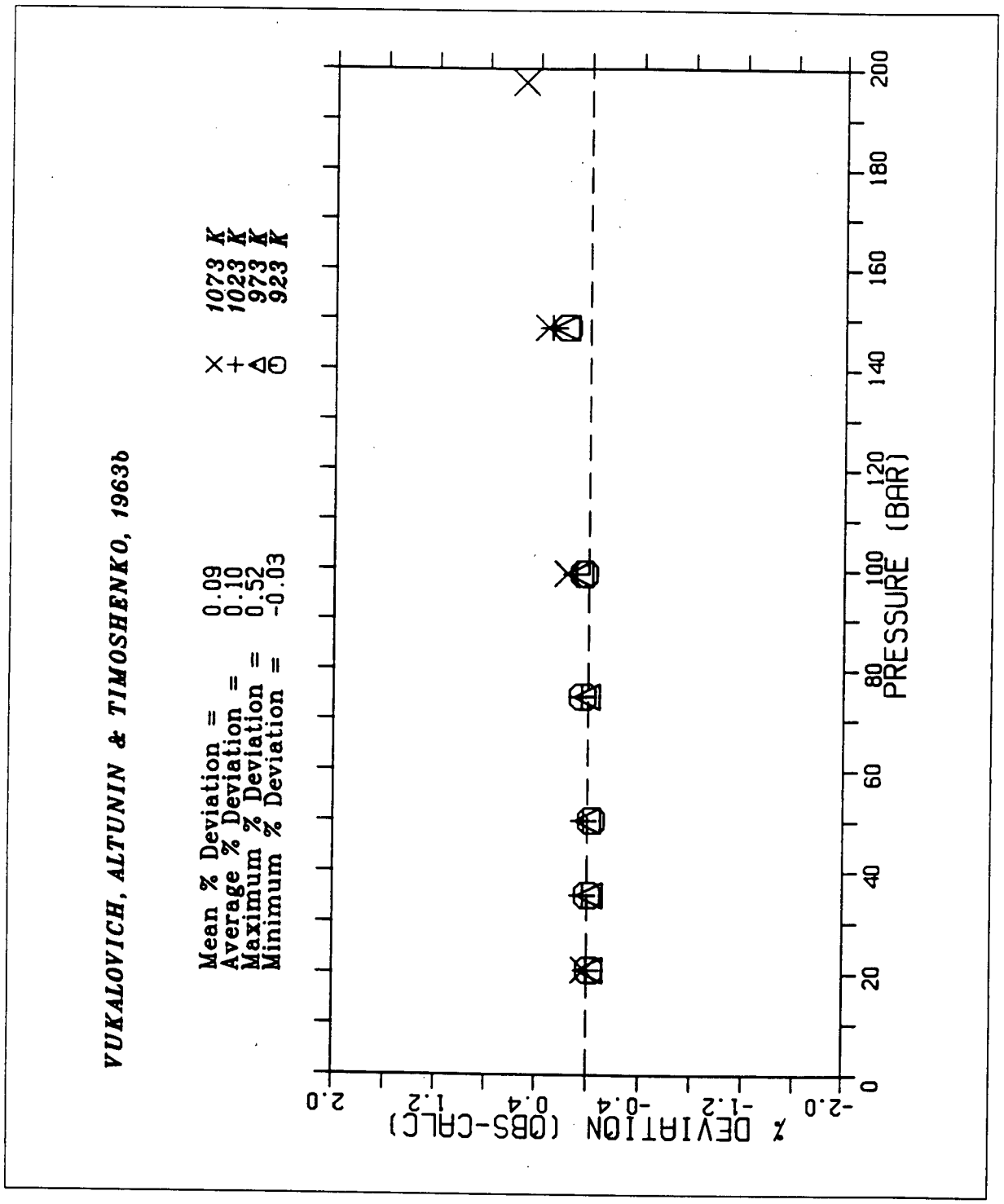

Figure D.34: Comparison of computed volumes with experimental data of Vukalovich *et al.* (1963b).

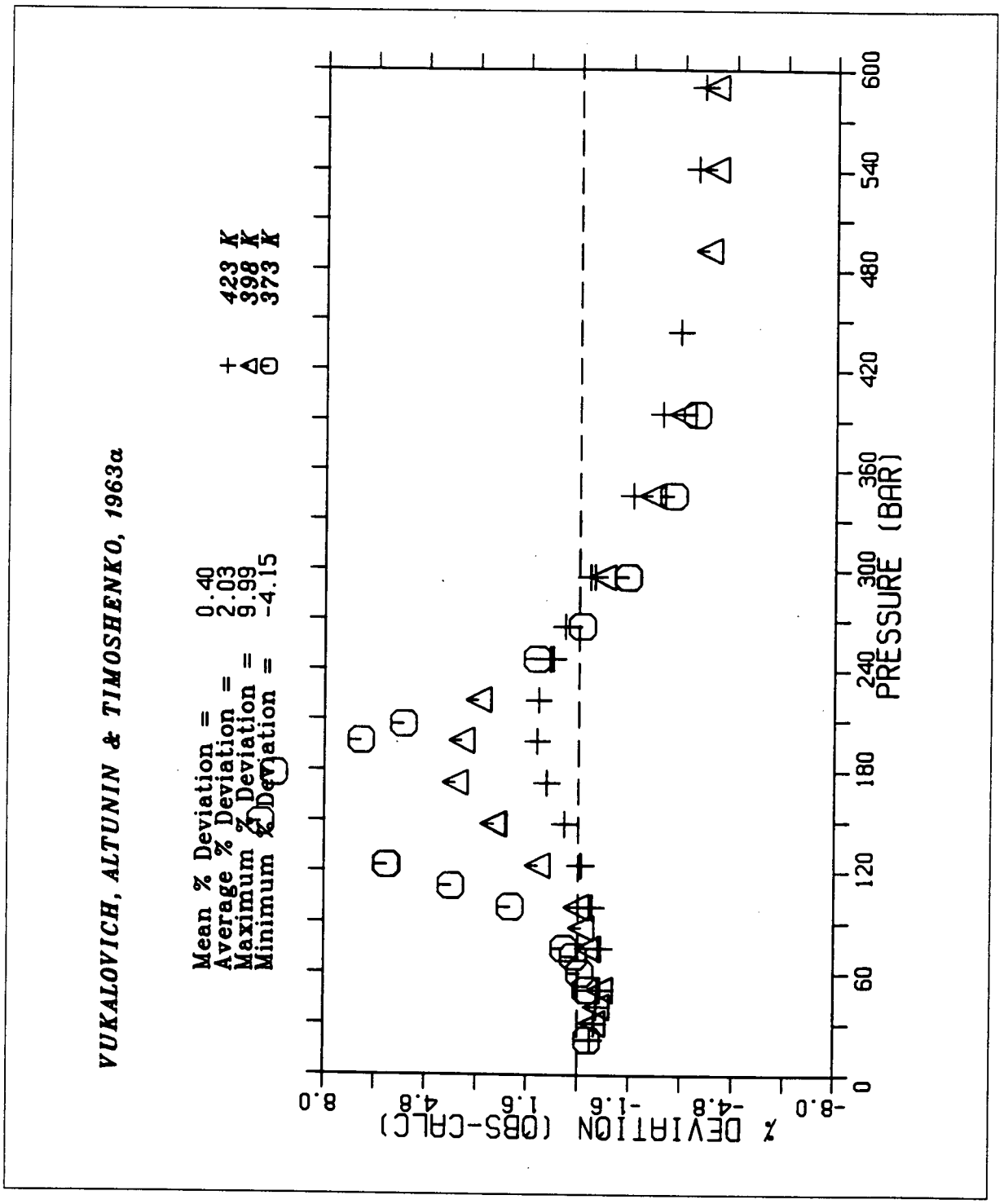

Figure D.35: Comparison of computed volumes with experimental data of Vukalovich *et al.* (1963a).

Appendix E

P–V–T–X Measurements: Data and Experimental Procedures of Existing Work

Existing *P-V-T-X* measurements on H_2O–CO_2 mixtures at supercritical conditions are recast in this appendix in terms of the molar excess volume on mixing. Figures E.36 to E.47 present the data in isothermal, isocompositional, pressure *vesrsus* excess volume plots. Figures E.48 to E.54 display the same data in graphs of fluid composition *versus* excess volume at constant pressure and temperature. Data are discussed in chapter 2.

A summary of the experimental methods used by the authors of *P-V-T-X* data is provided below including a discussion of uncertainties and some other aspects where appropriate. Two studies of the systems H_2O–Ar, H_2O–Xe and H_2O–CH_4 are included for comparative purposes. Several of the original publications or Ph.D. theses are written in German and in Russian.

Franck & Tödheide, 1959: H_2O–CO_2, 300-2000 bar, 400-750 °C: The authors use a cylindrical autoclave with 80 cm^3 volume and 66 mm OD and a Morey-type conical plug with a Bridgman seal made of copper. The OD to ID ratio is 1:3 with a wall thickness designed for 1000 hrs at 2000 bar and 750 °C. Pressure is measured with Bourdon gauges (0.6 and 1) which are filled with pure water and separated from the experiment through a valve. The furnace design combines two independent heating coils. Temperature is measured with 5 Pt-PtRh thermocouples (1 for absolute T, 3 along bomb, 1 in lid) located in 25 mm deep wells.

Starting materials are double–distilled water (conductivity $< 2.0^{-5}$ Ohm^{-1} cm^{-1}) and CO_2 of 99.7–99.8% purity (impurities: 15% O_2, 1% CO, 84% N_2). Moisture in CO_2 is reporetd to be 0.2 mg per liter.

The volume of the autoclave is 76.90 ± 0.05 cm^3 determined with the mercury method. The volume of connections is 5.7 ± 0.1 cm^3, some of which is added to the bomb volume. The authors assign 79.1 ± 0.25 to the measuring volume and 3.5 ± 0.2 to unheated connections and reproduce pure gas data (Kennedy, 1954, Holser & Kennedy, 1958, 1959) to within 1% accuracy. This procedure of determining the actual volume by calibration will eliminate some of the thermal gradient effects. Note that the data of Kennedy only extend to 1400 bar and measurements on pure gases are not reported.

The bomb is filled with liquid water and CO_2, with an uncertainty of 20 mg for water and 30 mg for CO_2. Connections are heated to empty its contents into the cold bomb. Measurements are taken during heating and cooling starting at 200 °C, with 50 K

intervals. The anticipated pressure in the bomb is preadjusted in the manometer capillary with a screw press to minimize exchange of gas during pressure measurement with the valve opened. The authors observe higher pressures on cooling compared to heating below 450 °C, with a maximum deviation of 50 kg/cm^2 at about 370 °C. They hypothesize on the extension of the two-phase region beyond the critical temperature of water. A similar observation was also made by Khitarov & Malinin (1956) in their experiments. Note that the critical region does not extend beyond the critical temperature of water (Tödheide & Franck, 1963). This must be either a metastable subcritical behaviour or the effect of metastably persisting species other than H_2O and CO_2.

Measurements are smoothed graphically with a mean deviation of all data of 0.39%. Corrections are applied due to the volume expansion of the autoclave and unheated connections but no details are reported. No data on volumes of pure fluids are reported. The computation of excess volumes for this appendix is based on the tabulated volumes of Kennedy (1954) and Holser & Kennedy (1958, 1959) for the pure fluids. This introduces the large uncertainties depicted in figurs E.36–E.45 and E.48–E.54. Compressibility factors (z) are reported with an uncertainty of 2.5% at total bomb concentrations of 10 mol/lit (1% from P, 0.2% from T, 1.3% from X_{CO_2}). A concentration of 10 mol/lit corresponds to about 1000 bar with pure CO_2 and 550 bar with pure H_2O. Uncertainties are larger at lower total concentrations, but are not specified. Extrapolated pressures from data by Khitarov & Malinin (1956) are up to 8 % higher than Franck & Tödheide's data. Ideal mixing yields compressibility factors that are only up to 5% too small compared to the measurements of Franck & Tödheide (1959).

Formation of H_2CO_3 is discussed: about 0.08 mol CO_2 are soluble in water at ambient pressure of which 0.1% is H_2CO_3. The authors partition the excess volume into a non–chemical part and a chemical part comparing their measurements to a van der Waal's equation with the following mixing rules that accont for the non–chemical contributions:

$$a_{\text{mix}} = X^2_{H_2O} a_{H_2O} + X^2_{CO_2} a_{CO_2} + 2X_{H_2O} X_{CO_2} \sqrt{a_{H_2O} a_{CO_2}}$$

$$b_{\text{mix}} = X^2_{H_2O} b_{H_2O} + X^2_{CO_2} b_{CO_2} + 2X_{H_2O} X_{CO_2} \left(\frac{\sqrt[3]{b_{wm}} + \sqrt[3]{b_{CO_2}}}{2} \right)^3$$

Note that these rules are for simple molecules with no or weak dipole moments, probably not a good approximation for H_2O and CO_2. The authors conclude that at 600 °C and $X = 0.5$ no more than 10% carbonic acid is present, probably much less. Measurements of the electrical conductivity (Franck, 1956) indicate no formation of ionic species above 400 °C. Note that this treatment of the problem of chemical association forms part of the basis on which de Santis *et al.* (1974) built their modification of the Redlich–Kwong equation of state which was adopted by Holloway (1977) and others (see chapter 2 for more deatils).

Tödheide & Franck, 1963, two-phase region to 3500 bar: The pressure vessel is made from ATS 113 with two conical Morey caps with copper Bridgman seals. The top cap contains 4 capillaries, 1 for filling and 3 for extracting samples for analyses. The capillaries for extraction tap at the base and at the top, and a third capillary is adjustable in its position. The base plug connects to a second vessel containing an electro-magnetically activated stirring mechanism. No volumes of any parts are reported. The bomb is of approximately 80 mm OD and 450 mm length. The sample chamber is about 25 mm by 300 mm (ca. 147 cm^3). Eight thermocouples are used for gradient control, 1 main, 5 along the side of the bomb, 1 in each cap, all in 18 mm deep wells. The furnace has 3 independent windings which are used to remove thermal gradients to better than 0.5 K. No volumes are measured in this study.

Water is doubly distilled and CO_2 is 99.7–99.8 % pure, with N_2, O_2 and minor CO. The high and low density phases are extracted (200–300 mg) into a series of evacuated containers and adsorption tubes (Mg-perchlorate and natron asbestos/Mg-perchlorate). The sample is filled into the autoclave at the temperature of interest until the desired pressure is achieved using calibrated injection pistons. Three samples of each phase are extracted at each pressure and temperature. The deviation from the mean is ± 0.15 mol-% in the liquid phase and ± 0.75 mol-% in the vapour phase. Equilibrium conditions are attained after 1 hour while stirring. Uncertainties are reported to be ± 1 % in pressure, ± 1 % in temperature, ± 0.5 mol-% in the liquid phase, and ± 1.0 mol-% in the gaseous phase. No details are provided on estimation of uncertainties. In particular, information about the treatment of volumes not at pressure and temperature of the experiemnt is not given.

Measurements are reported to agree with Wiebe & Gaddy (1939, 1940, 1941) and Wiebe (1941) up to 120 °C and 700 bar. The composition of the liquid phase agrees with Khitarov & Malinin (1958) and Malinin (1959) (330 °C, 500 bar), but deviations of the gas phase composition are as large as 4 mol-%.

The minimum of the critical curve is determined to be at 2.4–2.5 kbar, 266 °C and a mole fraction of CO_2 of 43 mol-%.

Gehrig, 1980: H_2O–CO_2–NaCl, 150–600 bar, 400-500 °C (to 3 kbar with NaCl): This author uses an apparatus that permits visual observation of the appearance of a new phase or its determination from the break in slopes of *P-T* curves at constant volume or *V-T* curves at constant pressure. This method provides precise measurements near phase boundaries or where densities of the two phases are nearly identical and cannot be determined reliably by the analytical method (i.e. Tödheide & Franck, 1963).

The autoclave is made from non–magnetic Ni–Cr–alloy (ATS 340) with dimensions of 400 mm length, 50 mm OD and 15 mm ID. A moveable piston allows the measuring volume to be adjusted. A VITON O–ring separates the pressure medium (water) chamber from the chamber containing the mixture. To protect the O-ring from excessive

temperatures a moveable cooling jacket is mounted externally at the position of the piston. This probably leads to temperature gradients within the cell. A sapphire window (10 mm thick) is mounted in the cap closing off the measuring volume. The other end contains a capillary for pressure medium access and a guide for a rod to determine the position of the piston with an externally mounted induction coil. Stirring is achieved by means of a magnetic stick agitated by an external magnet. Light is beamed through the window onto a platinum mirror mounted on the piston face which iluminates the sample volume. The furnace is wound directly onto the autoclave in four independent sections to allow thermal gradient control. Heating rates were less than 3 K/minute and less than 1 K/minute near phase transitions. Furnace sector temperatures are controlled with thermocouples mounted in wells in the pressure vessel wall. Temperature is measured with a Chromel-Alumel thermocouple mounted internally. Various modifications of the sapphire window were tested to minimize problems with salt leakage. Many measurements were performed in a cell without a window and with a fixed volume.

Temperature is measured with a resolution of 0.25 K. Pressure is measured on 3000 bar Heise-Bourdon gauge with 1 bar resolution. Volumes are measured via piston displacement which can be resolved inductively to 0.05 mm. The cell volume is calibrated with argon and carbon dioxide along isotherms. The volume correction term is expressed as 2nd-degree polynomial in temperature. The effect of pressure on the volume of the autoclave is assumed to be negligible (ca. 0.07 % per 1000 bar). Tri–distilled water was used and CO_2 of 99.8 % purity.

Errors are reported to be 0.5 % in pressure, 0.5 % in temperature (estimated), < 0.05 % in sample mass, 0.2–0.6 % in sample volume. The effect of the cooling jacket for the O-ring on the thermal field is not known, but might be substantial and will lead to an excessive apparent volume. There are some gradient measurements reported in an identical apparatus in the dissertation by Welsch (Karlsruhe, 1973), which show gradients increasing to 8 K at 500 °C. This effect translates into an overestimate of the volume of about 1 %.

Data on H_2O–CO_2 mixtures are reported in form of tabulated smoothed values from $X_{CO_2} = 0.1$–0.9, 150–600 bar and at 400, 450 and 500 °C. Volumes of pure fluids were measured but not reported. Data smoothing is carried out in V–X_{CO_2} sections constrained to obey the Gibbs–Duhem relationship. Smoothing was not constrained in V–P sections leading to a ragged apparance in several graphs of this appendix. Volumes for the pure gases were taken from the literature (Kennedy, 1954, Holser & Kennedy, 1958, 1959) in order to compute excess volumes on mixing from Gehrig's data. Activity coefficients are also tabulated based on the integrated excess volumes on mixing but details are not provided. Franck & Tödheide's volumes are up to 10 % smaller and the excess volumes up to 60 % smaller than Gehrig's measurements. Greenwood's (1973) data is in fair agreement but does not agree within stated uncertainties at many P–T–X conditions

(see graphs in this appendix).

Greenwood, 1969, 1973: H_2O–CO_2, 50–500 bar, 450–800 °C: The method and apparatus is described in great detail in Greenwood (1969). Measurement series were made in externally heated Morey bombs at constant temperature beginning with a CO_2–rich starting composition. Pressure is incrementally increased by injecting known amounts of H_2O, thus producing more H_2O–rich compositions along a given isotherm. The composition of the mixture at the end of a measurement series is determined as described in Greenwood (1961, 1967b) from which all compositions along the P–X_{CO_2} traverse can be determined by back calculation.

The volume was determined by various methods to ensure an acceptable accuracy of about 0.3–0.4 %. Temperatures are reported to be precise to ±0.3 K and accurate to ±1 K. Pressure is measured by calibrated Heise–Bourdon gauges with an estimated accuracy of 0.2 %. The calibration of the screw press used to inject H_2O shows maximum deviations of 0.085 % from the regression equation used to process the raw data. Data is smoothed to a polynomial in pressure and mole fraction for each isotherm that represent the observed compressibility factors to within 0.5 %. Tables of the compressibility z are presented in 50 K intervals.

In a subsequent publication Greenwood (1973) recasts his experiments into constrained polynomials with 12 coefficients for temperatures between 450 and 800 °C with 50 K intervals. Activity coefficients are tabulated at 50 K intervals between 450 and 800 °C at pressures of 100–500 bar. The polynomial equations obey the Gibbs–Duhem relationship and are used to represent Greenwood's data in the graphs of this appendix.

Shmulovich et al., *1980: H_2O–CO_2, 1–5 kbar, 400 and 500 °C:* These experiments were carried out at the Institute of Experimental Mineralogy, Academy of Sciences of the USSR, in Chernogolovska. A volume displacement method is used with an externally heated pressure vessel. The sample mixture is contained in a sealed gold capsule and the pressure medium is pure carbon dioxide. The volume of the sample is determined from the difference between two series of measurements, one with the filled gold capsule and one with the empty capsule. Measurements are performed at constant temperature starting from high pressure by incremental release of pressure medium.

Pressure is measured by calibrated Bourdon gauges (type SV 6000) and reported to be accurate to ±15 bar. The amount of gas in the capsule is determined after each run by weighing with an accuracy of ±0.05 %. Temperature gradients are controlled to better than 1 K.

The volumes measured are dependent on the P-V-T properties of CO_2 used as pressure medium. These properties were taken from Shmonov & Shmulovich (1974) obtained by a displacement method which might lead to systematic errors of the same sign in both studies. P-V-T measurements on pure H_2O show deviations from tabulations by

Burnham *et al.* (1969) of up to 0.5 %.

The overall accuracy is estimated at ±1.6 % at pressures 1.5–2 kbar and ±0.7 % at 4.5–5 kbar. Enough raw data is provided that one could revise the volumes of the mixtures given more accurate data for the pressure medium CO_2.

Excess volumes derived by the authors are tabulated at 400 °C (X_{CO_2}=0.623, 0.316, 0.087) and at 500 °C (X_{CO_2}=0.398, 0.227), at various pressures between 1 and 5 kbar.

Shmulovich et al., *1979: H_2O–CO_2, 0.4–5.7 kbar at 500 °C and 150–1000 bar at 500 °C:* The method is identical to that used by Shmulovich *et al.* (1980). The accuracy of the measured volumes is stated to be 0.2 %.

The authors report excess volumes on mixing at X_{CO_2}=0.2, 0.4 at 500 °C, and at X_{CO_2}=0.2, 0.4, 0.6, 0.8 at 400 °C. Some data is smoothed from measurements at X_{CO_2}=0.227, 0.398 (500 °C) and X_{CO_2}=0.2, 0.38, 0.6, 0.8 (400 °C). The volume of the mixture is not reported. Volumes of the pure fluids were adopted from Burnham *et al.* (1969) and Shmonov & Shmulovich (1974).

Most excess volumes are distinctly larger compared with other studies. Data obtained by Shmulovich *et al.* (1980) by a similar or identical method do not agree within uncertainties with this study where the two sets join together.

Khitarov & Malinin, 1956: H_2O–CO_2, 1–1800 kg/cm², 100–500 °C: The authors use an externally heated pressure vessel and measured the pressure generated at temperature by a known amount of mixture of known composition in a calibrated volume. The measurements are not precise with the largest uncertainties introdueced by the inadequate method of filling and mixing, and the rather large temperature uncertainty of ±2.5 K. The data are therefore not used in this analysis.

Welsch, 1973, H_2O–Xe, H_2O–CH_4, 300–2500 bar, 375–500 °C and 375–425 °C: These systems behave similarly to H_2O–CO_2, i.e. they all display temperature minima in the critical curve of the mixtures extending from the critical point of water to higher pressures. Methane is quite similar to CO_2 also with respect to its size and polarizibility. Methane, however, has no quadrupole moment. The temperature minimum of the CH_4–H_2O critical curve is at 353 °C, 990 bar, 38.3 cm³/mole and 25 mol-% methane. The temperature minimum of the CO_2-H_2O critical curve is at 266 °C, 2450 bar and 41.5 mol-% CO_2.

H_2O–CH_4: data is presented at 375, 400 and 425 °C between 400 and 2500 bar, plotted as a series of V_{excess}–X diagrams. At 400-500 bar all V_{excess} are positive, skewed towards the water-rich side with a maximum of about 33 cm³/mole at 400 °C and 400 bar. At higher pressures V_{excess} becomes negative on the water-rich and methane-rich side. At pressures above 1500 bar all V_{excess} are negative, not more than −5 cm³/mole, decreasing again at higher T (425 °C).

H_2O–Xe: V_{excess}–X plots are presented for 375, 400, 450, 500 °C at 300–2500 bar.

Largest V_{excess} are observed at 300 bar and 400 °C of 52 cm^3/mole, with curves skewed towards the water–rich side. Small negative V_{excess} are depicted at 375–400 °C on the water–rich side at pressures above 1000 bar.

Welsch also discusses the van der Waals equation of state and how it predicts the qualitative behaviour of the critical curve correctly in the systems Ar, Xe, CH_4 mixed with H_2O.

Greenwood, 1961, H_2O–Ar: 500–2000 bar, 500 °C; The system H_2O–Ar shows a different behaviour than mixtures of H_2O with Xe, CH_4 or CO_2 in that the critical curve proceeds to higher temperatures with rising pressure without the presence of a temperature minimum.

The method used by Greenwood (1961) consists of measuring pressure and temperature of a mixture contained in a known volume using an externally heated Morey–type pressure vessel. The composition of the mixture is determined after each experiemnt using a cold–trap to measure the amount of water and a manometer to determin argon. The uncertainties are estimated at 2 % for the composition of the mixture and 2 % for the molar volume. Measurements at 500 °C on pure H_2O agree well within uncertainties with measurements by Kennedy (1950). Date on pure argon at 150 °C is in good agreement with measurements by Michels *et al.* (1949).

Original measurements are reported and tabulated fugacities are determined from graphically smoothed data. The molar excess volume on mixing is displayed as a function of mole fraction and pressure. The largest excess volume (32 cm^3/mole) is observed at 500 bar.

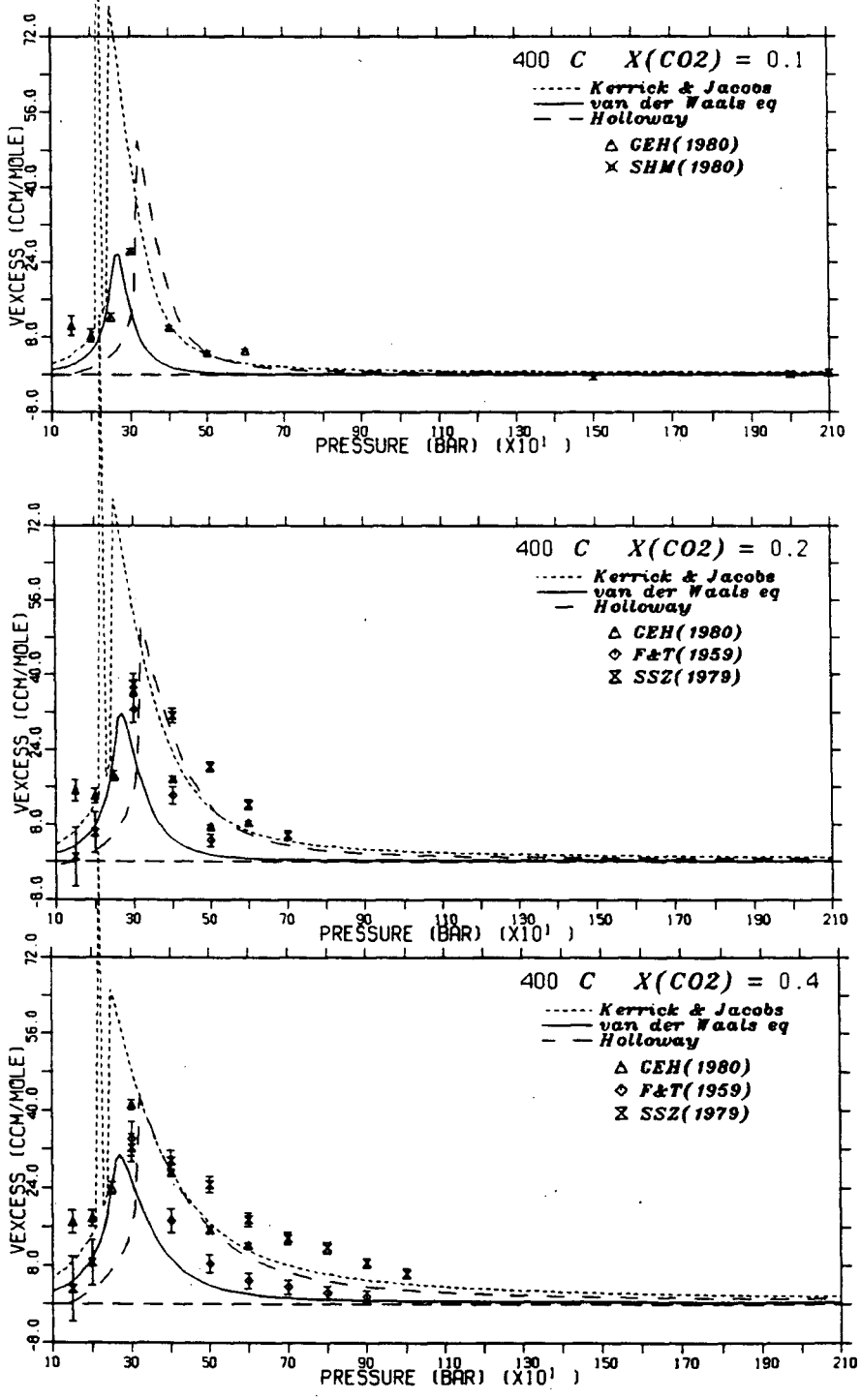

Figure E.36: $P - V_e$ graphs: 400 °C, X_{CO_2}=0.1–0.4. Data of Gehrig (GEH), Franck & Tödheide (F&T), Greenwood (GRE), Shmulovich *et al.* (SHM), and Shmulovich *et al.* (SSZ).

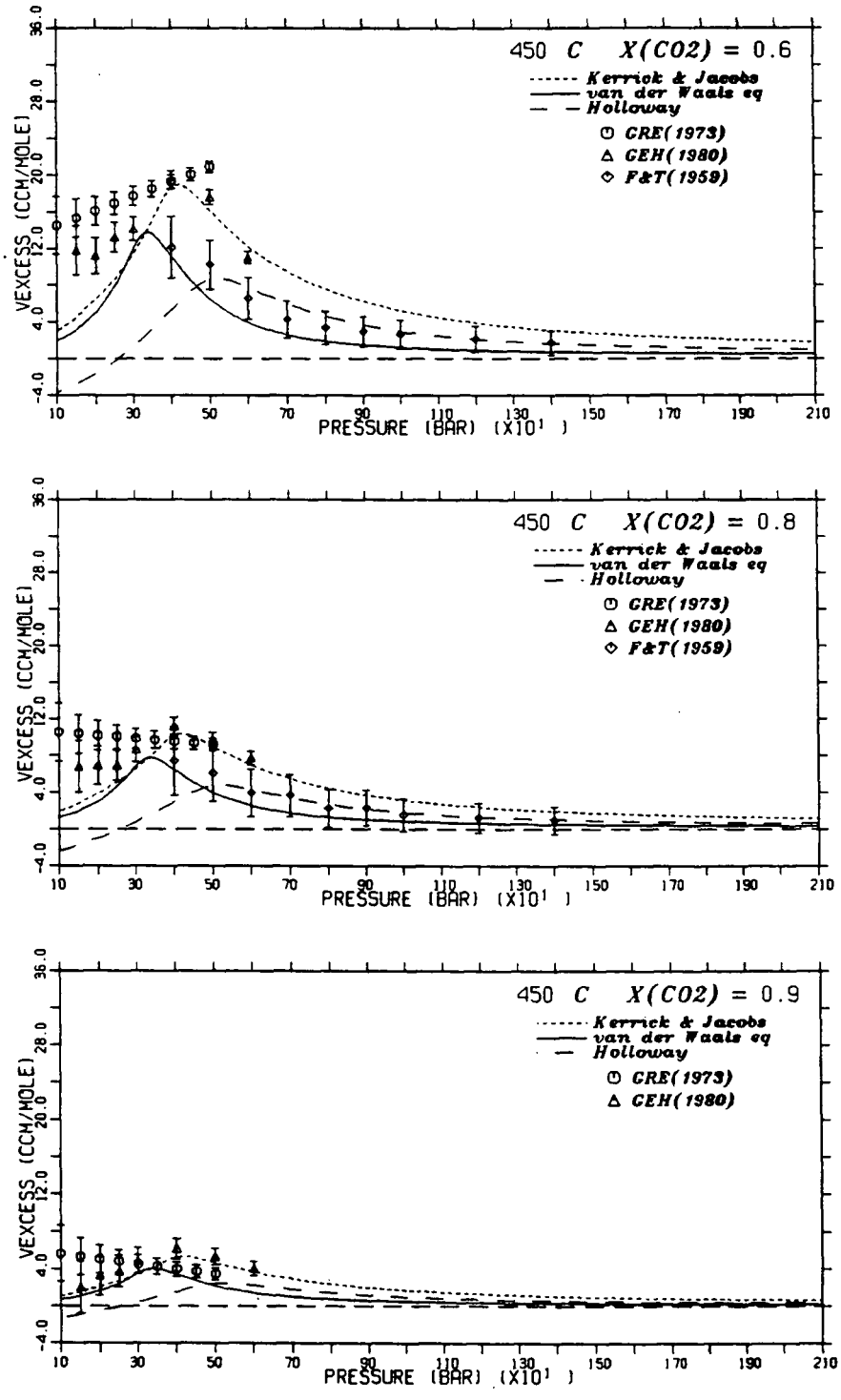

Figure E.37: $P - V_e$ graphs: 400 °C, X_{CO_2}=0.6–0.9. Data of Gehrig (GEH), Franck & Tödheide (F&T), Greenwood (GRE), Shmulovich *et al.* (SHM), and Shmulovich *et al.* (SSZ).

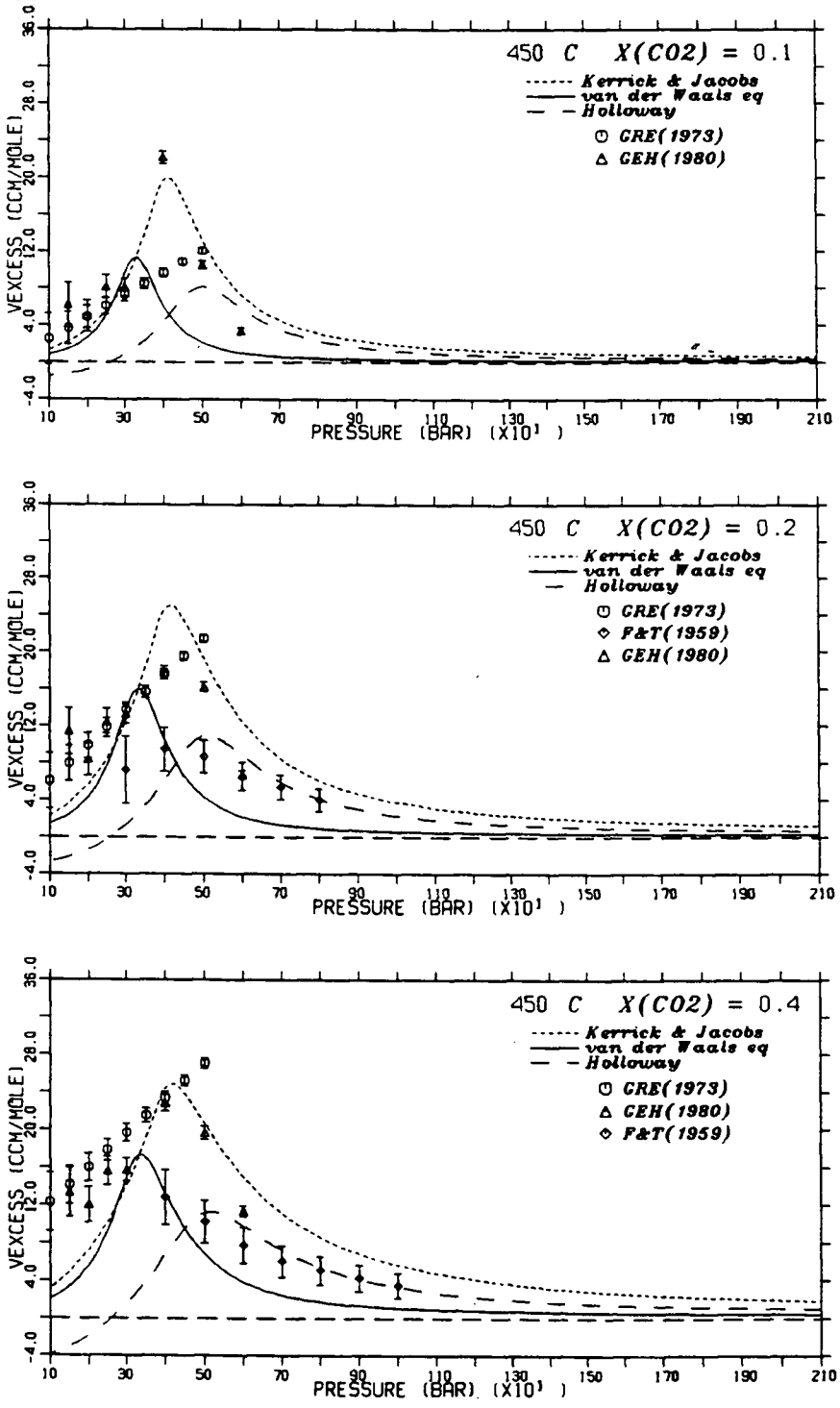

Figure E.38: $P - V_e$ graphs: 450 °C, X_{CO_2}=0.1–0.4. Data of Gehrig (GEH), Franck & Tödheide (F&T), Greenwood (GRE), Shmulovich *et al.* (SHM), and Shmulovich *et al.* (SSZ).

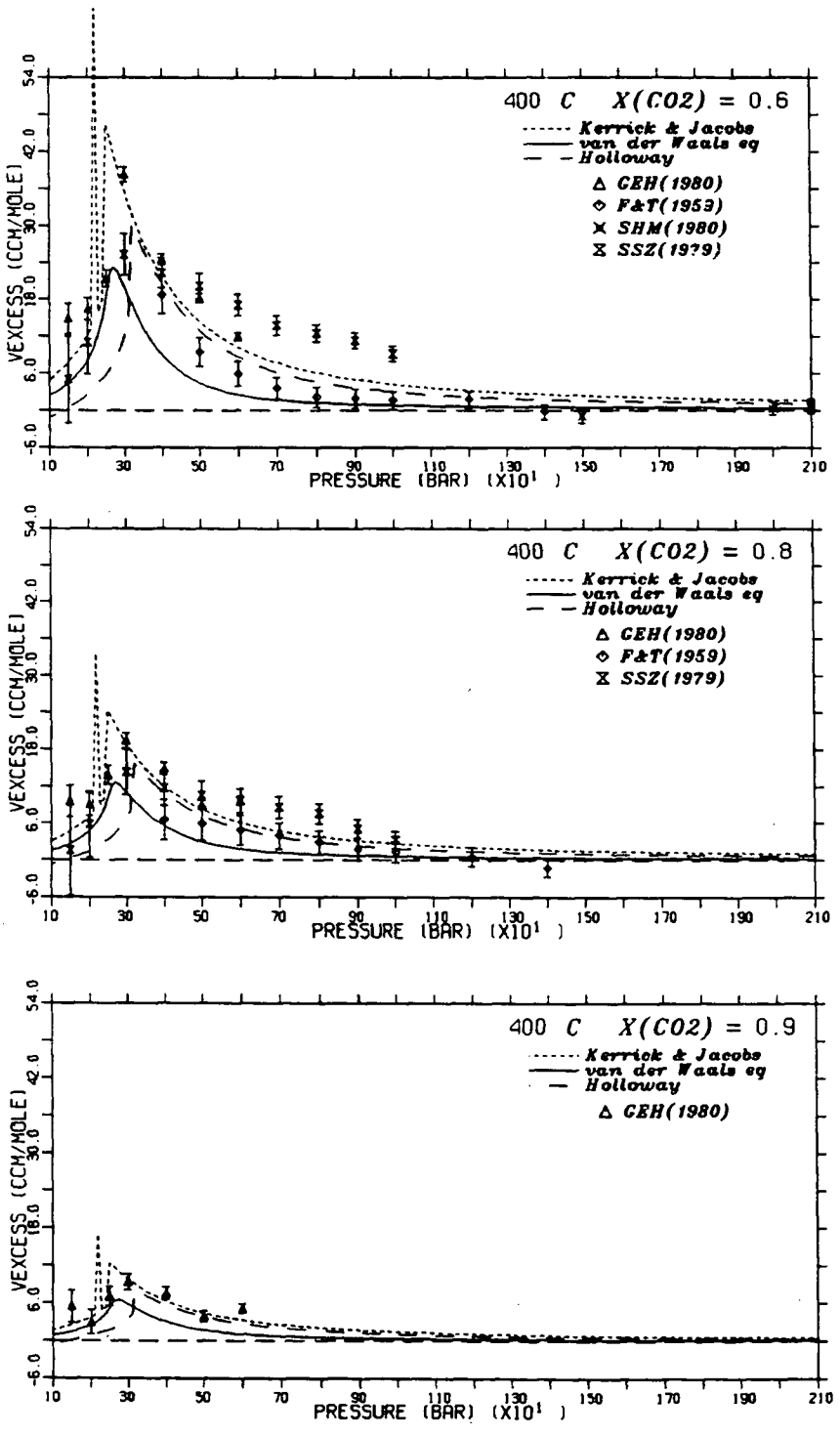

Figure E.39: $P - V_e$ graphs: 450 °C, X_{CO_2}=0.6–0.9. Data of Gehrig (GEH), Franck & Tödheide (F&T), Greenwood (GRE), Shmulovich *et al.* (SHM), and Shmulovich *et al.* (SSZ).

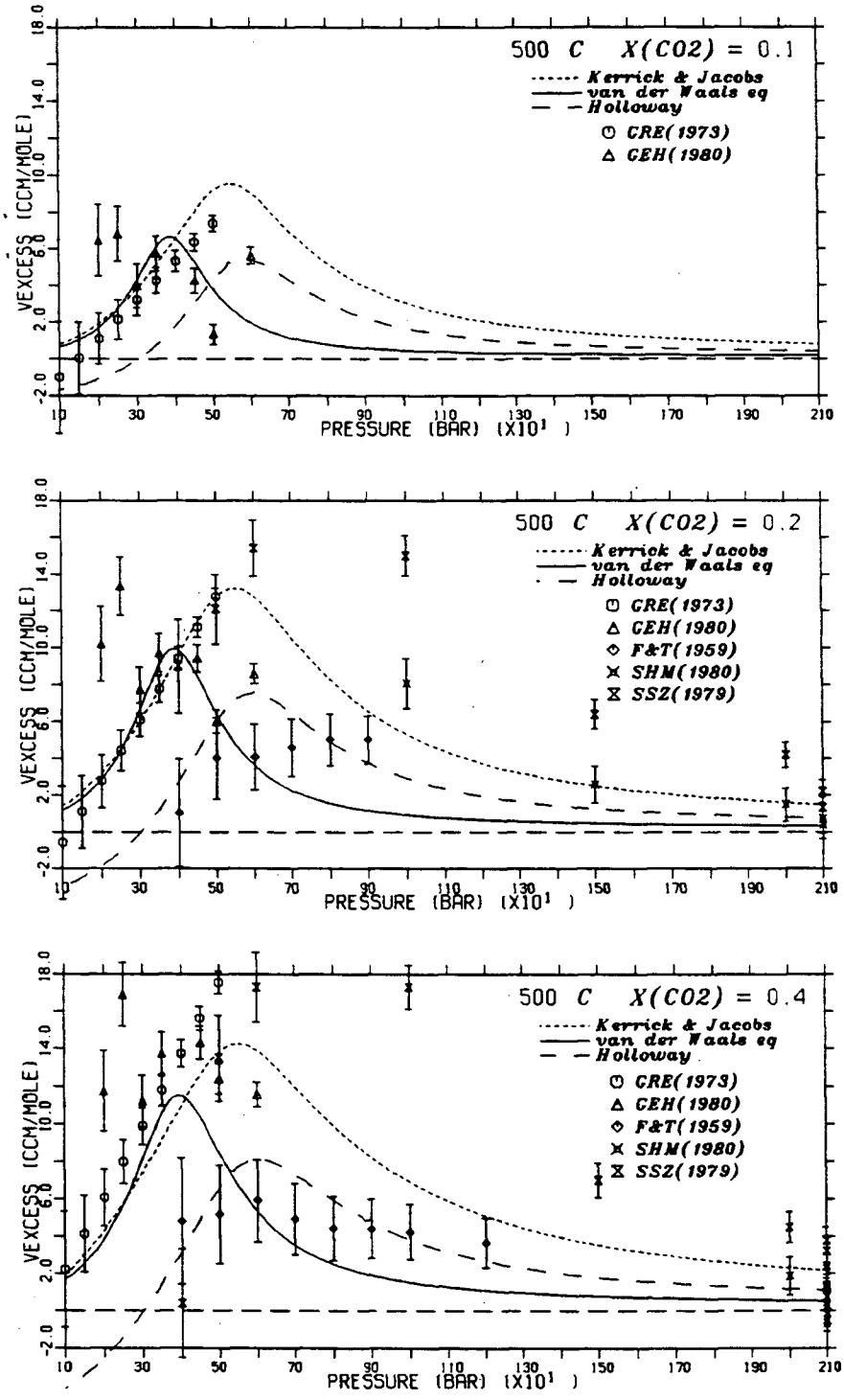

Figure E.40: $P - V_e$ graphs: 500 °C, X_{CO_2}=0.1–0.4. Data of Gehrig (GEH), Franck & Tödheide (F&T), Greenwood (GRE), Shmulovich *et al.* (SHM), and Shmulovich *et al.* (SSZ).

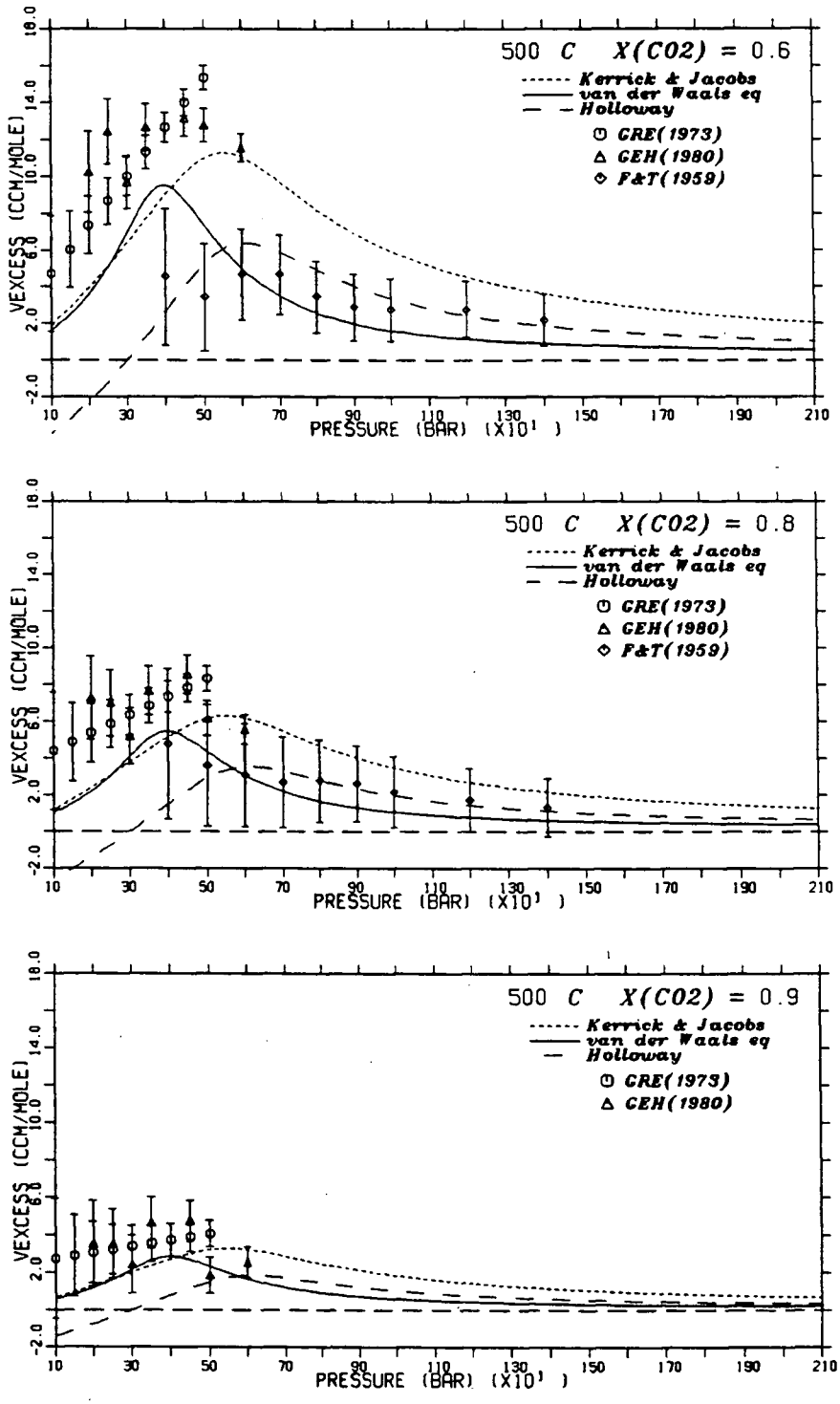

Figure E.41: $P - V_e$ graphs: 500 °C, X_{CO_2}=0.6–0.9. Data of Gehrig (GEH), Franck & Tödheide (F&T), Greenwood (GRE), Shmulovich *et al.* (SHM), and Shmulovich *et al.* (SSZ).

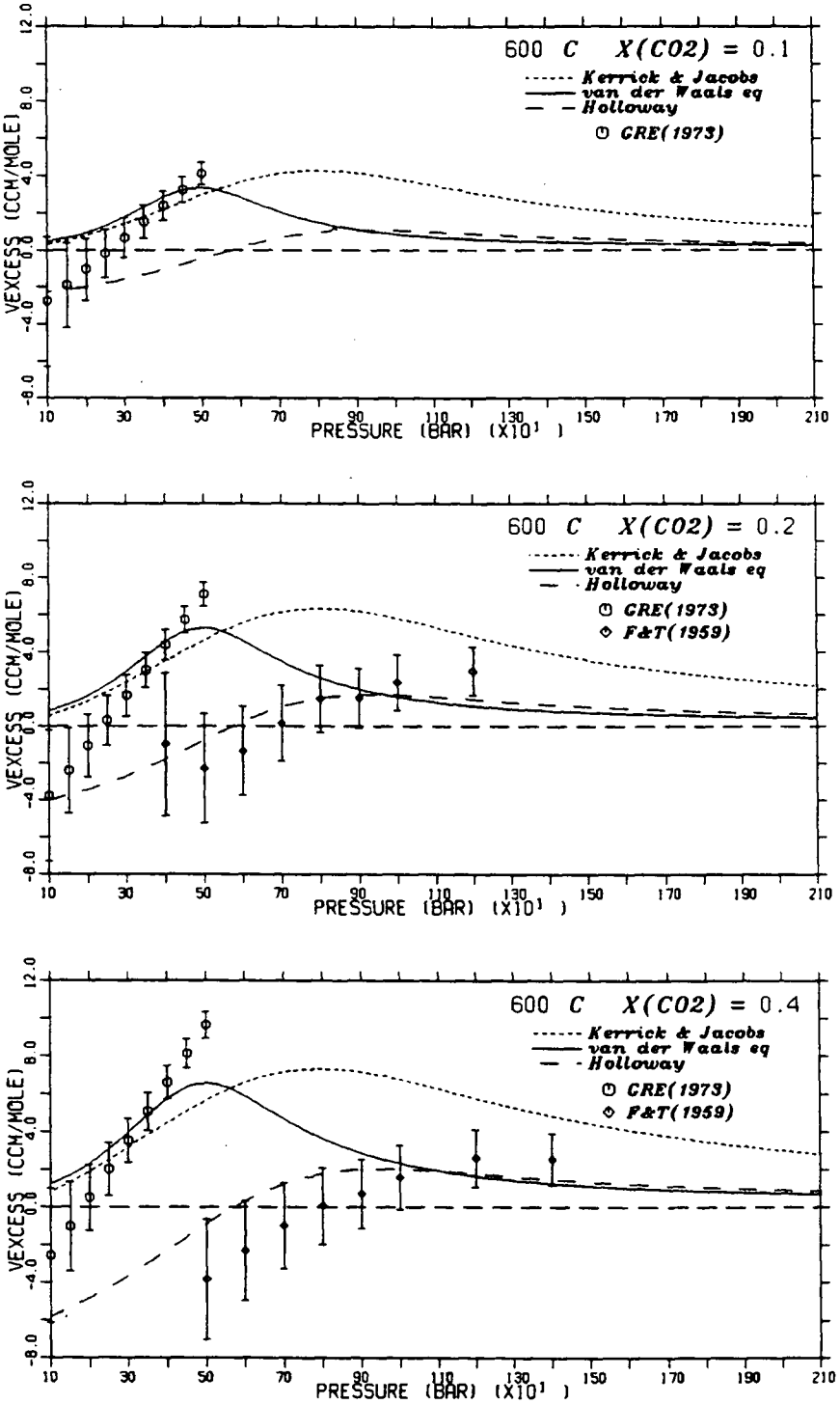

Figure E.42: $P - V_e$ graphs: 600 °C, X_{CO_2}=0.1–0.4. Data of Gehrig (GEH), Franck & Tödheide (F&T), Greenwood (GRE), Shmulovich *et al.* (SHM), and Shmulovich *et al.* (SSZ).

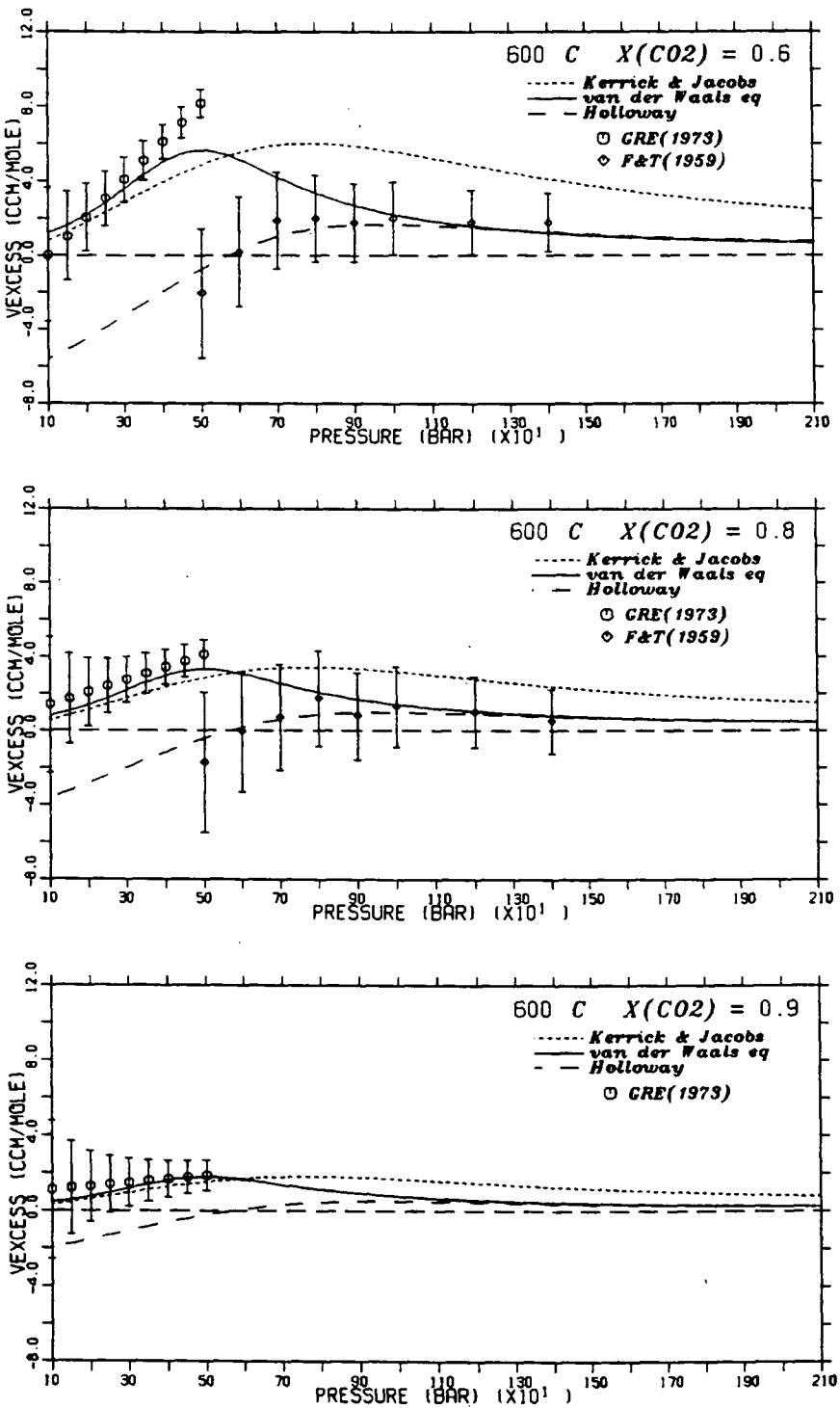

Figure E.43: $P - V_e$ graphs: 600 °C, X_{CO_2}=0.6–0.9. Data of Gehrig (GEH), Franck & Tödheide (F&T), Greenwood (GRE), Shmulovich *et al.* (SHM), and Shmulovich *et al.* (SSZ).

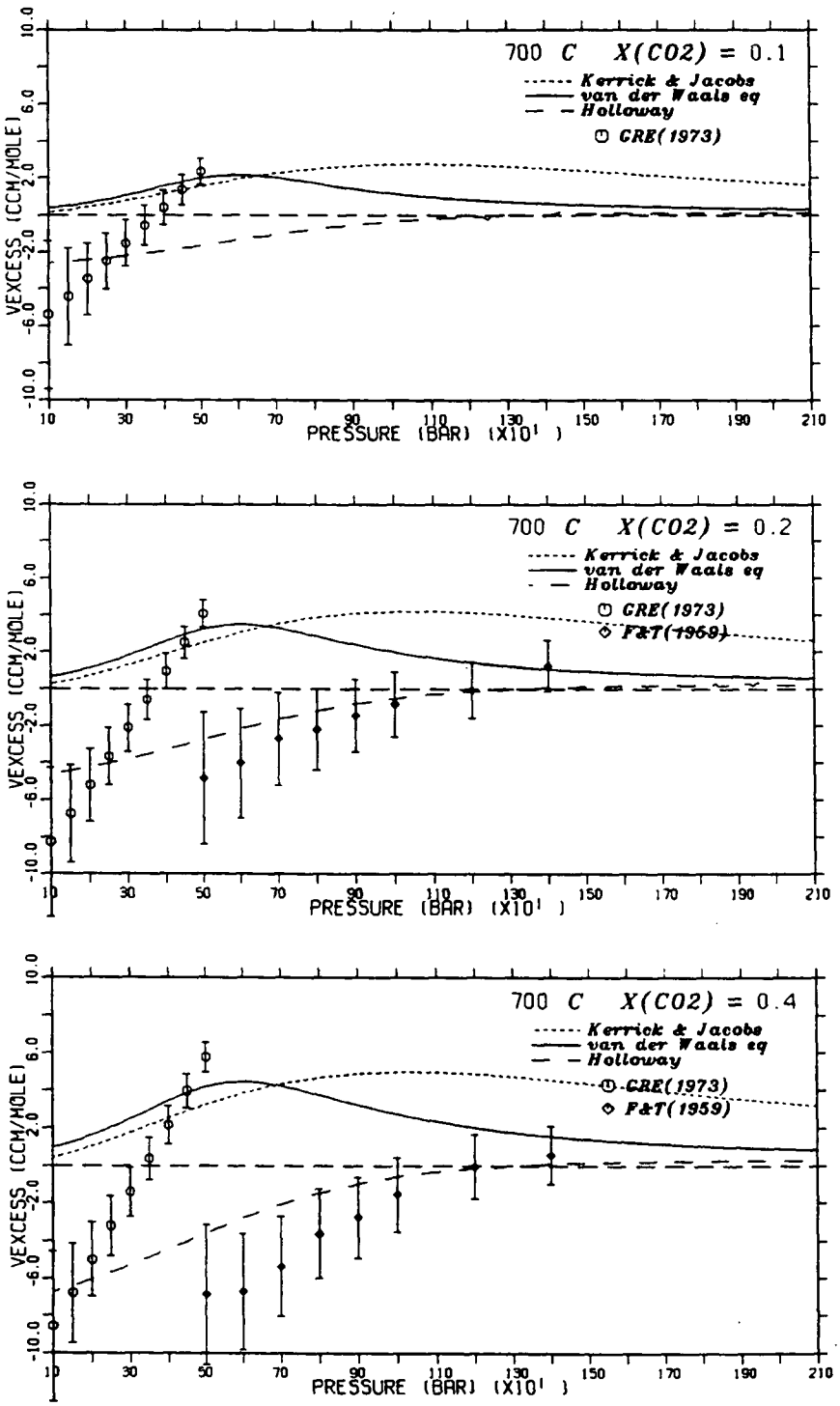

Figure E.44: $P - V_e$ graphs: 700 °C, X_{CO_2}=0.1–0.4. Data of Gehrig (GEH), Franck & Tödheide (F&T), Greenwood (GRE), Shmulovich *et al.* (SHM), and Shmulovich *et al.* (SSZ).

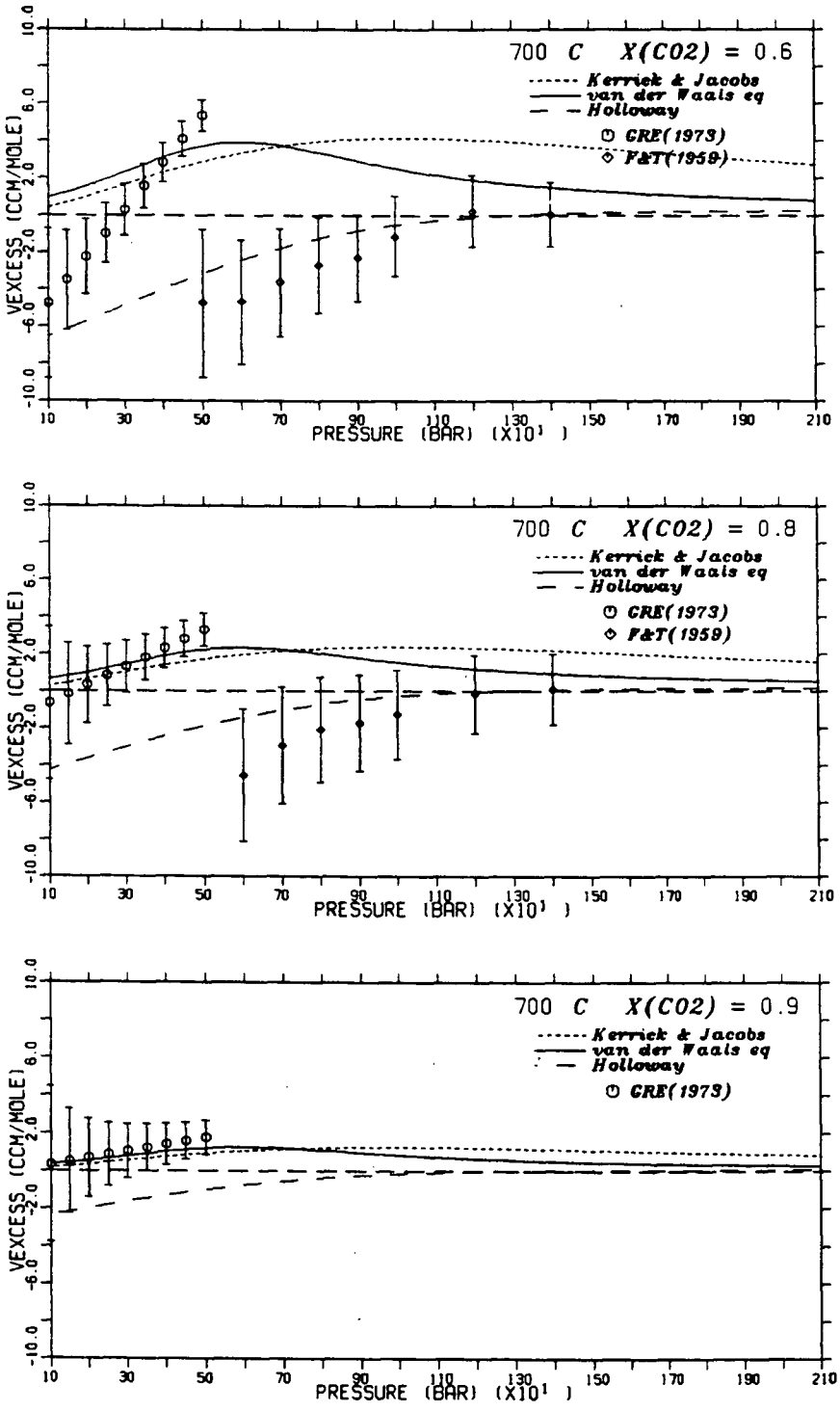

Figure E.45: $P - V_e$ graphs: 700 °C, X_{CO_2}=0.6–0.9. Data of Gehrig (GEH), Franck & Tödheide (F&T), Greenwood (GRE), Shmulovich *et al.* (SHM), and Shmulovich *et al.* (SSZ).

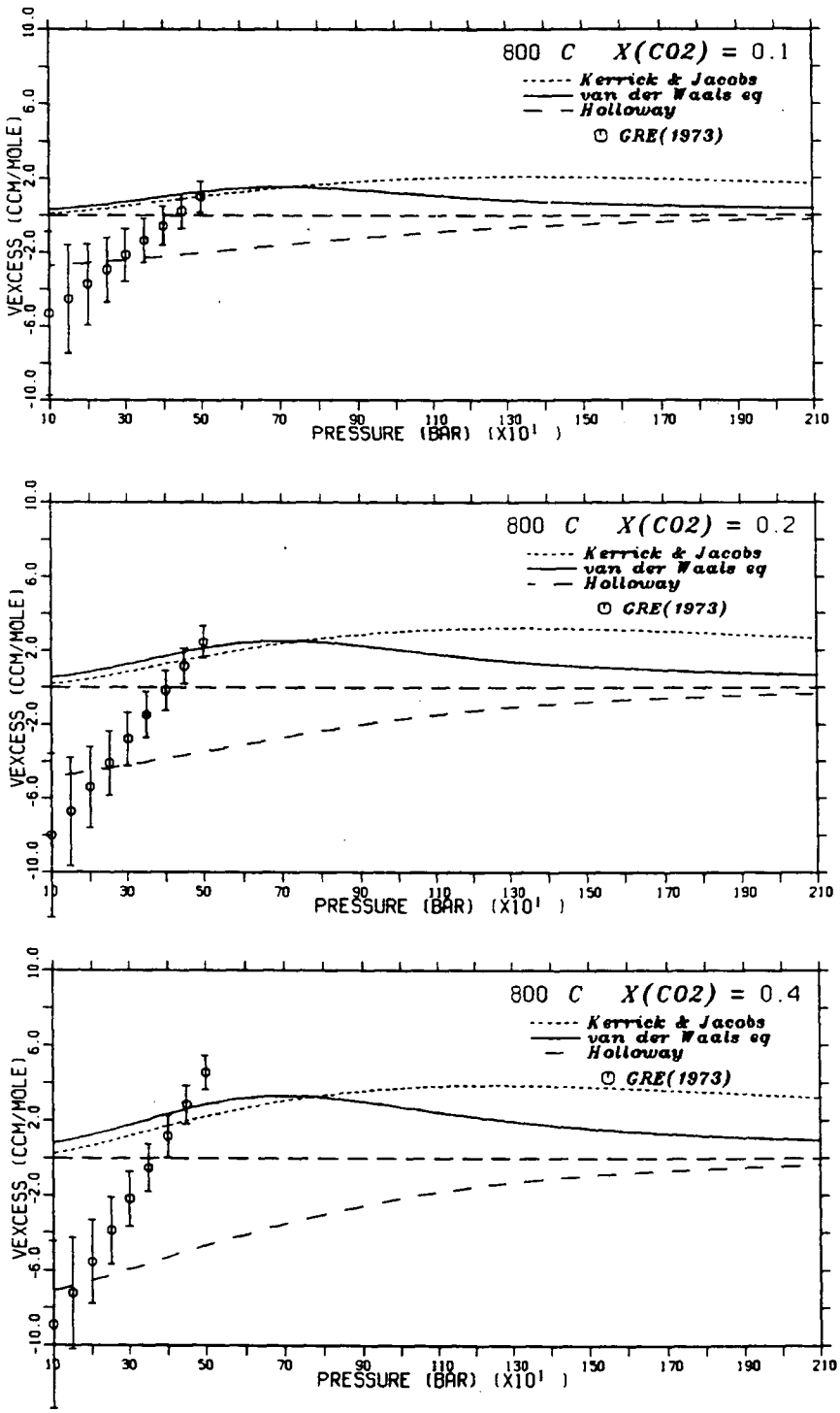

Figure E.46: $P - V_e$ graphs: 800 °C, X_{CO_2}=0.1–0.4. Data of Gehrig (GEH), Franck & Tödheide (F&T), Greenwood (GRE), Shmulovich *et al.* (SHM), and Shmulovich *et al.* (SSZ).

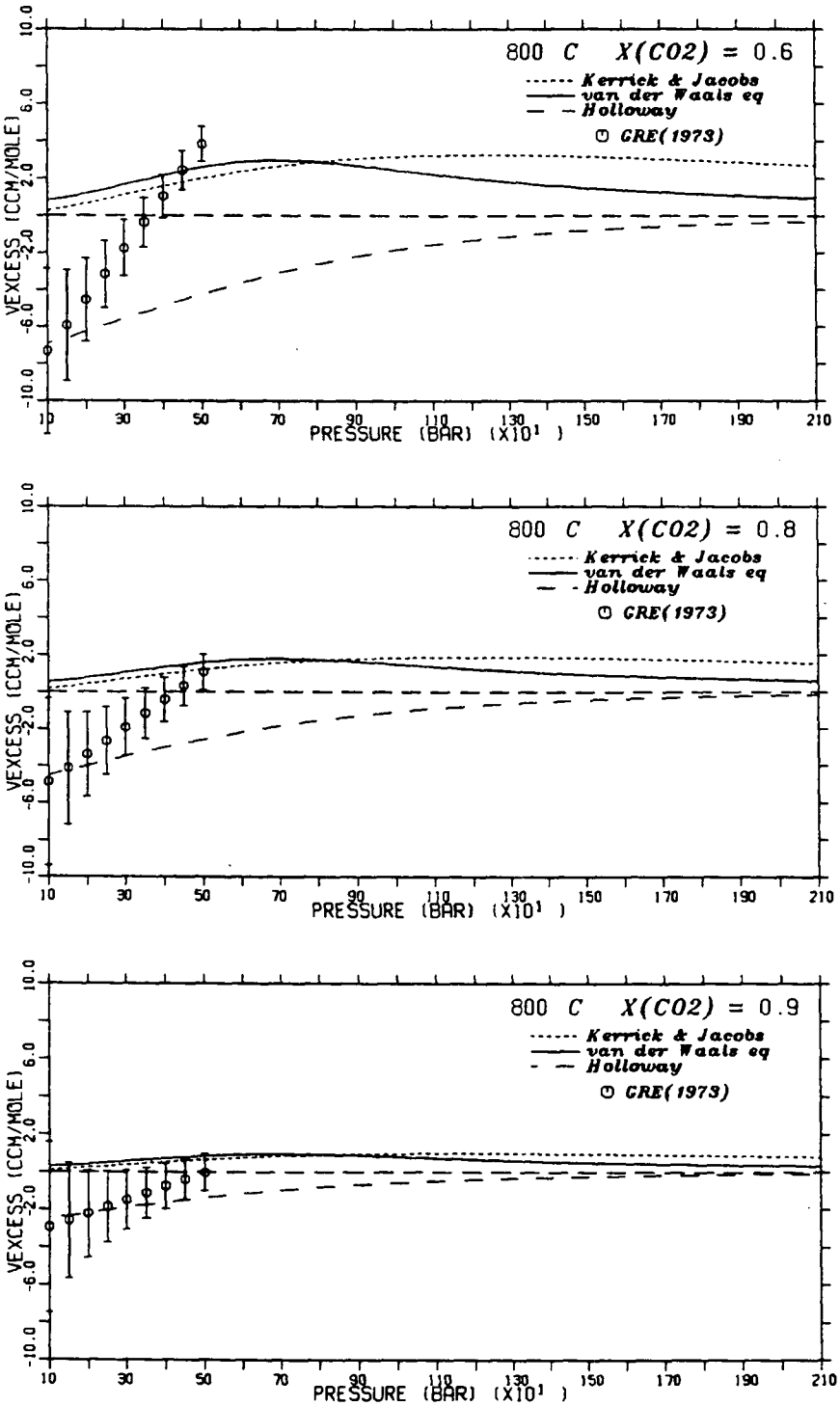

Figure E.47: $P - V_e$ graphs: 800 °C, X_{CO_2}=0.6–0.9. Data of Gehrig (GEH), Franck & Tödheide (F&T), Greenwood (GRE), Shmulovich *et al.* (SHM), and Shmulovich *et al.* (SSZ).

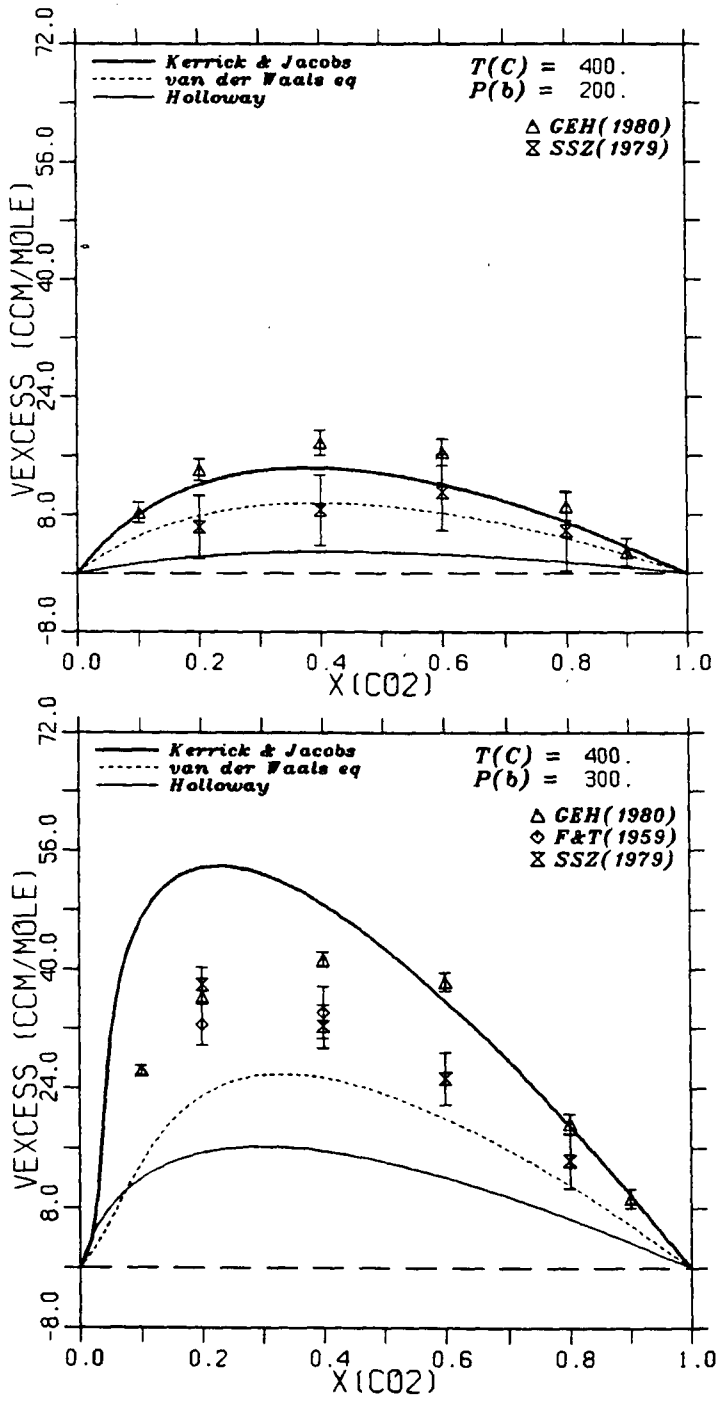

Figure E.48: $X - V_e$ graphs: 400 °C, 200 & 300 bar. Data of Gehrig (GEH), Franck & Tödheide (F&T), Greenwood (GRE), Shmulovich *et al.* (SHM), and Shmulovich *et al.* (SSZ).

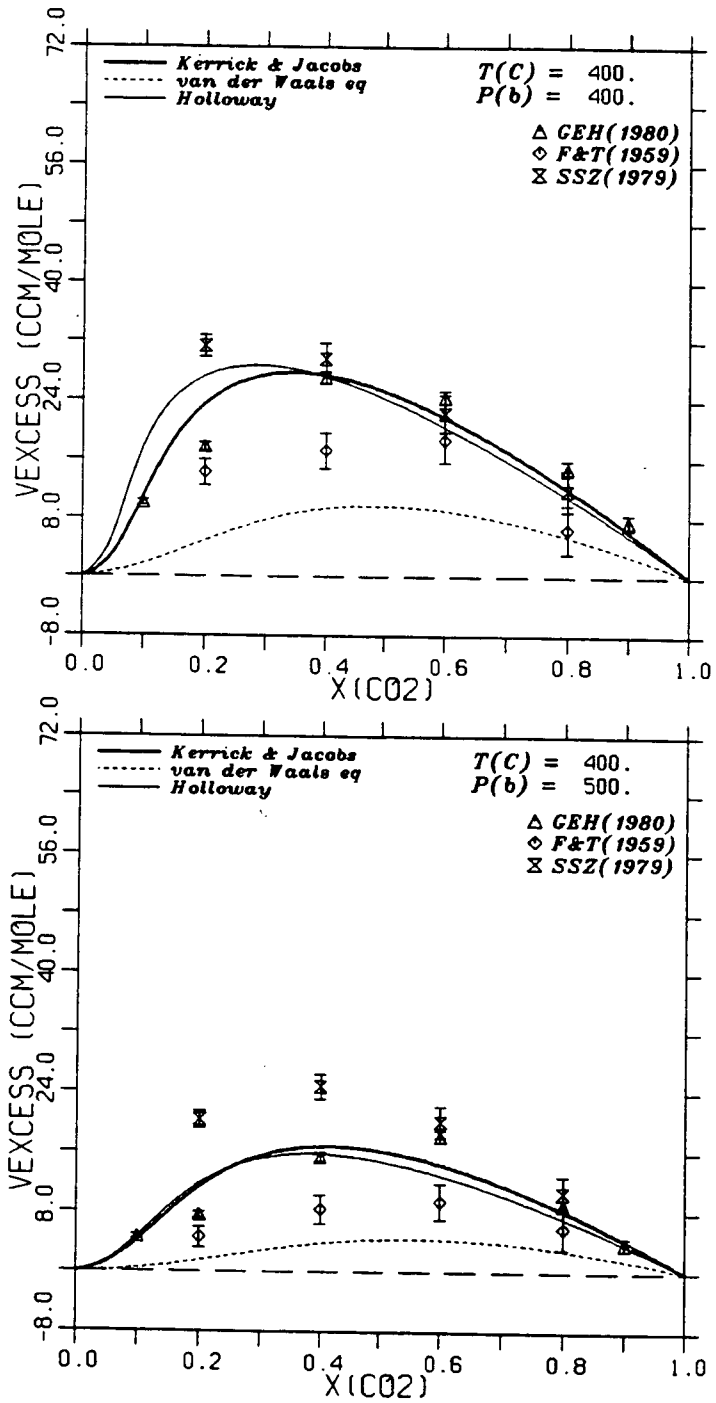

Figure E.49: $X - V_e$ graphs: 400 °C, 400 & 500 bar. Data of Gehrig (GEH), Franck & Tödheide (F&T), Greenwood (GRE), Shmulovich *et al.* (SHM), and Shmulovich *et al.* (SSZ).

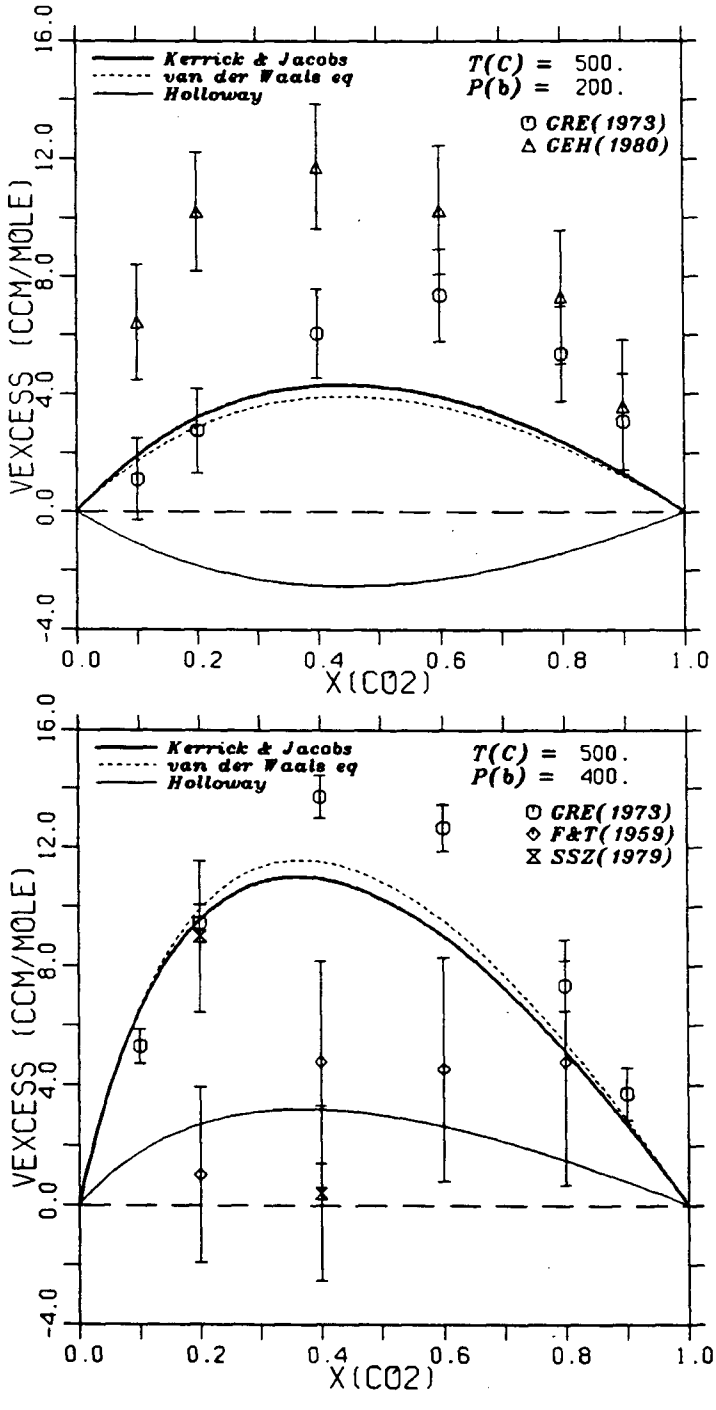

Figure E.50: $X - V_e$ graphs: 500 °C, 200 & 400 bar. Data of Gehrig (GEH), Franck & Tödheide (F&T), Greenwood (GRE), Shmulovich *et al.* (SHM), and Shmulovich *et al.* (SSZ).

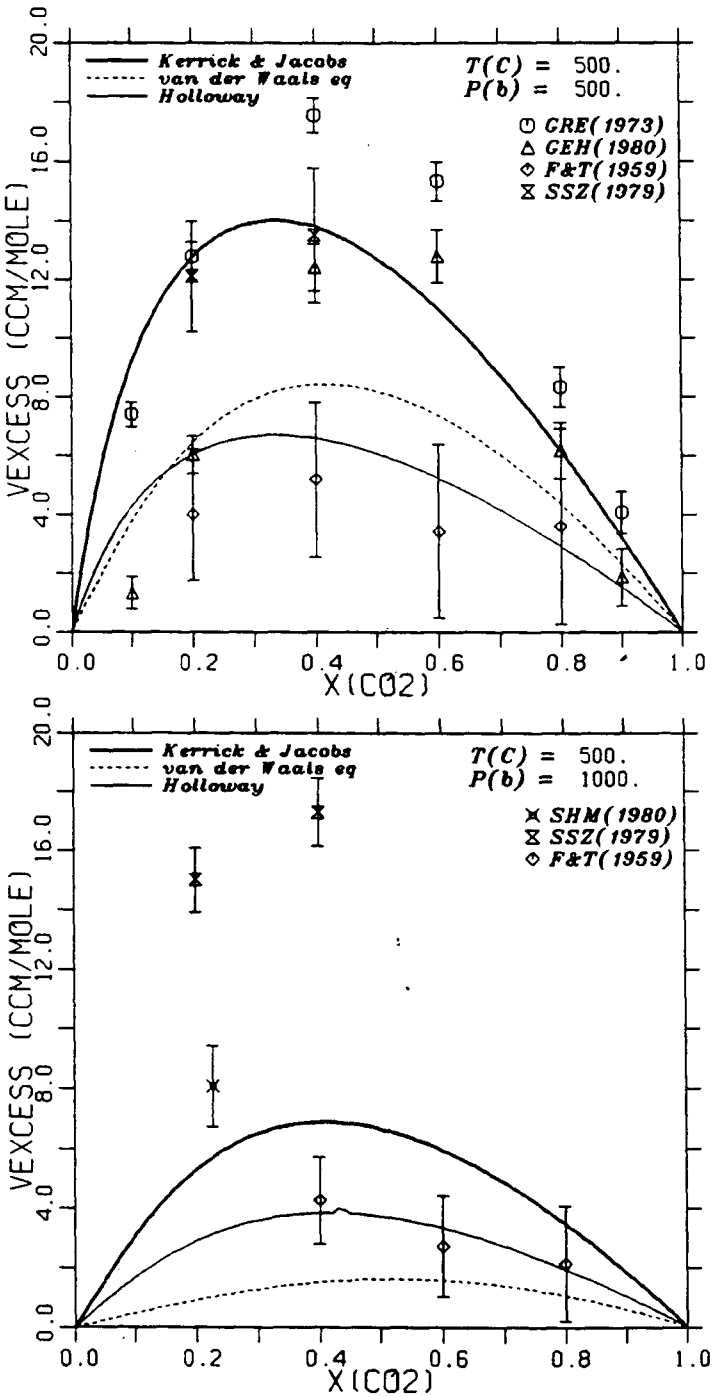

Figure E.51: $X - V_e$ graphs: 500 °C, 500 & 1000 bar. Data of Gehrig (GEH), Franck & Tödheide (F&T), Greenwood (GRE), Shmulovich *et al.* (SHM), and Shmulovich *et al.* (SSZ).

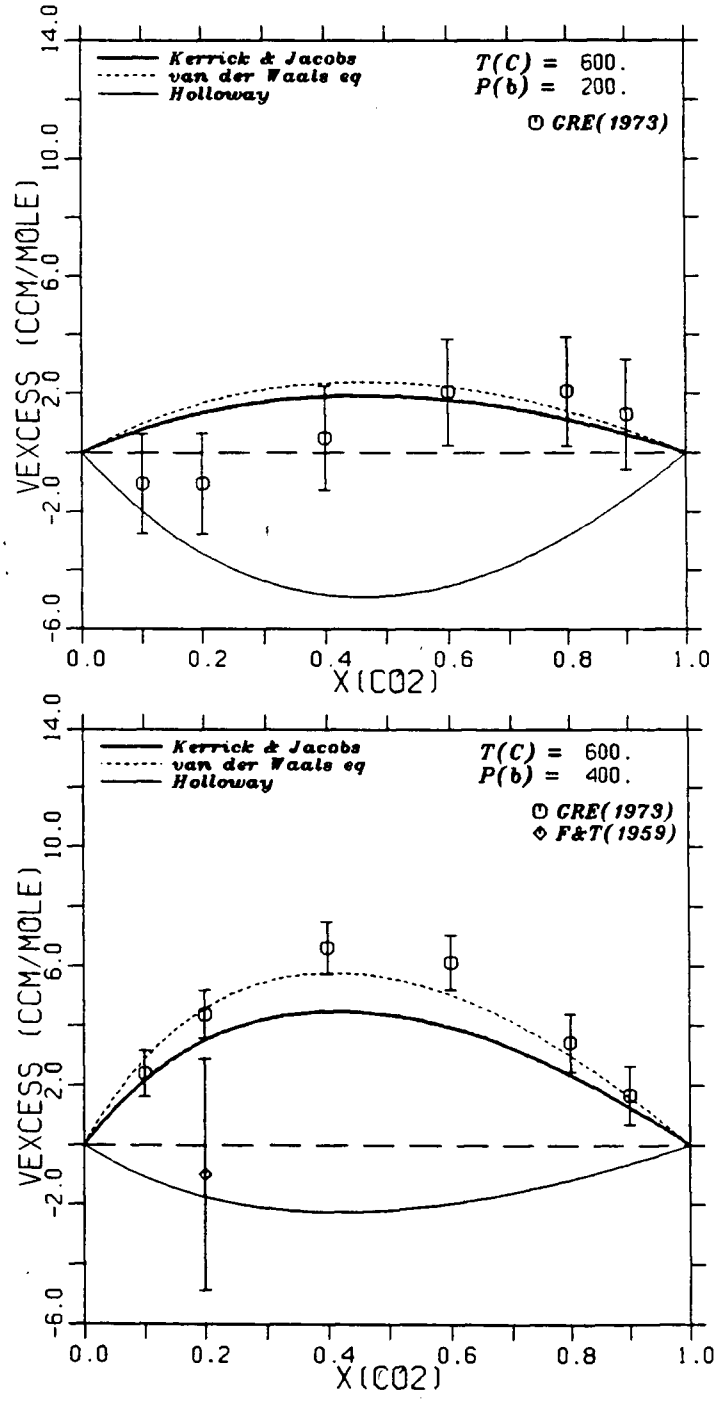

Figure E.52: $X - V_e$ graphs: 600 °C, 200 & 400 bar. Data of Gehrig (GEH), Franck & Tödheide (F&T), Greenwood (GRE), Shmulovich *et al.* (SHM), and Shmulovich *et al.* (SSZ).

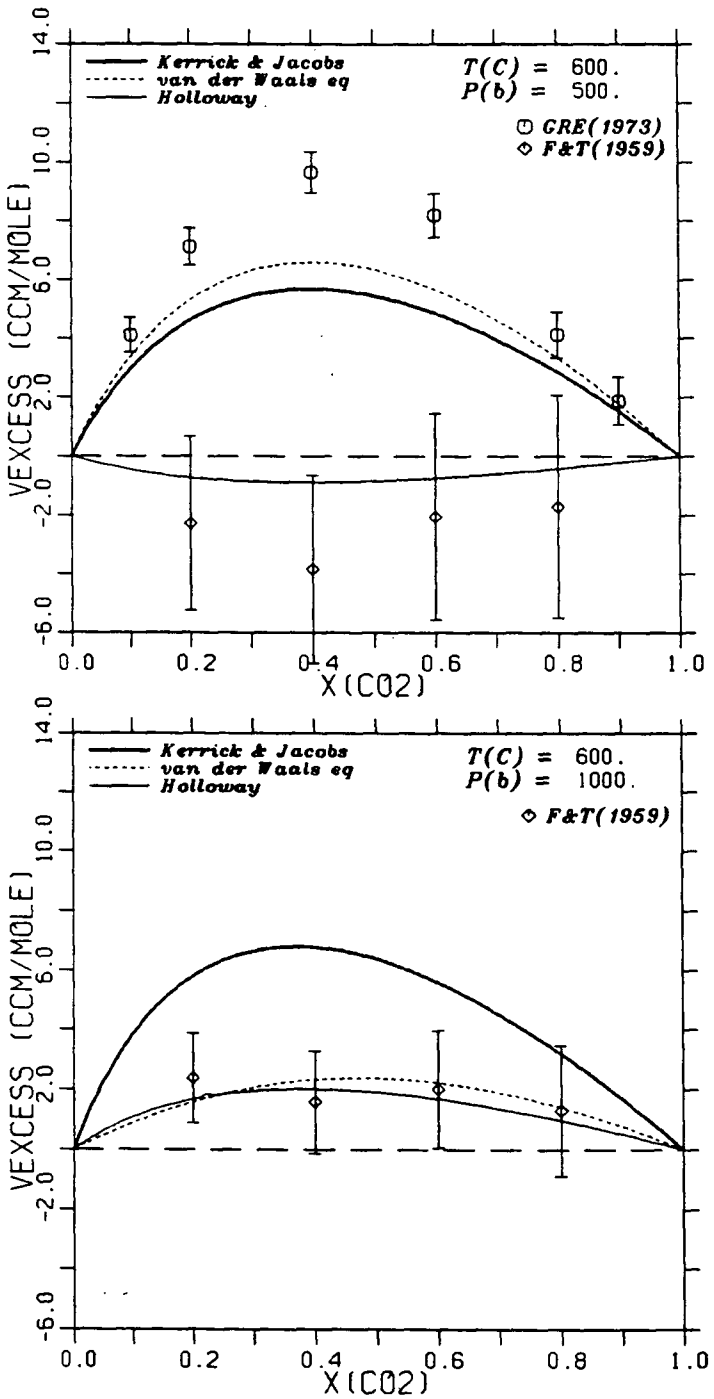

Figure E.53: $X - V_e$ graphs: 600 °C, 500 & 1000 bar. Data of Gehrig (GEH), Franck & Tödheide (F&T), Greenwood (GRE), Shmulovich *et al.* (SHM), and Shmulovich *et al.* (SSZ).

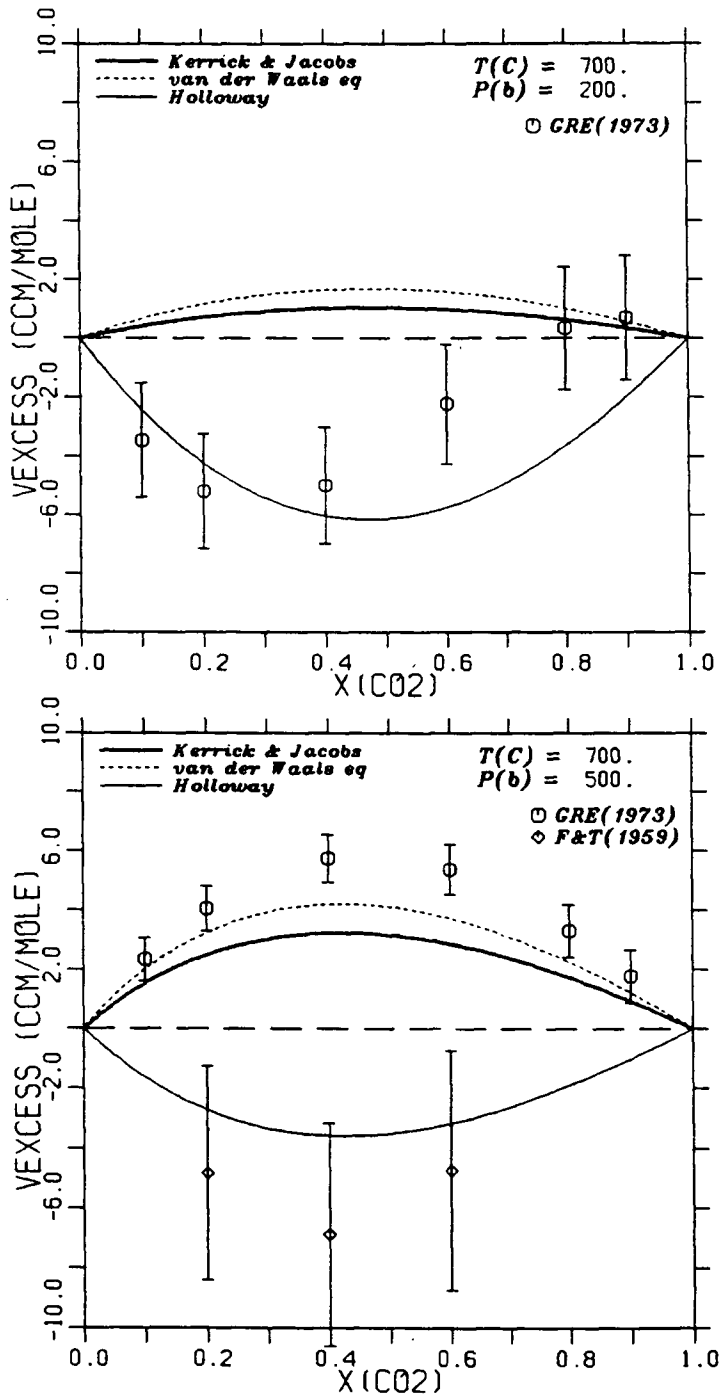

Figure E.54: $X - V_e$ graphs: 700 °C, 200 & 500 bar. Data of Gehrig (GEH), Franck & Tödheide (F&T), Greenwood (GRE), Shmulovich *et al.* (SHM), and Shmulovich *et al.* (SSZ).